

The relativistic nuclear dynamics

for the $SU(3)$ Goldstone bosons of chiral QCD

Schrift zur Habilitation

dem

Fachbereich Physik der
Technischen Universität Darmstadt

vorgelegt von

Matthias Friedrich Michael Lutz

aus Brühl bei Köln

Contents

1	Introduction	1
1.1	Fundamental aspects	2
1.2	Goldstone bosons in nuclear matter	4
1.3	Meson-baryon scattering	5
1.4	Perspectives	6
2	Chiral SU(3) symmetry and meson-baryon interactions	9
2.1	Baryon resonances and coupled channel dynamics	12
2.2	Relativistic chiral SU(3) interaction terms in large- N_c QCD	17
2.3	Quasi-local interaction terms	23
2.4	Explicit chiral symmetry breaking	26
3	Covariant meson–baryon scattering	33
3.1	On-shell reduction of the Bethe-Salpeter equation	34
3.2	Renormalization program	37
3.3	Weinberg-Tomozawa interaction and convergence of χ PT	45
3.4	Partial-wave decomposition of the Bethe-Salpeter equation	48
4	SU(3) coupled-channel dynamics	53
4.1	Construction of the effective interaction kernel	57
4.2	Chiral expansion and covariance	69
4.3	Crossing symmetry and the $S = 1$ channels	74
5	Goldstone bosons in cold nuclear matter	79
5.1	Self consistent and covariant nuclear dynamics	81
5.2	Covariant projector algebra method in nuclear matter	83
6	Results	89
6.1	Parameters	90
6.2	Axial-vector and meson-baryon coupling constants	94
6.3	Kaon- and antikaon-nucleon scattering	97
6.4	Analyticity and crossing symmetry	104
6.5	Antikaons and hyperon resonances in nuclear matter	108
7	Summary and outlook	127

Chapter 1

Introduction

The question whether and to what extent hadrons change their properties in a dense nuclear environment is an exciting subfield of nuclear and particle physics which attracts considerable attention in the community [1,2,3,4,5,6,7]. Several complementary approaches exist to study this question empirically. There is a long history for the study of pion- and kaon-nucleus scattering. Pion and kaon beams have been available at many facilities and a wealth of data has been collected. Also there exist data on level shifts of pionic and kaonic atoms. Phenomenological optical potentials were constructed that successfully describe the data set [8,9,10]. The optical potential reflects the in-medium properties of the mesons in cold nuclear matter for nuclear densities smaller or equal the nuclear saturation density. Furthermore, photon induced meson production off the nucleus offer a promising probe of in-medium effects [11,12].

A further important tool for the study of hadron properties in hot and dense matter is offered by the heavy ion facilities at GSI, CERN and BNL. A heavy ion reaction can be visualized as the creation of an initial hot and dense fireball, which after some evolution is assumed to freeze out to release the observed particles [13,14,15,16]. In this picture the measured hadron multiplicities are characterized by a freeze-out surface, temperature and baryon chemical potential. An alternative picture, avoiding any equilibrium assumption, is offered by transport model calculations which provide the bridge to a more microscopic understanding of heavy ion reactions [17,18,19,20,21,22,23,24,25,26,27,28]. The properties of the fireball may change dramatically if the energy of the heavy ion beam is varied. In the SPS (CERN) experiments, with typical energies per nucleon of $40 \text{ GeV} < E/N < 200 \text{ GeV}$, and more recently in the RHIC (BNL) experiments, with even larger energies, one attempts to create a fireball which is in the quark gluon plasma state [29]. There are indications that the temperatures reached are indeed sufficiently high, exceeding 200 MeV, as to melt the initial heavy ions into their quark and gluon constituents [30].

A complementary heavy ion program is pursued at GSI with typical energies of up to 2 GeV per nucleon. Here the initial fireball reaches nuclear densities of up to three times the density of nuclear saturation. The associated temperatures are typically smaller than 100 MeV. A spectacular finding of the KaoS collaboration at GSI was the enhanced subthreshold production of negatively charged kaons as compared to positively charged kaons in heavy ion reactions [31]. This may hint at a substantially decreased antikaon mass in a dense nuclear environment. Consequently there has been much theoretical effort to access the properties of kaons in nuclear matter [32,33,34,35,36,37,38,39,40,41,42,43,44,45]. A possible exciting consequence of a significantly reduced effective K^- mass could be that kaons condense in the interior of neutron stars [46,47].

Quantitative empirical constraints from heavy ion reactions, on the in-medium antikaon spectral functions require rather involved transport model calculations which are performed extensively by various groups [17, 18, 19, 20, 21, 22, 28]. The next generation of transport codes which are able to incorporate particles with finite width more consistently are being developed [25, 26, 27, 28]. This is of considerable importance when dealing with antikaons which are poorly described by a quasi-particle ansatz [41, 42]. It is an open challenge to find a microscopic understanding of the particle production data in heavy ion reactions. The challenges are many-fold. In particular one needs to derive improved microscopic input like in-medium reaction rates and spectral functions for hadrons to be used in transport model calculations.

In this work we will focus on the properties of antikaons in cold nuclear matter. We do not address the question how hadronic modes behave in a quark-gluon plasma environment. From an experimental point of view the pions, kaons and etas offer a particularly unique tool to study the nuclear many-body system since their in-medium properties are accessible in different types of experiments. Besides measuring pion, kaon and eta multiplicities in heavy-ion reactions one may scatter pions or kaons off nuclei or study the systems of negatively charged pions or antikaons bound at a nucleus via γ -spectroscopy. There is even the possibility that a eta meson may be bound at a nucleus forming an eta-atom [48, 49].

1.1 Fundamental aspects

The foundation of all theoretical attempts to describe and possibly predict hadron properties in a dense nuclear environment should be Quantum Chromo Dynamics (QCD), the fundamental theory of strong interactions. For an exposition of the basic concepts of QCD we refer to standard textbooks like [50]. The QCD Lagrangian predicts all hadron interactions in terms of quark and gluon degrees of freedom. At large momentum transfers QCD is extremely successful and predictive, because observable quantities can be evaluated perturbatively in a straightforward manner. At small momentum transfers, in contrast, QCD is less predictive so far due to its non-perturbative character. It is still an outstanding problem to systematically unravel the properties of QCD in its low-energy phase where the effective degrees of freedom are hadrons rather than quarks and gluons. That is a challenge since many of the most exciting phenomena of QCD, like the zoo of meson and baryon resonances, manifest themselves at low-energies. Also the fundamental question addressed in this work 'how do hadrons change their properties in dense nuclear matter' requires a solid understanding of QCD at small momentum transfer.

There are two promising paths along which one achieved and expects further significant progress. A direct evaluation of many observable quantities is possible by large scale numerical simulations where QCD is put on a finite lattice [51]. Though many static properties, like hadron ground-state properties, have been successfully reproduced by lattice calculations, the description of the wealth of hadronic scattering data is still outside the scope of that approach [51]. Also the determination of hadron properties at finite nuclear densities is still not feasible on the lattice [52, 53]. Here a complementary approach, effective field theory, is more promising at present. Rather than solving low-energy QCD in terms of quark and gluon degrees of freedom, inefficient at low energies, one aims at constructing an effective quantum field theory in terms of hadrons directly. The idea is to constrain that theory by as many properties of QCD as possible. This leads to a significant parameter reduction and a predictive power of the effective field theory

approach. In this spirit many effective field theory models, not all of which fully systematic, have been constructed and applied to the data set. Given the many empirical data points to be described, it is not always necessary to build in all constraints of QCD. Part of QCD's properties may enter the model indirectly once it successfully describes the data and provided that the model is not in conflict with the most basic properties of quantum field theory. The most difficult part in constructing a systematic effective field theory is the identification of its applicability domain and its accuracy level.

An effective field theory, which meets the above criteria, is the so called Chiral Perturbation Theory (χ PT) applicable in the flavor $SU(2)$ sector of low-energy QCD. This effective field theory is based on a simple observation, namely that QCD is chirally symmetric in the limiting case where the up and down current quark masses vanish $m_{u,d} = 0$. This implies in particular that the handedness of quarks is a conserved property in that limit. There is mounting empirical evidence that the QCD ground state breaks the chiral $SU(2)$ symmetry spontaneously in the limit $m_{u,d} = 0$. For instance the observation that hadrons do not occur in parity doublet states directly reflects that phenomenon. Also the smallness of the pion masses with $m_\pi \simeq 140$ MeV much smaller than the nucleon mass $m_N \simeq 940$ MeV, naturally fits into this picture once the pions are identified to be the Goldstone bosons of that spontaneously broken chiral symmetry. The merit of standard χ PT is that first it is based on an effective Lagrangian density constructed in accordance with all chiral constraints of QCD and second that it permits a systematic evaluation applying formal power counting rules [54]. In χ PT the finite but small values of the up and down quark masses $m_{u,d} \simeq 10$ MeV are taken into account as a small perturbation defining the finite masses of the Goldstone bosons. The smallness of the current quark masses on the typical chiral scale of 1 GeV explains the success of standard χ PT. For applications of χ PT to pion-nucleon scattering see [55, 56, 57, 58, 59].

It is of course tempting to generalize the chiral $SU(2)$ scheme to the $SU(3)$ flavor group which includes the strangeness sector. To construct the appropriate chiral $SU(3)$ Lagrangian is mathematically straightforward and has been done long ago (see e.g. [60]). The mass $m_s \simeq 10 m_{u,d}$ of the strange quark, though much larger than the up and down quark masses, is still small on the typical chiral scale of 1 GeV [61]. The required approximate Goldstone boson octet is readily found with the pions, kaons and the eta-meson. Nevertheless, important predictions of standard χ PT as applied to the $SU(3)$ flavor group are in stunning conflict with empirical observations. Most spectacular is the failure of the Weinberg-Tomozawa theorem [62, 63] which predicts an attractive K^- -proton scattering length, rather than the observed large and repulsive value. Progress can be made upon accepting a crucial observation that the power counting rules must not be applied to a certain subset of Feynman diagrams. Whereas for irreducible diagrams the chiral power counting rules are well justified, this is no longer necessarily the case for the irreducible diagrams [64]. The latter diagrams are enhanced as compared to irreducible diagrams and therefore may require a systematic resummation scheme in particular in the strangeness sectors. First intriguing works taking up this idea in the chiral context are given in [65, 66, 67, 68].

It is amusing to observe that this development may be viewed as a justification of the many K -matrix analyses in the 60's and the 70's which in spirit were already rather close to modern effective field theories only that chiral constraints were not considered. A severe drawback of those early attempts, where the inverse K -matrix is systematically expanded in a Taylor series, is that the number of free parameters increases excessively along with the number of terms kept in that Taylor series. For instance, the K -matrix analyses for the antikaon-nucleon scattering process, quite systematic close to threshold, involve up to 44 parameters which all need to be

adjusted to the data set [69, 70, 71, 72, 73]. Here modern effective field theories constitute an important advance once they successfully incorporate chiral constraints of QCD and therewith reduce the number of unknown parameters significantly.

1.2 Goldstone bosons in nuclear matter

We return to the main theme of this work to study the properties of Goldstone bosons in nuclear matter. Not only from an experimental but also from a theoretical point of view the pions and kaons, the lightest excitation of the QCD vacuum with masses of 140 MeV and 495 MeV respectively, are outstanding probes for exciting many-body dynamics. The Goldstone bosons are of particular interest since their in-medium properties reflect the structure of the nuclear many-body ground state. For example at high baryon densities one expects the chiral symmetry to be restored. One therefore anticipates that the Goldstone bosons change their properties substantially as one compresses nuclear matter.

Even though in the $SU(3)$ limit of QCD with degenerate current quark masses $m_u = m_d = m_s$ the pions and kaons have identical properties with respect to the strong interactions, they provide very different means to explore the nuclear many-body system. This is because the chiral $SU(3)$ symmetry is explicitly broken by a nuclear matter state with strangeness density zero, a typical property of matter produced in the laboratory. A pion, if inserted into isospin degenerate nuclear matter, probes rather directly the spontaneously broken or possibly restored chiral $SU(2)$ symmetry. A kaon, propagating in strangeness free nuclear matter, loses its chiral $SU(3)$ symmetry since the matter by itself explicitly breaks the $SU(3)$ symmetry. It is subject to three different phenomena: the spontaneously broken chiral $SU(3)$ symmetry, the explicit symmetry breaking of the small current quark masses and the explicit symmetry breaking of the nuclear matter bulk. The various effects are illustrated by recalling the effective pion and kaon masses in a dilute isospin symmetric nuclear matter gas. The low-density theorem [74, 33] predicts mass changes Δm_Φ^2 for any meson Φ in terms of its isospin averaged s-wave meson-nucleon scattering length $a_{\Phi N}$

$$\Delta m_\Phi^2 = -4\pi \left(1 + \frac{m_\Phi}{m_N}\right) a_{\Phi N} \rho + \mathcal{O}(\rho^{4/3}) \quad (1.1)$$

where ρ denotes the nuclear density. According to the above arguments one expects that the pion-nucleon scattering length $a_{\pi N} \sim m_\pi^2$ must vanish in the chiral $SU(2)$ limit since isospin symmetric nuclear matter conserves the Goldstone boson character of the pions at least at small densities. On the other hand, kaons lose their Goldstone boson properties and therefore one expects $a_{KN} \sim m_K$ and in particular $a_{K^-N} \neq a_{K^+N}$. This is demonstrated by the Weinberg-Tomozawa theorem which predicts the s-wave scattering length in terms of the chiral order parameter $f_\pi \simeq 93$ MeV :

$$a_{\pi N} = 0 + \mathcal{O}(m_\pi^2), \quad a_{K^\pm N} = \mp \frac{m_K}{4\pi f_\pi^2} + \mathcal{O}(m_K^2). \quad (1.2)$$

In the pion sector the Weinberg-Tomozawa theorem (1.2) is beautifully confirmed by the smallness of the empirical isospin averaged pion-nucleon scattering length $a_{\pi N} \simeq -0.01$ fm. In the kaon sector the Weinberg-Tomozawa theorem misses the empirical scattering K^+ nucleon

scattering length $a_{K+N} \simeq -0.3$ fm by about a factor of three. Even more spectacular is the disagreement of Weinberg-Tomozawa term in the K^- case where (1.2) predicts $a_{K-N} \simeq +0.9$ fm while the empirical K^- nucleon scattering length is $a_{K-N} \simeq (-0.6 + i 1.1)$ fm.

Whereas in conjunction with the low-density theorem the Weinberg-Tomozawa theorem predicts a decreased effective K^- mass, the empirical scattering length unambiguously states that there must be repulsion in the K^- channel at least at very small nuclear densities. The antikaon-nucleon scattering process is complicated due to the open inelastic $\pi\Sigma$ and $\pi\Lambda$ channels. This is reflected in the large imaginary part of the empirical K^- nucleon scattering length. A quite rich variety of phenomena arises from the presence of both the s-wave $\Lambda(1405)$ and p-wave $\Sigma(1385)$ resonances just below, and the d-wave $\Lambda(1520)$ resonance not too far above the antikaon-nucleon threshold. In nuclear matter there exist multiple modes with quantum numbers of the K^- resulting from the coupling of the various hyperon states to a nucleon-hole state. As a consequence the K^- spectral function shows a rather complex structure as a function of baryon density, kaon energy and momentum. This is illustrated by recalling the low-density theorem as applied for the energy dependence of the kaon self energy $\Pi_{\bar{K}}(\omega, \rho)$. The self energy is determined in terms of the s-wave kaon-nucleon scattering amplitude $f_{\bar{K}N}^{s\text{-wave}}(\sqrt{s})$ is

$$\Pi_{\bar{K}}(\omega, \rho) = -4\pi \left(1 + \frac{\omega}{m_N}\right) f_{\bar{K}N}^{s\text{-wave}}(m_N + \omega) \rho + \mathcal{O}(\rho^{4/3}), \quad (1.3)$$

where we assume zero kaon momentum. A pole contribution to $\Pi_{\bar{K}}(\omega, \rho)$ from a hyperon state with mass m_H , if sufficiently strong, may lead to a K^- like state of approximate energy $m_H - m_N$. Most important are the $\Lambda(1405)$ s-wave resonance and the $\Sigma(1385)$ p-wave resonance. An attractive modification of the antikaon spectral function was already anticipated in the 70's by the many K-matrix analyses of antikaon-nucleon scattering (see e.g. [69]) which predicted considerable attraction in the subthreshold s-wave K^- nucleon scattering amplitudes. In conjunction with the low-density theorem (1.3) this leads to an attractive antikaon spectral function in nuclear matter. As was pointed out in [41] the realistic evaluation of the antikaon self energy in nuclear matter requires a self consistent scheme. In particular the feedback effect of an attractive antikaon spectral function on the antikaon-nucleon scattering process was found to be important for the $\Lambda(1405)$ resonance structure in nuclear matter.

The quantitative evaluation of the antikaon spectral function in nuclear matter is still an outstanding problem. Further progress requires an improved understanding of the antikaon-nucleon scattering process in free space. In particular reliable subthreshold antikaon-nucleon scattering amplitudes are needed. The present data set for antikaon-nucleon scattering leaves much room for different theoretical extrapolations to subthreshold energies [69, 70, 71, 72, 73, 75, 76, 77, 65, 66, 78]. As a consequence the subthreshold $\bar{K}N$ scattering amplitudes of different analyses may differ by as much as a factor of two [65, 66] in the region of the $\Lambda(1405)$ resonance. Also the antikaon spectral function should be evaluated in an improved many-body treatment including the effects of p-wave interactions systematically.

1.3 Meson-baryon scattering

The meson-baryon scattering processes are an important test for effective field theories which aim at reproducing QCD at small energies, where the effective degrees of freedom are hadrons

rather than quarks and gluons. In this work we focus on the strangeness sector, because here the acceptable effective field theories are much less developed and also the empirical data set still leaves much room for different theoretical interpretations. In the near future the new DAΦNE facility at Frascati could deliver new data on kaon-nucleon scattering [79] and therewith help to establish a more profound understanding of the role played by the $SU(3)$ flavor symmetry in hadron interactions. At present the low-energy elastic K^+ -proton scattering data set leads to a rather well established K^+p scattering length with $a_{K^+p} \simeq 0.28 - 0.34$ fm [9]. Uncertainties exist, however, for the K^+ -neutron cross sections which are typically extracted from the scattering data of the $K^+d \rightarrow K^+pn, K^0pp$ reactions. Since data are available only for $p_{\text{lab}} > 350$ MeV the model dependence of the deuteron wave function, the final state interactions and the necessary extrapolations down to threshold lead to conflicting values for the K^+ -neutron scattering length [80]. A recent analysis [81] favors a repulsive and small value $a_{K^+n} \simeq 0.1$ fm. Since low-energy polarization data are not available for K^+ -nucleon scattering at present, the separate strength of the various p-wave channels can only be inferred from theory. This leads to large uncertainties in the p-wave scattering volumes [80].

The K^- -proton scattering length was only recently determined convincingly by a kaonic-hydrogen atom measurement [82]. In contrast to that the K^- -neutron scattering length remains model dependent [69, 70]. This reflects the fact that at low energies there are no K^- -deuteron scattering data available except for some K^-d branching ratios [83], which however are commonly not included in theoretical models of kaon-nucleon scattering. The rather complex multi-channel dynamics of the strangeness -1 channel is constrained by not too good quality low-energy elastic and inelastic K^-p scattering data [84] but rather precise K^-p threshold branching ratios [85]. Therefore the isospin one scattering amplitude is only indirectly constrained for instance by the $\Lambda\pi^0$ production data [86]. All this leaves much room for different theoretical extrapolations [69, 70, 71, 72, 73, 75, 76, 77, 78]. As a consequence the subthreshold $\bar{K}N$ scattering amplitudes, which determine the \bar{K} -spectral function in nuclear matter at leading order in the density expansion, are poorly controlled.

Therefore it is desirable to make use of the chiral symmetry constraints of QCD [65, 66, 67, 68]. The reliability of the extrapolated subthreshold scattering amplitudes can substantially be improved as compared to previous works [65, 66, 68], if s- and p-waves are considered in the analysis. This is important because the available data, in particular in the strangeness -1 channel, are much more precise for $p_{\text{lab}} > 200$ MeV than for $p_{\text{lab}} < 200$ MeV where one expects s-wave dominance.

1.4 Perspectives

In this work the relativistic chiral $SU(3)$ Lagrangian including an explicit baryon decuplet resonance field with $J^P = \frac{3}{2}^+$ is applied. The baryon decuplet field is an important ingredient, because it is part of the baryon ground state multiplet which arises in the large- N_c limit of QCD [87, 88]. Also the effects of a phenomenological baryon nonet d-wave resonance field with $J^P = \frac{3}{2}^-$ is considered. This is necessary because some of the p-wave strengths in the $\bar{K}N$ -system can be extracted from the present day data set reliably only via their interference effects with the d-wave resonance $\Lambda(1520)$. This is the first application of the chiral $SU(3)$ Lagrangian density to the kaon-nucleon and antikaon-nucleon system which systematically considers constraints

from the pion-nucleon sector. A convenient minimal chiral subtraction scheme for relativistic Feynman diagrams is proposed which complies manifestly with the standard chiral counting rule [89, 90, 91]. Furthermore it is argued that due to the rather large kaon mass the kaon-nucleon dynamics is non-perturbative in contrast to the pion-nucleon system where standard chiral perturbation theory (χ PT) can be applied successfully [55, 56, 57, 58, 59]. In the strangeness sectors a partial resummation scheme is required [92, 65, 66]. The Bethe-Salpeter equation for the scattering amplitude is solved with an interaction kernel truncated at chiral order Q^3 . Only those terms are included in the interaction kernel which are leading in the large- N_c limit of QCD [87, 88, 93, 94, 95]. An important aspect to be addressed concerns the independence of the on-shell scattering amplitude on the choice of chiral coordinates or the choice of interpolating fields. If one solves the Bethe-Salpeter equation with an interaction kernel evaluated in perturbation theory the resulting on-shell scattering amplitudes depend on the choice of interpolating fields even though physical quantities should be independent on that choice [96]. It will be demonstrated that this problem can be avoided by introducing an appropriate on-shell reduction scheme for the Bethe-Salpeter equation.

The s-, p- and d-wave contributions with $J = \frac{1}{2}, \frac{3}{2}$ in the scattering amplitude are considered. Detailed predictions for the poorly known meson-baryon coupling constants of the baryon octet and decuplet states will be made. It is found that the scattering amplitudes are quite sensitive to the precise values of the meson-baryon coupling constants permitting the determination of SU(3) symmetry breaking effects in the 3-point vertices. That observation justifies to include effects of chiral order Q^3 in the interaction kernel. At chiral order Q^2 one encounters 7 unknown symmetry conserving and 3 reasonably well known symmetry breaking parameters. At chiral order Q^3 the relevance of 4 unknown parameters is derived refining the quasi-local two-body vertices. Additional 10 parameters are required to describe SU(3) symmetry breaking effects in the meson-baryon coupling constants as well as those in the axial vector coupling constants of the baryon octet states. As a novel technical ingredient a covariant projector formalism is constructed. It is supplemented by a subtraction scheme rather than a cutoff scheme as employed previously [65, 66]. The renormalization scheme is an essential input for the chiral $SU(3)$ dynamics, because it leads to consistency with chiral counting rules and an approximate crossing symmetry of the subthreshold kaon-nucleon scattering amplitudes. In particular, the scheme avoids breaking the $SU(3)$ symmetry by channel dependent cutoff parameters as suggested in [65] and also an implicit sensitivity of the $\Lambda(1405)$ resonance structure on the cutoff parameter [66].

The set of parameters is adjusted successfully to describe the existing low-energy cross section data on kaon-nucleon and antikaon-nucleon scattering including angular distributions to good accuracy. At the same time a good description of the low-energy s- and p-wave pion-nucleon phase shifts as well as the empirical axial-vector coupling constants of the baryon octet states is achieved. Detailed predictions are given for the poorly known meson-baryon coupling constants of the baryon octet and decuplet states. Furthermore the many $SU(3)$ reaction amplitudes and cross sections like $\pi\Lambda \rightarrow \pi\Lambda, \pi\Sigma, \bar{K}N$ relevant for transport model simulations of heavy-ion reactions are presented. As a result of the analysis, particularly important for any microscopic description of antikaon propagation in dense nuclear matter, sizable contributions from the p-waves parts in the subthreshold K^- -nucleon forward scattering amplitude are predicted. Besides deriving a realistic antikaon spectral function first quantitative results on the in-medium structure of the p-wave $\Sigma(1385)$ and the d-wave $\Lambda(1520)$ resonances are obtained.

In chapter 2 a critical review of previous non-perturbative applications of the chiral SU(3) Lagrangian in the meson-baryon sector is given. It follows a discussion on the generic nature of

baryon resonances in view of their role played in chiral coupled channel theories. The chapter is closed by a series of more formal sections in which the parts of the relativistic chiral Lagrangian relevant for this work are constructed. All interaction terms are systematically analyzed in the $1/N_c$ expansion of QCD. In chapter 3 a formalism is developed how to properly treat the Bethe-Salpeter equation in a chiral coupled channel approach. Details on the renormalization scheme will be given. In chapter 4 the coupled channel effective interaction kernel in accordance with the scheme presented in chapter 3 is derived. A scheme-independent and covariant framework, in which self consistency for the in-medium meson spectral functions is implemented in terms of the vacuum meson-nucleon scattering amplitudes is developed in chapter 5. For the first time the scheme considers the in-medium mixing of s-, p- and d-waves in a self consistent manner. Any reader not primarily interested in the numerous technical developments may directly jump to the result chapter 6 which can be read independently.

The work presented here is based in large parts on collaborations with E.E. Kolomeitsev and C.L. Korpa [97, 98].

Chapter 2

Chiral SU(3) symmetry and meson-baryon interactions

In this chapter a detailed derivation of the constraints imposed on the meson-baryon scattering processes by the chiral SU(3) symmetry of QCD will be given. The discussion of the existing literature will emphasize the strangeness sectors since there exist various review articles on the pion-nucleon scattering process (see e.g. [101]). The latter process was studied in much more detail than the kaon and anti-kaon nucleon scattering processes, the focus of this work. After reviewing in some detail the more recent developments in the strangeness sectors the scope of this work will be defined. For earlier descriptions of the meson-baryon scattering data based on meson-exchange phenomenology we refer to standard review articles (see e.g. [102]). Before entering the many technical details on how to implement the chiral constraints into the coupled channel dynamics an exposition about the generic structure of baryon resonances will be offered in a separate section. This is important since we will encounter various baryon resonances in this work. As a result of the discussion a conjecture will be formulated as to what the nature of baryon resonances may be.

The first work by Kaiser, Siegel and Weise [65], who applied the chiral SU(3) Lagrangian to the low-energy antikaon-nucleon scattering data, described the elastic and inelastic scattering process in terms of a coupled channel Lippman-Schwinger equation. The scattering kernel was identified with the leading and subleading quasi-local interaction vertices of the chiral Lagrangian in a phenomenological manner. The power-divergencies, which arise when solving the Lippman-Schwinger equation, were tamed by phenomenological form factors. All together the scheme has 5 free parameters characterizing the strength of the leading and subleading quasi-local interaction vertices. Three additional parameters were required to model the form factors. The low-energy scattering data for laboratory momenta $p_{\text{lab}} < 200$ MeV were reproduced accurately in terms of s-wave dynamics only. In particular the s-wave $\Lambda(1405)$ resonance was generated dynamically by coupled channels effects. A criticism of this work was raised by Oset and Ramos [66] who pointed out that in [65] the $\eta \Sigma$, $\eta \Lambda$ and $K \Xi$ channels, indispensable ingredients of a chiral SU(3) theory, were not considered in the coupled channel scattering equations. Superficially these additional channels may appear unimportant since they are closed at small energies. However, the effect of those channels may turn important since they give rise to a particular renormalization of the leading open $\bar{K} N$, $\pi \Sigma$ and $\pi \Lambda$ channels. Oset and Ramos demonstrated that a reasonable fit of the low-energy scattering data was possible in terms of the leading Weinberg-Tomozawa interaction term and a suitable constructed universal form factor which was modelled by one

parameter only. They argued that the form factor represents higher order effects of the chiral Lagrangian in some way. From a fundamental point of view not much was gained as compared to previous K-matrix or potential model analyses of the scattering data. The interplay of form factor effects and the scattering kernel, constrained by the chiral $SU(3)$ symmetry in a phenomenological manner, remained puzzling in those early works. In particular, a fit to the scattering data required a fine-tuning of the form factors [66] which explicitly break the $SU(3)$ symmetry [65]. Moreover, the leading Weinberg-Tomozawa interaction was long known to be equivalent at low energies to an interaction kernel approximated by a simple t-channel vector meson exchange diagram if the vector-meson coupling constants were chosen in an universal manner [92]. A successful description of the low-energy scattering data was obtained previously by Siegel and Weise [92] in terms of the t-channel vector meson exchange diagram as the driving term in the coupled channel scattering equation. Such models, which reproduce the threshold strength as predicted by the leading chiral Weinberg-Tomozawa interaction, were originally proposed and studied by Wyld [103] and also by Dalitz, Wong and Rajasekaran [104]. In those early computations [103, 104] the t-channel vector-meson exchange was treated in the static approximation but already all inelastic channels required by the flavor $SU(3)$ symmetry were considered. The resulting coupled channel Schrödinger equation does not require any form factors to tame ultraviolet divergencies since the Yukawa type potential, which arises in the static approximation of the t-channel vector meson exchange diagram, is well behaved at short distances.

In order to make further progress and unravel the chiral $SU(3)$ structure of the meson-baryon scattering data a more systematic treatment of the chiral Lagrangian was asked for. In particular a more transparent scheme in which the interaction kernel and the scattering equation are considered on the same footing was desirable. A first important step in this direction was achieved in [67] where it was suggested to use a subtraction scheme rather than a phenomenological form factor. It was argued that the subtraction point is strongly constrained by the requirement that the associated relativistic loop integral should obey the chiral counting rule. Once a subtraction scheme is applied there is no need anymore for a fine-tuning of the parameters. Using a universal subtraction point for all partial waves and channels it was argued that the subtraction point should be identified with the hyperon mass as to protect the s-channel hyperon exchange contribution in the p-wave scattering amplitude. Then using the physical strength of the Weinberg-Tomozawa interaction as parameterized in terms of the pion decay constant $f_\pi \simeq 93$ MeV one obtained a parameter-free leading order description of the antikaon-nucleon s-wave dynamics. An additional strong argument as to why the subtraction point must be universal and close to the hyperon mass follows from dimensional regularization and the requirement that the theory should lead to crossing symmetric amplitudes, at least approximatively. This will be elaborated on in this work in great detail. In the more recent work Oller and Meissner [68] suggested a similar scheme where the value of the pion-decay constant and the subtraction point were varied as to obtain a quantitative description of the low-energy s-wave antikaon-nucleon scattering data. The resulting effective pion-decay constant was found to be significantly larger than the value required by the pion-nucleon scattering data¹.

¹Though the general strategy advocated by Oller and Meissner [68] is similar to that one applied previously in [99, 67] and used in this work, there are important technical differences. At leading order and in particular considering only s-wave dynamics the differences are of minor importance. However, when correction terms and higher partial waves, not studied in [68], are considered, this is not anymore the case and important differences arise. In the scheme of Oller and Meissner the crucial problem of how strength coming from the subtraction

The challenge, to obtain a simultaneous description of the low-energy pion-, kaon- and antikaon-nucleon scattering data remained. If different values of the chiral parameters are used in the various sectors the chiral SU(3) structure remains unclear. Obviously, one should consider chiral correction terms in a systematic way and treat the pion-, kaon-, and antikaon-nucleon scattering processes on equal footing. Also higher partial wave components, so far not studied in the strangeness sectors, should be evaluated. This defines the scope of this work. The analysis becomes necessarily much more involved but at the same time more rewarding since one may learn more about the chiral SU(3) symmetry. Of particular interest are the explicit SU(3) symmetry breaking effects which are so far only poorly understood.

It is emphasized that here the goal is not to describe pion-induced strangeness production off the nucleon. A solid understanding of such reactions $\pi N \rightarrow K\Lambda, K\Sigma, \dots$ requires the incorporation of the correlated two-pion production process which constitutes a major source of inelastic strength at these energies. That lies clearly outside the scope of this work which aims at understanding the scattering processes at low energies only. In this respect the antikaon-nucleon scattering process is better suited to unravel the chiral SU(3) symmetry of QCD quantitatively. For instance, the inelastic reactions $\bar{K}N \rightarrow \pi\Lambda, \pi\Sigma$ occur at energies where the phase space for the complicated three-body hadronic final states are still closed.

The incorporation of the correlated two-pion production into a chiral coupled channel theory is a quite ambitious enterprise, which we believe, however, to be feasible if the large- N_c constraints of QCD are used. The inclusion of vector mesons into the chiral Lagrangian as explicit degrees of freedom is subtle as to the fact that rigorous power counting rules do not exist. The effect of the implicit t-channel vector meson exchange contribution was suggested in [105, 106] to be incorporated by the N/D method of Chew and Mandelstam [107]. However, the question how to incorporate for instance the inelastic $\rho_\mu N$ or $\omega_\mu N$ channels into a chiral description of pion-nucleon scattering remains an open problem. We conjecture that this should be possible once the chiral expansion is combined with the $1/N_c$ expansion. The $1/N_c$ expansion provides an intuitive and possibly systematic guide as to why higher order loop diagrams involving multiple powers of the vector meson propagators are suppressed as the number of independent loop integrals in the diagram increases. Here we exploit the obvious observation that hadronic loop functions if visualized in terms of quark-gluon diagrams are suppressed in the $1/N_c$ expansion.

A phenomenological attempt by Caro Ramon et al. [108] to describe pion induced strangeness production within the chiral SU(3) Lagrangian but without the inclusion of the correlated two-pion production is obviously plagued by severe shortcomings. In particular, their description of differential cross sections, which includes s- and p-wave terms, leaves much room for improvements. It is unclear to what degree the SU(3) symmetry is obscured by form factor effects or the fact that chiral parameters were adjusted in the strangeness zero sector only. The more recent work [109], which also describes pion induced ηN and $K\Lambda$ production without the inclusion of the correlated two-pion production, is subject to similar objections. In particular the strong SU(3) symmetry breaking allowed for in the subtraction constants is difficult to understand. At this stage it may be advantageous to postpone the fundamental description of such reactions in terms of the chiral Lagrangian and rather improve the description of these reactions in terms of phenomenological approaches which do however incorporate the correlated two-pion production processes modelled in terms of effective $\rho_\mu N$ and $\pi\Delta_\mu$ channels [110, 111, 112, 113, 114, 99, 100]. The solid understanding of these reactions requires necessarily a profound theory for the struc-

coefficients is constrained by the chiral SU(3) symmetry remains obscure. This will be discussed in chapter 3.4 when presenting the technical details of our scheme.

ture of baryon resonances like for instance the s-wave $N(1535)$ and $N(1650)$ states. Since we will have to make assumptions on the nature of baryon resonances throughout this work we discuss this aspect in the following section in some detail.

2.1 Baryon resonances and coupled channel dynamics

There have been many discussions on how to incorporate the $\Delta(1232)$ isobar resonance into the chiral Lagrangian [115,116]. One legitimate point of view would be to insist that the two relevant small scales m_π and $m_\Delta - m_N$ are not correlated and that one should insist on $m_\pi \ll m_\Delta - m_N$, at least in the chiral limit where $m_\pi = 0$ but $m_\Delta \neq m_N$. In more physical terms the isobar degree of freedom would be integrated out and therefore would not appear as a fundamental field in the chiral Lagrangian. Obviously this point of view necessarily restricts the applicability of the chiral Lagrangian to threshold physics. For instance the well known rapid energy variation of the P_{33} pion-nucleon phase shift close to $\sqrt{s} \simeq 1232$ MeV can only be described in such a scheme if an infinite number of interaction terms in the chiral Lagrangian are considered. A more economical scheme arises if one accepts the physical values of m_π and $m_\Delta - m_N$ which suggest to set up an effective chiral field theory where one introduced so-called power counting rules with $m_\pi \sim m_\Delta - m_N \sim Q$ parametrically. With Q we denote any typical small scale of the system. A brief discussion of power counting rules will be given in section 2.2. Such a scheme is well justified if one incorporates an additional property of QCD into the effective field theory. If the number of colors, N_c , in QCD is considered as a free parameter a systematic expansion of hadron properties in powers of $1/N_c$ is feasible. At a given order, the $1/N_c$ expansion selects a well defined infinite set of quark-gluon diagrams which may be considered at the physical value $N_c = 3$. Even though at present it appears impossible to evaluate the sum of these diagrams, at any given order in that expansion it is possible to work out sum rules obeyed by hadronic observables. For instance at leading order in the $1/N_c$ expansion the nucleon and isobar masses are degenerate. This observation may serve as a justification for the counting rule $m_\pi \sim m_\Delta - m_N \sim Q$ in a combined chiral and $1/N_c$ expansion. The generalization to the chiral $SU(3)$ Lagrangian is straightforward. It necessarily involves baryon octet and decuplet fields since their mass parameters would be degenerate in the large- N_c limit of QCD up to small corrections from explicit $SU(3)$ symmetry breaking effects. The importance of the decuplet degrees of freedom for the antikaon-nucleon scattering process was pointed out in [67].

The picture becomes more complicated when baryons of the second generation are involved. Let us focus for a while on the s-wave baryon resonance $\Lambda(1405)$ which is known to play a dominant role in the antikaon-nucleon scattering process. Since there appears no fundamental reason at hand to insist on degenerate mass parameters of the $\Lambda(1115)$ ground state and the resonance state $\Lambda(1405)$ in the large- N_c or chiral limit of QCD, the incorporation of an explicit $\Lambda(1405)$ resonance field into the chiral Lagrangian would lead to the breakdown of power counting rules. As a consequence it would be unclear what diagrams to evaluate at given order implying an uncontrolled breaking of the chiral Ward identities. This is a disaster from a fundamental point of view. Thus, if the $\Lambda(1405)$ is within reach of the chiral $SU(3)$ Lagrangian it preferably be generated dynamically by coupled channel effects. Indeed, as is known from the many K-matrix analyses of the 70's the $\Lambda(1405)$ can be generated dynamically [117, 103, 104, 70, 71, 72]. This mechanism is confirmed beautifully by the recent applications of the chiral $SU(3)$ Lagrangian

to the antikaon-nucleon scattering process [65, 66, 67, 68].

An immediate question arises. To what extent is the dynamic generation of a baryon resonance consistent with the quite successful quark model picture of such states suggested by Isgur and Karl [118, 119, 120] where three constituent quarks are bound together by a confining potential? The answer of this question is nontrivial and we will not be able to offer a final answer. What we can do here is, however, to collect various arguments which at least illustrate the complexity of this problem. We do not claim originality for all of these arguments since they are in some way implicit in the literature even though it is difficult to associate them to a given person. As a result of this discussion we will formulate a conjecture as to what the nature of the baryon resonances may be. Before entering the discussion we emphasize that here we are concerned exclusively about baryon resonances build up from the light quarks of QCD, the up, down and strange quarks. For heavy quark systems there are convincing derivations of a non-relativistic confining potential which suffices to describe the interactions of heavy quarks [121]. The dynamics of the light quarks of QCD, on the other hand, is highly non-trivial and subject to controversial opinions. The problem is so complicated because for the light quarks a non-relativistic treatment of the bound state problem cannot be justified.

To some degree the problem may be simply a question of economy. What is the most natural description of the scattering data? Suppose some quark model predicts a bare resonance state of given mass. Then the coupling to the meson-baryon states gives rise to a finite hadronic decay width but also to a mass shift of the resonance. If the mass shift induced by the coupled channel dynamics is sufficiently large it may be more economical or at least legitimate to consider the resonance to be generated dynamically. It is difficult to imagine that the bare mass parameter is an observable quantity in this case. This suggests for instance that a bare-pole term in the scattering kernel may be Taylor expanded around the physical resonance mass provided that the bare pole position is outside the applicability domain of the effective field theory. The crucial question is therefore how important is the coupling of the bare resonance states to the final hadronic states [122]. The fact that baryon resonances exhibit large hadronic decay widths, not all of them well understood within the quark model approach so far, demonstrates that this is a non-trivial question. In this context it is important to realize, that channels which open only at energies larger than a given resonance mass may still give rise to a sizeable mass shift for that resonance.

It is instructive to return to the $1/N_c$ expansion strategy of QCD already touched upon above and discuss its implications for the baryon states. We would like to emphasize that the impressive success of the quark model in describing the properties of the baryon octet and decuplet ground states, like for instance their magnetic moments, can equivalently be obtained applying the $1/N_c$ expansion [93]. Only at the level of the second generation baryon resonances there appear important differences between the quark model approach and the $1/N_c$ expansion method [94, 95]. For the large- N_c baryon ground state properties the so called contracted $SU(6)$ spin-flavor symmetry, inherent in the quark model and also predicted by the $1/N_c$ expansion, is responsible for this remarkable success. A stringent test of the quark model dynamics is provided by the second and third generation of baryon resonances. It remains to be seen whether the predictions of present day quark model calculations [119], a large number of so far unobserved baryon resonances, comes true. The challenge is to reproduce the empirical baryon resonance spectrum and at the same time obtain a detailed description of the resonance decay channels. The question to be answered is whether it is efficient to classify baryon resonances not part of the large- N_c ground states as higher dimensional representations of a $O(3) \otimes SU(6)$ group or

whether it is more physical to consider those as a result of coupled channel dynamics. For instance the baryon octet and decuplet states form together the ground state **56**-plet. For the excited states this classification is indicative but hampered by the fact that it requires additional dynamical assumption on how to model the orbital excitation of a quark inside a resonance state consistently with the contracted $SU(6)$ spin-flavor symmetry of QCD. For the first excited resonance **56**-plet with negative parity there are hyperon resonance states which are so far not observed [123, 124]. Similarly the first **70**-plet of positive parity is incomplete containing a number of missing hyperon resonance states [125]. The latter multiplet assumes one quark to carry angular momentum $L = 1$. Of course one may say that this is a beautiful prediction anticipating that the missing states should eventually be observed in experiment. However, one also may be worried by the fact that the study of the excited resonance states reveals that operators that are subsubleading in the $1/N_c$ analysis are in fact describing the main splitting patterns observed in the multiplets, rather than the subleading operators [123, 124, 125]. Thus, it remains unclear whether the $1/N_c$ expansion converges for the excited baryon resonances. Moreover it was argued by Witten that the large- N_c picture of excited resonances is applicable for states with small total spin only [88, 126, 127]. In the Skyrme model for instance, a large- N_c realization of QCD, only states with $J \ll N_c$ are believed to be reliably described [88].

In the framework of the $1/N_c$ expansion the conjecture that resonances may be generated dynamically is quite attractive since it amounts to a significant parameter reduction. The interaction of the large- N_c meson and baryon ground states may be systematically constrained by the $1/N_c$ analysis and then would have to predict all excited resonance states. On the other hand a classification of the excited baryon resonance states as higher dimensional representations of the contracted $O(3) \otimes SU(6)$ group required for each multiplet a new tower of operators with unknown coefficients [123, 124, 125]. Of course any given quark model would predict the latter coefficients. However, one should not forget that there is no unique quark model so that strictly speaking the particular ansatz used for the inter-quark potential represents already a particular choice for an infinite set of parameters.

One may argue that the hadronic final state effect on a bare resonance state is suppressed by $1/N_c$. This follows at a formal level since any hadronic loop if visualized in terms of quark and gluon lines gives rise to that suppression factor $1/N_c$. Though this argument is certainly applicable in a world in which the parameter $N_c \gg 1$ is really large, it is less immediate for the physical case with $N_c = 3$. If for some reason a particular subset of hadronic loop diagrams is systematically enhanced by a factor larger than the suppression factor $1/N_c$ for $N_c = 3$ the above argument breaks down and one must sum that infinite set of hadronic diagrams. In this work we will argue that precisely the set of diagrams representing the hadronic final state effect on a bare resonance state are enhanced coherently by a typical factor 2π . Such diagrams are commonly called reducible in the sense that they give rise to unitarity cuts as compared to irreducible diagrams which build up the interaction kernel of the relativistic Bethe-Salpeter two-body scattering equation. Therefore we would expect that indeed the effect of the hadronic final state on a bare resonance state is non-perturbative and potentially large. That explains naturally why the chiral Lagrangian is able to generate for instance the $\Lambda(1405)$ resonance in terms of coupled channel dynamics. For a recent discussion of the competing picture in which the $\Lambda(1405)$ resonance is considered as a quark-model state we refer to [128]. The fact that the existence of the $\Lambda(1405)$ resonance is predicted by the chiral $SU(3)$ Lagrangian basically parameter free [67] we take as a strong indication that it is legitimate to consider at least part of the baryon resonances of the second and third generation as dynamically generated.

It is important to explore the consequence of this point of view. Since in the quark model and also in the large- N_c approach of QCD the excited resonances come in multiplets classified by the contracted spin-flavor $SU(6)$ group, the statement that one member of a given multiplet should lie outside the scope of the quark-model affects of course at the time the remaining members of that multiplet². For instance within the quark-model the s-wave $\Lambda(1405)$ and d-wave $\Lambda(1520)$ resonance states belong to the same **70**-plet [125]. Incidentally, the quark model has a notoriously difficult time to reproduce the empirical mass splitting of those states [128, 125]. However, if the $\Lambda(1405)$ resonance is a consequence of coupled channel dynamics than we would expect the same to hold for the $\Lambda(1520)$. Indeed there is an old speculation that the latter resonance may be formed as consequence of a strong $\bar{K}_\mu N$ channel [129, 130, 131]. Analogously, for the $SU(3)$ partner $N(1520)$ of the $\Lambda(1520)$ the $\rho_\mu N, \omega_\mu N$ would be the driving channels. For another member of the same **70**-plet, the s-wave $N(1535)$ resonance, there are hints from the t-channel vector meson exchange model of Wyld [103] and chiral coupled channel analyses [132, 133] that it may also be a state that is generated dynamically.

It is then natural to expect that the s-wave $N(1650)$ resonance, another member of the same **70**-plet, is of dynamic origin also. This conjecture was tested in a phenomenological coupled channel analysis of pion- and photon-nucleon scattering data which considered in particular the $\omega_\mu N$ and $\rho_\mu N$ channels [99, 100]. The s-wave $N(1535)$ and $N(1650)$ as well as the d-wave $N(1520)$ resonance were generated successfully by coupled channel effects. A similar chain of arguments may be applied for the remaining multiplets. For instance, the p-wave $N(1440)$ resonance studied in great detail by the Jülich group [134], was claimed to be of dynamic origin too. If that were true we would expect that the remaining 55 states of that **56**-plet [123, 124], more precisely the subset of states which exists, would also be of dynamic origin. Based on these observations it is tempting to conjecture that in fact all excited baryon resonance states, i.e. baryon states which do not belong to the baryon octet and decuplet states, are a consequence of coupled channel dynamics³.

There are two further interesting aspects we wish to discuss in connection with the conjecture formulated above. First we would like to comment on the possible parity doubling of resonance states with large mass and second on the Regge trajectory phenomena commonly used as a strong argument in favor of the quark-model [135, 136]. As was pointed out by Cohen and Glozman in recent papers [137, 138], the QCD operator product expansion [139] suggests that correlation functions of opposite parity should behave identically at high energies. Asymptotically the non-perturbative structure is caused by gluon dynamics which does not break the chiral symmetry. Therefore, if the operator product expansion is valid at energies where there are still resonance states visible, at least the high-energy tail thereof, one should conclude that high-mass baryon resonances must occur in parity doublets. Cohen and Glozman argue that indeed the known high mass baryon resonance states confirm this behavior. Though it is certainly premature to draw definite conclusion, if this is true it would pose a severe challenge to the quark-model picture [140]. Though by fine-tuning the quark model parameters one may obtain the approximate degeneracy of some states of opposite parity, it appears impossible to achieve this property for the infinite tower of states typical predicted by any quark model [140]. On the other hand in the coupled channel picture of resonance states this property can be im-

²Of course one may argue that the $\Lambda(1405)$ is not part of the **70**-plet. However, we find that point of view not very convincing since that would further increase the number of the so-called 'missing' resonance states.

³This conjecture would imply that a similar mechanism should explain excited meson resonances. These states would then be generated dynamically in terms of the large- N_c ground states, the pseudoscalar, the vector and axial-vector mesons, $\pi, \rho_\mu, \omega_\mu, a_\mu$ etc.

plemented very easily by an appropriate constraint on the scattering kernel. It is evident that if the scattering kernel in channels of opposite parity is degenerate at high energies the same would hold for resonances generated in those channels. In fact that constraint would naturally lead to a significant parameter reduction, a welcome effect. We turn to the discussion of the baryon Regge trajectories. A quark model with a linearly rising inter-quark potential can easily reproduce the empirical linear Regge trajectory behavior of the baryon resonance states [141]. How can this be achieved in the competing picture of resonance states? This is a serious challenge for the coupled channel mechanism which may ultimately favor the quark-model picture for highly excited resonances. Common wisdom is that a simple t-channel exchange driving the scattering kernel of a single channel problem can not produce a linear Regge trajectory [141]. However, we would conjecture that this may change once more channels are considered. In this respect it is encouraging that Diakonov and Petrov found a linear Regge trajectory for baryon resonances in the Skyrme model [142]. Even though we do not want to advocate this model to be realistic for baryon resonances it demonstrates that if sufficiently many inelastic channels, in case of the Skyrme model multiple pion emissions of a rotating chiral soliton, are considered one may have a chance to reproduce an approximatively linear Regge trajectory. It would be important to investigate this issue in more detail.

It is clear that in any case the rigorous study of baryon resonances requires extensive coupled channel calculations. On the one hand it is desirable to couple the bare three-quark states of the quark-model to the meson-baryon final states [122] in order to arrive at a more realistic description of the baryon resonances. Such calculation are similar in spirit to coupled channel analyses within generalized isobar models [110, 111, 112, 113, 114] where preformed baryon resonance states are part of the meson-baryon scattering kernel. On the other hand it is also useful to explore how far the competing picture where baryon resonances are generated dynamically can be carried [99, 100]. In this context it is illuminating to review a particular aspect of coupled channel analyses. Most generalized isobar model calculations so far employ the K-matrix approximation or extensions thereof [112, 113, 110]. There is a conceptual drawback of such computations. It is not guaranteed that the resulting scattering amplitudes satisfy dispersion-integral relations predicted by the micro causality property of quantum field theory. Analyticity is a fundamental property of the S-matrix and the analytic structure of the scattering amplitude plays an important role e.g. close to thresholds (see e.g. [143]). It is to be emphasized that this argument is not necessarily a valid objection against such calculations. By fitting the data set a particular model may satisfy the analyticity constraint approximatively. However, it would be useful to study this problem in detail and demonstrate to what extent the resulting amplitudes are consistent with their expected analyticity structure. A further property of the K-matrix approximation is the fact that it suppresses potentially large resonance mass shifts [134, 100]. Therefore the study of the question whether a given resonance is primarily a three-quark bound state or mainly a result of coupled channel dynamics should preferably be done in a framework that does not inherently suppress the formation of resonances. Such schemes have been developed [105, 106, 114, 99, 67, 100]. The question as to what is the nature of baryon resonances may be answered by a detailed coupled channel study where the bare resonance mass parameters and bare resonance coupling constants are considered as free parameters adjusted to the data set [134, 106]. Of course the model should be general enough as to avoid any bias of the analysis. If a given resonance is of dynamic origin one would expect that the result of such a fit would give either an extremely large bare resonance mass parameter or almost zero bare resonance coupling constants. It may well be that such an analysis will reveal some type of mixed sce-

nario. Even though it would be preferable to perform such analyses for all resonances separately, a tremendous challenge, it may be advantageous to allow for some minimal bias from large- N_c QCD. As discussed in some detail above, if for a given member of a large- N_c multiplet there are convincing analyses demonstrating that this resonance is of dynamic origin it is quite natural to 'give up' that multiplet and attempt a dynamic coupled channel interpretation also of the remaining so far observed states.

In this work the resonance physics is not the main theme. Rather the goal is to improve and better understand the chiral coupled channel approach elevating it onto more rigorous grounds and at the same time extending its applicability domain. Once the parameters of the chiral coupled channel approach are fixed by a fit to the low-energy data we will, however, investigate whether the scheme shows precursor effects of some baryon resonances at the edge of its applicability domain. If that is the case we take this as a hint or confirmation that those resonances may be of dynamic origin. The above discussion on the nature of baryon resonances was necessary since along the developments we will encounter various baryon resonances. Therefore it is quite useful to have a reasonable working hypothesis available that will guide us through the dark and dense forest of technical and physical difficulties towards the sunny glade of a profound understanding of hadronic interactions.

2.2 Relativistic chiral $SU(3)$ interaction terms in large- N_c QCD

In the following sections we present all chiral interaction terms to be used in the remaining chapters to describe the low-energy meson-baryon scattering data set. Particular emphasis is put on the constraints implied by the large- N_c analysis of QCD. The reader should not be discouraged by the many fundamental parameters introduced in this chapter. The empirical data set includes many hundreds of data points and will be reproduced rather accurately. Our scheme makes many predictions for poorly known or not known observable quantities like for example the p-wave scattering volumes of the kaon-nucleon scattering processes or the $SU(3)$ reactions like $\pi\Lambda \rightarrow \pi\Sigma$. In a more conventional meson-exchange approach, which lacks a systematic approximation scheme, many parameters are implicit in the so-called form factors. In a certain sense the parameters used in the form factors reflect the more systematically constructed and controlled quasi-local counter terms of the chiral Lagrangian.

We recall the interaction terms of the relativistic chiral $SU(3)$ Lagrangian density relevant for the meson-baryon scattering process. For details on the systematic construction principle see for example [60]. The basic building blocks of the chiral Lagrangian are

$$U_\mu = \frac{1}{2} e^{-i\frac{\Phi}{2f}} \left(\partial_\mu e^{i\frac{\Phi}{f}} + i \left[A_\mu, e^{i\frac{\Phi}{f}} \right]_+ \right) e^{-i\frac{\Phi}{2f}}, \quad B, \quad \Delta_\mu, \quad B_\mu^*, \quad (2.1)$$

where we include the pseudo-scalar meson octet field $\Phi(J^P=0^-)$, the baryon octet field $B(J^P=\frac{1}{2}^+)$, the baryon decuplet field $\Delta_\mu(J^P=\frac{3}{2}^+)$ and the baryon nonet resonance field $B_\mu^*(J^P=\frac{3}{2}^-)$ (see [144, 145, 146]).

In (2.1) we consider an external axial-vector source function A_μ which is required for the systematic evaluation of matrix elements of the axial-vector current. A corresponding term for the vector current is not shown in (2.1) because it will not be needed in this work. The axial-vector source function $A^\mu = \sum A_a^\mu \lambda^{(a)}$, the meson octet field $\Phi = \sum \Phi_a \lambda^{(a)}$ and the baryon

octet fields $B = \sum B_a \lambda^{(a)}/\sqrt{2}$, $B_\mu^* = B_{\mu,0}^*/\sqrt{3} + \sum B_{\mu,a}^* \lambda^{(a)}/\sqrt{2}$ are decomposed using the Gell-Mann matrices λ_a normalized by $\text{tr} \lambda_a \lambda_b = 2 \delta_{ab}$. The baryon decuplet field Δ^{abc} is completely symmetric and related to the physical states by

$$\begin{aligned} \Delta^{111} &= \Delta^{++}, & \Delta^{113} &= \Sigma^+/\sqrt{3}, & \Delta^{133} &= \Xi^0/\sqrt{3}, & \Delta^{333} &= \Omega^-, \\ \Delta^{112} &= \Delta^+/\sqrt{3}, & \Delta^{123} &= \Sigma^0/\sqrt{6}, & \Delta^{233} &= \Xi^-/\sqrt{3}, \\ \Delta^{122} &= \Delta^0/\sqrt{3}, & \Delta^{223} &= \Sigma^-/\sqrt{3}, \\ \Delta^{222} &= \Delta^-. \end{aligned} \quad (2.2)$$

The parameter f in (2.1) is determined by the weak decay widths of the charged pions and kaons properly corrected for chiral $SU(3)$ effects. Taking the average of the empirical decay parameters $f_\pi = 92.42 \pm 0.33$ MeV and $f_K \simeq 113.0 \pm 1.3$ MeV [147] one obtains the naive estimate $f \simeq 104$ MeV. This value is still within reach of the more detailed analysis [61] which lead to $f_\pi/f = 1.07 \pm 0.12$. As was emphasized in [148], the precise value of f is subject to large uncertainties.

Explicit chiral symmetry-breaking effects are included in terms of scalar and pseudo-scalar source fields χ_\pm proportional to the quark-mass matrix of QCD,

$$\chi_\pm = \frac{1}{2} \left(e^{+i \frac{\Phi}{2f}} \chi_0 e^{+i \frac{\Phi}{2f}} \pm e^{-i \frac{\Phi}{2f}} \chi_0 e^{-i \frac{\Phi}{2f}} \right), \quad (2.3)$$

where $\chi_0 \sim \text{diag}(m_u, m_d, m_s)$. All fields in (2.1) and (2.3) have identical properties under chiral $SU(3)$ transformations. The chiral Lagrangian consists of all possible interaction terms, formed with the fields $U_\mu, B, \Delta_\mu, B_\mu^*$ and χ_\pm and their respective covariant derivatives. Derivatives of the fields must be included in compliance with the chiral $SU(3)$ symmetry. This leads to the notion of a covariant derivative \mathcal{D}_μ which is identical for all fields in (2.1) and (2.3). For example, it acts on the baryon octet fields as

$$\begin{aligned} [\mathcal{D}_\mu, B]_- &= \partial_\mu B + \frac{1}{2} \left[e^{-i \frac{\Phi}{2f}} \left(\partial_\mu e^{+i \frac{\Phi}{2f}} \right) + e^{+i \frac{\Phi}{2f}} \left(\partial_\mu e^{-i \frac{\Phi}{2f}} \right), B \right]_- \\ &+ \frac{i}{2} \left[e^{-i \frac{\Phi}{2f}} A_\mu e^{+i \frac{\Phi}{2f}} - e^{+i \frac{\Phi}{2f}} A_\mu e^{-i \frac{\Phi}{2f}}, B \right]_-. \end{aligned} \quad (2.4)$$

The chiral Lagrangian is a powerful tool once it is combined with appropriate power counting rules leading to a systematic approximation strategy. One aims at describing hadronic interactions at low energy by constructing an expansion in small momenta and the small pseudo-scalar meson masses. The infinite set of Feynman diagrams are sorted according to their chiral powers. The minimal chiral power Q^ν of a given relativistic Feynman diagram,

$$\nu = 2 - \frac{1}{2} E_B + 2L + \sum_i V_i \left(d_i + \frac{1}{2} n_i - 2 \right), \quad (2.5)$$

is given in terms of the number of loops, L , the number, V_i , of vertices of type i with d_i 'small' derivatives and n_i baryon fields involved, and the number of external baryon lines E_B [64]. Here one calls a derivative small if it acts on the pseudo-scalar meson field or if it probes the virtuality of a baryon field. Explicit chiral symmetry-breaking effects are perturbative and included in the counting scheme with $\chi_0 \sim Q^2$. For a discussion of the relativistic chiral Lagrangian and its required systematic regrouping of interaction terms we refer to [90]. We will encounter explicit examples of this regrouping subsequently. The relativistic chiral Lagrangian requires a non-standard renormalization scheme. The MS or \overline{MS} minimal subtraction schemes of dimensional

regularization do not comply with the chiral counting rule [55]. However, an appropriately modified subtraction scheme for relativistic Feynman diagrams leads to manifest chiral counting rules [89, 90, 91]. Alternatively one may work with the chiral Lagrangian in its heavy-fermion representation [149] where an appropriate frame-dependent redefinition of the baryon fields leads to a more immediate manifestation of the chiral power counting rule (2.5). We will return to this issue in chapter 3.1 where we propose a simple modification of the \overline{MS} -scheme which leads to consistency with (2.5). Further subtleties of the chiral power counting rule (2.5) caused by the inclusion of an explicit baryon resonance field B_μ^* are addressed in chapter 4.1 when discussing the u-channel resonance exchange contributions.

In the πN sector the $SU(2)$ chiral Lagrangian was successfully applied [55, 56] demonstrating good convergence properties of the perturbative chiral expansion. In the $SU(3)$ sector the situation is more involved due in part to the rather large kaon mass $m_K \simeq m_N/2$. The perturbative evaluation of the chiral Lagrangian cannot be justified and one must change the expansion strategy. Rather than expanding directly the scattering amplitude one may expand the interaction kernel according to chiral power counting rules [64, 150]. The scattering amplitude then follows from the solution of a scattering equation like the Lipmann-Schwinger or the Bethe-Salpeter equation. This is analogous to the treatment of the $e^+ e^-$ bound-state problem of QED where a perturbative evaluation of the interaction kernel can be justified. The rationale behind this change of scheme lies in the observation that reducible diagrams are typically enhanced close to their unitarity threshold. The enhancement factor $(2\pi)^n$, measured relative to a reducible diagram with the same number of independent loop integrations, is given by the number, n , of reducible meson-baryon pairs in the diagram, i.e. the number of unitary iterations implicit in the diagram. In the πN sector this enhancement factor does not prohibit a perturbative treatment, because the typical expansion parameter of

$$\frac{m_\pi^2}{8\pi f^2} \simeq 0.1, \quad (2.6)$$

remains sufficiently small. In the $\bar{K}N$ sector, on the other hand, the factor $(2\pi)^n$ invalidates a perturbative treatment, because the typical expansion parameter would be

$$\frac{m_K^2}{8\pi f^2} \simeq 1. \quad (2.7)$$

This is in contrast to irreducible diagrams. They yield the typical expansion parameters

$$\frac{m_\pi}{4\pi f}, \quad \frac{m_K}{4\pi f}, \quad (2.8)$$

which justifies the perturbative evaluation of the scattering kernels. This issue will be taken up again later when exemplifying the enhancement factor (2π) in terms of the Weinberg-Tomozawa interaction term.

In the next chapter a formalism will be developed which defines how to construct the interaction kernel to be used in an 'on-shell reduced' Bethe-Salpeter equation. In the remainder of this chapter all interaction terms are collected that will be required for the construction of the leading orders interaction kernel. All terms of chiral order Q^2 but only the subset of chiral Q^3 -terms, those which are leading in the large- N_c limit, will be considered. Loop corrections to the Bethe-Salpeter kernel are neglected, because they carry minimal chiral order Q^3 and are $1/N_c$ suppressed. The chiral Lagrangian

$$\mathcal{L} = \sum_n \mathcal{L}^{(n)} + \sum_n \mathcal{L}_X^{(n)} \quad (2.9)$$

can be decomposed into terms of different classes $\mathcal{L}^{(n)}$ and $\mathcal{L}_\chi^{(n)}$. With an upper index n in $\mathcal{L}^{(n)}$ we indicate the number of fields in the interaction vertex. The lower index χ signals terms with explicit chiral symmetry breaking. Charge conjugation symmetry and parity invariance is assumed here. At leading chiral order the following interaction terms are required:

$$\begin{aligned}
\mathcal{L}^{(2)} &= \text{tr} \bar{B} \left(i \not{\partial} - \overset{\circ}{m}_{[8]} \right) B + \frac{1}{4} \text{tr} (\partial^\mu \Phi) (\partial_\mu \Phi) \\
&+ \text{tr} \bar{\Delta}_\mu \cdot \left(\left(i \not{\partial} - \overset{\circ}{m}_{[10]} \right) g^{\mu\nu} - i (\gamma^\mu \partial^\nu + \gamma^\nu \partial^\mu) + i \gamma^\mu \not{\partial} \gamma^\nu + \overset{\circ}{m}_{[10]} \gamma^\mu \gamma^\nu \right) \Delta_\nu \\
&+ \text{tr} \bar{B}_\mu^* \cdot \left(\left(i \not{\partial} - \overset{\circ}{m}_{[9]} \right) g^{\mu\nu} - i (\gamma^\mu \partial^\nu + \gamma^\nu \partial^\mu) + i \gamma^\mu \not{\partial} \gamma^\nu + \overset{\circ}{m}_{[9]} \gamma^\mu \gamma^\nu \right) B_\nu^* \\
\mathcal{L}^{(3)} &= \frac{F_{[8]}}{2f} \text{tr} \bar{B} \gamma_5 \gamma^\mu \left[(\partial_\mu \Phi), B \right]_- + \frac{D_{[8]}}{2f} \text{tr} \bar{B} \gamma_5 \gamma^\mu \left[(\partial_\mu \Phi), B \right]_+ \\
&- \frac{C_{[10]}}{2f} \text{tr} \left\{ \left(\bar{\Delta}_\mu \cdot (\partial_\nu \Phi) \right) \left(g^{\mu\nu} - \frac{1}{2} Z_{[10]} \gamma^\mu \gamma^\nu \right) B + \text{h.c.} \right\} \\
&+ \frac{D_{[9]}}{2f} \text{tr} \left\{ \bar{B}_\mu^* \cdot \left[(\partial_\nu \Phi) \left(g^{\mu\nu} - \frac{1}{2} Z_{[9]} \gamma^\mu \gamma^\nu \right) \gamma_5, B \right]_+ + \text{h.c.} \right\} \\
&+ \frac{F_{[9]}}{2f} \text{tr} \left\{ \bar{B}_\mu^* \cdot \left[(\partial_\nu \Phi) \left(g^{\mu\nu} - \frac{1}{2} Z_{[9]} \gamma^\mu \gamma^\nu \right) \gamma_5, B \right]_- + \text{h.c.} \right\} \\
&+ \frac{C_{[9]}}{8f} \text{tr} \left\{ \bar{B}_\mu^* \text{tr} \left[(\partial_\nu \Phi) \left(g^{\mu\nu} - \frac{1}{2} Z_{[9]} \gamma^\mu \gamma^\nu \right) \gamma_5, B \right]_+ + \text{h.c.} \right\}, \\
\mathcal{L}^{(4)} &= \frac{i}{8f^2} \text{tr} \bar{B} \gamma^\mu \left[\left[\Phi, (\partial_\mu \Phi) \right]_-, B \right]_-, \tag{2.10}
\end{aligned}$$

where we use the notations $[A, B]_\pm = AB \pm BA$ for $SU(3)$ matrices A and B . Note that the complete chiral interaction terms which lead to the terms in (2.10) are easily recovered by replacing $i \partial_\mu \Phi / f \rightarrow U_\mu$. A derivative acting on a baryon field in (2.10) must be understood as a covariant derivative with $\partial_\mu B \rightarrow [\mathcal{D}_\mu, B]_-$ and $\partial_\mu \Delta_\nu \rightarrow [\mathcal{D}_\mu, \Delta_\nu]_-$. The $SU(3)$ meson and baryon fields are written in terms of their isospin symmetric components

$$\begin{aligned}
\Phi &= \tau \cdot \pi + \alpha^\dagger \cdot K + K^\dagger \cdot \alpha + \eta \lambda_8, \\
\sqrt{2} B &= \alpha^\dagger \cdot N(939) + \lambda_8 \Lambda(1115) + \tau \cdot \Sigma(1195) + \Xi^t(1315) i \sigma_2 \cdot \alpha, \\
\alpha^\dagger &= \frac{1}{\sqrt{2}} (\lambda_4 + i \lambda_5, \lambda_6 + i \lambda_7), \quad \tau = (\lambda_1, \lambda_2, \lambda_3), \tag{2.11}
\end{aligned}$$

with the isospin doublet fields $K = (K^+, K^0)^t$, $N = (p, n)^t$ and $\Xi = (\Xi^0, \Xi^-)^t$. The isospin Pauli matrix σ_2 acts exclusively in the space of isospin doublet fields (K, N, Ξ) and the matrix valued isospin doublet α (see [97]). For this work we chose the isospin basis, because isospin breaking effects are important only in the $\bar{K}N$ channel. Note that in (2.11) the numbers in the parentheses indicate the approximate mass of the baryon octet fields and $(\dots)^t$ means matrix transposition. Analogously we write the baryon resonance field B_μ^* as

$$\begin{aligned}
\sqrt{2} B_\mu^* &= \left(\sqrt{\frac{2}{3}} \cos \vartheta - \lambda_8 \sin \vartheta \right) \Lambda_\mu(1520) + \alpha^\dagger \cdot N_\mu(1520) \\
&+ \left(\sqrt{\frac{2}{3}} \sin \vartheta + \lambda_8 \cos \vartheta \right) \Lambda_\mu(1690) + \tau \cdot \Sigma_\mu(1670) + \Xi_\mu^t(1820) i \sigma_2 \cdot \alpha, \tag{2.12}
\end{aligned}$$

where we allow for singlet-octet mixing by means of the mixing angle ϑ (see [146]). The parameters $\overset{\circ}{m}_{[8]}$, $\overset{\circ}{m}_{[9]}$ and $\overset{\circ}{m}_{[10]}$ in (2.10) denote the baryon masses in the chiral $SU(3)$ limit.

Furthermore the products of an anti-decuplet field $\bar{\Delta}$ with a decuplet field Δ and an octet field Φ transform as $SU(3)$ octets

$$\begin{aligned} (\bar{\Delta} \cdot \Delta)_b^a &= \bar{\Delta}_{bcd} \Delta^{acd}, & (\bar{\Delta} \cdot \Phi)_b^a &= \epsilon^{kla} \bar{\Delta}_{knb} \Phi_l^n, \\ (\Phi \cdot \Delta)_b^a &= \epsilon_{klb} \Phi_n^l \Delta^{kna}, \end{aligned} \quad (2.13)$$

where ϵ_{abc} is the completely anti-symmetric pseudo-tensor. For the isospin decomposition of $\bar{\Delta} \cdot \Delta$, $\bar{\Delta} \cdot \Phi$ and $\Phi \cdot \Delta$ we refer to [97].

The parameters $F_{[8]} \simeq 0.45$ and $D_{[8]} \simeq 0.80$ are constrained by the weak decay widths of the baryon octet states [151] (see also Tab. 2.1) and $C_{[10]} \simeq 1.6$ can be estimated from the hadronic decay width of the baryon decuplet states. The parameter $Z_{[10]}$ in (2.10) may be best determined in an $SU(3)$ analysis of meson-baryon scattering. While in the pion-nucleon sector it can be absorbed into the quasi-local 4-point interaction terms to chiral accuracy Q^2 [152] (see also [97]) this is no longer possible if the scheme is extended to $SU(3)$. Our detailed analysis reveals that the parameter $Z_{[10]}$ is relevant already to order Q^2 if a simultaneous chiral analysis of the pion-nucleon and kaon-nucleon scattering processes is performed. The resonance parameters may be estimated by an update of the analysis [146]. That leads to the values

$$F_{[9]} \simeq 1.8, \quad D_{[9]} \simeq 0.84, \quad C_{[9]} \simeq 2.5. \quad (2.14)$$

The singlet-octet mixing angle $\vartheta \simeq 28^\circ$ confirms the finding of [145] that the $\Lambda(1520)$ resonance is predominantly a flavor singlet state. The value for the background parameter $Z_{[9]}$ of the $J^P = \frac{3}{2}^-$ resonance is expected to be rather model dependent, because it is unclear so far how to incorporate the $J^P = \frac{3}{2}^-$ resonance in a controlled approximation scheme. As will be explained in detail $Z_{[9]}$ will drop out completely in our scheme (see chapters 4.1-4.2).

The empirical values of $F_{[8]}$, $D_{[8]}$ and $C_{[10]}$ are consistent with the expectation from large- N_c counting rules which predict for example $C_{[10]}/D_{[8]} = 2 + \mathcal{O}(1/N_c)$ [153]. The large- N_c scaling of a chiral interaction term is easily worked out applying the operator analysis proposed in [154]. Interaction terms involving baryon fields are represented by matrix elements of many-body operators in the large- N_c ground-state baryon multiplet $|\mathcal{B}\rangle$. A n-body operator is the product of n factors formed exclusively in terms of the bilinear quark-field operators J_i , $G_i^{(a)}$ and $T^{(a)}$. These operators are characterized fully by their commutation relations,

$$\begin{aligned} [G_i^{(a)}, G_j^{(b)}]_- &= \frac{1}{4} i \delta_{ij} f_c^{ab} T^{(c)} + \frac{1}{2} i \epsilon_{ij}^k \left(\frac{1}{3} \delta^{ab} J_k + d_c^{ab} G_k^{(c)} \right), \\ [J_i, J_j]_- &= i \epsilon_{ij}^k J_k, \quad [T^{(a)}, T^{(b)}]_- = i f_c^{ab} T^{(c)}, \\ [T^{(a)}, G_i^{(b)}]_- &= i f_c^{ab} G_i^{(c)}, \quad [J_i, G_j^{(a)}]_- = i \epsilon_{ij}^k G_k^{(a)}, \quad [J_i, T^{(a)}]_- = 0. \end{aligned} \quad (2.15)$$

The algebra (2.15), which reflects the so-called contracted spin-flavor symmetry of QCD, leads to a transparent derivation of the many sum rules implied by the various infinite subclasses of QCD quark-gluon diagrams as collected to a given order in the $1/N_c$ expansion. A convenient realization of the algebra (2.15) is obtained in terms of non-relativistic, flavor-triplet and color N_c -multiplet field operators q and q^\dagger as

$$\begin{aligned} J_i &= q^\dagger \left(\frac{\sigma_i^{(q)}}{2} \otimes 1 \right) q, & T^{(a)} &= q^\dagger \left(1 \otimes \frac{\lambda^{(a)}}{2} \right) q, \\ G_i^{(a)} &= q^\dagger \left(\frac{\sigma_i^{(q)}}{2} \otimes \frac{\lambda^{(a)}}{2} \right) q. \end{aligned} \quad (2.16)$$

If the fermionic field operators q and q^\dagger are assigned anti-commutation rules the algebra (2.15) follows. The Pauli spin matrices $\sigma_i^{(q)}$ act on the two-component spinors of the fermion fields q, q^\dagger and the Gell-Mann matrices λ_a on their flavor components. Here one needs to emphasize that the non-relativistic quark-field operators q and q^\dagger should not be identified with the quark-field operators of the QCD Lagrangian [93, 94, 95]. Rather, they constitute an effective tool to represent the operator algebra (2.15) which allows for an efficient derivation of the large- N_c sum rules of QCD. A systematic truncation scheme results in the operator analysis, because a n -body operator is assigned the suppression factor N_c^{1-n} [88]. The analysis is complicated by the fact that matrix elements of $T^{(a)}$ and $G_i^{(a)}$ may be of order N_c in the baryon ground state $|\mathcal{B}\rangle$. That implies for instance that matrix elements of the $(2n+1)$ -body operator $(T_a T^{(a)})^n T^{(c)}$ are not suppressed relative to the matrix elements of the one-body operator $T^{(c)}$. The systematic large- N_c operator analysis relies on the observation that matrix elements of the spin operator J_i , on the other hand, are always of order N_c^0 . Then a set of identities shows how to systematically represent the infinite set of many-body operators, which one may write down to a given order in the $1/N_c$ expansion, in terms of a finite number of operators. This leads to a convenient scheme with only a finite number of operators at given order [154]. Typical examples of the required operator identities read

$$\begin{aligned}
[T_a, T^{(a)}]_+ - [J_i, J^{(i)}]_+ &= \frac{1}{6} N_c (N_c + 6), \quad [T_a, G_i^{(a)}]_+ = \frac{2}{3} (3 + N_c) J_i, \\
27 [T_a, T^{(a)}]_+ - 12 [G_i^{(a)}, G_a^{(i)}]_+ &= 32 [J_i, J^{(i)}]_+, \\
d_{abc} [T^{(a)}, T^{(b)}]_+ - 2 [J_i, G_c^{(i)}]_+ &= -\frac{1}{3} (N_c + 3) T_c, \\
d_{bc}^a [G_a^{(i)}, G_i^{(b)}]_+ + \frac{9}{4} d_{abc} [T^{(a)}, T^{(b)}]_+ &= \frac{10}{3} [J_i, G_c^{(i)}]_+, \\
d_{ab}^c [T^{(a)}, G_i^{(b)}]_+ = \frac{1}{3} [J_i, T^{(c)}]_+ - \frac{1}{3} \epsilon_{ijk} f_{ab}^c [G_a^{(j)}, G_b^{(k)}]_+. &
\end{aligned} \tag{2.17}$$

For instance the first identity in (2.17) shows how to avoid that infinite tower $(T_a T^{(a)})^n T^{(c)}$ discussed above. Note that the 'parameter' N_c enters in (2.17) as a mean to classify the possible realizations of the algebra (2.15).

As a first and simple example recall the large- N_c structure of the 3-point vertices. One readily establishes two operators with parameters g and h at leading order in the $1/N_c$ expansion [154]:

$$\langle \mathcal{B}' | \mathcal{L}^{(3)} | \mathcal{B} \rangle = \frac{1}{f} \langle \mathcal{B}' | g G_i^{(c)} + h J_i T^{(c)} | \mathcal{B} \rangle \text{tr} \lambda_c \nabla^{(i)} \Phi + \mathcal{O} \left(\frac{1}{N_c} \right). \tag{2.18}$$

Further possible terms in (2.18) are either redundant or suppressed in the $1/N_c$ expansion. For example, the two-body operator $i f_{abc} G_i^{(a)} T^{(b)} \sim N_c^0$ is reduced by applying the relation

$$i f_{ab}^c [G_i^{(a)}, T^{(b)}]_- = i f_{ab}^c i f^{ab}_d G_i^{(d)} = -3 G_i^{(c)}.$$

In order to make use of the large- N_c result it is necessary to evaluate the matrix elements in (2.18) at $N_c = 3$ where one has a **56**-plet with $|\mathcal{B}\rangle = |B(a), \Delta(ijk)\rangle$. Most economically this is achieved with the completeness identity $1 = |B\rangle\langle B| + |\Delta\rangle\langle \Delta|$ in conjunction with

$$\begin{aligned}
T_c |B_a(\chi)\rangle &= i f_{abc} |B^{(b)}(\chi)\rangle, \quad J^{(i)} |B_a(\chi)\rangle = \frac{1}{2} \sigma_{\chi'\chi}^{(i)} |B_a(\chi')\rangle, \\
G_c^{(i)} |B_a(\chi)\rangle &= \left(\frac{1}{2} d_{abc} + \frac{1}{3} i f_{abc} \right) \sigma_{\chi'\chi}^{(i)} |B^{(b)}(\chi')\rangle \\
&\quad + \frac{1}{\sqrt{2} 2} \left(\epsilon_l^{jk} \lambda_{mj}^{(c)} \lambda_{nk}^{(a)} \right) S_{\chi'\chi}^{(i)} |\Delta^{(lmn)}(\chi')\rangle,
\end{aligned} \tag{2.19}$$

where $S_i S_j^\dagger = \delta_{ij} - \sigma_i \sigma_j / 3$ and $\lambda_a \lambda_b = \frac{2}{3} \delta_{ab} + (i f_{abc} + d_{abc}) \lambda^{(c)}$. In (2.19) the baryon octet states $|B_b(\chi)\rangle$ are labelled according to their $SU(3)$ octet index $a = 1, \dots, 8$ with the two spin states represented by $\chi = 1, 2$. Similarly the decuplet states $|\Delta_{lmn}(\chi')\rangle$ are listed with $l, m, n = 1, 2, 3$ as defined in (2.2). Note that the expressions (2.19) may be verified using the quark-model wave functions for the baryon octet and decuplet states. The result (2.19) is however much more general than the quark-model, because it follows from the structure of the ground-state baryons in the large- N_c limit of QCD only. Matching the interaction vertices of the relativistic chiral Lagrangian onto the static matrix elements arising in the large- N_c operator analysis requires a non-relativistic reduction. It is standard to decompose the 4-component Dirac fields B and Δ_μ into baryon octet and decuplet spinor fields $B(\chi)$ and $\Delta(\chi)$:

$$(B, \Delta_\mu) \rightarrow \begin{pmatrix} \left(\frac{1}{2} + \frac{1}{2} \sqrt{1 + \frac{\nabla^2}{M^2}} \right)^{\frac{1}{2}} (B(\chi), S_\mu \Delta(\chi)) \\ \frac{(\sigma \cdot \nabla)}{\sqrt{2} M} \left(1 + \sqrt{1 + \frac{\nabla^2}{M^2}} \right)^{-\frac{1}{2}} (B(\chi), S_\mu \Delta(\chi)) \end{pmatrix}, \quad (2.20)$$

where M denotes the baryon octet and decuplet mass in the large- N_c limit. At leading order one finds $S_\mu = (0, S_i)$ with the transition matrices S_i introduced in (2.19). It is then straightforward to expand in powers of ∇/M and achieve the desired matching. This leads for example to the identification $D_{[8]} = g$, $F_{[8]} = 2g/3 + h$ and $C_{[10]} = 2g$. Operators at subleading order in (2.18) then parameterize the deviation from $C_{[10]} \simeq 2D_{[8]}$.

2.3 Quasi-local interaction terms

Consider the two-body interaction terms to chiral order Q^2 . From phase space consideration it is evident that at this order there are only terms which contribute to the meson-baryon s-wave scattering lengths, the s-wave effective range parameters and the p-wave scattering volumes. Higher partial waves are not affected at this order. The various contributions are grouped according to their scalar, vector or tensor nature as

$$\mathcal{L}_2^{(4)} = \mathcal{L}^{(S)} + \mathcal{L}^{(V)} + \mathcal{L}^{(T)}, \quad (2.21)$$

where the lower index k in $\mathcal{L}_k^{(n)}$ denotes the minimal chiral order of the interaction vertex. In the relativistic framework one observes mixing of the partial waves in the sense that for instance $\mathcal{L}^{(S)}, \mathcal{L}^{(V)}$ contribute to the s-wave channels and $\mathcal{L}^{(S)}, \mathcal{L}^{(T)}$ to the p-wave channels. We write

$$\begin{aligned} \mathcal{L}^{(S)} &= \frac{g_0^{(S)}}{8f^2} \text{tr} \bar{B} B \text{tr} (\partial_\mu \Phi) (\partial^\mu \Phi) + \frac{g_1^{(S)}}{8f^2} \text{tr} \bar{B} (\partial_\mu \Phi) \text{tr} (\partial^\mu \Phi) B \\ &+ \frac{g_F^{(S)}}{16f^2} \text{tr} \bar{B} \left[[(\partial_\mu \Phi), (\partial^\mu \Phi)]_+, B \right]_- + \frac{g_D^{(S)}}{16f^2} \text{tr} \bar{B} \left[[(\partial_\mu \Phi), (\partial^\mu \Phi)]_+, B \right]_+, \\ \mathcal{L}^{(V)} &= \frac{g_0^{(V)}}{16f^2} \left(\text{tr} \bar{B} i \gamma^\mu (\partial^\nu B) \text{tr} (\partial_\nu \Phi) (\partial_\mu \Phi) + \text{h.c.} \right) \\ &+ \frac{g_1^{(V)}}{32f^2} \text{tr} \bar{B} i \gamma^\mu \left((\partial_\mu \Phi) \text{tr} (\partial_\nu \Phi) (\partial^\nu B) + (\partial_\nu \Phi) \text{tr} (\partial_\mu \Phi) (\partial^\nu B) + \text{h.c.} \right) \end{aligned}$$

$$\begin{aligned}
& + \frac{g_F^{(V)}}{32f^2} \left(\text{tr } \bar{B} i \gamma^\mu \left[[(\partial_\mu \Phi), (\partial_\nu \Phi)]_+, (\partial^\nu B) \right]_- + \text{h.c.} \right) \\
& + \frac{g_D^{(V)}}{32f^2} \left(\text{tr } \bar{B} i \gamma^\mu \left[[(\partial_\mu \Phi), (\partial_\nu \Phi)]_+, (\partial^\nu B) \right]_+ + \text{h.c.} \right), \\
\mathcal{L}^{(T)} & = \frac{g_1^{(T)}}{8f^2} \text{tr } \bar{B} (\partial_\mu \Phi) i \sigma^{\mu\nu} \text{tr } (\partial_\nu \Phi) B \\
& + \frac{g_D^{(T)}}{16f^2} \text{tr } \bar{B} i \sigma^{\mu\nu} \left[[(\partial_\mu \Phi), (\partial_\nu \Phi)]_-, B \right]_+ \\
& + \frac{g_F^{(T)}}{16f^2} \text{tr } \bar{B} i \sigma^{\mu\nu} \left[[(\partial_\mu \Phi), (\partial_\nu \Phi)]_-, B \right]_-. \tag{2.22}
\end{aligned}$$

It is clear that if the heavy-baryon expansion is applied to (2.22) the quasi-local 4-point interactions can be mapped onto corresponding terms of the heavy-baryon formalism presented for example in [155]. Inherent in the relativistic scheme is the presence of redundant interaction terms which requires that a systematic regrouping of the interaction terms is performed. This will be discussed below in more detail when introducing the quasi-local counter terms at chiral order Q^3 .

The large- N_c counting rules are applied in order to estimate the relative importance of the quasi-local Q^2 -terms in (2.22). Terms which involve a single-flavor trace are enhanced as compared to the double-flavor trace terms. This is because a flavor trace in an interaction term is necessarily accompanied by a corresponding color trace if visualized in terms of quark and gluon lines. A color trace signals a quark loop and therefore provides the announced $1/N_c$ suppression factor [87, 88]. The counting rules are nevertheless subtle, because a certain combination of double trace expressions can be rewritten in terms of a single-flavor trace term [156]

$$\begin{aligned}
& \text{tr } (\bar{B} B) \text{tr } (\Phi \Phi) + 2 \text{tr } (\bar{B} \Phi) \text{tr } (\Phi B) \\
= & \text{tr } [\bar{B}, \Phi]_- [B, \Phi]_- + \frac{3}{2} \text{tr } \bar{B} \left[[\Phi, \Phi]_+, B \right]_+. \tag{2.23}
\end{aligned}$$

Thus, one expects for example that both parameters $g_0^{(S)}$ and $g_1^{(S)}$ may be large separately but the combination $2g_0^{(S)} - g_1^{(S)}$ should be small. A more detailed operator analysis leads to

$$\begin{aligned}
\langle \mathcal{B}' | \mathcal{L}_2^{(4)} | \mathcal{B} \rangle & = \frac{1}{16f^2} \langle \mathcal{B}' | O_{ab}(g_1, g_2) | \mathcal{B} \rangle \text{tr } [(\partial_\mu \Phi), \lambda^{(a)}]_- [(\partial^\mu \Phi), \lambda^{(b)}]_- \\
& + \frac{1}{16f^2} \langle \mathcal{B}' | O_{ab}(g_3, g_4) | \mathcal{B} \rangle \text{tr } [(\partial_0 \Phi), \lambda^{(a)}]_- [(\partial_0 \Phi), \lambda^{(b)}]_- \\
& + \frac{1}{16f^2} \langle \mathcal{B}' | O_{ab}^{(ij)}(g_5, g_6) | \mathcal{B} \rangle \text{tr } [(\nabla_i \Phi), \lambda^{(a)}]_- [(\nabla_j \Phi), \lambda^{(b)}]_-, \\
O_{ab}(g, h) & = g d_{abc} T^{(c)} + h [T_a, T_b]_+ + \mathcal{O} \left(\frac{1}{N_c} \right), \\
O_{ab}^{(ij)}(g, h) & = i \epsilon^{ijk} i f_{abc} \left(g G_k^{(c)} + h J_k T^{(c)} \right) + \mathcal{O} \left(\frac{1}{N_c} \right). \tag{2.24}
\end{aligned}$$

It was checked that other forms for the coupling of the operators O_{ab} to the meson fields do not lead to new structures. The matching of the coupling constants $g_{1,\dots,6}$ onto those of (2.22)

is straight forward. Identifying the leading terms in the non-relativistic expansion, we obtain

$$\begin{aligned}
g_0^{(S)} &= \frac{1}{2} g_1^{(S)} = \frac{2}{3} g_D^{(S)} = -2 g_2, & g_F^{(S)} &= -3 g_1, \\
g_0^{(V)} &= \frac{1}{2} g_1^{(V)} = \frac{2}{3} g_D^{(V)} = -2 \frac{g_4}{M}, & g_F^{(V)} &= -3 \frac{g_3}{M}, \\
g_1^{(T)} &= 0, & g_F^{(T)} &= -g_5 - \frac{3}{2} g_6, & g_D^{(T)} &= -\frac{3}{2} g_5,
\end{aligned} \tag{2.25}$$

where M is the large- N_c value of the baryon octet mass. Thus, to chiral order Q^2 there are only six leading large- N_c coupling constants.

Continue with the quasi-local counter terms to chiral order Q^3 . It is useful to discuss first a set of redundant interaction terms:

$$\begin{aligned}
\mathcal{L}^{(R)} &= \frac{h_0^{(1)}}{8f^2} \text{tr}(\partial^\mu \bar{B}) (\partial_\nu B) \text{tr}(\partial_\mu \Phi) (\partial^\nu \Phi) \\
&+ \frac{h_1^{(1)}}{16f^2} \text{tr}(\partial^\mu \bar{B}) (\partial_\nu \Phi) \text{tr}(\partial_\mu \Phi) (\partial^\nu B) \\
&+ \frac{h_1^{(1)}}{16f^2} \text{tr}(\partial^\mu \bar{B}) (\partial_\mu \Phi) \text{tr}(\partial^\nu \Phi) (\partial_\nu B), \\
&+ \frac{h_F^{(1)}}{16f^2} \text{tr}(\partial^\mu \bar{B}) \left[[(\partial_\mu \Phi), (\partial^\nu \Phi)]_+, (\partial_\nu B) \right]_- \\
&+ \frac{h_D^{(1)}}{16f^2} \text{tr}(\partial^\mu \bar{B}) \left[[(\partial_\mu \Phi), (\partial^\nu \Phi)]_+, (\partial_\nu B) \right]_+.
\end{aligned} \tag{2.26}$$

Performing the non-relativistic expansion of (2.26) one finds that the leading moment is of chiral order Q^2 . Formally the terms in (2.26) are transformed into terms of subleading order Q^3 by subtracting $\mathcal{L}^{(V)}$ of (2.22) with $g^{(V)} = \overset{\circ}{m}_{[8]} h^{(1)}$. Bearing this in mind the terms of (2.26) define particular interaction vertices of chiral order Q^3 . Note that by analogy with (2.24) and (2.25) we expect the coupling constants $h_F^{(1)}$ and $h_D^{(1)}$ with $h_1^{(1)} = 2h_0^{(1)} = 4h_D^{(1)}/3$ to be leading in the large- N_c limit. A complete collection of counter terms of chiral order Q^3 is presented in [97]. Including the four terms of (2.26) we find ten independent interaction terms which all contribute exclusively to the s- and p-wave channels. Here the two additional terms with $h_F^{(2)}$ and $h_F^{(3)}$ which are leading in the large- N_c expansion are presented:

$$\begin{aligned}
\mathcal{L}_3^{(4)} &= \mathcal{L}^{(R)} - \mathcal{L}^{(V)} [g^{(V)} = \overset{\circ}{m}_{[8]} h^{(1)}] \\
&+ \frac{h_F^{(2)}}{32f^2} \text{tr} \bar{B} i \gamma^\mu \left[[(\partial_\mu \Phi), (\partial_\nu \Phi)]_-, (\partial^\nu B) \right]_- + \text{h.c.} \\
&+ \frac{h_F^{(3)}}{16f^2} \text{tr} \bar{B} i \gamma^\alpha \left[[(\partial_\alpha \partial_\mu \Phi), (\partial^\mu \Phi)]_-, B \right]_-.
\end{aligned} \tag{2.27}$$

The interaction vertices in (2.27) can be mapped onto corresponding static matrix elements of the large- N_c operator analysis

$$\begin{aligned}
\langle \mathcal{B}' | \mathcal{L}_3^{(4)} | \mathcal{B} \rangle &= \frac{h_2}{16f^2} \langle \mathcal{B}' | i f_{abc} T^{(c)} | \mathcal{B} \rangle \partial_\mu \left(\text{tr} [(\partial_0 \Phi), \lambda^{(a)}]_- [(\partial^\mu \Phi), \lambda^{(b)}]_- \right) \\
&+ \frac{h_3}{16f^2} \langle \mathcal{B}' | i f_{abc} T^{(c)} | \mathcal{B} \rangle \text{tr} [(\partial_0 \partial_\mu \Phi), \lambda^{(a)}]_- [(\partial^\mu \Phi), \lambda^{(b)}]_-,
\end{aligned} \tag{2.28}$$

where $h_F^{(2)} \sim h_2$ and $h_F^{(3)} \sim h_3$. To summarize the result for the quasi-local chiral interaction vertices of order Q^3 : at leading order the $1/N_c$ expansion leads to four relevant parameters $h_{F,D}^{(1)}$ and $h_F^{(2)}$ and $h_F^{(3)}$, only. Also one should stress that the $SU(3)$ structure of the Q^3 terms as they contribute to the s- and p-wave channels differ from the $SU(3)$ structure of the Q^2 terms. For instance the $g^{(S)}$ coupling constants contribute to the p-wave channels with four independent $SU(3)$ tensors. In contrast, to order Q^3 the parameters $h_F^{(2)}$ and $h_F^{(3)}$, which are in fact the only parameters contribution to the p-wave channels to this order, contribute with a different and independent $SU(3)$ tensor. This is to be compared with the static $SU(3)$ prediction that leads to six independent tensors:

$$8 \otimes 8 = 1 \oplus 8_S \oplus 8_A \oplus 10 \oplus \overline{10} \oplus 27. \quad (2.29)$$

Part of the predictive power of the chiral Lagrangian results, because chiral $SU(3)$ symmetry selects certain subsets of all $SU(3)$ symmetric tensors to a given chiral order.

2.4 Explicit chiral symmetry breaking

There remain the interaction terms proportional to χ_{\pm} which break the chiral $SU(3)$ symmetry explicitly. Here all relevant terms of chiral order Q^2 [55, 65] and Q^3 [157] are collected. It is convenient to visualize the symmetry-breaking fields χ_{\pm} of (2.3) in their expanded forms:

$$\chi_+ = \chi_0 - \frac{1}{8f^2} \left[\Phi, \left[\Phi, \chi_0 \right]_+ \right]_+ + \mathcal{O}(\Phi^4), \quad \chi_- = \frac{i}{2f} \left[\Phi, \chi_0 \right]_+ + \mathcal{O}(\Phi^3). \quad (2.30)$$

Begin with the 2-point interaction vertices which all result exclusively from chiral interaction terms linear in χ_+ . They read:

$$\begin{aligned} \mathcal{L}_\chi^{(2)} &= -\frac{1}{4} \text{tr} \Phi \left[\chi_0, \Phi \right]_+ + 2 \text{tr} \bar{B} \left(b_D \left[\chi_0, B \right]_+ + b_F \left[\chi_0, B \right]_- + b_0 B \text{tr} \chi_0 \right) \\ &+ 2 d_D \text{tr} \left(\bar{\Delta}_\mu \cdot \Delta^\mu \right) \chi_0 + 2 d_0 \text{tr} \left(\bar{\Delta}_\mu \cdot \Delta^\mu \right) \text{tr} \chi_0 \\ &+ \text{tr} \bar{B} \left(i \not{\partial} - \overset{\circ}{m}_{[8]} \right) \left(\zeta_0 B \text{tr} \chi_0 + \zeta_D \left[B, \chi_0 \right]_+ + \zeta_F \left[B, \chi_0 \right]_- \right), \\ \chi_0 &= \frac{1}{3} \left(m_\pi^2 + 2 m_K^2 \right) 1 + \frac{2}{\sqrt{3}} \left(m_\pi^2 - m_K^2 \right) \lambda_8, \end{aligned} \quad (2.31)$$

where we normalized χ_0 to give the pseudo-scalar mesons their isospin averaged masses. The first term in (2.31) leads to the finite masses of the pseudo-scalar mesons. Note that at chiral order Q^2 one has $m_\eta^2 = 4(m_K^2 - m_\pi^2)/3$. The parameters b_D , b_F , and d_D are determined at leading order by the baryon octet and decuplet mass splitting

$$\begin{aligned} m_{[8]}^{(\Sigma)} - m_{[8]}^{(\Lambda)} &= \frac{16}{3} b_D (m_K^2 - m_\pi^2), \quad m_{[8]}^{(\Xi)} - m_{[10]}^{(N)} = -8 b_F (m_K^2 - m_\pi^2), \\ m_{[10]}^{(\Sigma)} - m_{[10]}^{(\Delta)} &= m_{[8]}^{(\Xi)} - m_{[10]}^{(\Sigma)} = m_{[10]}^{(\Omega)} - m_{[10]}^{(\Xi)} = -\frac{4}{3} d_D (m_K^2 - m_\pi^2). \end{aligned} \quad (2.32)$$

The empirical baryon masses lead to the estimates $b_D \simeq 0.06 \text{ GeV}^{-1}$, $b_F \simeq -0.21 \text{ GeV}^{-1}$, and $d_D \simeq -0.49 \text{ GeV}^{-1}$. For completeness we recall the leading large- N_c operators for the baryon

mass splitting (see e.g. [153]):

$$\begin{aligned}
\langle \mathcal{B}' | \mathcal{L}_\chi^{(2)} | \mathcal{B} \rangle &= \langle \mathcal{B}' | b_1 T^{(8)} + b_2 [J^{(i)}, G_i^{(8)}]_+ | \mathcal{B} \rangle + \mathcal{O}\left(\frac{1}{N_c^2}\right), \\
b_D &= -\frac{\sqrt{3}}{16} \frac{3b_2}{m_K^2 - m_\pi^2}, \quad b_F = -\frac{\sqrt{3}}{16} \frac{2b_1 + b_2}{m_K^2 - m_\pi^2}, \\
d_D &= -\frac{3\sqrt{3}}{8} \frac{b_1 + 2b_2}{m_K^2 - m_\pi^2},
\end{aligned} \tag{2.33}$$

where we matched the symmetry-breaking parts with λ_8 . One observes that the empirical values for $b_D + b_F$ and d_D are remarkably consistent with the large- N_c sum rule $b_D + b_F \simeq \frac{1}{3} d_D$. The parameters b_0 and d_0 are more difficult to access. They determine the deviation of the octet and decuplet baryon masses from their chiral $SU(3)$ limit values $\hat{m}_{[8]}$ and $\hat{m}_{[10]}$:

$$\begin{aligned}
m_{[8]}^{(N)} &= \hat{m}_{[8]} - 2m_\pi^2(b_0 + 2b_F) - 4m_K^2(b_0 + b_D - b_F), \\
m_{[10]}^{(\Delta)} &= \hat{m}_{[10]} - 2m_\pi^2(d_0 + d_D) - 4m_K^2 d_0,
\end{aligned} \tag{2.34}$$

where terms of chiral order Q^3 are neglected. The size of the parameter b_0 is commonly encoded into the pion-nucleon sigma term

$$\sigma_{\pi N} = -2m_\pi^2(b_D + b_F + 2b_0) + \mathcal{O}(Q^3). \tag{2.35}$$

Note that the former standard value $\sigma_{\pi N} = (45 \pm 8)$ MeV of [158] is currently under debate [159].

The parameters ζ_0, ζ_D and ζ_F are required to cancel a divergent term in the baryon wavefunction renormalization as it follows from the one loop self-energy correction or equivalently the unitarization of the s-channel baryon exchange term. It will be demonstrated explicitly that within our approximation they will not have any observable effect. They lead to a renormalization of the three-point vertices only, which can be accounted for by a redefinition of the parameters in (2.37). Thus, one may simply drop these interaction terms.

The predictive power of the chiral Lagrangian lies in part in the strong correlation of vertices of different degrees as implied by the non-linear fields U_μ and χ_\pm . A powerful example is given by the two-point vertices introduced in (2.31). Since they result from chiral interaction terms linear in the χ_+ -field (see (2.30)), they induce particular meson-octet baryon-octet interaction vertices:

$$\begin{aligned}
\mathcal{L}_\chi^{(4)} &= \frac{i}{16f^2} \text{tr} \bar{B} \gamma^\mu \left[[\Phi, (\partial_\mu \Phi)]_- , \zeta_0 B \text{tr} \chi_0 + \zeta_D [B, \chi_0]_+ + \zeta_F [B, \chi_0]_- \right]_- \\
&+ \frac{i}{16f^2} \text{tr} \left[\zeta_0 \bar{B} \text{tr} \chi_0 + \zeta_D [\bar{B}, \chi_0]_+ + \zeta_F [\bar{B}, \chi_0]_- , [\Phi, (\partial_\mu \Phi)]_- \right]_- \gamma^\mu B \\
&- \frac{1}{4f^2} \text{tr} \bar{B} \left(b_D \left[[\Phi, [\Phi, \chi_0]_+]_+ , B \right]_+ + b_F \left[[\Phi, [\Phi, \chi_0]_+]_+ , B \right]_- \right) \\
&- \frac{b_0}{4f^2} \text{tr} \bar{B} B \text{tr} \left[\Phi, [\Phi, \chi_0]_+ \right]_+ .
\end{aligned} \tag{2.36}$$

To chiral order Q^3 there are no further four-point interaction terms with explicit chiral symmetry breaking.

Next turn to the three-point vertices with explicit chiral symmetry breaking. Here the chiral Lagrangian permits two types of interaction terms written as $\mathcal{L}_\chi^{(3)} = \mathcal{L}_{\chi,+}^{(3)} + \mathcal{L}_{\chi,-}^{(3)}$. In $\mathcal{L}_{\chi,+}^{(3)}$ we

collect 16 axial-vector terms, which result form chiral interaction terms linear in the χ_+ field (see (2.30)), with a priori unknown coupling constants $F_{0,\dots,9}$ and $C_{0,\dots,5}$,

$$\begin{aligned}
\mathcal{L}_{\chi,+}^{(3)} &= \frac{1}{4f} \text{tr} \bar{B} \gamma_5 \gamma^\mu \left([(\partial_\mu \Phi), F_0 [\chi_0, B]_+ + F_1 [\chi_0, B]_-]_+ \right) + \text{h.c.} \\
&+ \frac{1}{4f} \text{tr} \bar{B} \gamma_5 \gamma^\mu \left([(\partial_\mu \Phi), F_2 [\chi_0, B]_+ + F_3 [\chi_0, B]_-]_- \right) + \text{h.c.} \\
&+ \frac{1}{2f} \text{tr} \bar{B} \gamma_5 \gamma^\mu \left(F_4 [[\chi_0, (\partial_\mu \Phi)]_+, B]_+ + F_5 [[\chi_0, (\partial_\mu \Phi)]_+, B]_- \right) \\
&+ \frac{1}{4f} \text{tr} \bar{B} \gamma_5 \gamma^\mu \left(F_6 B \text{tr} (\chi_0 (\partial_\mu \Phi)) + F_7 (\partial_\mu \Phi) \text{tr} (\chi_0 B) \right) + \text{h.c.} \\
&+ \frac{1}{2f} \text{tr} \bar{B} \gamma_5 \gamma^\mu \left(F_8 [(\partial_\mu \Phi), B]_+ \text{tr} \chi_0 + F_9 [(\partial_\mu \Phi), B]_- \text{tr} \chi_0 \right) \\
&- \frac{1}{2f} \text{tr} \left\{ C_0 (\bar{\Delta}_\mu \cdot [\chi_0, (\partial_\mu \Phi)]_+ + C_1 (\bar{\Delta}_\mu \cdot [\chi_0, (\partial_\mu \Phi)]_-) B + \text{h.c.} \right\} \\
&- \frac{1}{2f} \text{tr} \left\{ (\bar{\Delta}_\mu \cdot (\partial_\mu \Phi)) (C_2 [\chi_0, B]_+ + C_3 [\chi_0, B]_- + \text{h.c.}) \right\} \\
&- \frac{C_4}{2f} \text{tr} \left\{ (\bar{\Delta}_\mu \cdot \chi_0) [(\partial_\mu \Phi), B]_- + \text{h.c.} \right\} \\
&- \frac{C_5}{2f} \text{tr} \left\{ (\bar{\Delta}_\mu \cdot (\partial_\mu \Phi)) B + \text{h.c.} \right\} \text{tr} \chi_0 .
\end{aligned} \tag{2.37}$$

Similarly in $\mathcal{L}_{\chi,-}^{(3)}$ the remaining terms which result from chiral interaction terms linear in χ_- are collected. There are three pseudo-scalar interaction terms with $\bar{F}_{4,5,6}$ and four additional terms parameterized by $\delta F_{4,5,6}$ and δC_0

$$\begin{aligned}
\mathcal{L}_{\chi,-}^{(3)} &= \frac{1}{2f} \text{tr} \bar{B} \left[2i \gamma_5 \hat{m}_{[8]} \bar{F}_4 [\chi_0, \Phi]_+ + \gamma_5 \gamma^\mu \delta F_4 [\chi_0, (\partial_\mu \Phi)]_+, B \right]_+ \\
&+ \frac{1}{2f} \text{tr} \bar{B} \left[2i \gamma_5 \hat{m}_{[8]} \bar{F}_5 [\chi_0, \Phi]_+ + \gamma_5 \gamma^\mu \delta F_5 [\chi_0, (\partial_\mu \Phi)]_+, B \right]_- \\
&+ \frac{1}{2f} \text{tr} \bar{B} \left(2i \gamma_5 \hat{m}_{[8]} \bar{F}_6 \text{tr} (\chi_0 \Phi) + \gamma_5 \gamma^\mu \delta F_6 \text{tr} (\chi_0 (\partial_\mu \Phi)) \right) B \\
&- \frac{\delta C_0}{2f} \text{tr} \left(\bar{\Delta}_\mu \cdot [\chi_0, (\partial_\mu \Phi)]_+ B + \text{h.c.} \right) .
\end{aligned} \tag{2.38}$$

While the parameters F_i and C_i contribute to matrix elements of the $SU(3)$ axial-vector current A_a^μ , none of the terms in (2.38) contribute. This follows once the external axial-vector current is restored. In (2.37) this is achieved with the replacement $\partial^\mu \Phi_a \rightarrow \partial^\mu \Phi_a + 2f A_a^\mu$ (see (2.1)). Though it is obvious that the pseudo-scalar terms in (2.38) proportional to \bar{F}_i do not contribute to the axial-vector current, it is less immediate that the terms proportional to δF_i and δC_i also do not contribute. Moreover, the latter terms appear redundant, because terms with identical structure at the 3-point level are already listed in (2.38). Here one needs to realize that the terms proportional to δF_i and δC_i result from chiral interaction terms linear in $[\mathcal{D}_\mu, \chi_-]_-$ while the terms proportional to F_i, C_i result from chiral interaction terms linear in U_μ .

The pseudo-scalar parameters \bar{F}_i and also δF_i lead to a tree-level Goldberger-Treiman discrepancy. For instance, we have

$$f g_{\pi NN} - g_A m_N = 2 m_N m_\pi^2 (\bar{F}_4 + \delta F_4 + \bar{F}_5 + \delta F_5) + \mathcal{O}(Q^3) , \tag{2.39}$$

where we introduced the pion-nucleon coupling constant $g_{\pi NN}$ and the axial-vector coupling constant of the nucleon g_A . The corresponding generalized Goldberger-Treiman discrepancies for the remaining axial-vector coupling constants of the baryon octet states follow easily from the replacement rule $F_i \rightarrow F_i + \bar{F}_i + \delta F_i$ for $i = 4, 5, 6$ (see also [160]). It is to be emphasized that (2.39) must not be confronted directly with the Goldberger-Treiman discrepancy as discussed in [161, 162, 160], because it necessarily involves the $SU(3)$ parameter f rather than $f_\pi \simeq 92$ MeV or $f_K \simeq 113$ MeV.

The effect of the axial-vector interaction terms in (2.37) is twofold. First, they lead to renormalized values of the $F_{[8]}, D_{[8]}$ and $C_{[10]}$ parameters in (2.10). Secondly they induce interesting $SU(3)$ symmetry-breaking effects which are proportional to $(m_K^2 - m_\pi^2) \lambda_8$. Note that the renormalization of the $F_{[8]}, D_{[8]}$ and $C_{[10]}$ parameters requires care, because it is necessary to discriminate between the renormalization of the axial-vector current and the renormalization of the meson-baryon coupling constants. The parameters F_R, D_R and C_R are introduced as they enter matrix elements of the axial-vector current:

$$\begin{aligned} F_R &= F_{[8]} + (m_\pi^2 + 2m_K^2) \left(F_9 + \frac{2}{3} (F_2 + F_5) \right) , \\ D_R &= D_{[8]} + (m_\pi^2 + 2m_K^2) \left(F_8 + \frac{2}{3} (F_0 + F_4) \right) , \\ C_R &= C_{[10]} + (m_\pi^2 + 2m_K^2) \left(C_5 + \frac{2}{3} (C_0 + C_2) \right) . \end{aligned} \quad (2.40)$$

and the renormalized parameters $F_{A,P}, D_{A,P}$ and C_A as they are relevant for the meson-baryon 3-point vertices:

$$\begin{aligned} F_A &= F_R + \frac{2}{3} (m_\pi^2 + 2m_K^2) \delta F_5 , & D_A &= D_R + \frac{2}{3} (m_\pi^2 + 2m_K^2) \delta F_4 , \\ F_P &= \frac{2}{3} (m_\pi^2 + 2m_K^2) \bar{F}_5 , & D_P &= \frac{2}{3} (m_\pi^2 + 2m_K^2) \bar{F}_4 , \\ C_A &= C_R + \frac{2}{3} (m_\pi^2 + 2m_K^2) \delta C_0 . \end{aligned} \quad (2.41)$$

The index A or P indicates whether the meson couples to the baryon via an axial-vector vertex (A) or a pseudo-scalar vertex (P). It is clear that the effects of (2.40) and (2.41) break the chiral symmetry but do not break the $SU(3)$ symmetry. In this work the renormalized parameters F_R, D_R and C_R are used. Note that one can always choose the parameters F_8, F_9 and C_5 to obtain $F_R = F_{[8]}$, $D_R = D_{[8]}$ and $C_R = C_{[10]}$. In order to distinguish the renormalized values from their bare values one needs to determine the parameters F_8, F_9 and C_5 by investigating higher-point Green functions. This is beyond the scope of this work.

The number of parameters inciting $SU(3)$ symmetry-breaking effects can be reduced significantly by the large- N_c analysis. Recall the five leading operators presented in [154]:

$$\begin{aligned} \langle \mathcal{B}' | \mathcal{L}_\chi^{(3)} | \mathcal{B} \rangle &= \frac{1}{f} \langle \mathcal{B}' | O_i^{(a)}(\tilde{c}) | \mathcal{B} \rangle \text{tr} \lambda_a \nabla^{(i)} \Phi + 4 \langle \mathcal{B}' | O_i^{(a)}(c) | \mathcal{B} \rangle A_a^{(i)} , \\ O_i^{(a)}(c) &= c_1 (d^{8a}_b G_i^{(b)} + \frac{1}{3} \delta^{a8} J_i) + c_2 (d^{8a}_b J_i T^{(b)} + \delta^{a8} J_i) \\ &\quad + c_3 [G_i^{(a)}, T^{(8)}]_+ + c_4 [T^{(a)}, G_i^{(8)}]_+ + c_5 [J^2, [T^{(8)}, G_i^{(a)}]_-]_- . \end{aligned} \quad (2.42)$$

It is important to observe that the parameters c_i and \tilde{c}_i are a priori independent. They are correlated by the chiral $SU(3)$ symmetry only. With (2.19) it is straightforward to map the interaction terms (2.42), which all break the $SU(3)$ symmetry linearly, onto the chiral vertices of (2.37) and (2.38). This procedure relates the parameters c_i and \tilde{c}_i . One finds that the

	g_A (Exp.)	F_R	D_R	c_1	c_2	c_3	c_4	c_5
$n \rightarrow p e^- \bar{\nu}_e$	1.267 ± 0.004	1	1	$\frac{5}{3\sqrt{3}}$	$\frac{1}{\sqrt{3}}$	$\frac{5}{\sqrt{3}}$	$\frac{1}{\sqrt{3}}$	0
$\Sigma^- \rightarrow \Lambda e^- \bar{\nu}_e$	0.601 ± 0.015	0	$\sqrt{\frac{2}{3}}$	$\frac{\sqrt{2}}{3}$	0	0	0	0
$\Lambda \rightarrow p e^- \bar{\nu}_e$	-0.889 ± 0.015	$-\sqrt{\frac{3}{2}}$	$-\frac{1}{\sqrt{6}}$	$\frac{1}{2\sqrt{2}}$	$\frac{1}{2\sqrt{2}}$	$-\frac{3}{2\sqrt{2}}$	$\frac{1}{2\sqrt{2}}$	0
$\Sigma^- \rightarrow n e^- \bar{\nu}_e$	0.342 ± 0.015	-1	1	$-\frac{1}{6\sqrt{3}}$	$\frac{1}{2\sqrt{3}}$	$\frac{1}{2\sqrt{3}}$	$-\frac{\sqrt{3}}{2}$	0
$\Xi^- \rightarrow \Lambda e^- \bar{\nu}_e$	0.306 ± 0.061	$\sqrt{\frac{3}{2}}$	$-\frac{1}{\sqrt{6}}$	$-\frac{1}{6\sqrt{2}}$	$-\frac{1}{2\sqrt{2}}$	$-\frac{1}{2\sqrt{2}}$	$-\frac{5}{2\sqrt{2}}$	0
$\Xi^- \rightarrow \Sigma^0 e^- \bar{\nu}_e$	0.929 ± 0.112	$\frac{1}{\sqrt{2}}$	$\frac{1}{\sqrt{2}}$	$-\frac{5}{6\sqrt{6}}$	$-\frac{1}{2\sqrt{6}}$	$-\frac{5}{2\sqrt{6}}$	$-\frac{1}{2\sqrt{6}}$	0

Table 2.1: Axial-vector coupling constants for the weak decay processes of the baryon octet states. The empirical values for g_A are taken from [163]. Here we do not consider $SU(3)$ symmetry-breaking effects of the vector current. The last seven columns give the coefficients of the axial-vector coupling constants g_A decomposed into the F_R , D_R and c_i parameters.

matching is possible for all operators leaving only ten independent parameters c_i , $\tilde{c}_{1,2}$, $\bar{c}_{1,2}$ and a rather than the twenty-three F_i , C_i and $\delta F_i, \delta C_i$ and \bar{F}_i parameters in (2.37,2.38). Simple algebra leads to $c_i = \tilde{c}_i$ for $i = 3, 4, 5$ and

$$\begin{aligned}
F_1 &= -\frac{\sqrt{3}}{2} \frac{c_3}{m_K^2 - m_\pi^2}, & F_2 &= -\frac{\sqrt{3}}{2} \frac{c_4}{m_K^2 - m_\pi^2}, & F_3 &= -\frac{1}{\sqrt{3}} \frac{c_3 + c_4}{m_K^2 - m_\pi^2}, \\
F_4 &= -\frac{\sqrt{3}}{4} \frac{c_1}{m_K^2 - m_\pi^2}, & F_5 &= -\frac{\sqrt{3}}{4} \frac{\frac{2}{3}c_1 + c_2}{m_K^2 - m_\pi^2}, & F_6 &= -\frac{\sqrt{3}}{2} \frac{\frac{2}{3}c_1 + c_2}{m_K^2 - m_\pi^2}, \\
C_0 &= -\frac{\sqrt{3}}{2} \frac{c_1}{m_K^2 - m_\pi^2}, & C_1 &= -\frac{\sqrt{3}}{2} \frac{c_3 - c_4 + 3c_5}{m_K^2 - m_\pi^2}, \\
C_3 &= -\sqrt{3} \frac{c_3}{m_K^2 - m_\pi^2}, & C_4 &= -\sqrt{3} \frac{c_4}{m_K^2 - m_\pi^2}, & F_{0,7} &= C_{2,5} = 0,
\end{aligned} \tag{2.43}$$

and

$$\begin{aligned}
\bar{F}_4 &= -\frac{\sqrt{3}}{4} \frac{\tilde{c}_1}{m_K^2 - m_\pi^2}, & \delta F_4 &= -\frac{\sqrt{3}}{4} \frac{\delta c_1}{m_K^2 - m_\pi^2}, \\
\bar{F}_5 &= -\frac{\sqrt{3}}{4} \frac{\frac{2}{3}\tilde{c}_1 + \tilde{c}_2 + a}{m_K^2 - m_\pi^2}, & \delta F_5 &= -\frac{\sqrt{3}}{4} \frac{\frac{2}{3}\delta c_1 + \delta c_2 - a}{m_K^2 - m_\pi^2}, \\
\bar{F}_6 &= -\frac{\sqrt{3}}{2} \frac{\frac{2}{3}\tilde{c}_1 + \tilde{c}_2 + a}{m_K^2 - m_\pi^2}, & \delta F_6 &= -\frac{\sqrt{3}}{2} \frac{\frac{2}{3}\delta c_1 + \delta c_2 - a}{m_K^2 - m_\pi^2}, \\
\delta C_0 &= -\frac{\sqrt{3}}{2} \frac{\tilde{c}_1 - c_1}{m_K^2 - m_\pi^2}, & \delta c_i &= \tilde{c}_i - c_i - \bar{c}_i.
\end{aligned} \tag{2.44}$$

In (2.44) the pseudo-scalar parameters $\bar{F}_{4,5,6}$ are expressed in terms of the more convenient dimensionless parameters $\tilde{c}_{1,2}$ and a . Here we insist that an expansion analogous to (2.42) holds also for the pseudo-scalar vertices in (2.38).

The analysis of [163], which considers constraints from the weak decay processes of the baryon octet states and the strong decay widths of the decuplet states, obtains $c_2 \simeq -0.15$ and

$c_3 \simeq 0.09$ but finds values of c_1 and c_4 which are compatible with zero⁴. In Tab. (2.1) we reproduce the axial-vector coupling constants as given in [163] relevant for the various baryon octet weak-decay processes. Besides $C_A + 2\tilde{c}_1/\sqrt{3}$, the empirical strong-decay widths of the decuplet states constrain the parameters c_3 and c_4 only, as is evident from the expressions for the decuplet widths,

$$\begin{aligned}\Gamma_{[10]}^{(\Delta)} &= \frac{m_N + E_N}{2\pi f^2} \frac{p_{\pi N}^3}{12 m_{[10]}^{(\Delta)}} \left(C_A + \frac{2}{\sqrt{3}} (\tilde{c}_1 + 3c_3) \right)^2, \\ \Gamma_{[10]}^{(\Sigma)} &= \frac{m_\Lambda + E_\Lambda}{2\pi f^2} \frac{p_{\pi\Lambda}^3}{24 m_{[10]}^{(\Sigma)}} \left(C_A + \frac{2}{\sqrt{3}} \tilde{c}_1 \right)^2 \\ &\quad + \frac{m_\Sigma + E_\Sigma}{3\pi f^2} \frac{p_{\pi\Sigma}^3}{24 m_{[10]}^{(\Sigma)}} \left(C_A + \frac{2}{\sqrt{3}} (\tilde{c}_1 + 6c_4) \right)^2, \\ \Gamma_{[10]}^{(\Xi)} &= \frac{m_\Xi + E_\Xi}{2\pi f^2} \frac{p_{\pi\Xi}^3}{24 m_{[10]}^{(\Xi)}} \left(C_A + \frac{2}{\sqrt{3}} (\tilde{c}_1 - 3c_3 + 3c_4) \right)^2,\end{aligned}\tag{2.45}$$

where for example $m_\Delta = \sqrt{m_N^2 + p_{\pi N}^2} + \sqrt{m_\pi^2 + p_{\pi N}^2}$ and $E_N = \sqrt{m_N^2 + p_{\pi N}^2}$. For instance, the values $C_A + 2\tilde{c}_1/\sqrt{3} \simeq 1.7$, $c_3 \simeq 0.09$ and $c_4 \simeq 0.0$ together with $f \simeq f_\pi \simeq 93$ MeV lead to isospin averaged partial decay widths of the decuplet states which are compatible with the present day empirical estimates. It is clear that the six data points for the baryon octet decays can be reproduced by a suitable adjustment of the six parameters F_R , D_R and $c_{1,2,3,4}$. The non-trivial issue is to what extent the explicit $SU(3)$ symmetry-breaking pattern in the axial-vector coupling constants is consistent with the symmetry-breaking pattern in the meson-baryon coupling constants. Here a possible strong energy dependence of the decuplet self-energies may invalidate the use of the simple expressions (2.45). A more direct comparison with the meson-baryon scattering data may be required.

An implicit assumption one relies on if Tab. 2.1 is applied should be mentioned. In a strict chiral expansion the Q^2 effects included in that table are incomplete. There are various one-loop diagrams which are not considered but carry chiral order Q^2 also. However, in a combined chiral and $1/N_c$ expansion it is natural to neglect such loop effects, because they are suppressed by $1/N_c$. This is immediate with the large- N_c scaling rules $m_\pi \sim N_c^0$ and $f \sim \sqrt{N_c}$ [87,88] together with the fact that the one-loop effects are proportional to $m_{K,\pi}^2/(4\pi f^2)$ [164]. On the other hand, it is evident from (2.18) and (2.42) that the $SU(3)$ symmetry-breaking contributions are not necessarily suppressed by $1/N_c$. This approach differs from previous calculations [164,165,166,167] where emphasis was put on the one-loop corrections of the axial-vector current rather than the quasi-local counter terms which were not considered. It is clear that part of the one-loop effects, in particular their renormalization scale dependence, can be absorbed into the counter terms considered in this work.

The large- N_c counting issue will be taken up again when discussing the approximate scattering kernel and also when presenting the final set of parameters, obtained from a fit to the data set.

⁴The parameters of [163] are obtained with $c_i \rightarrow -\sqrt{3}c_i/2$ and $a = D_R + (c_1 + 3c_3)/\sqrt{3}$ and $b = F_R - 2a/3 + (2c_1/3 + c_2 + 2c_3 + c_4)/\sqrt{3}$. The analysis of [163] does not determine the parameter c_5 .

Chapter 3

Covariant meson–baryon scattering

In this chapter the basic concepts required for a relativistic coupled-channel effective field theory of meson–baryon scattering are introduced. The formalism is developed first for the case of elastic πN scattering for simplicity. The next chapter is then devoted to the inclusion of inelastic channels which leads to the coupled-channel approach. The developments rely on an 'old' idea present in the literature for many decades. One aims at reducing the complexity of the relativistic Bethe-Salpeter equation by a suitable reduction scheme constrained to preserve the relativistic unitarity cuts [168, 169, 170]. A famous example is the Blankenbecler-Sugar scheme [168] which reduces the Bethe-Salpeter equation to a 3-dimensional integral equation. For a beautiful variant developed for pion-nucleon scattering, see the work by Gross and Surya [169]. In this work a scheme is derived which is more suitable for the relativistic chiral Lagrangian. It is not attempted to establish a numerical solution of the four dimensional Bethe-Salpeter equation based on phenomenological form factors and interaction kernels [171]. The merit of the chiral Lagrangian is that a major part of the complexity is already eliminated by having reduced non-local interactions to 'quasi' local interactions involving a finite number of derivatives only. The scheme is therefore constructed to be particularly transparent and efficient for the typical case of 'quasi' local interaction terms. A further important aspect to be addressed in this section concerns the independence of the on-shell scattering amplitude on the choice of chiral coordinates or the choice of interpolating fields. If one solves the Bethe-Salpeter equation with an interaction kernel evaluated in perturbation theory the resulting on-shell scattering amplitude depends on the choice of interpolating fields even though physical quantities should be independent on that choice [96]. It will be demonstrated that this problem can be avoided by introducing an appropriate on-shell reduction scheme for the Bethe-Salpeter equation. In the course of developing the approach a modified subtraction scheme within dimensional regularization is proposed. The latter complies manifestly with the chiral counting rule (2.5).

Consider the on-shell pion-nucleon scattering amplitude

$$\begin{aligned} \langle \pi^i(\bar{q}) N(\bar{p}) | T | \pi^j(q) N(p) \rangle &= (2\pi)^4 \delta^4(p + q - \bar{p} - \bar{q}) \\ &\times \bar{u}(\bar{p}) T_{\pi N \rightarrow \pi N}^{ij}(\bar{q}, \bar{p}; q, p) u(p) \end{aligned} \quad (3.1)$$

where $\delta^4(\dots)$ guarantees energy-momentum conservation and $u(p)$ is the nucleon isospin-doublet spinor. In quantum field theory the scattering amplitude $T_{\pi N \rightarrow \pi N}$ is obtained by solving the Bethe-Salpeter matrix equation

$$T(\bar{k}, k; w) = K(\bar{k}, k; w) + \int \frac{d^4 l}{(2\pi)^4} K(\bar{k}, l; w) G(l; w) T(l, k; w) ,$$

$$G(l; w) = -i S_N(\tfrac{1}{2} w + l) D_\pi(\tfrac{1}{2} w - l), \quad (3.2)$$

defined in terms of the Bethe-Salpeter scattering kernel $K(\bar{k}, k; w)$, the nucleon propagator $S_N(p) = 1/(\not{p} - m_N + i\epsilon)$ and the pion propagator $D_\pi(q) = 1/(q^2 - m_\pi^2 + i\epsilon)$. Self energy corrections in the propagators are suppressed and therefore not considered in this work. In (5.8) convenient kinematical variables are used:

$$w = p + q = \bar{p} + \bar{q}, \quad k = \tfrac{1}{2}(p - q), \quad \bar{k} = \tfrac{1}{2}(\bar{p} - \bar{q}), \quad (3.3)$$

where q, p, \bar{q} and \bar{p} are the initial and final pion and nucleon 4-momenta. Here there is no need to specify the form of the scattering kernel K since the discussion is generic and does not depend on the particular form of the interaction. The Bethe-Salpeter equation (5.8) implements Lorentz invariance and unitarity for the two-body scattering process. It involves the off-shell continuation of the on-shell scattering amplitude introduced in (5.5). Only the on-shell limit with $\bar{p}^2, p^2 \rightarrow m_N^2$ and $\bar{q}^2, q^2 \rightarrow m_\pi^2$ carries direct physical information. In quantum field theory the off-shell form of the scattering amplitude reflects the particular choice of the pion and nucleon interpolating fields chosen in the Lagrangian density and therefore can be altered basically at will by a redefinition of the fields [172, 156].

It is convenient to decompose the interaction kernel and the resulting scattering amplitude in isospin invariant components

$$K_{ij}(\bar{k}, k; w) = \sum_I K_I(\bar{k}, k; w) P_{ij}^{(I)}, \quad T_{ij}(\bar{k}, k; w) = \sum_I T_I(\bar{k}, k; w) P_{ij}^{(I)} \quad (3.4)$$

with the isospin projection matrices $P_{ij}^{(I)}$. For pion-nucleon scattering one has:

$$P_{ij}^{(\frac{1}{2})} = \frac{1}{3} \sigma_i \sigma_j, \quad P_{ij}^{(\frac{3}{2})} = \delta_{ij} - \frac{1}{3} \sigma_i \sigma_j, \quad \sum_k P_{ik}^{(I)} P_{kj}^{(I')} = \delta_{II'} P_{ij}^{(I)}. \quad (3.5)$$

The ansatz (3.4) decouples the Bethe-Salpeter equation into the two isospin channels $I = 1/2$ and $I = 3/2$.

3.1 On-shell reduction of the Bethe-Salpeter equation

It is important to construct a systematic reduction scheme for the Beth-Salpeter equation as to arrive at a formulation in which the on-shell scattering amplitudes are independent on the choice of chiral coordinates or the choice of interpolating fields. The interaction kernel is decomposed into an 'on-shell irreducible' part \bar{K} and 'on-shell reducible' terms K_L and K_R [90] which vanish if evaluated with on-shell kinematics either in the incoming or outgoing channel respectively

$$K = \bar{K} + K_L + K_R + K_{LR}, \quad \bar{u}_N(\bar{p}) K_L \Big|_{\text{on-shell}} = 0 = K_R u_N(p) \Big|_{\text{on-shell}}. \quad (3.6)$$

The term K_{LR} disappears if evaluated with either incoming or outgoing on-shell kinematics. The notion of an on-shell irreducible kernel \bar{K} is not unique per se and needs further specifications. The precise definition of a particular choice of on-shell irreducibility will be provided when

constructing covariant partial-wave projectors. In this subsection the generic consequences of decomposing the interaction kernel according to (3.6) are studied. With this decomposition of the interaction kernel the scattering amplitude can be written as follows

$$\begin{aligned}
T &= \bar{T} - (K_L + K_{LR}) \cdot (1 - G \cdot K)^{-1} \cdot G \cdot (K_R + K_{LR}) - K_{LR} \\
&+ (K_L + K_{LR}) \cdot (1 - G \cdot K)^{-1} + (1 - K \cdot G)^{-1} \cdot (K_R + K_{LR}), \\
\bar{T} &= (1 - V \cdot G)^{-1} \cdot V,
\end{aligned} \tag{3.7}$$

where we use operator notation with, e.g., $T = K + K \cdot G \cdot T$ representing the Bethe-Salpeter equation (5.8). The effective interaction V in (3.7) is given by

$$\begin{aligned}
V &= (\bar{K} + K_R \cdot G \cdot X) \cdot (1 - G \cdot K_L - G \cdot K_{LR} \cdot G \cdot X)^{-1}, \\
X &= (1 - (K_R + K_{LR}) \cdot G)^{-1} \cdot (\bar{K} + K_L)
\end{aligned} \tag{3.8}$$

without any approximations. It should be emphasized that the interaction kernels V and K are equivalent on-shell by construction. This follows from (3.7) and (3.6), which predict the equivalence of T and \bar{T} for on-shell kinematics

$$\bar{u}_N(\bar{p}) T u_N(p) \Big|_{\text{on-shell}} \equiv \bar{u}_N(\bar{p}) \bar{T} u_N(p) \Big|_{\text{on-shell}}.$$

To what extent does the formalism (3.6-3.8) help in constructing an approximation scheme to the Bethe-Salpeter equation which does not show an unwanted dependence on the choice of fields? In order to streamline the following discussion it is written

$$O = \sum O_n, \quad \text{for } O = K, V, T, \dots, \tag{3.9}$$

where the moments O_n are defined with respect to some perturbative expansion. At leading order, say $n = 1$, it is evident that given a particular notion of on-shell irreducibility the moment $\bar{K}_1 = \bar{T}_1$ does not depend on the choice of fields. The conclusion relies on the equivalence theorem which implies that on-shell quantities do not depend on the choice of fields if evaluated systematically at given order in perturbation theory. The \bar{O} -notation is used for any object, $O = K, V, T, \dots$, as introduced in (3.6). If one truncates $V \rightarrow V_1 = \bar{K}_1$ the resulting on-shell equivalent amplitude $\hat{T} = (1 - V_1 \cdot G)^{-1} \cdot V_1$ is invariant under field redefinitions provided that the two-particle propagator G is invariant also¹. The extension of this argument to subleading orders is subtle. For instance there is no reason to expect the invariance of

$$\hat{T} = (1 - \sum_{i=1}^n V_i \cdot G)^{-1} \cdot \sum_{j=1}^n V_j, \tag{3.10}$$

at order n . Moreover it is evident that subleading moments of \bar{K}_n may depend on the choice of fields simply because they are not observable quantities. On the other hand, given any notion of on-shell irreducibility the moments \bar{T}_n are invariant as a direct consequence of the equivalence

¹This assumption can be justified upon an appropriate renormalization of the two-particle propagator G (see (3.35)). One may simply identify G_R with the bare two-particle propagator written in terms of physical mass parameters.

theorem. It is then straightforward to identify the uniquely induced effective interaction kernel V_{eff} ,

$$V_{\text{eff}} = \left(1 + \bar{T} \cdot G\right)^{-1} \cdot \bar{T}, \quad \bar{T} = \overline{(1 - K \cdot G)^{-1} \cdot K} = (1 - V_{\text{eff}} \cdot G)^{-1} \cdot V_{\text{eff}}, \quad (3.11)$$

which is invariant under field redefinitions by construction. The moments $V_{\text{eff},n}$ follow by expanding the result (3.11). That may be inconvenient for a given notion of on-shell irreducibility but is in principle straight forward. To conclude it is possible to construct the invariant effective interaction V_{eff} once one agrees on a particular notion of on-shell irreducibility. Of course there are infinite many ways to do so, but this is welcome since we may exploit that freedom as to simplify the process of solving the Bethe-Salpeter equation.

In this work the guide will be the question how the result (3.11) relates to the more explicit and convenient formalism (3.6-3.8). In general there appears no transparent relation of V_{eff} and V . Only for a particular choice of on-shell irreducibility there is a simple relation. This difficulty reflects a subtle property of the effective invariant interaction, namely $V_{\text{eff}} \neq \bar{V}_{\text{eff}}$. Only if one succeeds in introducing a specific form of on-shell irreducibility that is invariant under unitary iteration,

$$\bar{K} \cdot G \cdot \bar{K} = \overline{\bar{K} \cdot G \cdot \bar{K}}, \quad (3.12)$$

for any interaction kernel K , one obtains $V_{\text{eff}} = \bar{V}_{\text{eff}}$. Given (3.12) the effective interaction kernel $V_{\text{eff}}[K]$ can now be constructed in perturbation theory applying the convenient formalism (3.6-3.8). Here $V[K]$ as given in (3.8) is considered as a functional in K . Within this notation one obtains

$$\left(V_{\text{eff}}[K]\right)_{n+1} = \left(\overline{V^{(n)}[K]}\right)_{n+1}, \quad V^{(n+1)}[K] = V[V^{(n)}[K]], \quad V^{(1)}[K] = V[K]. \quad (3.13)$$

To summarize the crucial property of the on-shell reduction scheme (3.6-3.8,3.13). Given that scheme using different chiral coordinates or fields does lead to the same on-shell scattering amplitude \bar{T} provided that the effective interaction V_{eff} is evaluated systematically to a given order in perturbation theory. It is left to establish a notion of on-shell irreducibility that is consistent with (3.12). This will be accomplished when constructing covariant partial-wave projectors.

As an explicit simple example for the application of the formalism (3.7,3.8) consider the s-channel nucleon pole diagram as a particular contribution to the interaction kernel $K(\bar{k}, k; w)$ in (5.8). In the isospin 1/2 channel its contribution evaluated with the pseudo-vector pion-nucleon vertex reads

$$K(\bar{k}, k; w) = -\frac{3g_A^2}{4f^2} \gamma_5 \left(\frac{1}{2} \psi - \bar{k}\right) \frac{1}{\psi - m_N - \Delta m_N(w)} \gamma_5 \left(\frac{1}{2} \psi - k\right), \quad (3.14)$$

where a wave-function and mass renormalization $\Delta m_N(w)$ is included for later convenience². The various components of the kernel according to (3.6) are derived readily

$$\begin{aligned} \bar{K} &= -\frac{3g_A^2}{4f^2} \frac{(\psi - m_N)^2}{\psi + \bar{m}_N}, & K_{LR} &= \frac{3g_A^2}{4f^2} \left(\not{p} - m_N\right) \frac{1}{\psi + \bar{m}_N} \left(\not{p} - m_N\right), \\ K_L &= \frac{3g_A^2}{4f^2} \left(\not{p} - m_N\right) \frac{\psi - m_N}{\psi + \bar{m}_N}, & K_R &= \frac{3g_A^2}{4f^2} \frac{\psi - m_N}{\psi + \bar{m}_N} \left(\not{p} - m_N\right), \end{aligned} \quad (3.15)$$

²The corresponding counter terms in the chiral Lagrangian (2.31) are linear combinations of b_0, b_D and b_F and ζ_0, ζ_D and ζ_F .

where $\bar{m}_N = m_N + \gamma_5 \Delta m_N(w) \gamma_5$. The solution of the Bethe-Salpeter equation is derived in two steps. First solve for the auxiliary object X in (3.8)

$$\begin{aligned} X &= \frac{3g_A^2}{4f^2} (\not{p} - \not{\psi}) \frac{1}{\psi + \bar{m}_N} (\psi - m_N) \\ &+ \frac{3g_A^2}{4f^2} (\not{p} + \not{\psi} - 2m_N) \frac{3g_A^2 I_\pi^{(l)}}{4f^2 (\psi + \bar{m}_N) + 3g_A^2 I_\pi} \frac{\psi - m_N}{\psi + \bar{m}_N}, \end{aligned} \quad (3.16)$$

where one encounters the pionic tadpole integrals:

$$I_\pi = i \int \frac{d^d l}{(2\pi)^d} \frac{\mu^{4-d}}{l^2 - m_\pi^2 + i\epsilon}, \quad I_\pi^{(l)} = i \int \frac{d^d l}{(2\pi)^d} \frac{\mu^{4-d} \not{l}}{l^2 - m_\pi^2 + i\epsilon}, \quad (3.17)$$

properly regularized for space-time dimension d in terms of the renormalization scale μ . Since $I_\pi^{(l)} = 0$ and $K_R \cdot G \cdot (\bar{K} + K_L) \equiv 0$ for our example the expression (3.16) reduces to $X = \bar{K} + K_L$. The effective potential $V(w)$ and the on-shell equivalent scattering amplitude \bar{T} follow

$$\begin{aligned} V(w) &= -\frac{3g_A^2}{4f^2} \frac{(\psi - m_N)^2}{\psi + \bar{m}_N} \left(1 + \frac{3g_A^2 I_\pi}{4f^2} \frac{\psi - m_N}{\psi + \bar{m}_N} \right)^{-1}, \\ \bar{T}(w) &= \frac{1}{1 - V(w) J_{\pi N}(w)} V(w). \end{aligned} \quad (3.18)$$

The divergent loop function $J_{\pi N}$ in (3.18) defined via $\bar{K} \cdot G \cdot \bar{K} = \bar{K} J_{\pi N} \bar{K}$ may be decomposed into scalar master-loop functions $I_{\pi N}(\sqrt{s})$ and I_N, I_π with

$$\begin{aligned} J_{\pi N}(w) &= \left(m_N + \frac{w^2 + m_N^2 - m_\pi^2}{2w^2} \psi \right) I_{\pi N}(\sqrt{s}) + \frac{I_N - I_\pi}{2w^2} \psi, \\ I_{\pi N}(\sqrt{s}) &= -i \int \frac{d^d l}{(2\pi)^d} \frac{\mu^{4-d}}{l^2 - m_\pi^2} \frac{1}{(w-l)^2 - m_N^2}, \\ I_N &= i \int \frac{d^d l}{(2\pi)^d} \frac{\mu^{4-d}}{l^2 - m_N^2 + i\epsilon} \end{aligned} \quad (3.19)$$

where $s = w^2$. The result (3.18) gives an explicit example of the powerful formula (3.7). The Bethe-Salpeter equation may be solved in two steps. Once the effective potential V is evaluated the scattering amplitude \bar{T} is given in terms of the loop function $J_{\pi N}$ which is independent on the form of the interaction. In chapter 3.3 the result (3.18) will be generalized by constructing a complete set of covariant projectors. The latter will define a particular notion of on-shell irreducibility. Before discussing the result (3.18) in more detail an appropriate regularization and renormalization scheme for the relativistic loop functions in (3.19) is developed.

3.2 Renormalization program

An important requisite of the chiral Lagrangian is a consistent regularization and renormalization scheme for its loop diagrams. The regularization scheme should respect all symmetries built into the theory but should also comply with the power counting rule (2.5). The standard

MS or \overline{MS} subtraction scheme of dimensional regularization appears inconvenient, because it contradicts standard chiral power counting rules if applied to relativistic Feynman diagrams [173, 174]. A modified subtraction scheme for relativistic diagrams, properly regularized in space-time dimensions d , which complies with the chiral counting rule (2.5) manifestly, will be suggested.

The discussion centers around the one-loop functions I_π , I_N and $I_{\pi N}(\sqrt{s})$ introduced in (3.19). One encounters some freedom how to regularize and renormalize those master-loop functions, which are typical representatives for all one-loop diagrams [90]. Recall their well-known properties at $d = 4$. The loop function $I_{\pi N}(\sqrt{s})$ is rendered finite by one subtraction, for example at $\sqrt{s} = 0$,

$$\begin{aligned} I_{\pi N}(\sqrt{s}) &= \frac{1}{16\pi^2} \left(\frac{p_{\pi N}}{\sqrt{s}} \left(\ln \left(1 - \frac{s - 2p_{\pi N}\sqrt{s}}{m_\pi^2 + m_N^2} \right) - \ln \left(1 - \frac{s + 2p_{\pi N}\sqrt{s}}{m_\pi^2 + m_N^2} \right) \right) \right. \\ &\quad \left. + \left(\frac{1}{2} \frac{m_\pi^2 + m_N^2}{m_\pi^2 - m_N^2} - \frac{m_\pi^2 - m_N^2}{2s} \right) \ln \left(\frac{m_\pi^2}{m_N^2} \right) + 1 \right) + I_{\pi N}(0), \\ p_{\pi N}^2 &= \frac{s}{4} - \frac{m_N^2 + m_\pi^2}{2} + \frac{(m_N^2 - m_\pi^2)^2}{4s}. \end{aligned} \quad (3.20)$$

One finds $I_{\pi N}(m_N) - I_{\pi N}(0) = (4\pi)^{-2} + \mathcal{O}(m_\pi/m_N) \sim Q^0$ in conflict with the expected minimal chiral power Q . On the other hand the leading chiral power of the subtracted loop function complies with the prediction of the standard chiral power counting rule (2.5) with $I_{\pi N}(\sqrt{s}) - I_{\pi N}(\mu_S) \sim Q$ rather than the anomalous power Q^0 provided that $\mu_S \sim m_N$ holds. The anomalous contribution is eaten up by the subtraction constant $I_{\pi N}(\mu_S)$. This can be seen by expanding the loop function

$$\begin{aligned} I_{\pi N}(\sqrt{s}) &= i \frac{\sqrt{\phi_{\pi N}}}{8\pi m_N} + \frac{\sqrt{\phi_{\pi N}}}{16\pi^2 m_N} \ln \left(\frac{\sqrt{s} - m_N + \sqrt{\phi_{\pi N}}}{\sqrt{s} - m_N - \sqrt{\phi_{\pi N}}} \right) \\ &\quad + \frac{\sqrt{m_\pi^2 - \mu_N^2}}{8\pi m_N} - \frac{\sqrt{\mu_N^2 - m_\pi^2}}{16\pi^2 m_N} \ln \left(\frac{\mu_N + \sqrt{\mu_N^2 - m_\pi^2}}{\mu_N - \sqrt{\mu_N^2 - m_\pi^2}} \right) \\ &\quad - \frac{\sqrt{s} - \mu_S}{16\pi^2 m_N} \ln \left(\frac{m_\pi^2}{m_N^2} \right) + \mathcal{O} \left(\frac{(\mu_S - m_N)^2}{m_N^2}, Q^2 \right) + I_{\pi N}(\mu_S), \end{aligned} \quad (3.21)$$

in powers of $\sqrt{s} - m_N \sim Q$ and $\mu_N = \mu_S - m_N$. Here $\phi_{\pi N} = (\sqrt{s} - m_N)^2 - m_\pi^2$ is an approximate phase-space factor.

From the simple example of $I_{\pi N}(\sqrt{s})$ in (3.20) it becomes clear that a manifest realization of the chiral counting rule (2.5) is closely linked to the subtraction scheme implicit in any regularization scheme. A priori it is unclear in which way the subtraction constants of various loop functions are related by the pertinent symmetries³. Here dimensional regularization has proven to be an extremely powerful tool to regularize and to subtract loop functions in accordance with all symmetries. Therefore, it is useful to recall the expressions for the master-loop function I_N , and I_π and $I_{\pi N}(m_N)$ as they follow in dimensional regularization:

$$I_N = m_N^2 \frac{\Gamma(1 - d/2)}{(4\pi)^2} \left(\frac{m_N^2}{4\pi\mu^2} \right)^{(d-4)/2}$$

³This aspect was not addressed satisfactorily in [90, 91].

$$= \frac{m_N^2}{(4\pi)^2} \left(-\frac{2}{4-d} + \gamma - 1 - \ln(4\pi) + \ln \left(\frac{m_N^2}{\mu^2} \right) + \mathcal{O}(4-d) \right), \quad (3.22)$$

where d is the dimension of space-time and γ the Euler constant. The analogous result for the pionic tadpole follows by replacing the nucleon mass m_N in (3.22) by the pion mass m_π . The merit of dimensional regularization is that one is free to subtract all poles at $d = 4$ including any specified finite term without violating any of the pertinent symmetries. In the \overline{MS} -scheme the pole $1/(4-d)$ is subtracted including the finite part $\gamma - \ln(4\pi)$. This leads to

$$\begin{aligned} I_{N,\overline{MS}} &= \frac{m_N^2}{(4\pi)^2} \left(-1 + \ln \left(\frac{m_N^2}{\mu^2} \right) \right), & I_{\pi,\overline{MS}} &= \frac{m_\pi^2}{(4\pi)^2} \left(-1 + \ln \left(\frac{m_\pi^2}{\mu^2} \right) \right), \\ I_{\pi N,\overline{MS}}(m_N) &= -\frac{1}{(4\pi)^2} \ln \left(\frac{m_N^2}{\mu^2} \right) - \frac{m_\pi}{16\pi m_N} + \mathcal{O} \left(\frac{m_\pi^2}{m_N^2} \right). \end{aligned} \quad (3.23)$$

The result (3.23) confirms the expected chiral power for the pionic tadpole $I_\pi \sim Q^2$. However, a striking disagreement with the chiral counting rule (2.5) is found for the \overline{MS} -subtracted loop functions $I_{\pi N} \sim Q^0$ and $I_N \sim Q^0$. Recall that for the subtracted loop function $I_{\pi N}(\sqrt{s}) - I_{\pi N}(m_N) \sim Q$ the expected minimal chiral power is manifest (see (3.21)). It is instructive to trace the source of the anomalous chiral powers. By means of the identities

$$\begin{aligned} I_{\pi N}(m_N) &= \frac{I_\pi - I_N}{m_N^2 - m_\pi^2} + I_{\pi N}(m_N) - I_{\pi N}(0), \\ I_{\pi N}(m_N) - I_{\pi N}(0) &= \frac{1}{(4\pi)^2} - \frac{m_\pi}{16\pi m_N} \left(1 - \frac{m_\pi^2}{8m_N^2} \right) \\ &\quad + \frac{1}{(4\pi)^2} \left(1 - \frac{3}{2} \ln \left(\frac{m_\pi^2}{m_N^2} \right) \right) \frac{m_\pi^2}{m_N^2} + \mathcal{O} \left(\frac{m_\pi^4}{m_N^4}, d-4 \right), \end{aligned} \quad (3.24)$$

it appears that once the subtraction scheme has been specified for the tadpole terms I_π and I_N the required subtractions for the remaining master-loop functions are unique. In (3.24) the algebraic consistency identity is applied⁴:

$$I_\pi - I_N = (m_N^2 - m_\pi^2) I_{\pi N}(0), \quad (3.25)$$

which holds for any value of the space-time dimension d , and expanded the finite expression $I_{\pi N}(m_N) - I_{\pi N}(0)$ in powers of m_π/m_N at $d = 4$. The result (3.24) seems to show that one either violates the desired chiral power for the nucleonic tadpole, I_N , or the one for the loop function $I_{\pi N}(m_N)$. One may for example subtract the pole at $d = 4$ including the finite constant

$$\gamma - 1 - \ln(4\pi) + \ln \left(\frac{m_N^2}{\mu^2} \right).$$

That leads to a vanishing nucleonic tadpole $I_N \rightarrow 0$, which would be consistent with the expectation $I_N \sim Q^3$, but we find $I_{\pi N}(m_N) \rightarrow 1/(4\pi)^2 + \mathcal{O}(m_\pi)$, in disagreement with the expectation $I_{\pi N}(m_N) \sim Q$. This problem can be solved if one succeeds in defining a subtraction scheme which acts differently on $I_{\pi N}(0)$ and $I_{\pi N}(m_N)$. It is stressed that this is legitimate, because $I_{\pi N}(0)$ probes our effective theory outside its applicability domain. Mathematically this can be

⁴Note that (3.25) leads to a well-behaved loop function $J_{\pi N}(w)$ at $w = 0$ (see (3.19)).

achieved most economically and consistently by subtracting a pole in $I_{\pi N}(\sqrt{s})$ at $d = 3$ which arises in the limit $m_\pi/m_N \rightarrow 0$. To be explicit recall the expression for $I_{\pi N}(\sqrt{s})$ at arbitrary space-time dimension d (see eg. [89]):

$$I_{\pi N}(\sqrt{s}) = \left(\frac{m_N}{\mu}\right)^{d-4} \frac{\Gamma(2-d/2)}{(4\pi)^{d/2}} \int_0^1 dz C^{d/2-2},$$

$$C = z^2 - \frac{s - m_N^2 - m_\pi^2}{m_N^2} z(1-z) + \frac{m_\pi^2}{m_N^2} (1-z)^2 - i\epsilon. \quad (3.26)$$

The explicit representation (3.26) demonstrates that at $d = 3$ the loop function $I_{\pi N}(\sqrt{s})$ is finite at $\sqrt{s} = 0$ but infinite at $\sqrt{s} = m_N$ if one applies the limit $m_\pi/m_N \rightarrow 0$. One finds:

$$I_{\pi N}(m_N) = \frac{1}{8\pi} \frac{\mu}{m_N} \frac{1}{d-3} - \frac{1}{16\pi} \frac{\mu}{m_N} \left(\ln(4\pi) + \ln\left(\frac{\mu^2}{m_N^2}\right) + \frac{\Gamma'(1/2)}{\sqrt{\pi}} \right)$$

$$+ \mathcal{O}\left(\frac{m_\pi}{m_N}, d-3\right). \quad (3.27)$$

A minimal chiral subtraction scheme is now introduced. It may be viewed as a simplified variant of the scheme of Becher and Leutwyler in [89]. As usual one first needs to evaluate the contributions to an observable quantity at arbitrary space-time dimension d . The result shows poles at $d = 4$ and $d = 3$ if considered in the non-relativistic limit with $m_\pi/m_N \rightarrow 0$. Our modified subtraction scheme is defined by the replacement rules:

$$\frac{1}{d-3} \rightarrow -\frac{m_N}{2\pi\mu}, \quad \frac{2}{d-4} \rightarrow \gamma - 1 - \ln(4\pi) + \ln\left(\frac{m_N^2}{\mu^2}\right), \quad (3.28)$$

where it is understood that poles at $d = 3$ are isolated in the non-relativistic limit with $m_\pi/m_N \rightarrow 0$. The $d = 4$ poles are isolated with the ratio m_π/m_N at its physical value. The limit $d \rightarrow 4$ is applied after the pole terms are replaced according to (3.28). It is to be emphasized that there are no infrared singularities in the residuum of the $1/(d-3)$ -pole terms. In particular we observe that the anomalous subtraction implied in (3.28) does not lead to a potentially troublesome pion-mass dependence of the counter terms⁵. To make contact with a non-relativistic scheme one needs to expand the loop function in powers of p/m_N where p represents any external three momentum.

The results for the loop functions I_N , I_π and $I_{\pi N}(m_N)$ as implied by the subtraction prescription (3.28) are:

$$\bar{I}_N = 0, \quad \bar{I}_\pi = \frac{m_\pi^2}{(4\pi)^2} \ln\left(\frac{m_\pi^2}{m_N^2}\right),$$

$$\bar{I}_{\pi N}(m_N) = -\frac{m_\pi}{16\pi m_N} \left(1 - \frac{m_\pi^2}{8m_N^2}\right)$$

$$+ \frac{1}{(4\pi)^2} \left(1 - \frac{1}{2} \ln\left(\frac{m_\pi^2}{m_N^2}\right)\right) \frac{m_\pi^2}{m_N^2} + \mathcal{O}\left(\frac{m_\pi^4}{m_N^4}\right), \quad (3.29)$$

⁵In the scheme of Becher and Leutwyler [89] a pion-mass dependent subtraction scheme for the scalar one-loop functions is suggested. To be specific the master-loop function $I_{\pi N}(\sqrt{s})$ is subtracted by a regular polynomial in s, m_N and m_π of infinite order. In our scheme we subtract only a constant which agrees with the non-relativistic limit of the suggested polynomial of Becher and Leutwyler. Our subtraction constant does not depend on the pion mass.

where the ‘ $\bar{}$ ’ signals a subtracted loop functions⁶. The result shows that now the loop functions behave according to their expected minimal chiral power (2.5). Note that the one-loop expressions (3.29) do no longer depend on the renormalization scale μ introduced in dimensional regularization⁷. This should not be too surprising, because the renormalization prescription (3.28) has a non-trivial effect on the counter terms of the chiral Lagrangian. Note that the prescription (3.28) defines also a unique subtraction for higher loop functions in the same way the \overline{MS} -scheme does. The renormalization scale dependence will be explicit at the two-loop level reflecting the presence of so-called overall divergencies.

It was checked that all scalar one-loop functions, subtracted according to (3.28), comply with their expected minimal chiral power (2.5). Typically, loop functions which are finite at $d = 4$ are not affected by the subtraction prescription (3.28). Also, loop functions involving pion propagators only do not show singularities at $d = 3$ and therefore can be related easily to the corresponding loop functions of the \overline{MS} -scheme. Though, in the nucleon sector it may be tedious to relate the standard \overline{MS} -scheme to the scheme introduced here, in particular when multi-loop diagrams are considered, it is asserted that a well defined prescription for regularizing all divergent loop integrals is proposed. A prescription which is far more convenient than the \overline{MS} -scheme, because it complies manifestly with the chiral counting rule (2.5)⁸.

If one were to perform calculations within standard chiral perturbation theory in terms of the relativistic chiral Lagrangian everything is all set for any computation. However, as advocated before a non-perturbative chiral theory is asked for. That requires a more elaborate renormalization program, because it is necessary to discriminate carefully reducible and irreducible diagrams and sum the reducible diagrams to infinite order. The idea is to take over the renormalization program of standard chiral perturbation theory to the interaction kernel. In order to apply the standard perturbative renormalization program for the interaction kernel one has to move all divergent parts lying in reducible diagrams into the interaction kernel. That problem is solved in part by constructing an on-shell equivalent interaction kernel according to (3.6-3.8). It is evident that the ‘moving’ of divergencies needs to be controlled by an additional renormalization condition. Any such condition imposed should be constructed so as to respect crossing symmetry approximatively. While standard chiral perturbation theory leads directly to cross symmetric amplitudes at least approximatively, it is not automatically so in a resummation scheme.

Before introducing the general scheme the above issues are examined explicitly in terms of the example worked out in detail in the previous section. Taking the s-channel nucleon pole

⁶ The renormalized loop function $J_{\pi N}(w)$ is no longer well-behaved at $w = 0$. This was expected and does not cause any harm, because the point $\sqrt{s} = 0$ is far outside the applicability domain of our effective field theory.

⁷One may make contact with the non-relativistic so-called PDS-scheme of [175] by slightly modifying the replacement rule for the pole at $d = 3$. With

$$\frac{1}{d-3} \rightarrow 1 - \frac{m_N}{2\pi\mu}, \quad I_{\pi N}(m_N) \rightarrow \frac{1}{16\pi} \frac{2\mu - m_\pi}{m_N} + \mathcal{O}\left(\frac{m_\pi^2}{m_N^2}\right),$$

power counting is manifest if one counts $\mu \sim Q$. This is completely analogous to the PDS-scheme

⁸It is unclear how to set up a prescription in the presence of two massive fields with respective masses m_1 and m_2 and $m_1 \gg m_2$. For the decuplet baryons one may count $m_{[8]} - m_{[10]} \sim Q$ as suggested by large- N_c counting arguments and therefore start with a common mass for the baryon octet and decuplet states. The presence of the B_μ^* field in the chiral Lagrangian does cause a problem. Since we include the B_μ^* field only at tree-level in the interaction kernel of pion-nucleon and kaon-nucleon scattering, we do not further investigate the possible problems in this work. Formally one may avoid such problems all together if one counts $m_{[8]} - m_{[9]} \sim Q$ even though this assignment may not be effective.

term as the driving term in the Bethe-Salpeter equation the explicit result (3.18) was derived. First its implicit nucleon mass renormalization is discussed. The result (3.18) shows a pole at the physical nucleon mass with $\psi = -m_N$, only if the mass-counter term Δm_N in (3.14) is identified as follows

$$\Delta m_N = \frac{3g_A^2}{4f^2} 2m_N \left(m_\pi^2 I_{\pi N}(m_N) - I_N \right). \quad (3.30)$$

In the \overline{MS} -scheme the divergent parts of Δm_N , or more precisely the renormalization scale dependent parts, may be absorbed into the nucleon bare mass [173]. Renormalization within the chiral minimal subtraction scheme is achieved by the replacements $I_{\pi N} \rightarrow \bar{I}_{\pi N}$, $I_\pi \rightarrow \bar{I}_\pi$ and $I_N \rightarrow \bar{I}_N = 0$. The result (3.30) together with (3.29) then reproduces the well known result [173, 174]

$$\Delta m_N = -\frac{3g_A^2 m_\pi^3}{32\pi f^2} + \dots,$$

commonly derived in terms of the one-loop nucleon self energy $\Sigma_N(p)$. In order to offer a more direct comparison of (3.18) with the nucleon self-energy $\Sigma_N(p)$ recall the one-loop result

$$\begin{aligned} \Sigma_N(p) = \frac{3g_A^2}{4f^2} & \left(m_N \left(m_\pi^2 I_{\pi N}(\sqrt{p^2}) - I_N \right) - \not{p} \left(\frac{p^2 - m_N^2}{2p^2} I_\pi + \frac{p^2 + m_N^2}{2p^2} I_N \right. \right. \\ & \left. \left. + \left(\frac{(p^2 - m_N^2)^2}{2p^2} - m_\pi^2 \frac{p^2 + m_N^2}{2p^2} \right) I_{\pi N}(\sqrt{p^2}) \right) \right), \end{aligned} \quad (3.31)$$

in terms of the convenient master-loop function $I_{\pi N}(\sqrt{p^2})$ and the tadpole terms I_N and I_π . It is emphasized that the expression (3.31) is valid for arbitrary space-time dimension d . The wave-function renormalization, \mathcal{Z}_N , of the nucleon can be read off (3.31) leading to

$$\begin{aligned} \mathcal{Z}_N^{-1} &= 1 - \frac{\partial \Sigma_N}{\partial \not{p}} \Big|_{\not{p}=m_N} = 1 - \frac{3g_A^2}{4f^2} \left(2m_\pi^2 m_N \frac{\partial I_{\pi N}(\sqrt{p^2})}{\partial \sqrt{p^2}} \Big|_{p^2=m_N^2} - I_\pi \right) \\ &= 1 - \frac{3g_A^2}{4f^2} \frac{m_\pi^2}{(4\pi)^2} \left(-4 - 3 \ln \left(\frac{m_\pi^2}{m_N^2} \right) + 3\pi \frac{m_\pi}{m_N} + \mathcal{O} \left(\frac{m_\pi^2}{m_N^2} \right) \right), \end{aligned} \quad (3.32)$$

where in the last line of (3.32) relies on the minimal chiral subtraction scheme (3.28). The result (3.32) agrees with the expressions obtained previously in [173, 174, 89]. Note that in (3.32) the contribution of the counter terms ζ_0 , ζ_D and ζ_F are suppressed.

It is illuminating to discuss the role played by the pionic tadpole contribution, I_π , from $V(w)$ in (3.18) and from $J_{\pi N}(w)$ in (3.19). In the mass renormalization (3.30) both tadpole contributions cancel identically. If one dropped the pionic tadpole term I_π in the effective interaction $V(w)$ one would find a mass renormalization

$$\Delta m_N \sim m_N I_\pi / f^2 \sim Q^2, \quad (3.33)$$

in conflict with the expected minimal chiral power $\Delta m_N \sim Q^3$ (see (3.30)). Therefore it is mandatory to 'move' all tadpole contributions from the loop function $J_{\pi N}(w)$ to the effective interaction kernel $V(w)$ if the latter is evaluated in perturbation theory. This is readily achieved by splitting the meson-baryon propagator

$$G = \mathcal{Z}_N (G_R + \Delta G), \quad (3.34)$$

into two terms G_R and ΔG . The form of ΔG is chosen such that the renormalized loop function implied by G_R is free of reduced tadpole contributions. This procedure renormalizes the effective interaction kernel $V(w) \rightarrow V_R(w)$ as follows

$$\bar{T}_R = \frac{\mathcal{Z}_N}{1 - V \cdot G} \cdot V = \frac{1}{1 - V_R \cdot G_R} \cdot V_R, \quad V_R = \frac{\mathcal{Z}_N}{1 - \mathcal{Z}_N V \cdot \Delta G} \cdot V, \quad (3.35)$$

where the renormalized scattering amplitude

$$\bar{T}_R = \mathcal{Z}_N^{\frac{1}{2}} \bar{T} \mathcal{Z}_N^{\frac{1}{2}}, \quad (3.36)$$

as implied by the LSZ reduction scheme is introduced. Now the cancellation of the pionic tadpole contributions is easily implemented by applying the chiral expansion to $V_R(w)$. The renormalized interaction kernel $V_R(w)$ is real by construction.

The renormalization scheme is still incomplete⁹. It is necessary to specify how to absorb the remaining logarithmic divergence in $I_{\pi N}(\sqrt{s})$. The strategy is to move all divergences from the unitarity loop function $J_{\pi N}(w)$ into the renormalized potential $V_R(w)$ via (3.35). For the effective potential one may then apply the standard perturbative renormalization program. The remaining ambiguity is fixed by the renormalization condition that the effective potential $V_R(w)$ matches the scattering amplitudes at a subthreshold energy $\sqrt{s} = \mu_S$:

$$\bar{T}_R(\mu_S) = V_R(\mu_S). \quad (3.37)$$

The choice for the subtraction point μ_S is rather well determined by the crossing symmetry constraint. In fact one is lead almost uniquely to the convenient point $\mu_S = m_N$. For the case of pion-nucleon scattering one observes that the renormalized effective interaction V_R is real only if $m_N - m_\pi < \mu_S < m_N + m_\pi$ holds. The first condition reflects the s-channel unitarity cut with $\Im I_{\pi N}(\mu_S) = 0$ only if $\mu_S < m_N + m_\pi$. The second condition signals the u-channel unitarity cut. A particular convenient choice for the subtraction point is $\mu_S = m_N$, because it protects the nucleon pole term contribution. It leads to

$$\begin{aligned} \bar{T}_R(w) &= V_R(w) + \mathcal{O}\left((\psi + m_N)^0\right) \\ &= -\frac{3(\mathcal{Z}_N g_A)^2}{4f^2} \frac{4m_N^2}{\psi + m_N} + \mathcal{O}\left((\psi + m_N)^0\right), \end{aligned} \quad (3.38)$$

if the renormalized loop function is subtracted in such a way that

$$I_{\pi N,R}(m_N) = 0, \quad I'_{\pi N,R}(m_N) = 0, \quad (3.39)$$

hold in $J_{\pi N}(w)$ as specified in (3.19). It is insisted on a minimal subtraction for the scalar loop function $I_{\pi N}(\sqrt{s})$ 'inside' the full loop function $J_{\pi N}(w)$ as suggested by dimensional regularization. According to (3.20) one subtraction suffices to render $I_{\pi N}(\sqrt{s})$ finite. A direct subtraction for $J_{\pi N}(w)$ would require a subtraction polynomial that would not be specified by the simple renormalization condition (3.37) and would most likely be at odds with chiral symmetry constraints. It is stressed that the double subtraction in $I_{\pi N}(\sqrt{s})$ is necessary in order to meet the condition (3.37). Only with $I'_{\pi N,R}(m_N) = 0$ the renormalized effective potential $V_R(w)$ in (3.38) represents the s-channel nucleon pole term in terms of the physical coupling constant $\mathcal{Z}_N g_A$

⁹Here the most general case not necessarily imposing the minimal chiral subtraction scheme (3.28) is discussed.

properly. For example, it is evident that if V_R is truncated at chiral order Q^2 one finds $\mathcal{Z}_N = 1$. The one-loop wave-function renormalization (3.32) is needed if one considers the Q^3 -terms in V_R .

One observes that the subtracted loop function $I_{\pi N}(\sqrt{s}) - I_{\pi N}(\mu_S)$ is in fact independent on the subtraction point to order Q^2 if one counted $\mu_S - m_N \sim Q^2$. In this case one derives from (3.21) the expression

$$\begin{aligned} I_{\pi N}(\sqrt{s}) - I_{\pi N}(\mu_S) &= i \frac{\sqrt{\phi_{\pi N}}}{8 \pi m_N} + \frac{m_\pi}{16 \pi m_N} - \frac{\sqrt{s} - m_N}{16 \pi^2 m_N} \ln \left(\frac{m_\pi^2}{m_N^2} \right) \\ &+ \frac{\sqrt{\phi_{\pi N}}}{16 \pi^2 m_N} \ln \left(\frac{\sqrt{s} - m_N + \sqrt{\phi_{\pi N}}}{\sqrt{s} - m_N - \sqrt{\phi_{\pi N}}} \right) + \mathcal{O}(Q^2), \end{aligned} \quad (3.40)$$

where $\phi_{\pi N} = (\sqrt{s} - m_N)^2 - m_\pi^2$. The result (3.40) suggests that one may set up a systematic expansion scheme in powers of $\mu_S - m_N \sim Q^2$. The subtraction-scale independence of physical results then implies that all powers $(\mu_S - m_N)^n$ cancel except for the leading term with $n = 0$. In this sense one may say that the scattering amplitude is independent of the subtraction point μ_S . Note that such a scheme does not necessarily require a perturbative expansion of the scattering amplitude. It may be advantageous instead to restore that minimal μ_S -dependence in the effective potential V , leading to a subtraction scale independent scattering amplitude at given order in $(\mu_S - m_N)$. Equivalently, it is legitimate to directly insist on the ‘physical’ subtraction with $\mu_S = m_N$. There is a further important point to be made: we would reject a conceivable scheme in which the inverse effective potential V^{-1} is expanded in chiral powers, even though it would obviously facilitate the construction of that minimal μ_S -dependence. As examined in detail in [90] expanding the inverse effective potential requires a careful analysis as to determine if the effective potential has a zero within its applicability domain. If this is the case one must reorganize the expansion scheme. This is particularly cumbersome in a coupled-channel scenario where one must ensure that $\det V \neq 0$ holds. Since in the $SU(3)$ limit the Weinberg-Tomozawa interaction term, which is the first term in the chiral expansion of V , leads to $\det V_{WT} = 0$ (see (4.16)) one should not pursue this path ¹⁰.

An important further aspect, the approximate crossing symmetry, needs to be addressed. It will turn out that this problem is closely related to the renormalization program required to define the scattering equation. At first, one may insist on either a strict perturbative scheme or an approach which performs a simultaneous iteration of the s- and u-channel in order to meet the crossing symmetry constraint. It is pointed out, however, that a simultaneous iteration of the s- and u-channel is not required, if the s-channel iterated and u-channel iterated amplitudes match at subthreshold energies $\sqrt{s} \simeq \mu_S \simeq m_N$ to high accuracy. This is a sufficient condition in the chiral framework, because the overlap of the applicability domains of the s- and u-channel iterated amplitudes are restricted to a small matching window at subthreshold energies in any case. This will be discussed in more detail in chapter 4.3. Crossing symmetry is not necessarily observed in a cutoff regularized approach. In the scheme developed here the meson-baryon scattering process is *perturbative* below the s- and u-channel unitarity thresholds by construction and therefore meets the crossing symmetry constraints approximatively. *Non-perturbative* effects as implied by the unitarization are then expected at energies outside the matching window.

¹⁰There is a further strong indication that the expansion of the inverse effective potential indeed requires a reorganization. The effective p-wave interaction kernel is troublesome, because the nucleon-pole term together with a smooth background term will lead necessarily to a non-trivial zero.

Before turning to the coupled channel formalism it is instructive to study the degree of convergence of standard χ PT. The poor convergence of the standard χ PT scheme in the $\bar{K}N$ sector will be illustrated.

3.3 Weinberg-Tomozawa interaction and convergence of χ PT

Consider the Weinberg-Tomozawa interaction term $K_{WT}(\bar{k}, k; w)$ as the driving term in the Bethe-Salpeter equation. This is an instructive example because it exemplifies the non-perturbative nature of the strangeness channels and it also serves as a transparent first test of the renormalization scheme. The on-shell equivalent scattering amplitude $\bar{T}_{WT}(w)$ is

$$\begin{aligned} V_{WT}(w) &= \left(1 - \frac{c}{4f^2} I_L\right)^{-1} \frac{c}{4f^2} \left(2\psi - 2M - I_{LR} \frac{c}{4f^2}\right) \left(1 - I_R \frac{c}{4f^2}\right)^{-1}, \\ \bar{T}_{WT}(w) &= \frac{1}{1 - V_{WT}(w) J(w)} V_{WT}(w), \quad K_{WT}(\bar{k}, k; w) = c \frac{\not{k} + \not{\bar{k}}}{4f^2}, \end{aligned} \quad (3.41)$$

where the Bethe-Salpeter scattering equation (5.8) was solved algebraically following the construction (3.6,3.7). The result is obtained by replacing the typical building blocks in (3.8) according to

$$\begin{aligned} K_R \cdot G &\rightarrow I_R, & G \cdot K_L &\rightarrow I_L, & K_R \cdot G \cdot K_L &\rightarrow I_{LR}, \\ I_L &= I_R = I_M, & I_{LR} &= (\psi - M) I_M, \end{aligned} \quad (3.42)$$

with the mesonic tadpole loop I_M introduced in (3.17). The meson-baryon loop function $J(w)$ is defined for the πN system in (3.19). The coupling constants c specify the strength of the Weinberg-Tomozawa interaction in a given meson-baryon channel with isospin I . Note that (3.41) is written in a way such that coupled channel effects are easily included by identifying the proper matrix structure of its building blocks. A detailed account of these effects will be presented in subsequent chapters. It is emphasized that the mesonic tadpole I_M cannot be absorbed systematically in f , in particular when the coupled-channel generalization of (3.41) with its non-diagonal matrix c is considered. Note that at leading chiral order Q the tadpole contribution should be dropped in the effective interaction V in any case.

It is instructive to consider the s-wave $\bar{K}N$ scattering lengths up to second order in the Weinberg-Tomozawa interaction vertex. The coefficients

$$c_{\bar{K}N \rightarrow \bar{K}N}^{(0)} = 3, \quad c_{\bar{K}N \rightarrow \bar{K}N}^{(1)} = 1, \quad (3.43)$$

lead to

$$\begin{aligned} 4\pi \left(1 + \frac{m_K}{m_N}\right) a_{\bar{K}N}^{(I=0)} &= \frac{3}{2} \frac{m_K}{f^2} \left(1 + \frac{3m_K^2}{16\pi^2 f^2} \left(\pi - \ln\left(\frac{m_K^2}{m_N^2}\right)\right)\right) + \dots, \\ 4\pi \left(1 + \frac{m_K}{m_N}\right) a_{\bar{K}N}^{(I=1)} &= \frac{1}{2} \frac{m_K}{f^2} \left(1 + \frac{m_K^2}{16\pi^2 f^2} \left(\pi - \ln\left(\frac{m_K^2}{m_N^2}\right)\right)\right) + \dots, \end{aligned} \quad (3.44)$$

where only the s-channel iteration effects following from (3.41) are included. The loop function $I_{\bar{K}N}(\sqrt{s})$ was subtracted at the nucleon mass and all tadpole contributions are dropped. Though

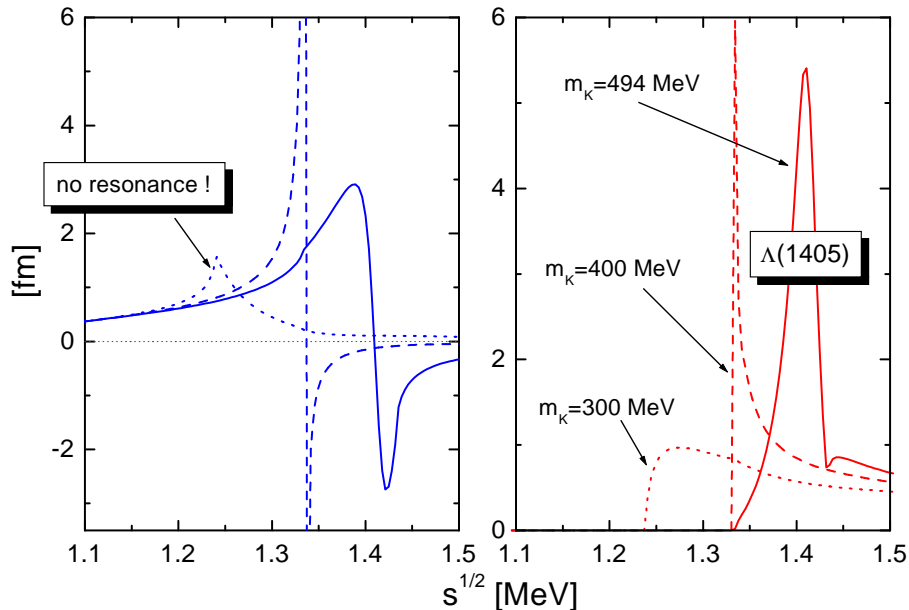


Figure 3.1: Real and imaginary part of the isospin zero s-wave K^- -nucleon scattering amplitude as it follows from the $SU(3)$ Weinberg-Tomozawa interaction term in a coupled channel calculation. It is used $f = 93$ MeV. The subtraction point is identified with the $\Lambda(1116)$ mass.

the expressions (3.44) are incomplete in the χ PT framework (terms of chiral order Q^2 and Q^3 terms are neglected) it is highly instructive to investigate the convergence property of a reduced chiral Lagrangian with the Weinberg-Tomozawa interaction only. According to (3.44) the relevant expansion parameter $m_K^2/(8\pi f^2) \simeq 1$ is about one in the $\bar{K}N$ sector. One observes the enhancement factor 2π as compared to irreducible diagrams which would lead to the typical factor $m_K^2/(4\pi f)^2$. The perturbative treatment of the Weinberg-Tomozawa interaction term is therefore unjustified and a change in approximation scheme is required. In the isospin zero $\bar{K}N$ system the Weinberg-Tomozawa interaction if iterated to all orders in the s-channel (3.41) leads to a pole in the scattering amplitude at subthreshold energies $\sqrt{s} < m_N + m_K$. This pole is a precursor of the $\Lambda(1405)$ resonance [104, 92, 65, 66, 67].

In Fig. 3.1, which was published previously in [67], the final result based on the leading interaction term of the chiral $SU(3)$ Lagrangian density as suggested by Tomozawa and Weinberg is shown. If taken as input for the multi-channel Bethe-Salpeter equation, properly furnished with a renormalization scheme leading to a subtraction point close to the baryon octet mass, a rich structure of the scattering amplitude arises [67]. Details for the coupled-channel generalization of (3.41) are presented in the subsequent chapters. Fig. 3.1 shows the s-wave solution of the multi-channel Bethe-Salpeter as a function of the kaon mass. For physical kaon masses the isospin zero scattering amplitude exhibits a resonance structure at energies where one would expect the $\Lambda(1405)$ resonance. It is pointed out that the resonance structure disappears as the kaon mass is decreased. Already at a hypothetical kaon mass of 300 MeV the $\Lambda(1405)$ resonance is no longer formed. Fig. 3.1 demonstrates that the chiral $SU(3)$ Lagrangian is necessarily non-perturbative in the strangeness sector. This confirms the findings of [65, 66]. In previous works, however, the $\Lambda(1405)$ resonance is the result of a fine-tuned cutoff parameter which gives rise to a different

kaon mass dependence of the scattering amplitude [66]. In the scheme developed here the choice of subtraction point close to the baryon octet mass follows necessarily from the compliance of the expansion scheme with approximate crossing symmetry. Moreover, the identification of the subtraction point with the Λ -mass in the isospin zero channel protects the hyperon exchange s-channel pole contribution and therefore avoids possible pathologies at subthreshold energies.

In the light of the above arguments it is important to study their possible relevance for the pion-nucleon sector. The chiral $SU(2)$ Lagrangian has been successfully applied to pion-nucleon scattering in standard chiral perturbation theory [56,57,58]. Here the typical expansion parameter $m_\pi^2/(8\pi f^2) \ll 1$ characterizing the unitarization is sufficiently small and one would expect good convergence properties. The application of the chiral $SU(3)$ Lagrangian to pion-nucleon scattering on the other hand is not completely worked out so far. In the $SU(3)$ world the πN channel couples for example to the $K\Sigma$ channel. Thus, the slow convergence of the unitarization in the $K\Sigma$ channel suggests to expand the interaction kernel rather than the scattering amplitude also in the strangeness zero channel. This may improve the convergence properties of the chiral expansion and extend its applicability domain to larger energies. Also, if the same set of parameters are to be used in the pion-nucleon and kaon-nucleon sectors the analogous partial resummation of higher order counter terms included by solving the Bethe-Salpeter equation should be applied. Such effects are illustrated for the case of the Weinberg-Tomozawa interaction. With

$$c_{\pi N \rightarrow \pi N}^{(\frac{3}{2})} = -1, \quad c_{\pi N \rightarrow K\Sigma}^{(\frac{3}{2})} = -1, \quad (3.45)$$

the isospin three half s-wave pion-nucleon scattering length, $a_{\pi N}^{(\frac{3}{2})}$, receives the typical correction terms

$$\begin{aligned} 4\pi \left(1 + \frac{m_\pi}{m_N} \right) a_{\pi N}^{(\frac{3}{2})} = & -\frac{m_\pi}{2f^2} \left(1 - \frac{m_\pi^2}{16\pi^2 f^2} \left(\pi - \ln \left(\frac{m_\pi^2}{m_N^2} \right) \right) \right) \\ & - \frac{(m_\pi + m_K)^2}{32\pi^2 f^2} \left(-1 - \frac{1}{2} \ln \left(\frac{m_K^2}{m_\Sigma^2} \right) \right) \\ & + \pi \left(\frac{3m_K}{4m_N} - \frac{m_\Sigma - m_N}{2m_K} \right) + \mathcal{O}(Q^2) \Big) + \mathcal{O}(m_\pi^2). \end{aligned} \quad (3.46)$$

Again, exclusively the unitary correction terms are considered. Note that the ratio $(m_\Sigma - m_N)/m_K$ arises in (3.46), because we first expand in powers of m_π and only then expand further with $m_\Sigma - m_N \sim Q^2$ and $m_K^2 \sim Q^2$. The correction terms in (3.46) induced by the kaon-hyperon loop, which is subtracted at the nucleon mass, exemplify the fact that the parameter f is renormalized by the strangeness sector and therefore must not be identified with the chiral limit value of f as derived for the $SU(2)$ chiral Lagrangian. This is evident if one confronts the Weinberg-Tomozawa theorem of the chiral $SU(2)$ symmetry with (3.46). The expression (3.46) demonstrates further that this renormalization of f appears poorly convergent in the kaon mass. Note in particular the anomalously large term $\pi m_K/m_N$. Hence it is advantageous to consider the partial resummation induced by a unitary coupled channel treatment of pion-nucleon scattering.

3.4 Partial-wave decomposition of the Bethe-Salpeter equation

The Bethe-Salpeter equation (5.8) can be solved analytically for quasi-local interaction terms which typically arise in the chiral Lagrangian. The scattering equation is decoupled by introducing relativistic projection operators $Y_n^{(\pm)}(\bar{q}, q; w)$ with good total angular momentum:

$$\begin{aligned}
Y_n^{(\pm)}(\bar{q}, q; w) &= \frac{1}{2} \left(\frac{\psi}{\sqrt{w^2}} \pm 1 \right) \bar{Y}_{n+1}(\bar{q}, q; w) \\
&\quad - \frac{1}{2} \left(\not{q} - \frac{w \cdot \bar{q}}{w^2} \psi \right) \left(\frac{\psi}{\sqrt{w^2}} \mp 1 \right) \left(\not{q} - \frac{w \cdot q}{w^2} \psi \right) \bar{Y}_n(\bar{q}, q; w) , \\
\bar{Y}_n(\bar{q}, q; w) &= \sum_{k=0}^{[(n-1)/2]} \frac{(-)^k (2n-2k)!}{2^n k! (n-k)! (n-2k-1)!} Y_{\bar{q}\bar{q}}^k Y_{\bar{q}q}^{n-2k-1} Y_{qq}^k , \\
Y_{\bar{q}\bar{q}} &= \frac{(w \cdot \bar{q})(\bar{q} \cdot w)}{w^2} - \bar{q} \cdot \bar{q} , \quad Y_{qq} = \frac{(w \cdot q)(q \cdot w)}{w^2} - q \cdot q , \\
Y_{\bar{q}q} &= \frac{(w \cdot \bar{q})(q \cdot w)}{w^2} - \bar{q} \cdot q .
\end{aligned} \tag{3.47}$$

For the readers convenience we provide the leading order projectors $Y_n^{(\pm)}$ relevant for the $J = \frac{1}{2}$ and $J = \frac{3}{2}$ channels explicitly:

$$\begin{aligned}
Y_0^{(\pm)}(\bar{q}, q; w) &= \frac{1}{2} \left(\frac{\psi}{\sqrt{w^2}} \pm 1 \right) , \\
Y_1^{(\pm)}(\bar{q}, q; w) &= \frac{3}{2} \left(\frac{\psi}{\sqrt{w^2}} \pm 1 \right) \left(\frac{(\bar{q} \cdot w)(w \cdot q)}{w^2} - (\bar{q} \cdot q) \right) \\
&\quad - \frac{1}{2} \left(\not{q} - \frac{w \cdot \bar{q}}{w^2} \psi \right) \left(\frac{\psi}{\sqrt{w^2}} \mp 1 \right) \left(\not{q} - \frac{w \cdot q}{w^2} \psi \right) .
\end{aligned} \tag{3.48}$$

The objects $Y_n^{(\pm)}(\bar{q}, q; w)$ are constructed to have the following convenient property: suppose that the interaction kernel K in (5.8) can be expressed as linear combinations of the $Y_n^{(\pm)}(\bar{q}, q; w)$ with a set of coupling functions $V^{(\pm)}(\sqrt{s}, n)$, which may depend on the variable s ,

$$K(\bar{k}, k; w) = \sum_{n=0}^{\infty} \left(V^{(+)}(\sqrt{s}; n) Y_n^{(+)}(\bar{q}, q; w) + V^{(-)}(\sqrt{s}; n) Y_n^{(-)}(\bar{q}, q; w) \right) \tag{3.49}$$

with $w = p + q$, $k = (p - q)/2$ and $\bar{k} = (\bar{p} - \bar{q})/2$. Then in a given isospin channel the unique solution reads

$$\begin{aligned}
T(\bar{k}, k; w) &= \sum_{n=0}^{\infty} \left(M^{(+)}(\sqrt{s}; n) Y_n^{(+)}(\bar{q}, q; w) + M^{(-)}(\sqrt{s}; n) Y_n^{(-)}(\bar{q}, q; w) \right) , \\
M^{(\pm)}(\sqrt{s}; n) &= \frac{V^{(\pm)}(\sqrt{s}; n)}{1 - V^{(\pm)}(\sqrt{s}; n) J^{(\pm)}(\sqrt{s}; n)} ,
\end{aligned} \tag{3.50}$$

with a set of divergent loop functions $J_{\pi N}^{(\pm)}(\sqrt{s}; n)$ defined by

$$\begin{aligned}
J_{\pi N}^{(\pm)}(\sqrt{s}; n) Y_n^{(\pm)}(\bar{q}, q; w) &= -i \int \frac{d^4 l}{(2\pi)^4} Y_n^{(\pm)}(\bar{q}, l; w) S_N(w - l) \\
&\quad \times D_{\pi}(l) Y_n^{(\pm)}(l, q; w) .
\end{aligned} \tag{3.51}$$

It is underlined that the definition of the loop functions in (3.51) is non trivial, because it assumes that $Y_n^{(\pm)} \cdot G \cdot Y_n^{(\pm)}$ is indeed proportional to $Y_n^{(\pm)}$. An explicit derivation of this property, which is in fact closely linked to our renormalization scheme, is given in [97]. Recall that the loop functions $J_{\pi N}^{(\pm)}(\sqrt{s}; n)$, which are badly divergent, have a finite and well-defined imaginary part

$$\Im J_{\pi N}^{(\pm)}(\sqrt{s}; n) = \frac{p_{\pi N}^{2n+1}}{8\pi\sqrt{s}} \left(\frac{\sqrt{s}}{2} + \frac{m_N^2 - m_\pi^2}{2\sqrt{s}} \pm m_N \right). \quad (3.52)$$

It will be specified how to renormalize the loop functions. In dimensional regularization the loop functions can be written as linear combinations of scalar one loop functions $I_{\pi N}(\sqrt{s})$, I_π , I_N and $I^{(n)}$,

$$I^{(n)} = i \int \frac{d^4 l}{(2\pi)^4} (l^2)^n, \quad (3.53)$$

According to our renormalization procedure we drop $I^{(n)}$, the tadpole contributions I_π , I_N and replace $I_{\pi N}(s)$ by $I_{\pi N}(\sqrt{s}) - I_{\pi N}(\mu_S)$. This leads to

$$\begin{aligned} J_{\pi N}^{(\pm)}(\sqrt{s}; n) &= p_{\pi N}^{2n}(\sqrt{s}) \left(\frac{\sqrt{s}}{2} + \frac{m_N^2 - m_\pi^2}{2\sqrt{s}} \pm m_N \right) \Delta I_{\pi N}(\sqrt{s}), \\ \Delta I_{\pi N}(\sqrt{s}) &= I_{\pi N}(\sqrt{s}) - I_{\pi N}(\mu_S), \end{aligned} \quad (3.54)$$

with the master loop function $I_{\pi N}(\sqrt{s})$ and $p_{\pi N}(\sqrt{s})$ given in (3.20). In the center of mass frame $p_{\pi N}$ represents the relative momentum. It is to be emphasized that the loop functions $J_{\pi N}^{(\pm)}(\sqrt{s}; n)$ are renormalized in accordance with (3.37) and (3.35) where $\mu_S = m_N^{11}$. This leads to tadpole-free loop functions and also to $M^{(\pm)}(m_N, n) = V^{(\pm)}(m_N, n)$. The behavior of the loop functions $J_{\pi N}^{(\pm)}(\sqrt{s}, n)$ close to threshold

$$\Im J_{\pi N}^{(+)}(\sqrt{s}, n) \sim p_{\pi N}^{2n+1}, \quad \Im J_{\pi N}^{(-)}(\sqrt{s}, n) \sim p_{\pi N}^{2n+3}, \quad (3.55)$$

already tells the angular momentum, l , of a given channel with $l = n$ for the $'+''$ and $l = n + 1$ for the $'-'$ channel.

It is instructive to compare the form of the unitarity loop functions (3.54) with those suggested by Oller and Meissner [68] as they arise in the N/D method of Chew and Mandelstam [107]. Despite the conceptual differences it is useful to compare the form of the final unitarity loop functions generated by the two schemes. In any approach that is unitary the partial wave amplitudes, $M^{(\pm)}(\sqrt{s}; n)$, may be cast into the form (3.50). Therefore different schemes may be compared at the level of the unitarity loop function $J^{(\pm)}(\sqrt{s}; n)$ and the effective interaction kernel $V^{(\pm)}(\sqrt{s}; n)$. It is evident that, once the precise form of the unitarity loop functions $J^{(\pm)}(\sqrt{s}, n)$ is specified it is well defined how to evaluate the effective interaction kernel in perturbation theory. In [105, 106, 68] it was suggested to take

$$\frac{p_{\pi N}^{2l+1}}{8\pi\sqrt{s}}, \quad (3.56)$$

¹¹ Note that consistency with the renormalization condition (3.37) requires a further subtraction in the loop function $J_{\pi N}^{(-)}(\sqrt{s}, 0)$ if the potential $V_{\pi N}^{(-)}(\sqrt{s}, 0) \sim 1/(s - m_N^2 + i\epsilon)$ exhibits the s-channel nucleon pole (see (3.38)).

as the imaginary part of the unitarity loop function of given angular momentum l and then reconstruct the real part of the loop function by means of a subtracted dispersion-integral representation. That requires the determination of $l+1$ subtraction constants [105], which leads to a flood of free parameters that are not controlled systematically by the chiral SU(3) symmetry. This is particularly cumbersome when dealing with many coupled channels all of which would require a priori independent subtraction coefficients. On the other hand, in the scheme developed here the application of dimensional regularization strongly constrains the subtraction procedure leaving one universal subtraction point μ_S which is fixed by the requirement that chiral counting rules and approximative crossing symmetry hold. Here the construction of the covariant projection operators (3.47) proves particularly useful since by means of those it is possible to apply dimensional regularization required to control the subtraction parameters in conformity with symmetry constraints. It was demonstrated that all reduced tadpole contributions (see e.g. (3.19)) must be moved into the effective interaction $V^{(\pm)}(\sqrt{s}; n)$ as to avoid an anomalous chiral power of the baryon mass renormalization which otherwise would arise when solving the scattering equation. An independent argument that lead to the same renormalization requirement was based on the observation that the orthogonality of covariant projectors with different total angular momentum J follows only if all reduced tadpole contributions are considered as part of the effective interaction. A further important difference are the prefactors $E_N \pm m_N$ in (3.54), which are required in a covariant scheme but were dropped in [68]. If those factors would be restored into the scheme of Oller and Meissner, already the s-wave unitarity loop function required two subtraction constants.

The Bethe-Salpeter equation (3.50) decouples into reduced scattering amplitudes $M^{(\pm)}(\sqrt{s}, n)$ with well-defined angular momentum. In order to unambiguously identify the total angular momentum J we recall the partial-wave decomposition of the on-shell scattering amplitude [84]. The latter amplitude T is decomposed into invariant amplitudes $F_{\pm}^{(I)}(s, t)$ carrying good isospin,

$$T = \sum_I \left(\frac{1}{2} \left(\frac{\psi}{\sqrt{w^2}} + 1 \right) F_+^{(I)}(s, t) + \frac{1}{2} \left(\frac{\psi}{\sqrt{w^2}} - 1 \right) F_-^{(I)}(s, t) \right) P_I, \quad (3.57)$$

where $s = (p + q)^2 = w^2$ and $t = (\bar{q} - q)^2$ and P_I are the isospin projectors introduced in (3.5). The choice of invariant amplitudes is not unique. The particular choice used in (3.57) is particularly convenient to make contact with the covariant projection operators (3.47). For different choices, see [84]. The amplitudes $F_{\pm}(s, t)$ are decomposed into partial-wave amplitudes $f_{J=l\pm\frac{1}{2}}^{(l)}(s)$ with [84]:

$$\begin{aligned} F_+(s, t) &= \frac{8\pi\sqrt{s}}{E + m_N} \sum_{n=1}^{\infty} \left(f_{J=n+\frac{1}{2}}^{(n-1)}(\sqrt{s}) - f_{J=n-\frac{1}{2}}^{(n+1)}(\sqrt{s}) \right) P'_n(\cos\theta), \\ F_-(s, t) &= \frac{8\pi\sqrt{s}}{E - m_N} \sum_{n=1}^{\infty} \left(f_{J=n-\frac{1}{2}}^{(n)}(\sqrt{s}) - f_{J=n+\frac{1}{2}}^{(n)}(\sqrt{s}) \right) P'_n(\cos\theta), \\ P'_n(\cos\theta) &= \sum_{k=0}^{[(n-1)/2]} \frac{(-)^k (2n-2k)!}{2^n k! (n-k)! (n-2k-1)!} (\cos\theta)^{n-2k-1}, \end{aligned} \quad (3.58)$$

where $[n/2] = (n-1)/2$ for n odd and $[n/2] = n/2$ for n even. $P'_n(z)$ is the derivative of the Legendre polynomials. In the center of mass frame E represents the nucleon energy and θ the

scattering angle:

$$E = \frac{1}{2} \sqrt{s} + \frac{m_N^2 - m_\pi^2}{2\sqrt{s}}, \quad t = (\bar{q} - q)^2 = -2p_{\pi N}^2 (1 - \cos \theta). \quad (3.59)$$

The unitarity condition formulated for the partial-wave amplitudes $f_J^{(l)}$ leads to their representation in terms of the scattering phase shifts $\delta_J^{(l)}$

$$p_{\pi N} f_{J=l\pm\frac{1}{2}}^{(l)}(\sqrt{s}) = \frac{1}{2i} \left(e^{2i\delta_{J=l\pm\frac{1}{2}}^{(l)}(s)} - 1 \right) = \frac{1}{\cot \delta_{J=l\pm\frac{1}{2}}^{(l)}(s) - i}. \quad (3.60)$$

One can now match the reduced amplitudes $M_n^{(\pm)}(s)$ of (3.50) and the partial-wave amplitudes $f_{J=l\pm\frac{1}{2}}^{(l)}(s)$

$$f_{J=l\pm\frac{1}{2}}^{(l)}(\sqrt{s}) = \frac{p_{\pi N}^{2J-1}}{8\pi\sqrt{s}} \left(\frac{\sqrt{s}}{2} + \frac{m_N^2 - m_\pi^2}{2\sqrt{s}} \pm m_N \right) M^{(\pm)}(\sqrt{s}, J - \frac{1}{2}). \quad (3.61)$$

It is useful to consider the basic building block $\bar{Y}_n(\bar{q}, q; w)$ of the covariant projectors $Y_n^{(\pm)}(\bar{q}, q; w)$ in (3.47) and observe the formal similarity with $P'_n(\cos \theta)$ in (3.58). In fact in the center of mass frame with $w_{cm} = (\sqrt{s}, 0)$ one finds $p_{\pi N}^{2n-2} P'_n(\cos \theta) = Y_n(\bar{q}, q; w_{cm})$. This observation leads to a straightforward proof of (3.50) and (3.51). It is sufficient to prove the loop-orthogonality of the projectors in the center of mass frame, because they are free of kinematical singularities [97]. One readily finds that the imaginary part of the unitary products $Y_n^{(\pm)} G Y_m^{(\pm)}$ vanish unless both projectors are the same. It follows that the unitary product of projectors which are expected to be orthogonal can at most be a real polynomial involving the tadpole functions I_π, I_N and $I^{(n)}$. Then the renormalization procedure as described in chapter 3.2 leads to (3.50) and (3.51). It is emphasized that the argument relies crucially on the fact that the projectors are free of kinematical singularities in q and \bar{q} . This implies in particular that the object $Y_n(\bar{q}, q; w)$ must not be identified with $p_{\pi N}^{2n-2} P'_n(\cos \theta)$ as one may expect naively.

It is necessary to return to the assumption made in (3.49) that the interaction kernel K can be decomposed in terms of the covariant projectors. Of course this is not possible for a general interaction kernel K . It is pointed out, however, that the set of projectors (3.47) can be used to introduce a particular notion of on-shell irreducibility defining what is meant with \bar{K} in (3.6). The on-shell irreducible kernel \bar{K} is identified by decomposing the interaction kernel according to

$$\begin{aligned} \bar{K}^{(I)}(\bar{q}, q; w) &= \sum_{n=0}^{\infty} \left(\bar{K}_+^{(I)}(\sqrt{s}; n) Y_n^{(+)}(\bar{q}, q; w) + \bar{K}_-^{(I)}(\sqrt{s}; n) Y_n^{(-)}(\bar{q}, q; w) \right), \\ \bar{K}_\pm^{(I)}(\sqrt{s}; n) &= \int_{-1}^1 \frac{dz}{2} \frac{K_\pm^{(I)}(s, t)}{p_{\pi N}^{2n}} P_n(z) \\ &\quad + \int_{-1}^1 \frac{dz}{2} \left(\frac{1}{2} \sqrt{s} + \frac{m_N^2 - m_\pi^2}{2\sqrt{s}} \mp m_N \right)^2 \frac{K_\mp^{(I)}(s, t)}{p_{\pi N}^{2n+2}} P_{n+1}(z), \end{aligned} \quad (3.62)$$

where $t = -2p_{\pi N}^2(1 - x)$ and $K_\pm^{(I)}(s, t)$ follows from the decomposition of the interaction kernel K into the scalar components $K_\pm^{(I)}(s, t)$,

$$K^{(I)}(\bar{q}, q; w) \Big|_{\text{on-shell}} = \frac{1}{2} \left(\frac{\psi}{\sqrt{w^2}} + 1 \right) K_+^{(I)}(s, t) + \frac{1}{2} \left(\frac{\psi}{\sqrt{w^2}} - 1 \right) K_-^{(I)}(s, t). \quad (3.63)$$

Then $K - \bar{K}$ is on-shell reducible by construction and therefore can be decomposed into K_L , K_R and K_{LR} . The decomposition in (3.62) generalizes the partial wave decomposition of the scattering kernel, usually defined only in the center of mass frame. Now, with a well defined notion of on-shell irreducibility, that complies with (3.12), one can apply (3.13) to set up a systematic expansion of the on-shell reduced effective scattering kernel V_{eff} . The merit of the formulation presented here lies in the fact that for a given choice of the chiral Lagrangian it is in principal straight forward to reconstruct the off-shell part of the scattering amplitude as it may be required for calculations of higher n-point Green's functions or current-current correlation functions. If one aims at an evaluation of the on-shell scattering amplitudes only it is of course equivalent to evaluate the partial wave amplitudes $M^{(\pm)}(\sqrt{s}, n)$ to a given order and derive from the representation (3.50) the effective interaction $V_{\text{eff}}^{(\pm)}(\sqrt{s}, n)$ to that same order. The latter calculational scheme relies of course on the form of the loop functions as derived above.

Chapter 4

SU(3) coupled-channel dynamics

The Bethe-Salpeter equation (5.8) is readily generalized for a coupled channel system. The chiral $SU(3)$ Lagrangian with baryon octet and pseudo-scalar meson octet couples the $\bar{K}N$ system to five inelastic channels $\pi\Sigma$, $\pi\Lambda$, $\eta\Lambda$, $\eta\Sigma$ and $K\Xi$ and the πN system to the three channels $K\Sigma$, ηN and $K\Lambda$. The strangeness plus one sector with the KN channel is treated separately in chapter 4.3 when discussing constraints from crossing symmetry. For simplicity good isospin symmetry is assumed in the following discussion. How to deal with isospin symmetry breaking effects is described in [97]. In order to set up a convenient notation consider for example the two-body meson-baryon interaction terms in (2.22) in momentum space. The Lagrangian density $\mathcal{L}(x)$ in coordinate space is related to its momentum space representation through

$$\begin{aligned}\int d^4x \mathcal{L}(x) &= \int \frac{d^4k}{(2\pi)^4} \frac{d^4\bar{k}}{(2\pi)^4} \frac{d^4w}{(2\pi)^4} \mathcal{L}(\bar{k}, k; w), \\ R(q, p) &= \int d^4x d^4y e^{-iqx - ipy} \Phi(x) B(y),\end{aligned}\quad (4.1)$$

where the bilinear field $R(q, p)$ is introduced in terms of the meson and baryon fields $\Phi(x)$ and $B(y)$. In momentum space $\mathcal{L}(\bar{k}, k; w)$ determines the scattering kernel $K(\bar{k}, k; w)$ as is required for the Bethe-Salpeter equation rather directly in the following way

$$\begin{aligned}\mathcal{L}(\bar{k}, k; w) &= \sum_{I=0, \frac{1}{2}, 1, \frac{3}{2}} R^{(I)\dagger}(\bar{q}, \bar{p}) \gamma_0 K^{(I)}(\bar{k}, k; w) R^{(I)}(q, p), \\ R^{(0)} &= \begin{pmatrix} \frac{1}{\sqrt{2}} K^\dagger N \\ \frac{1}{\sqrt{3}} \vec{\pi}_c \vec{\Sigma} \\ \eta_c \Lambda \\ \frac{1}{\sqrt{2}} K^t i \sigma_2 \Xi \end{pmatrix}, \quad \vec{R}^{(1)} = \begin{pmatrix} \frac{1}{\sqrt{2}} K^\dagger \vec{\sigma} N \\ \frac{1}{i\sqrt{2}} \vec{\pi}_c \times \vec{\Sigma} \\ \vec{\pi}_c \Lambda \\ \eta_c \vec{\Sigma} \\ \frac{1}{\sqrt{2}} K^t i \sigma_2 \vec{\sigma} \Xi \end{pmatrix}, \\ R^{(\frac{1}{2})} &= \begin{pmatrix} \frac{1}{\sqrt{3}} \pi_c \cdot \sigma N \\ \frac{1}{\sqrt{3}} \Sigma \cdot \sigma K \\ \eta_c N \\ K \Lambda \end{pmatrix}, \quad R^{(\frac{3}{2})} = \begin{pmatrix} \pi_c \cdot S N \\ \Sigma \cdot S K \end{pmatrix}.\end{aligned}\quad (4.2)$$

In (4.2) the pion field and the eta field are decomposes with $\vec{\pi} = \vec{\pi}_c + \vec{\pi}_c^\dagger$ and $\eta = \eta_c + \eta_c^\dagger$ ¹. Also the isospin decomposition of (2.11) is applied. The isospin 1/2 to 3/2 transition matrices S_i in (4.2) are normalized by $S_i^\dagger S_j = \delta_{ij} - \sigma_i \sigma_j / 3$.

The merit of the notation (4.2) is threefold. First, the phase convention for the isospin states is specified. Second, it defines the convention for the interaction kernel K in the Bethe-Salpeter equation. Last it provides also a convenient scheme to read off the isospin decomposition for the interaction kernel K directly from the interaction Lagrangian (see [97]). The coupled channel Bethe-Salpeter matrix equation reads

$$\begin{aligned} T_{ab}^{(I)}(\bar{k}, k; w) &= K_{ab}^{(I)}(\bar{k}, k; w) + \sum_{c,d} \int \frac{d^4l}{(2\pi)^4} K_{ac}^{(I)}(\bar{k}, l; w) G_{cd}^{(I)}(l; w) T_{db}^{(I)}(l, k; w), \\ G_{cd}^{(I)}(l; w) &= -i D_{\Phi(I,d)}(\frac{1}{2}w - l) S_{B(I,d)}(\frac{1}{2}w + l) \delta_{cd} \end{aligned} \quad (4.3)$$

where $D_{\Phi(I,d)}(q)$ and $S_{B(I,d)}(p)$ denote the meson propagator and baryon propagator respectively for a given channel d with isospin I . The matrix structure of the coupled-channel interaction kernel $K_{ab}(\bar{k}, k; w)$ is defined via (4.2) and

$$\begin{aligned} \Phi(0, a) &= (\bar{K}, \pi, \eta, K)_a, & B(0, a) &= (N, \Sigma, \Lambda, \Xi)_a, \\ \Phi(1, a) &= (\bar{K}, \pi, \pi, \eta, K)_a, & B(1, a) &= (N, \Sigma, \Lambda, \Sigma, \Xi)_a, \\ \Phi(\frac{1}{2}, a) &= (\pi, K, \eta, K)_a, & B(\frac{1}{2}, a) &= (N, \Sigma, N, \Lambda)_a, \\ \Phi(\frac{3}{2}, a) &= (\pi, K)_a, & B(\frac{3}{2}, a) &= (N, \Sigma)_a. \end{aligned} \quad (4.4)$$

The on-shell equivalent coupled channel interaction kernel V_{eff} of (3.8,3.13) will be constructed. To leading chiral orders it is legitimate to identify $V_{ab}^{(I)}$ with $\bar{K}_{ab}^{(I)}$ of (3.6), because the loop corrections in (3.8) are of minimal chiral power Q^3 (see (2.5)). To chiral order Q^3 the interaction kernel receives additional terms from one loop diagrams involving the on-shell reducible interaction kernels $K_{L,R}$ as well as from irreducible one-loop diagrams. In the notation of (3.6) one finds

$$V = \bar{K} + K_R \cdot G \cdot \bar{K} + \bar{K} \cdot G \cdot K_L + K_R \cdot G \cdot K_L + \mathcal{O}(Q^4). \quad (4.5)$$

Typically the Q^3 terms induced by $K_{L,R}$ in (4.5) are tadpoles (see e.g. (3.18,3.41)). The only non-trivial contribution arise from the on-shell reducible parts of the u-channel baryon octet terms. However, by construction those contributions have the same form as the irreducible Q^3 loop-correction terms of \bar{K} . In particular they do not show the typical enhancement factor of 2π associated with the s-channel unitarity cuts. In the large- N_c limit all loop correction terms to V are necessarily suppressed by $1/N_c$. This follows, because any hadronic loop function if visualized in terms of quark-gluon diagrams involves at least one quark-loop, which in turn is $1/N_c$ suppressed [87, 88]. Thus, it is legitimate to take $V = \bar{K}$ in this work.

¹ For a neutral scalar field $\phi(x) = \phi_c(x) + \phi_c^\dagger(x)$ with mass m we write

$$\phi_c(0, \vec{x}) = \int \frac{d^3k}{(2\pi)^3} \frac{e^{i\vec{k}\cdot\vec{x}}}{2\omega_k} a(\vec{k}), \quad \phi_c^\dagger(0, \vec{x}) = \int \frac{d^3k}{(2\pi)^3} \frac{e^{-i\vec{k}\cdot\vec{x}}}{2\omega_k} a^\dagger(\vec{k})$$

where $\omega_k = (m^2 + \vec{k}^2)^{\frac{1}{2}}$ and $[a(k), a^\dagger(k')]_- = (2\pi)^3 2\omega_k \delta^3(k - k')$. In (4.2) terms are suppressed which do not contribute to the two-body scattering process at tree-level. For example terms like $\bar{N} \eta_c N \eta_c$ or $\bar{N} \eta_c^\dagger N \eta_c^\dagger$ are dropped.

The baryon octet and decuplet exchange contributions ask for special attention. Individually the baryon exchange diagrams are of forbidden order N_c . Only the complete large- N_c baryon ground state multiplet with $J = (\frac{1}{2}, \dots, \frac{N_c}{2})$ leads to an exact cancellation and a scattering amplitude of order N_c^0 [126]. However this cancellation persists only in the limit of degenerate baryon octet $\overset{\circ}{m}_{[8]}$ and decuplet mass $\overset{\circ}{m}_{[10]}$. With $m_\pi < \overset{\circ}{m}_{[10]} - \overset{\circ}{m}_{[8]}$ the cancellation is incomplete and thus leads to an enhanced sensitivity of the scattering amplitude on the physical baryon-exchange contributions. Therefore one should sum the $1/N_c$ suppressed contributions of the form

$$\left(\frac{\overset{\circ}{m}_{[10]} - \overset{\circ}{m}_{[8]}}{m_\pi} \right)^n \sim \frac{1}{N_c^n}. \quad (4.6)$$

This is taken into account by evaluating the baryon-exchange contributions to subleading chiral orders but avoid the expansion in either $(\overset{\circ}{m}_{[10]} - \overset{\circ}{m}_{[8]})/m_\pi$ or $m_\pi/(\overset{\circ}{m}_{[10]} - \overset{\circ}{m}_{[8]})$. We also include the $SU(3)$ symmetry-breaking counter terms of the 3-point meson-baryon vertices and the quasi-local two-body counter terms of chiral order Q^3 which are leading in the $1/N_c$ expansion. Note that the quasi-local two-body counter terms of large chiral order are not necessarily suppressed by $1/N_c$ relatively to the terms of low chiral order. This is plausible, because for example a t-channel vector-meson exchange, which has a definite large- N_c scaling behavior, leads to contributions in all partial waves. Thus, quasi-local counter terms with different partial-wave characteristics may have identical large- N_c scaling behavior even though they carry different chiral powers. In chapter 3.3 it was observed that reducible diagrams are enhanced close to their unitarity threshold. The typical enhancement factor of 2π per unitarity cut, measured relatively to irreducible diagrams (see (3.44)), is larger than the number of colors $N_c = 3$ of our world. Therefore it is justified to perform the partial $1/N_c$ resummation of all reducible diagrams implied by solving the on-shell reduced Bethe-Salpeter equation (3.7).

By analogy with (3.50) the coupled-channel scattering amplitudes $T_{ab}^{(I)}$ are decomposed into their on-shell equivalent partial-wave amplitudes $M_{ab}^{(I,\pm)}$

$$\begin{aligned} \bar{T}_{ab}^{(I)}(\bar{k}, k; w) &= \sum_{n=0}^{\infty} M_{ab}^{(I,+)}(\sqrt{s}; n) Y_n^{(+)}(\bar{q}, q; w) \\ &+ \sum_{n=0}^{\infty} M_{ab}^{(I,-)}(\sqrt{s}; n) Y_n^{(-)}(\bar{q}, q; w), \end{aligned} \quad (4.7)$$

where $k = \frac{1}{2}w - q$ and $\bar{k} = \frac{1}{2}w - \bar{q}$ and $s = w_\mu w^\mu$. The covariant projectors $Y_n^{(\pm)}(\bar{q}, q; w)$ were introduced in (3.47). Equations for the differential cross sections as expressed in terms of the partial-wave amplitudes $M_{ab}^{(\pm)}$ can be found in [97]. The form of the scattering amplitude (4.7) follows, because the effective interaction kernel $V_{ab}^{(I)}$ of (3.8) is decomposed accordingly

$$\begin{aligned} V_{ab}^{(I)}(\bar{k}, k; w) &= \sum_{n=0}^{\infty} V_{ab}^{(I,+)}(\sqrt{s}; n) Y_n^{(+)}(\bar{q}, q; w) \\ &+ \sum_{n=0}^{\infty} V_{ab}^{(I,-)}(\sqrt{s}; n) Y_n^{(-)}(\bar{q}, q; w). \end{aligned} \quad (4.8)$$

The coupled-channel Bethe-Salpeter equation (4.3) reduces to a convenient matrix equation for the effective interaction kernel $V_{ab}^{(I)}$ and the invariant amplitudes $M_{ab}^{(I,\pm)}$

$$M_{ab}^{(I,\pm)}(\sqrt{s}; n) = V_{ab}^{(I,\pm)}(\sqrt{s}; n)$$

$$+ \sum_{c,d} V_{ac}^{(I,\pm)}(\sqrt{s}; n) J_{cd}^{(I,\pm)}(\sqrt{s}; n) M_{db}^{(I,\pm)}(\sqrt{s}; n), \quad (4.9)$$

which is readily solved with:

$$M_{ab}^{(I,\pm)}(\sqrt{s}; n) = \left[\left(1 - V^{(I,\pm)}(\sqrt{s}; n) J^{(I,\pm)}(\sqrt{s}; n) \right)^{-1} V^{(I,\pm)}(\sqrt{s}; n) \right]_{ab}. \quad (4.10)$$

It remains to specify the coupled-channel loop matrix function $J_{ab}^{(I,\pm)} \sim \delta_{ab}$, which is diagonal in the coupled channel space. The diagonal elements read

$$\begin{aligned} J_{aa}^{(I,\pm)}(\sqrt{s}; n) &= \left(\frac{\sqrt{s}}{2} + \frac{m_{B(I,a)}^2 - m_{\Phi(I,a)}^2}{2\sqrt{s}} \pm m_{B(I,a)} \right) \Delta I_{\Phi(I,a)B(I,a)}^{(k)}(\sqrt{s}) \\ &\times \left(\frac{s}{4} - \frac{m_{B(I,a)}^2 + m_{\Phi(I,a)}^2}{2} + \frac{(m_{B(I,a)}^2 - m_{\Phi(I,a)}^2)^2}{4s} \right)^n, \\ \Delta I_{\Phi(I,a)B(I,a)}^{(k)}(\sqrt{s}) &= I_{\Phi(I,a)B(I,a)}(\sqrt{s}) \\ &- \sum_{l=0}^k \frac{1}{l} (\sqrt{s} - \mu_S)^l \left(\frac{\partial}{\partial \sqrt{s}} \right)^l \Big|_{\sqrt{s}=\mu_S} I_{\Phi(I,a)B(I,a)}(\sqrt{s}). \end{aligned} \quad (4.11)$$

The index a labels a specific channel consisting of a meson-baryon pair of given isospin $(\Phi(I, a), B(I, a))$. In particular $m_{\Phi(I,a)}$ and $m_{B(I,a)}$ denote the empirical isospin averaged meson and baryon octet mass respectively. The scalar master-loop integral, $I_{\Phi(I,a)B(I,a)}(\sqrt{s})$, was introduced explicitly in (3.20) for the pion-nucleon channel. Note that we do not use the expanded form of (3.21). The subtraction point is identified with $\mu_S = m_\Lambda$ and $\mu_S = m_\Sigma$ in the isospin zero and isospin one channel respectively so as to protect the hyperon s-channel pole structures. Similarly we use $\mu_S = m_N$ in the pion-nucleon sectors. In the p-wave loop functions $J^{(-)}(\sqrt{s}, 0)$ and $J^{(+)}(\sqrt{s}, 1)$ a double subtraction of the internal master-loop function with $k = 1$ in (4.11) is performed whenever a large- N_c baryon ground state manifests itself with a s-channel pole contribution in the associated partial-wave scattering amplitude. In all remaining channels it is used $k = 0$ in (4.11). This leads to consistency with the renormalization condition (3.37), in particular in the large- N_c limit with $m_{[8]} = m_{[10]}$.

The on-shell irreducible interaction kernel $\bar{K}_{ab}^{(I)}$ in (4.5) needs to be identified. The result (3.62) is generalized to the case of inelastic scattering. This leads to the matrix structure of the interaction kernel K_{ab} defined in (4.2). In a given partial wave the effective interaction kernel $\bar{K}_{ab}^{(I,\pm)}(\sqrt{s}; n)$ reads:

$$\begin{aligned} \bar{K}_{ab}^{(I)} &= \sum_{n=0}^{\infty} \left(\bar{K}_{ab}^{(I,+)}(\sqrt{s}; n) Y_n^{(+)}(\bar{q}, q; w) + \bar{K}_{ab}^{(I,-)}(\sqrt{s}; n) Y_n^{(-)}(\bar{q}, q; w) \right), \\ \bar{K}_{ab}^{(I,\pm)}(\sqrt{s}; n) &= \int_{-1}^1 \frac{dz}{2} \frac{K_{ab}^{(I,\pm)}(s, t_{ab}^{(I)})}{(p_a^{(I)} p_b^{(I)})^n} P_n(z) \\ &+ \int_{-1}^1 \frac{dz}{2} \left(E_a^{(I)} \mp m_{B(I,a)} \right) \left(E_b^{(I)} \mp m_{B(I,b)} \right) \frac{K_{ab}^{(I,\mp)}(s, t_{ab}^{(I)})}{(p_a^{(I)} p_b^{(I)})^{n+1}} P_{n+1}(z), \end{aligned} \quad (4.12)$$

where $P_n(z)$ are the Legendre polynomials and

$$\begin{aligned} t_{ab}^{(I)} &= m_{\Phi(I,a)}^2 + m_{\Phi(I,b)}^2 - 2\omega_a^{(I)}\omega_b^{(I)} + 2p_a^{(I)}p_b^{(I)}z, \quad E_a^{(I)} = \sqrt{s} - \omega_a^{(I)}, \\ \omega_a^{(I)} &= \frac{s + m_{\Phi(I,a)}^2 - m_{B(I,a)}^2}{2\sqrt{s}}, \quad \left(p_a^{(I)}\right)^2 = \left(\omega_a^{(I)}\right)^2 - m_{\Phi(I,a)}^2. \end{aligned} \quad (4.13)$$

The construction of the on-shell irreducible interaction kernel requires the identification of the invariant amplitudes $K_{ab}^{(I,\pm)}(s,t)$ in a given channel ab :

$$K_{ab}^{(I)} \Big|_{\text{on-sh.}} = \frac{1}{2} \left(\frac{\psi}{\sqrt{w^2}} + 1 \right) K_{ab}^{(I,+)}(s,t) + \frac{1}{2} \left(\frac{\psi}{\sqrt{w^2}} - 1 \right) K_{ab}^{(I,-)}(s,t). \quad (4.14)$$

It is underlined that the approach developed here deviates from the common chiral expansion scheme as implied by the heavy-fermion representation of the chiral Lagrangian. A strict chiral expansion of the unitarity loop function $I_{\Phi(I,a)B(I,a)}(\sqrt{s})$ does not reproduce the correct s -channel unitarity cut. One must perform an infinite summation of interaction terms in the heavy-fermion chiral Lagrangian to recover the correct threshold behavior. This is achieved more conveniently by working directly with the manifest relativistic scheme, where it is natural to write down the loop functions in terms of the physical masses. In this work results are systematically expressed in terms of physical parameters avoiding the use of bare parameters like $\hat{m}_{[8]}$ whenever possible.

4.1 Construction of the effective interaction kernel

After having specified the basic ingredients of the chiral coupled channel approach it is necessary to collect all terms of the chiral Lagrangian as they contribute to the interaction kernel $K_{ab}^{(I)}(\bar{k}, k; w)$ of (4.3) to chiral order Q^3 :

$$\begin{aligned} K^{(I)}(\bar{k}, k; w) &= K_{WT}^{(I)}(\bar{k}, k; w) + K_{s-[8]}^{(I)}(\bar{k}, k; w) + K_{u-[8]}^{(I)}(\bar{k}, k; w) \\ &+ K_{s-[10]}^{(I)}(\bar{k}, k; w) + K_{u-[10]}^{(I)}(\bar{k}, k; w) + K_{s-[9]}^{(I)}(\bar{k}, k; w) \\ &+ K_{u-[9]}^{(I)}(\bar{k}, k; w) + K_{[8][8]}^{(I)}(\bar{k}, k; w) + K_{\chi}^{(I)}(\bar{k}, k; w). \end{aligned} \quad (4.15)$$

The contributions to the interaction kernel will be written in a form which facilitates the derivation of $K_{ab}^{(I,\pm)}(s,t)$ in (4.12). It is then straightforward to derive the on-shell irreducible interaction kernel V .

To start the discussion of the various terms in (4.15) consider the Weinberg-Tomozawa interaction term $K_{WT}^{(I)}$ in (2.10). To chiral order Q^3 the effects of the baryon wave-function renormalization factors \mathcal{Z} and of further counter terms introduced in (2.36) must be considered. All together one finds

$$\left[K_{WT}^{(I)}(\bar{k}, k; w) \right]_{ab} = \left[C_{WT}^{(I)} \right]_{ab} \left(1 + \frac{1}{2} \Delta\zeta_{B(I,a)} + \frac{1}{2} \Delta\zeta_{B(I,b)} \right) \frac{\not{q} + \not{q}'}{4f^2}. \quad (4.16)$$

The dimensionless coefficient matrix $C_{WT}^{(I)}$ of the Weinberg-Tomozawa interaction is given in Tab. 4.1 for the strangeness minus one channels and in [97] for the strangeness zero channels. The constants $\Delta\zeta_{B(c)}$ in (4.16) receive contributions from the baryon octet wave-function

renormalization factors \mathcal{Z} and the parameters ζ_0, ζ_D and ζ_F of (2.36):

$$\begin{aligned}
\Delta\zeta &= \zeta + \mathcal{Z} - 1 + \dots, \\
\zeta_N &= (\zeta_0 + 2\zeta_F) m_\pi^2 + (2\zeta_0 + 2\zeta_D - 2\zeta_F) m_K^2, \\
\zeta_\Lambda &= (\zeta_0 - \frac{2}{3}\zeta_D) m_\pi^2 + (2\zeta_0 + \frac{8}{3}\zeta_D) m_K^2, \\
\zeta_\Sigma &= (\zeta_0 + 2\zeta_D) m_\pi^2 + 2\zeta_0 m_K^2, \\
\zeta_\Xi &= (\zeta_0 - 2\zeta_F) m_\pi^2 + (2\zeta_0 + 2\zeta_D + 2\zeta_F) m_K^2.
\end{aligned} \tag{4.17}$$

The dots in (4.17) represent corrections terms of order Q^3 and further contributions from irreducible one-loop diagrams not considered here. It is pointed out that the coupling constants ζ_0, ζ_D and ζ_F , which appear to renormalize the strength of the Weinberg-Tomozawa interaction term, also contribute to the baryon wave-function factor \mathcal{Z} as is evident from (2.31). In fact, it will be demonstrated that the explicit and implicit dependence via the wave-function renormalization factors \mathcal{Z} cancel identically to leading order. Generalizing (3.32) the wave-function renormalization constants for the $SU(3)$ baryon octet fields are derived

$$\begin{aligned}
\mathcal{Z}_{B(c)}^{-1} - 1 &= \zeta_{B(c)} - \frac{1}{4f^2} \sum_a \xi_{B(I,a)} m_{\Phi(I,a)}^2 \left(G_{\Phi(I,a)B(I,a)}^{(B(c))} \right)^2, \\
\xi_{B(I,a)} &= 2m_{B(c)} \left. \frac{\partial I_{\Phi(I,a)B(I,a)}(\sqrt{s})}{\partial \sqrt{s}} \right|_{\sqrt{s}=m_{B(c)}} - \frac{I_{\Phi(I,a)B(I,a)}}{m_{\Phi(I,a)}^2} + \mathcal{O}(Q^4),
\end{aligned} \tag{4.18}$$

where the sum in (4.18) includes all $SU(3)$ channels as listed in (4.2). The result (4.18) is expressed in terms of the dimensionless coupling constants $G_{\Phi B}^{(B)}$. For completeness all required 3-point coupling coefficients are collected:

$$\begin{aligned}
G_{\pi N}^{(N)} &= \sqrt{3}(F + D), \quad G_{K\Sigma}^{(N)} = -\sqrt{3}(F - D), \quad G_{\eta N}^{(N)} = \frac{1}{\sqrt{3}}(3F - D), \\
G_{K\Lambda}^{(N)} &= -\frac{1}{\sqrt{3}}(3F + D), \quad G_{\bar{K}N}^{(\Lambda)} = \sqrt{2}G_{K\Lambda}^{(N)}, \quad G_{\pi\Sigma}^{(\Lambda)} = 2D, \\
G_{\eta\Lambda}^{(\Lambda)} &= -\frac{2}{\sqrt{3}}D, \quad G_{K\Xi}^{(\Lambda)} = -\sqrt{\frac{2}{3}}(3F - D), \quad G_{\bar{K}N}^{(\Sigma)} = \sqrt{\frac{2}{3}}G_{K\Sigma}^{(N)}, \\
G_{\pi\Sigma}^{(\Sigma)} &= -\sqrt{8}F, \quad G_{\pi\Lambda}^{(\Sigma)} = \frac{1}{\sqrt{3}}G_{\pi\Sigma}^{(\Lambda)}, \quad G_{\eta\Sigma}^{(\Sigma)} = \frac{2}{\sqrt{3}}D, \\
G_{K\Xi}^{(\Sigma)} &= \sqrt{2}(F + D), \quad G_{\bar{K}\Lambda}^{(\Xi)} = -\frac{1}{\sqrt{2}}G_{K\Xi}^{(\Lambda)}, \quad G_{\bar{K}\Sigma}^{(\Xi)} = -\sqrt{\frac{3}{2}}G_{K\Xi}^{(\Sigma)}, \\
G_{\eta\Xi}^{(\Xi)} &= -\frac{1}{\sqrt{3}}(3F + D), \quad G_{\pi\Xi}^{(\Xi)} = \sqrt{3}(F - D),
\end{aligned} \tag{4.19}$$

to leading chiral order Q^0 . The loop function $I_{\Phi(I,a)B(I,a)}(\sqrt{s})$ and the mesonic tadpole term $I_{\Phi(I,a)}$ are the obvious generalizations of $I_{\pi N}(\sqrt{s})$ and I_π introduced in (3.20). It is emphasized that the contribution $\zeta_{B(c)}$ in (4.18) is identical to the corresponding contribution in $\Delta\zeta_{B(c)}$. Therefore, if all one-loop effects are dropped, one finds the result

$$\mathcal{Z}^{-1} = 1 + \zeta, \quad \Delta\zeta = 0 + \mathcal{O}\left(Q^3, \frac{1}{N_c}Q^2\right). \tag{4.20}$$

Given the renormalization condition (3.37), which requires the baryon s-channel pole contribution to be represented by the renormalized effective potential V_R , it follows that (4.20) holds here. This argument relies on the requirement that the loop correction to \mathcal{Z} as given in (4.18) must be considered as part of the renormalized effective potential V_R . Consequently such loop

corrections should be dropped as they are suppressed by the factor Q^3/N_c . It is evident that the one-loop contribution to the baryon \mathcal{Z} -factor is naturally moved into V_R by that double subtraction with $k = 1$ in (4.11), as explained previously.

It is illuminating to explore whether the parameters ζ_0, ζ_D and ζ_F can be dialed to give $\mathcal{Z} = 1$. In the $SU(3)$ limit with degenerate meson and also degenerate baryon masses one finds a degenerate wave-function renormalization factor \mathcal{Z}

$$\begin{aligned} \mathcal{Z}^{-1} - 1 = & 3\zeta_0 + 2\zeta_D - \frac{m_\pi^2}{(4\pi f)^2} \left(\frac{5}{3} D^2 + 3F^2 \right) \left(-4 - 3 \ln \left(\frac{m_\pi^2}{m_N^2} \right) \right) \\ & + 3\pi \frac{m_\pi}{m_N} + \mathcal{O} \left(\frac{m_\pi^2}{m_N^2} \right), \end{aligned} \quad (4.21)$$

where the minimal chiral subtraction prescription (3.28) was applied. The result (4.21) agrees identically with the $SU(2)$ -result (3.32) if one formally replaces g_A^2 by $4F^2 + \frac{20}{9}D^2$ in (3.32). It is clear from (4.21) that in the $SU(3)$ limit the counter term $3\zeta_0 + 2\zeta_D$ may be dialed so as to impose $\mathcal{Z} = 1$. This is no longer possible once the explicit $SU(3)$ symmetry-breaking effects are included. Note however that consistency of the perturbative renormalization procedure suggests that for hypothetical $SU(3)$ -degenerate ξ -factors in (4.18) it should be possible to dial ζ_0, ζ_D and ζ_F so as to find $\mathcal{Z}_B = 1$ for all baryon octet fields. This is expected, because for example in the \overline{MS} -scheme one finds a $SU(3)$ -symmetric renormalization scale² dependence of $\xi_{B(c)}$ in (4.18) with $\xi_{B(c)} \sim \ln \mu^2$. Indeed in this case the choice

$$\begin{aligned} \zeta_0 = \frac{\xi}{4f^2} \left(\frac{26}{9} D^2 + 2F^2 \right), \quad \zeta_D = \frac{\xi}{4f^2} \left(-D^2 + 3F^2 \right), \\ \zeta_F = \frac{\xi}{4f^2} \frac{10}{3} D F, \end{aligned} \quad (4.22)$$

would lead to $\mathcal{Z} = 1$ for all baryon octet wave functions. The $SU(3)$ symmetry-breaking effects in the baryon wave-function renormalization factors will be discussed again below. They affect the meson-baryon 3-point vertices at subleading order.

The s- and u-channel exchange diagrams of the baryon octet contribute as follows

$$\begin{aligned} \left[K_{s-[\bar{8}]}^{(I)}(\bar{k}, k; w) \right]_{ab} &= - \sum_{c=1}^3 \left(\not{q} - R_{L,ab}^{(I,c)} \right) \frac{[C_{[\bar{8}}]^{(I,c)}]_{ab}}{4f^2 (\psi + m_{[\bar{8}}]^{(c)})} \left(\not{q} - R_{R,ab}^{(I,c)} \right), \\ \left[K_{u-[\bar{8}]}^{(I)}(\bar{k}, k; w) \right]_{ab} &= \sum_{c=1}^4 \frac{[\tilde{C}_{[\bar{8}}]^{(I,c)}]_{ab}}{4f^2} \left(\psi + m_{[\bar{8}}]^{(c)} + \tilde{R}_{L,ab}^{(I,c)} + \tilde{R}_{R,ab}^{(I,c)} \right. \\ &\quad \left. - \left(\not{p} + m_{[\bar{8}}]^{(c)} + \tilde{R}_{L,ab}^{(I,c)} \right) \frac{1}{\tilde{\psi} + m_{[\bar{8}}]^{(c)}} \left(\not{p} + m_{[\bar{8}}]^{(c)} + \tilde{R}_{R,ab}^{(I,c)} \right) \right), \end{aligned} \quad (4.23)$$

where $\tilde{w}_\mu = p_\mu - \bar{q}_\mu$. The index c in (4.23) labels the baryon octet exchange with $c \rightarrow (N, \Lambda, \Sigma, \Xi)$. In particular $m_{[\bar{8}}]^{(c)}$ denotes the physical baryon octet masses and $R^{(I,c)}$ and $\tilde{R}^{(I,c)}$ characterize the ratios of pseudo-vector to pseudo-scalar terms in the meson-baryon vertices. The dimensionless

²Note that in the minimal chiral subtraction scheme the counter terms $\zeta_{0,D,F}$ are already renormalization scale independent. The consistency of this procedure follows from the symmetry conserving property of dimensional regularization.

	$C_{WT}^{(0)}$	$C_{N_{[8]}}^{(0)}$	$C_{\Lambda_{[8]}}^{(0)}$	$C_{\Sigma_{[8]}}^{(0)}$	$C_{\Delta_{[10]}}^{(0)}$	$C_{\Sigma_{[10]}}^{(0)}$	$\tilde{C}_{N_{[8]}}^{(0)}$	$\tilde{C}_{\Lambda_{[8]}}^{(0)}$	$\tilde{C}_{\Sigma_{[8]}}^{(0)}$	$\tilde{C}_{\Xi_{[8]}}^{(0)}$	$\tilde{C}_{\Delta_{[10]}}^{(0)}$	$\tilde{C}_{\Sigma_{[10]}}^{(0)}$	$\tilde{C}_{\Xi_{[10]}}^{(0)}$
11	3	0	1	0	0	0	0	0	0	0	0	0	0
12	$\sqrt{\frac{3}{2}}$	0	1	0	0	0	$\sqrt{\frac{2}{3}}$	0	0	0	$2\sqrt{\frac{2}{3}}$	0	0
13	$\frac{3}{\sqrt{2}}$	0	1	0	0	0	$\sqrt{2}$	0	0	0	0	0	0
14	0	0	1	0	0	0	0	$\frac{1}{2}$	$-\frac{3}{2}$	0	0	$-\frac{3}{2}$	0
22	4	0	1	0	0	0	0	$\frac{1}{3}$	-1	0	0	-1	0
23	0	0	1	0	0	0	0	0	$\sqrt{3}$	0	0	$\sqrt{3}$	0
24	$-\sqrt{\frac{3}{2}}$	0	1	0	0	0	0	0	0	$-\sqrt{\frac{2}{3}}$	0	0	$-\sqrt{\frac{2}{3}}$
33	0	0	1	0	0	0	0	1	0	0	0	0	0
34	$-\frac{3}{\sqrt{2}}$	0	1	0	0	0	0	0	0	$-\sqrt{2}$	0	0	$-\sqrt{2}$
44	3	0	1	0	0	0	0	0	0	0	0	0	0
	$C_{WT}^{(1)}$	$C_{N_{[8]}}^{(1)}$	$C_{\Lambda_{[8]}}^{(1)}$	$C_{\Sigma_{[8]}}^{(1)}$	$C_{\Delta_{[10]}}^{(1)}$	$C_{\Sigma_{[10]}}^{(1)}$	$\tilde{C}_{N_{[8]}}^{(1)}$	$\tilde{C}_{\Lambda_{[8]}}^{(1)}$	$\tilde{C}_{\Sigma_{[8]}}^{(1)}$	$\tilde{C}_{\Xi_{[8]}}^{(1)}$	$\tilde{C}_{\Delta_{[10]}}^{(1)}$	$\tilde{C}_{\Sigma_{[10]}}^{(1)}$	$\tilde{C}_{\Xi_{[10]}}^{(1)}$
11	1	0	0	1	0	1	0	0	0	0	0	0	0
12	1	0	0	1	0	1	$-\frac{2}{3}$	0	0	0	$\frac{2}{3}$	0	0
13	$\sqrt{\frac{3}{2}}$	0	0	1	0	1	$\sqrt{\frac{2}{3}}$	0	0	0	0	0	0
14	$\sqrt{\frac{3}{2}}$	0	0	1	0	1	$\sqrt{\frac{2}{3}}$	0	0	0	0	0	0
15	0	0	0	1	0	1	0	$-\frac{1}{2}$	$-\frac{1}{2}$	0	0	$-\frac{1}{2}$	0
22	2	0	0	1	0	1	0	$-\frac{1}{3}$	$\frac{1}{2}$	0	0	$\frac{1}{2}$	0
23	0	0	0	1	0	1	0	0	-1	0	0	-1	0
24	0	0	0	1	0	1	0	0	1	0	0	1	0
25	-1	0	0	1	0	1	0	0	0	$\frac{2}{3}$	0	0	$\frac{2}{3}$
33	0	0	0	1	0	1	0	0	1	0	0	1	0
34	0	0	0	1	0	1	0	$\frac{1}{\sqrt{3}}$	0	0	0	0	0
35	$\sqrt{\frac{3}{2}}$	0	0	1	0	1	0	0	0	$-\sqrt{\frac{2}{3}}$	0	0	$-\sqrt{\frac{2}{3}}$
44	0	0	0	1	0	1	0	0	1	0	0	1	0
45	$\sqrt{\frac{3}{2}}$	0	0	1	0	1	0	0	0	$-\sqrt{\frac{2}{3}}$	0	0	$-\sqrt{\frac{2}{3}}$
55	1	0	0	1	0	1	0	0	0	0	0	0	0
	$C_{WT}^{(2)}$	$C_{N_{[8]}}^{(2)}$	$C_{\Lambda_{[8]}}^{(2)}$	$C_{\Sigma_{[8]}}^{(2)}$	$C_{\Delta_{[10]}}^{(2)}$	$C_{\Sigma_{[10]}}^{(2)}$	$\tilde{C}_{N_{[8]}}^{(2)}$	$\tilde{C}_{\Lambda_{[8]}}^{(2)}$	$\tilde{C}_{\Sigma_{[8]}}^{(2)}$	$\tilde{C}_{\Xi_{[8]}}^{(2)}$	$\tilde{C}_{\Delta_{[10]}}^{(2)}$	$\tilde{C}_{\Sigma_{[10]}}^{(2)}$	$\tilde{C}_{\Xi_{[10]}}^{(2)}$
11	-2	0	0	0	0	0	0	$\frac{1}{3}$	$\frac{1}{2}$	0	0	$\frac{1}{2}$	0

Table 4.1: Weinberg-Tomozawa interaction strengths and baryon exchange coefficients of the strangeness minus one channels as defined in (4.16) and (4.23).

matrices $C_{[8]}$ and $\tilde{C}_{[8]}$ give the renormalized strengths of the s-channel and u-channel baryon exchanges respectively. They are expressed most conveniently in terms of s-channel $C_{B(c)}$ and u-channel $\tilde{C}_{B(c)}$ coefficient matrices

$$\begin{aligned} \left[C_{[8]}^{(I,c)} \right]_{ab} &= \left[C_{B(c)}^{(I)} \right]_{ab} \bar{A}_{\Phi(I,a)B(I,a)}^{(B(c))} \bar{A}_{\Phi(I,b)B(I,b)}^{(B(c))} , \\ \left[\tilde{C}_{[8]}^{(I,c)} \right]_{ab} &= \left[\tilde{C}_{B(c)}^{(I)} \right]_{ab} \bar{A}_{\Phi(I,b)B(I,a)}^{(B(c))} \bar{A}_{\Phi(I,a)B(I,b)}^{(B(c))} , \end{aligned} \quad (4.24)$$

and the renormalized three-point coupling constants \bar{A} . According to the LSZ-scheme the bare coupling constants, A , are related to the renormalized coupling constants, \bar{A} , by means of the baryon octet \mathcal{Z} -factors:

$$\bar{A}_{\Phi(I,a)B(I,b)}^{(B(c))} = \mathcal{Z}_{B(c)}^{\frac{1}{2}} A_{\Phi(I,a)B(I,b)}^{(B(c))} \mathcal{Z}_{B(I,b)}^{\frac{1}{2}} . \quad (4.25)$$

At leading order Q^0 the bare coupling constants $A = G(F, D) + \mathcal{O}(Q^2)$ are specified in (4.19). The chiral correction terms to the coupling constants A and R will be discussed in great detail later. In the convention applied here the s-channel coefficients $C_{B(c)}$ are either one or zero and the u-channel coefficients $\tilde{C}_{B(c)}$ represent appropriate Fierz factors resulting from the interchange of initial and final meson states. To illustrate the notation explicitly the coefficients are listed in Tab. 4.1 for the strangeness minus one channels. For the strangeness zero channel see [97]. It is stressed that the expressions for the s- and u-channel exchange contributions (4.23) depend on the result (4.20), because there would otherwise be a factor $\mathcal{Z}^{-1}/(1 + \zeta)$ in front of both contributions. That would necessarily lead to an asymmetry in the treatment of s-versus u-channel, simply because the s-channel contribution would be further renormalized by the unitarization. In contrast, in the present scheme the proper balance of s- and u-channel exchange contributions in the scattering amplitude as is required for the realization of the large- N_c cancellation mechanism [126] is observed.

The $SU(3)$ symmetry-breaking effects in the meson-baryon coupling constants are particularly interesting. The 3-point vertices have pseudo-vector and pseudo-scalar components determined by $F_i + \delta F_i$ and \tilde{F}_i of (2.37,2.38) respectively. Collect first the symmetry-breaking terms in the axial-vector coupling constants A introduced in (4.25). They are of chiral order Q^2 but lead to particular Q^3 -correction terms in the scattering amplitudes. One finds

$$\begin{aligned} A &= G(F_A, D_A) - \frac{2}{\sqrt{3}} (m_K^2 - m_\pi^2) \Delta A , \quad \tilde{F}_i = F_i + \delta F_i , \\ \Delta A_{\pi N}^{(N)} &= 3(F_1 + F_3) - F_0 - F_2 + 2(\tilde{F}_4 + \tilde{F}_5) , \\ \Delta A_{K\Sigma}^{(N)} &= \frac{3}{2}(F_1 - F_3) + \frac{1}{2}(F_0 - F_2) - \tilde{F}_4 + \tilde{F}_5 , \\ \Delta A_{\eta N}^{(N)} &= -F_1 + 3F_3 + \frac{1}{3}F_0 - F_2 + \frac{2}{3}\tilde{F}_4 - 2\tilde{F}_5 + 2(\tilde{F}_6 + \frac{4}{3}\tilde{F}_4) , \\ \Delta A_{K\Lambda}^{(N)} &= -\frac{1}{2}F_1 - \frac{3}{2}F_3 + \frac{1}{2}F_0 + \frac{3}{2}F_2 + \frac{1}{3}\tilde{F}_4 + \tilde{F}_5 + (F_7 + \frac{4}{3}F_0) , \\ \Delta A_{\bar{K}N}^{(\Lambda)} &= \sqrt{2} \Delta A_{K\Lambda}^{(N)} , \\ \Delta A_{\pi\Sigma}^{(\Lambda)} &= \frac{4}{\sqrt{3}} \tilde{F}_4 + \sqrt{3}(F_7 + \frac{4}{3}F_0) , \\ \Delta A_{\eta\Lambda}^{(\Lambda)} &= \frac{4}{3}(F_0 + \tilde{F}_4) + 2(\tilde{F}_6 + \frac{4}{3}\tilde{F}_4) + 2(F_7 + \frac{4}{3}F_0) , \\ \Delta A_{K\Xi}^{(\Lambda)} &= -\frac{1}{\sqrt{2}}(F_0 + F_1) + \frac{3}{\sqrt{2}}(F_2 + F_3) - \frac{\sqrt{2}}{3}(\tilde{F}_4 - 3\tilde{F}_5) - \sqrt{2}(F_7 + \frac{4}{3}F_0) , \end{aligned}$$

$$\begin{aligned}
\Delta A_{\bar{K}N}^{(\Sigma)} &= \sqrt{\frac{2}{3}} \Delta A_{\bar{K}\Sigma}^{(N)}, \quad \Delta A_{\pi\Sigma}^{(\Sigma)} = -4\sqrt{\frac{2}{3}}(F_2 + \tilde{F}_5), \quad \Delta A_{\pi\Lambda}^{(\Sigma)} = \frac{1}{\sqrt{3}} \Delta A_{\pi\Sigma}^{(\Lambda)}, \\
\Delta A_{\eta\Sigma}^{(\Sigma)} &= \frac{4}{3}(F_0 - \tilde{F}_4) + 2(\tilde{F}_6 + \frac{4}{3}\tilde{F}_4), \\
\Delta A_{\bar{K}\Xi}^{(\Sigma)} &= -\sqrt{\frac{3}{2}}(F_1 + F_3) + \sqrt{\frac{1}{6}}(F_0 + F_2) - \sqrt{\frac{2}{3}}(\tilde{F}_4 + \tilde{F}_5), \\
\Delta A_{\bar{K}\Lambda}^{(\Xi)} &= -\frac{1}{\sqrt{2}} \Delta A_{\bar{K}\Xi}^{(\Lambda)}, \quad \Delta A_{\bar{K}\Sigma}^{(\Xi)} = -\sqrt{\frac{3}{2}} \Delta A_{\bar{K}\Xi}^{(\Sigma)}, \\
\Delta A_{\eta\Xi}^{(\Xi)} &= F_1 + 3F_3 + \frac{1}{3}F_0 + F_2 + \frac{2}{3}\tilde{F}_4 + 2\tilde{F}_5 + 2(\tilde{F}_6 + \frac{4}{3}\tilde{F}_4), \\
\Delta A_{\pi\Xi}^{(\Xi)} &= F_0 + 3F_1 - F_2 - 3F_3 + 2(\tilde{F}_5 - \tilde{F}_4), \tag{4.26}
\end{aligned}$$

where the renormalized coupling constants D_A and F_A are given in (2.41) and $G(F, D)$ in (4.19). It is emphasized that to order Q^2 the effect of the \mathcal{Z} -factors in (4.25) can be accounted for by the following redefinition of the F_R, D_R and F_i parameters in (4.26)

$$\begin{aligned}
F_R &\rightarrow F_R + \left(2m_K^2 + m_\pi^2\right) \left(\zeta_0 + \frac{2}{3}\zeta_D\right) F_R, \\
D_R &\rightarrow D_R + \left(2m_K^2 + m_\pi^2\right) \left(\zeta_0 + \frac{2}{3}\zeta_D\right) D_R, \\
F_0 &\rightarrow F_0 + \zeta_D D_R, \quad F_1 \rightarrow F_1 + \zeta_F F_R, \quad F_2 \rightarrow F_2 + \zeta_D F_R, \\
F_3 &\rightarrow F_3 + \zeta_F F_R, \quad F_7 \rightarrow F_7 - \frac{4}{3}\zeta_D D_R. \tag{4.27}
\end{aligned}$$

As a consequence the parameters ζ_0, ζ_D and ζ_F are redundant in the approximation applied here and can therefore be dropped. It is legitimate to identify the bare coupling constants A with the renormalized coupling constants \bar{A} . The same renormalization holds for the matrix elements of the axial-vector current.

Recall the large- N_c result (2.43). The many parameters F_i and δF_i in (4.26) are expressed in terms of the seven parameters c_i and $\delta c_i = \tilde{c}_i - c_i - \bar{c}_i$. We give explicitly the axial-vector coupling constants, which are most relevant for the pion-nucleon and kaon-nucleon scattering processes, in terms of those large- N_c parameters

$$\begin{aligned}
A_{\pi N}^{(N)} &= \sqrt{3} \left(F_A + D_A\right) + \frac{5}{3} \left(c_1 + \delta c_1\right) + c_2 + \delta c_2 - a + 5c_3 + c_4, \\
A_{\bar{K}N}^{(\Lambda)} &= -\sqrt{\frac{2}{3}} \left(3F_A + D_A\right) + \frac{1}{\sqrt{2}} \left(c_1 + \delta c_1 + c_2 + \delta c_2 - a - 3c_3 + c_4\right), \\
A_{\bar{K}N}^{(\Sigma)} &= -\sqrt{2} \left(F_A - D_A\right) - \frac{1}{\sqrt{6}} \left(\frac{1}{3} \left(c_1 + \delta c_1\right) - c_2 - \delta c_2 + a - c_3 + 3c_4\right), \\
A_{\pi\Sigma}^{(\Lambda)} &= 2D_A + \frac{2}{\sqrt{3}} \left(c_1 + \delta c_1\right), \tag{4.28}
\end{aligned}$$

where

$$F_A = F_R - \frac{\beta}{\sqrt{3}} \left(\frac{2}{3}\delta c_1 + \delta c_2 - a\right), \quad D_A = D_R - \frac{\beta}{\sqrt{3}} \delta c_1, \quad \beta = \frac{m_K^2 + m_\pi^2/2}{m_K^2 - m_\pi^2}. \tag{4.29}$$

The result (4.28) shows that the axial-vector coupling constants $A_{\pi N}^{(N)}$, $A_{\bar{K}N}^{(\Lambda)}$, $A_{\bar{K}N}^{(\Sigma)}$ and $A_{\pi\Sigma}^{(\Lambda)}$, can be fine tuned with c_i in (2.43) to be off their $SU(3)$ limit values. Moreover, the $SU(3)$ symmetric contribution proportional to F_A or D_A deviate from their corresponding F_R and D_R values relevant for matrix elements of the axial-vector current, once non-zero values for $\delta c_{1,2}$ are established. However, the values of F_R, D_R and c_i are strongly constrained by the weak decay widths of the baryon-octet states (see Tab. 2.1). Thus, the $SU(3)$ symmetry-breaking pattern

in the axial-vector current and the one in the meson-baryon axial-vector coupling constants are closely linked.

It is left to specify the pseudo-scalar part, P , of the meson-baryon vertices introduced in (2.38). In (4.23) their effect was encoded into the R and \tilde{R} parameters with $R, \tilde{R} \sim \bar{F} \sim \bar{c}, a$. Applying the large- N_c result of (2.44) we obtain

$$\begin{aligned}
R_{L,ab}^{(I,c)} A_{\Phi(I,a)B(I,a)}^{(B(c))} &= \left(m_{B(I,a)} + m_{B(c)} \right) P_{\Phi(I,a)B(I,a)}^{(B(c))}, \\
R_{R,ab}^{(I,c)} A_{\Phi(I,b)B(I,b)}^{(B(c))} &= \left(m_{B(I,b)} + m_{B(c)} \right) P_{\Phi(I,b)B(I,b)}^{(B(c))}, \\
\tilde{R}_{L,ab}^{(I,c)} A_{\Phi(I,b)B(I,a)}^{(B(c))} &= \left(m_{B(I,a)} + m_{B(c)} \right) P_{\Phi(I,b)B(I,a)}^{(B(c))}, \\
\tilde{R}_{R,ab}^{(I,c)} A_{\Phi(I,a)B(I,b)}^{(B(c))} &= \left(m_{B(I,b)} + m_{B(c)} \right) P_{\Phi(I,a)B(I,b)}^{(B(c))}, \\
P_{\pi N}^{(N)} &= -\left(\frac{5}{3} \bar{c}_1 + \bar{c}_2 + a \right) (\beta - 1), \quad P_{K\Sigma}^{(N)} = -\left(\frac{1}{3} \bar{c}_1 - \bar{c}_2 - a \right) \left(\beta + \frac{1}{2} \right), \\
P_{\eta N}^{(N)} &= \frac{7}{3} \bar{c}_1 + \bar{c}_2 + a - \beta \left(\frac{1}{3} \bar{c}_1 + \bar{c}_2 + a \right), \\
P_{K\Lambda}^{(N)} &= \left(\bar{c}_1 + \bar{c}_2 + a \right) \left(\beta + \frac{1}{2} \right), \quad P_{\bar{K}N}^{(\Lambda)} = \sqrt{2} P_{K\Lambda}^{(N)}, \\
P_{\pi\Sigma}^{(\Lambda)} &= -\frac{2}{\sqrt{3}} \bar{c}_1 (\beta - 1), \quad P_{\eta\Lambda}^{(\Lambda)} = \frac{2}{3} \bar{c}_1 (5 + \beta) + 2\bar{c}_2 + 2a, \\
P_{K\Xi}^{(\Lambda)} &= \frac{1}{\sqrt{2}} \left(\frac{1}{3} \bar{c}_1 + \bar{c}_2 + a \right) (2\beta + 1), \quad P_{\bar{K}N}^{(\Sigma)} = \sqrt{\frac{2}{3}} P_{K\Sigma}^{(N)}, \\
P_{\pi\Sigma}^{(\Sigma)} &= \sqrt{\frac{2}{3}} \left(\frac{4}{3} \bar{c}_1 + 2\bar{c}_2 + 2a \right) (\beta - 1), \quad P_{\pi\Lambda}^{(\Sigma)} = \frac{1}{\sqrt{3}} P_{\pi\Sigma}^{(\Lambda)}, \\
P_{\eta\Sigma}^{(\Sigma)} &= 2\bar{c}_1 \left(1 - \frac{1}{3} \beta \right) + 2\bar{c}_2 + 2a, \\
P_{K\Xi}^{(\Sigma)} &= -\frac{1}{\sqrt{6}} \left(\frac{5}{3} \bar{c}_1 + \bar{c}_2 + a \right) (2\beta + 1), \quad P_{\bar{K}\Lambda}^{(\Xi)} = -\frac{1}{\sqrt{2}} P_{K\Xi}^{(\Lambda)}, \\
P_{\bar{K}\Sigma}^{(\Xi)} &= -\sqrt{\frac{3}{2}} P_{K\Xi}^{(\Sigma)}, \quad P_{\eta\Xi}^{(\Xi)} = \frac{11}{3} \bar{c}_1 + 3\bar{c}_2 + 3a + \beta (\bar{c}_1 + \bar{c}_2 + a), \\
P_{\pi\Xi}^{(\Xi)} &= \left(\frac{1}{3} \bar{c}_1 - \bar{c}_2 - a \right) (\beta - 1), \tag{4.30}
\end{aligned}$$

where $\beta \simeq 1.12$ was introduced in (4.29). The pseudo-scalar meson-baryon vertices show $SU(3)$ symmetric contribution linear in $\beta \bar{c}_i$ and symmetry-breaking terms proportional to \bar{c}_i . It is emphasized that, even though the physical meson-baryon coupling constants, $G = A + P$, are the sum of their axial-vector and pseudo-scalar components, it is important to carefully discriminate both types of vertices, because they give rise to quite different behaviors for the partial-wave amplitudes off the baryon-octet pole. Such effects are expected to be particularly important in the strangeness sectors since there (4.30) leads to $P_{\bar{K}N}^{(\Lambda,\Sigma)} \sim m_K^2$ to be compared to $P_{\pi N}^{(N)} \sim m_\pi^2$.

Next study the decuplet exchange terms $K_{s-[10]}^{(I)}$ and $K_{u-[10]}^{(I)}$ in (4.15). Their respective interaction kernels are written in a form which facilitates the identification of their on-shell irreducible parts

$$\begin{aligned}
K_{s-[10]}^{(I)}(\bar{k}, k; w) &= \sum_{c=1}^2 \frac{C_{[10]}^{(I,c)}}{4f^2} \left(\frac{\bar{q} \cdot q}{\psi - m_{[10]}^{(c)}} - \frac{(\bar{q} \cdot w)(w \cdot q)}{(m_{[10]}^{(c)})^2 (\psi - m_{[10]}^{(c)})} \right) \\
&+ \frac{1}{3} \left(\not{q} + \frac{\bar{q} \cdot w}{m_{[10]}^{(c)}} \right) \frac{1}{\psi + m_{[10]}^{(c)}} \left(\not{q} + \frac{w \cdot q}{m_{[10]}^{(c)}} \right) - \frac{Z_{[10]}}{3m_{[10]}^{(c)}} \not{q} \not{q}
\end{aligned}$$

$$\begin{aligned}
& - \frac{Z_{[10]}^2}{6(m_{[10]}^{(c)})^2} \not{q} \left(\psi - 2m_{[10]}^{(c)} \right) \not{q} + Z_{[10]} \not{q} \frac{w \cdot q}{3(m_{[10]}^{(c)})^2} \\
& + Z_{[10]} \frac{\bar{q} \cdot w}{3(m_{[10]}^{(c)})^2} \not{q} \Big), \\
K_{u-[10]}^{(I)}(\bar{k}, k; w) &= \sum_{c=1}^3 \frac{\tilde{C}_{[10]}^{(I,c)}}{4f^2} \left(\frac{\bar{q} \cdot q}{\not{\psi} - m_{[10]}^{(c)}} - \frac{(\bar{q} \cdot \tilde{w})(\tilde{w} \cdot q)}{(m_{[10]}^{(c)})^2 (\not{\psi} - m_{[10]}^{(c)})} \right. \\
& + \frac{1}{3} \left(\not{p} + m_{[10]}^{(c)} + \frac{q \cdot \tilde{w}}{m_{[10]}^{(c)}} \right) \frac{1}{\not{\psi} + m_{[10]}^{(c)}} \left(\not{p} + m_{[10]}^{(c)} + \frac{\tilde{w} \cdot \bar{q}}{m_{[10]}^{(c)}} \right) \\
& - \frac{\tilde{w} \cdot (q + \bar{q})}{3m_{[10]}^{(c)}} - \frac{1}{3} \left(\psi + m_{[10]}^{(c)} \right) \\
& + \frac{Z_{[10]}}{3(m_{[10]}^{(c)})^2} \left(\not{q} (\tilde{w} \cdot q) + (\bar{q} \cdot \tilde{w}) \not{q} + m_{[10]}^{(c)} (\not{q} \not{q} - 2(\bar{q} \cdot q)) \right) \\
& \left. - \frac{Z_{[10]}^2}{6(m_{[10]}^{(c)})^2} \left(\not{p} \not{\psi} \not{p} - \tilde{w}^2 \psi + 2m_{[10]}^{(c)} (\not{q} \not{q} - 2q \cdot q) \right) \right). \tag{4.31}
\end{aligned}$$

The index c in (4.31) labels the decuplet exchange with $c \rightarrow (\Delta_{[10]}, \Sigma_{[10]}, \Xi_{[10]})$. The dimensionless matrices $C_{[10]}^{(I,c)}$ and $\tilde{C}_{[10]}^{(I,c)}$ characterize the strength of the s-channel and u-channel resonance exchanges respectively. Here we apply the notation introduced in (4.24) also for the resonance exchange contributions. In particular the decuplet coefficients $C_{[10]}^{(I,c)}$ and $\tilde{C}_{[10]}^{(I,c)}$ are determined by

$$\begin{aligned}
A &= G(C_A) - \frac{2}{\sqrt{3}} (m_K^2 - m_\pi^2) \Delta A, \quad \tilde{C}_0 = C_0 + \delta C_0, \\
\Delta A_{\pi N}^{(\Delta_{[10]})} &= \sqrt{2} \left(-\frac{1}{\sqrt{3}} C_2 + \sqrt{3} C_3 + \frac{2}{\sqrt{3}} \tilde{C}_0 \right), \\
\Delta A_{K\Sigma}^{(\Delta_{[10]})} &= -\sqrt{2} \left(\frac{2}{\sqrt{3}} C_2 - \frac{1}{\sqrt{3}} \tilde{C}_0 + \sqrt{3} C_1 \right), \\
\Delta A_{\bar{K}N}^{(\Sigma_{[10]})} &= \sqrt{\frac{2}{3}} \left(-\frac{1}{\sqrt{3}} C_2 + \sqrt{3} C_3 - \frac{1}{\sqrt{3}} \tilde{C}_0 - \sqrt{3} C_1 \right) - \sqrt{2} C_4, \\
\Delta A_{\pi\Sigma}^{(\Sigma_{[10]})} &= -\sqrt{\frac{2}{3}} \left(\frac{2}{\sqrt{3}} C_2 + \frac{2}{\sqrt{3}} \tilde{C}_0 \right) - 2\sqrt{2} C_4, \\
\Delta A_{\pi\Lambda}^{(\Sigma_{[10]})} &= \frac{2}{\sqrt{3}} (C_2 - \tilde{C}_0), \quad \Delta A_{\eta\Sigma}^{(\Sigma_{[10]})} = \frac{2}{\sqrt{3}} C_2 - \frac{2}{\sqrt{3}} \tilde{C}_0, \\
\Delta A_{\bar{K}\Xi}^{(\Sigma_{[10]})} &= -\sqrt{\frac{2}{3}} \left(-\frac{1}{\sqrt{3}} C_2 - \sqrt{3} C_3 - \frac{1}{\sqrt{3}} \tilde{C}_0 + \sqrt{3} C_1 \right) + \sqrt{2} C_4, \\
\Delta A_{\bar{K}\Lambda}^{(\Xi_{[10]})} &= -\frac{1}{\sqrt{3}} \tilde{C}_0 - \sqrt{3} C_1 - \frac{1}{\sqrt{3}} (3C_4 + 2C_2), \\
\Delta A_{\bar{K}\Sigma}^{(\Xi_{[10]})} &= \frac{2}{\sqrt{3}} C_2 - \frac{1}{\sqrt{3}} \tilde{C}_0 - \sqrt{3} C_1 + \sqrt{3} C_4, \\
\Delta A_{\eta\Xi}^{(\Xi_{[10]})} &= \frac{1}{\sqrt{3}} C_2 + \sqrt{3} C_3 + \frac{2}{\sqrt{3}} \tilde{C}_0 + \sqrt{3} C_4, \\
\Delta A_{\pi\Xi}^{(\Xi_{[10]})} &= \frac{1}{\sqrt{3}} C_2 + \sqrt{3} C_3 - \frac{2}{\sqrt{3}} \tilde{C}_0 - \sqrt{3} C_4, \tag{4.32}
\end{aligned}$$

where the $SU(3)$ symmetric contributions $G(C)$ are

$$\begin{aligned}
G_{\pi N}^{(\Delta_{[10]})} &= \sqrt{2} C, & G_{K\Sigma}^{(\Delta_{[10]})} &= -\sqrt{2} C, & G_{\bar{K}N}^{(\Sigma_{[10]})} &= \sqrt{\frac{2}{3}} C, \\
G_{\pi\Sigma}^{(\Sigma_{[10]})} &= -\sqrt{\frac{2}{3}} C, & G_{\pi\Lambda}^{(\Sigma_{[10]})} &= -C, & G_{\eta\Sigma}^{(\Sigma_{[10]})} &= C, & G_{K\Xi}^{(\Sigma_{[10]})} &= -\sqrt{\frac{2}{3}} C, \\
G_{\bar{K}\Lambda}^{(\Xi_{[10]})} &= C, & G_{\bar{K}\Sigma}^{(\Xi_{[10]})} &= C, & G_{\eta\Xi}^{(\Xi_{[10]})} &= -C, & G_{\pi\Xi}^{(\Xi_{[10]})} &= -C.
\end{aligned} \tag{4.33}$$

Recall that to leading order in the $1/N_c$ expansion the five symmetry-breaking parameters C_i introduced in (2.37) are all given in terms of the c_i parameters (2.43). The parameter $\delta C_0 \sim \tilde{c}_1 - c_1$ and also implicitly \tilde{C}_R (see (2.41)) probe the \tilde{c}_1 parameter introduced in (2.42). All c_i parameters but c_5 are determined to a large part by the weak decay widths of the baryon octet states. The \tilde{c}_1 parameter is constrained strongly by the $SU(3)$ symmetry-breaking pattern of the meson-baryon-octet coupling constants (2.42).

The baryon octet resonance contributions $K_{s-[9]}^{(I)}$ and $K_{u-[9]}^{(I)}$ require special attention, because the way to incorporate systematically these resonances in a chiral $SU(3)$ scheme is not clear. We present first the s-channel and u-channel contributions as they follow from (2.10) at tree-level

$$\begin{aligned}
K_{s-[9]}^{(I)}(\bar{k}, k; w) &= \sum_{c=0}^4 \frac{C_{[9]}^{(I,c)}}{4f^2} \left(-\frac{\bar{q} \cdot q}{\psi + m_{[9]}^{(c)}} + \frac{(\bar{q} \cdot w)(w \cdot q)}{(m_{[9]}^{(c)})^2 (\psi + m_{[9]}^{(c)})} \right. \\
&\quad \left. - \frac{1}{3} \left(\not{q} - \frac{\bar{q} \cdot w}{m_{[9]}^{(c)}} \right) \frac{1}{\psi - m_{[9]}^{(c)}} \left(\not{q} - \frac{w \cdot q}{m_{[10]}^{(c)}} \right) \right), \\
K_{u-[9]}^{(I)}(\bar{k}, k; w) &= \sum_{c=0}^4 \frac{\tilde{C}_{[9]}^{(I,c)}}{4f^2} \left(-\frac{\bar{q} \cdot q}{\tilde{\psi} + m_{[9]}^{(c)}} + \frac{(\bar{q} \cdot \tilde{w})(\tilde{w} \cdot q)}{(m_{[9]}^{(c)})^2 (\tilde{\psi} + m_{[9]}^{(c)})} \right. \\
&\quad \left. - \frac{1}{3} \left(\not{p} - m_{[9]}^{(c)} - \frac{q \cdot \tilde{w}}{m_{[9]}^{(c)}} \right) \frac{1}{\tilde{\psi} - m_{[9]}^{(c)}} \left(\not{p} - m_{[9]}^{(c)} - \frac{\tilde{w} \cdot \bar{q}}{m_{[9]}^{(c)}} \right) \right. \\
&\quad \left. - \frac{\tilde{w} \cdot (q + \bar{q})}{3m_{[9]}^{(c)}} + \frac{1}{3} (\psi - m_{[9]}^{(c)}) \right) \\
&\quad - \frac{Z_{[9]}}{3(m_{[9]}^{(c)})^2} \left(\not{q} (\tilde{w} \cdot q) + (\bar{q} \cdot \tilde{w}) \not{q} - m_{[9]}^{(c)} (\not{q} \not{q} - 2(\bar{q} \cdot q)) \right) \\
&\quad + \frac{(Z_{[9]})^2}{6(m_{[9]}^{(c)})^2} \left(\not{p} \not{\tilde{w}} \not{p} - \tilde{w}^2 \psi - 2m_{[9]}^{(c)} (\not{q} \not{q} - 2q \cdot q) \right)
\end{aligned} \tag{4.34}$$

where the index $c \rightarrow (\Lambda(1520), N(1520), \Lambda(1690), \Sigma(1680), \Xi(1820))$ extends over the nonet resonance states. The coefficient matrices $C_{[9]}^{(I,c)}$ and $\tilde{C}_{[9]}^{(I,c)}$ are constructed by analogy with those of the octet and decuplet contributions (see (4.19,4.24)). In particular one has $C_{B^*(c)}^{(I)} = C_{B(c)}^{(I)}$ and $\tilde{C}_{B^*(c)}^{(I)} = \tilde{C}_{B(c)}^{(I)}$. The coupling constants $A_{\Phi B}^{(B^*)} = G_{\Phi B}^{(B)}(F_{[9]}, D_{[9]})$ are given in terms of the $F_{[9]}$ and $D_{[9]}$ parameters introduced in (2.10) for all contributions except those of the $\Lambda(1520)$ and $\Lambda(1690)$ resonances

$$G_{\bar{K}N}^{(\Lambda(1520))} = \sqrt{\frac{2}{3}} (3F_{[9]} + D_{[9]}) \sin \vartheta + \sqrt{3} C_{[9]} \cos \vartheta,$$

$$\begin{aligned}
G_{\pi\Sigma}^{(\Lambda(1520))} &= -2 D_{[9]} \sin \vartheta + \frac{3}{\sqrt{2}} C_{[9]} \cos \vartheta , \\
G_{\eta\Lambda}^{(\Lambda(1520))} &= \frac{2}{\sqrt{3}} D_{[9]} \sin \vartheta + \sqrt{\frac{3}{2}} C_{[9]} \cos \vartheta , \\
G_{K\Xi}^{(\Lambda(1520))} &= \sqrt{\frac{2}{3}} \left(3 F_{[9]} - D_{[9]} \right) \sin \vartheta - \sqrt{3} C_{[9]} \cos \vartheta ,
\end{aligned} \tag{4.35}$$

and

$$\begin{aligned}
G_{\bar{K}N}^{(\Lambda(1690))} &= -\sqrt{\frac{2}{3}} \left(3 F_{[9]} + D_{[9]} \right) \cos \vartheta + \sqrt{3} C_{[9]} \sin \vartheta , \\
G_{\pi\Sigma}^{(\Lambda(1690))} &= 2 D_{[9]} \cos \vartheta + \frac{3}{\sqrt{2}} C_{[9]} \sin \vartheta , \\
G_{\eta\Lambda}^{(\Lambda(1690))} &= -\frac{2}{\sqrt{3}} D_{[9]} \cos \vartheta + \sqrt{\frac{3}{2}} C_{[9]} \sin \vartheta , \\
G_{K\Xi}^{(\Lambda(1690))} &= -\sqrt{\frac{2}{3}} \left(3 F_{[9]} - D_{[9]} \right) \cos \vartheta - \sqrt{3} C_{[9]} \sin \vartheta .
\end{aligned} \tag{4.36}$$

The baryon nonet field B_μ^* asks for special considerations in a chiral $SU(3)$ scheme as there is no straightforward systematic approximation strategy. Given that the baryon octet and decuplet states are degenerate in the large- N_c limit, it is natural to impose $m_{[10]} - m_{[8]} \sim Q$. In contrast with that there is no fundamental reason to insist on $m_{N(1520)} - m_N \sim Q$, for example. But, only with $m_{[9]} - m_{[8]} \sim Q$ is it feasible to establish consistent power counting rules needed for the systematic evaluation of the chiral Lagrangian. The presence of the baryon nonet resonance states in the large- N_c limit of QCD is far from obvious. Referring to the detailed exposition in chapter 2.1, our opinion differs here from the one expressed in [123, 124, 125] where the d-wave baryon octet resonance states are considered as part of an excited large- N_c **70**-plet. It was argued that reducible diagrams summed by the Bethe-Salpeter equation are typically enhanced by a factor of 2π relatively to irreducible diagrams. Therefore there are a priori two extreme possibilities: the baryon resonances are a consequence of important coupled channel dynamics or they are already present in the interaction kernel. As was motivated in detail in chapter 2.1 we favor the latter case.

The description of resonances has a subtle consequence for the treatment of the u-channel baryon resonance exchange contributions. If a resonance is formed primarily by the coupled channel dynamics one should not include an explicit bare u-channel resonance contribution in the interaction kernel. The then necessarily strong energy dependence of the resonance self-energy would invalidate the use of (4.34), because for physical energies $\sqrt{s} > m_N + m_\pi$ the resonance self-energy is probed far off the resonance pole. This argument has non-trivial implications for the chiral $SU(3)$ dynamics. Naively one may object that the effect of the u-channel baryon resonance exchange contribution in (4.34) can be absorbed to good accuracy into chiral two-body interaction terms in any case. However, while this is true in a chiral $SU(2)$ scheme this is no longer possible in a chiral $SU(3)$ approach. This follows because chiral symmetry selects a specific subset of all possible $SU(3)$ -symmetric two-body interaction terms to given chiral order. In particular one finds that the effect of the $Z_{[9]}$ parameter in (4.34) can not be absorbed into the chiral two-body parameters $g^{(S)}, g^{(V)}$ or $g^{(T)}$ of (2.22). For that reason we discriminate two possible scenarios. In scenario I we conjecture that the baryon nonet resonance states are primarily generated by the coupled channel dynamics of the vector-meson baryon-octet channels. Therefore in this scenario the u-channel resonance exchange contribution of (4.34) is neglected and only its s-channel contribution is included as a reminiscence of the neglected vector meson channels. This is analogous the treatment of the $\Lambda(1405)$ resonance, which is generated dynamically in the chiral $SU(3)$ scheme (see Fig. 3.1). Here a s-channel

pole term is generated by the coupled channel dynamics but the associated u-channel term is effectively left out as a much suppressed contribution. In scenario II we explicitly include the s- and the u-channel resonance exchange contributions as given in (4.34), thereby assuming that the resonance was preformed already in the large- N_c limit of QCD and only slightly affected by the coupled channel dynamics. According to the discussion of chapter 2.1 one may expect that the data set should favor scenario I): if one member of the **70**-plet is dynamically generated the remaining members should be of dynamic origin too. Since the $\Lambda(1405)$ appears to be the result of coupled channel dynamics the same should hold for the baryon nonet states, in particular the $\Lambda(1520)$.

Detailed analyses of the data set clearly favor scenario I). It appears impossible to obtain any reasonable fit within scenario II). The inclusion of the u-channel resonance exchange contributions destroys the subtle balance of chiral s-wave range terms. From a physical point of view this mechanism is easily understood. Once the coupling constants of the baryon nonet states to the meson bayron final state are estimated in terms of the resonance decay width, the u-channel diagrams predict quite large s-wave effective range terms that can not be reabsorbed into the quasi-local counter terms of the chiral Lagrangian. Therefore an attempt to fit the antikaon-nucleon scattering data in scenario II) is unable to generate the s-wave $\Lambda(1405)$ resonance and support the proper resonance structure for the nonet states at the same time. Thus, all results presented in this work will be based on scenario I). In this scenario the background parameter $Z_{[9]}$ drops out completely (see (4.42)).

Consider the quasi-local two-body interaction terms $K_{[8][8]}^{(I)}$ and $K_\chi^{(I)}$ in (4.15). It is convenient to represent the strength of an interaction term in a given channel $(I, a) \rightarrow (I, b)$ by means of the dimensionless coupling coefficients $[C_{\dots}^{(I)}]_{ab}$. The $SU(3)$ structure of the interaction terms $\mathcal{L}^{(S)}$ and $\mathcal{L}^{(V)}$ in (2.22) are characterized by the coefficients $C_0^{(I)}$, $C_1^{(I)}$, $C_D^{(I)}$, $C_F^{(I)}$ and $\mathcal{L}^{(T)}$ by $\bar{C}_1^{(I)}$, $\bar{C}_D^{(I)}$ and $\bar{C}_F^{(I)}$. Similarly the interaction terms (2.31) which break chiral symmetry explicitly are written in terms of the coefficients $C_{\pi,0}^{(I)}$, $C_{\pi,D}^{(I)}$, $C_{\pi,F}^{(I)}$ and $C_{K,0}^{(I)}$, $C_{K,D}^{(I)}$, $C_{K,F}^{(I)}$. We have

$$\begin{aligned}
K_{[8][8]}^{(I)}(\bar{k}, k; w) &= \frac{\bar{q} \cdot q}{4f^2} \left(g_0^{(S)} C_0^{(I)} + g_1^{(S)} C_1^{(I)} + g_D^{(S)} C_D^{(I)} + g_F^{(S)} C_F^{(I)} \right) \\
&+ \frac{1}{16f^2} \left(\not{q}(p + \bar{p}) \cdot \bar{q} + \not{\bar{q}}(p + \bar{p}) \cdot q \right) \left(g_0^{(V)} C_0^{(I)} + g_1^{(V)} C_1^{(I)} \right) \\
&+ \frac{1}{16f^2} \left(\not{q}(p + \bar{p}) \cdot \bar{q} + \not{\bar{q}}(p + \bar{p}) \cdot q \right) \left(g_D^{(V)} C_D^{(I)} + g_F^{(V)} C_F^{(I)} \right) \\
&+ \frac{i}{4f^2} \left(\bar{q}^\mu \sigma_{\mu\nu} q^\nu \right) \left(g_1^{(T)} \bar{C}_1^{(I)} + g_D^{(T)} \bar{C}_D^{(I)} + g_F^{(T)} \bar{C}_F^{(I)} \right), \\
K_\chi^{(I)}(\bar{k}, k; w) &= \frac{b_0}{f^2} \left(m_\pi^2 C_{\pi,0}^{(I)} + m_K^2 C_{K,0}^{(I)} \right) + \frac{b_D}{f^2} \left(m_\pi^2 C_{\pi,D}^{(I)} + m_K^2 C_{K,D}^{(I)} \right) \\
&+ \frac{b_F}{f^2} \left(m_\pi^2 C_{\pi,F}^{(I)} + m_K^2 C_{K,F}^{(I)} \right), \tag{4.37}
\end{aligned}$$

where the coefficients $C_{\dots,ab}^{(I)}$ are listed in Tab. 4.2 for the strangeness minus one channels but shown in [97] for the strangeness zero channels. A complete listing of the Q^3 quasi-local two-body interaction terms can be found in [97].

	$C_{\pi,0}^{(0)}$	$C_{\pi,D}^{(0)}$	$C_{\pi,F}^{(0)}$	$C_{K,0}^{(0)}$	$C_{K,D}^{(0)}$	$C_{K,F}^{(0)}$	$C_0^{(0)}$	$C_1^{(0)}$	$C_D^{(0)}$	$C_F^{(0)}$	$\bar{C}_1^{(0)}$	$\bar{C}_D^{(0)}$	$\bar{C}_F^{(0)}$
11	0	0	0	-4	-6	-2	2	2	3	1	2	1	3
12	0	$-\sqrt{\frac{3}{2}}$	$\sqrt{\frac{3}{2}}$	0	$-\sqrt{\frac{3}{2}}$	$\sqrt{\frac{3}{2}}$	0	$\sqrt{6}$	$\sqrt{\frac{3}{2}}$	$-\sqrt{\frac{3}{2}}$	$\sqrt{6}$	$-\sqrt{\frac{3}{2}}$	$\sqrt{\frac{3}{2}}$
13	0	$\frac{1}{\sqrt{2}}$	$\frac{3}{\sqrt{2}}$	0	$-\frac{5}{3\sqrt{2}}$	$-\frac{5}{\sqrt{2}}$	0	$\sqrt{2}$	$\frac{1}{3\sqrt{2}}$	$\frac{1}{\sqrt{2}}$	$\sqrt{2}$	$\frac{1}{\sqrt{2}}$	$\frac{3}{\sqrt{2}}$
14	0	0	0	0	0	0	0	-3	0	0	-1	0	0
22	-4	-4	0	0	0	0	2	4	2	0	2	0	4
23	0	$-\frac{4}{\sqrt{3}}$	0	0	0	0	0	$\sqrt{3}$	$\frac{2}{\sqrt{3}}$	0	$\sqrt{3}$	0	0
24	0	$\sqrt{\frac{3}{2}}$	$\sqrt{\frac{3}{2}}$	0	$\sqrt{\frac{3}{2}}$	$\sqrt{\frac{3}{2}}$	0	$-\sqrt{6}$	$-\sqrt{\frac{3}{2}}$	$-\sqrt{\frac{3}{2}}$	$-\sqrt{6}$	$-\sqrt{\frac{3}{2}}$	$-\sqrt{\frac{3}{2}}$
33	$\frac{4}{3}$	$\frac{28}{9}$	0	$-\frac{16}{3}$	$-\frac{64}{9}$	0	2	2	2	0	0	0	0
34	0	$-\frac{1}{\sqrt{2}}$	$\frac{3}{\sqrt{2}}$	0	$\frac{5}{3\sqrt{2}}$	$-\frac{5}{\sqrt{2}}$	0	$-\sqrt{2}$	$-\frac{1}{3\sqrt{2}}$	$\frac{1}{\sqrt{2}}$	$-\sqrt{2}$	$\frac{1}{\sqrt{2}}$	$-\frac{3}{\sqrt{2}}$
44	0	0	0	-4	-6	2	2	2	3	-1	2	-1	3
	$C_{\pi,0}^{(1)}$	$C_{\pi,D}^{(1)}$	$C_{\pi,F}^{(1)}$	$C_{K,0}^{(1)}$	$C_{K,D}^{(1)}$	$C_{K,F}^{(1)}$	$C_0^{(1)}$	$C_1^{(1)}$	$C_D^{(1)}$	$C_F^{(1)}$	$\bar{C}_1^{(1)}$	$\bar{C}_D^{(1)}$	$\bar{C}_F^{(1)}$
11	0	0	0	-4	-2	2	2	0	1	-1	0	-1	1
12	0	-1	1	0	-1	1	0	0	1	-1	0	-1	1
13	0	$\frac{1}{\sqrt{6}}$	$\sqrt{\frac{3}{2}}$	0	$\frac{1}{\sqrt{6}}$	$\sqrt{\frac{3}{2}}$	0	0	$-\frac{1}{\sqrt{6}}$	$-\sqrt{\frac{3}{2}}$	0	$\frac{1}{\sqrt{6}}$	$\sqrt{\frac{3}{2}}$
14	0	$-\sqrt{\frac{3}{2}}$	$\sqrt{\frac{3}{2}}$	0	$\frac{5}{\sqrt{6}}$	$-\frac{5}{\sqrt{6}}$	0	0	$-\frac{1}{\sqrt{6}}$	$\frac{1}{\sqrt{6}}$	0	$-\sqrt{\frac{3}{2}}$	$\sqrt{\frac{3}{2}}$
15	0	0	0	0	0	0	0	1	0	0	-1	0	0
22	-4	-4	0	0	0	0	2	-1	2	0	1	0	2
23	0	0	0	0	0	0	0	0	0	0	0	$-2\sqrt{\frac{2}{3}}$	0
24	0	0	$4\sqrt{\frac{2}{3}}$	0	0	0	0	0	0	$-2\sqrt{\frac{2}{3}}$	0	0	0
25	0	1	1	0	1	1	0	0	-1	-1	0	-1	-1
33	-4	$-\frac{4}{3}$	0	0	0	0	2	0	$\frac{2}{3}$	0	0	0	0
34	0	$-\frac{4}{3}$	0	0	0	0	0	1	$\frac{2}{3}$	0	-1	0	0
35	0	$\frac{1}{\sqrt{6}}$	$-\sqrt{\frac{3}{2}}$	0	$\frac{1}{\sqrt{6}}$	$-\sqrt{\frac{3}{2}}$	0	0	$-\frac{1}{\sqrt{6}}$	$\sqrt{\frac{3}{2}}$	0	$-\frac{1}{\sqrt{6}}$	$\sqrt{\frac{3}{2}}$
44	$\frac{4}{3}$	$-\frac{4}{3}$	0	$-\frac{16}{3}$	0	0	2	0	$\frac{2}{3}$	0	0	0	0
45	0	$-\sqrt{\frac{3}{2}}$	$-\sqrt{\frac{3}{2}}$	0	$\frac{5}{\sqrt{6}}$	$\frac{5}{\sqrt{6}}$	0	0	$-\frac{1}{\sqrt{6}}$	$-\frac{1}{\sqrt{6}}$	0	$\sqrt{\frac{3}{2}}$	$\sqrt{\frac{3}{2}}$
55	0	0	0	-4	-2	-2	2	0	1	1	0	1	1
	$C_{\pi,0}^{(2)}$	$C_{\pi,D}^{(2)}$	$C_{\pi,F}^{(2)}$	$C_{K,0}^{(2)}$	$C_{K,D}^{(2)}$	$C_{K,F}^{(2)}$	$C_0^{(2)}$	$C_1^{(2)}$	$C_D^{(2)}$	$C_F^{(2)}$	$\bar{C}_1^{(2)}$	$\bar{C}_D^{(2)}$	$\bar{C}_F^{(2)}$
11	-4	-4	0	0	0	0	2	1	2	0	-1	0	-2

Table 4.2: Coefficients of quasi-local interaction terms in the strangeness minus one channels as defined in (4.37).

4.2 Chiral expansion and covariance

It remains to perform a chiral expansion of the interaction kernel (4.15). This is necessary since here the relativistic chiral Lagrangian is applied. In contrast, if the heavy-baryon representation of the chiral Lagrangian is used part of the chiral expansion is already implemented at the level of the Lagrangian. A novel chiral expansion strategy for the interaction kernel will be proposed that complies manifestly with covariance.

For this purpose it is instructive to cast the meson energy ω and the baryon energy E introduced in (4.12) into the following form

$$\begin{aligned}\omega_a^{(I)}(\sqrt{s}) &= \sqrt{s} - m_{B(I,a)}^{(I)} - \frac{\phi_a^{(I)}(\sqrt{s})}{2\sqrt{s}}, & E_a^{(I)}(\sqrt{s}) &= m_{B(I,a)} + \frac{\phi_a^{(I)}(\sqrt{s})}{2\sqrt{s}}, \\ \phi_a^{(I)}(\sqrt{s}) &= \left(\sqrt{s} - m_{B(I,a)}\right)^2 - m_{\Phi(I,a)}^2,\end{aligned}\tag{4.38}$$

expressed in terms of the approximate phase-space factor ϕ . It is sufficient to consider the above kinematical variables since it is assumed that the partial wave decomposition of the scattering kernel was performed previously. In the standard counting scheme the meson energy ω is assigned the formal power Q . On the other hand, the baryon energy $E = m + \mathcal{O}(Q^2)$ is interpreted as a leading term, the baryon mass (more precisely its chiral limit value) and a series of correction terms. As a consequence also the Mandelstam variable, $\sqrt{s} = \omega + E$, is split into an infinite hierarchy of terms characterized by increasing chiral orders. Here it is proposed to count

$$\sqrt{s} \sim Q^0,\tag{4.39}$$

instead, a manifest covariant assignment. Then the representation (4.38) suggests that it may be advantageous to write the meson energy ω as a sum of two terms, the first of order Q and the second term of order Q^2 . This is achieved once the formal powers are assigned as follows

$$\sqrt{s} \sim Q^0, \quad \phi_a^{(I)}/\sqrt{s} \sim Q^2, \quad m_{\Phi(I,a)}^2 \sim Q^2.\tag{4.40}$$

A unique decomposition of the meson energy ω into the leading term $\sqrt{s} - m \sim Q$ and the subleading term $-\phi/(2\sqrt{s}) \sim Q^2$ is implied. It is stressed that the assignment leads to m as the leading chiral moment of the baryon energy E .

The implications of the novel covariant power counting assignment are first exemplified for the case of the quasi-local two-body interaction terms. It is straight forward to derive the effective interaction kernel relevant for the s- and p-wave channels

$$\begin{aligned}V_{[8][8]}^{(I,+)}(\sqrt{s}; 0) &= \frac{1}{4f^2} \left(g_0^{(S)} + \sqrt{s} g_0^{(V)}\right) \left(\sqrt{s} - M^{(I)}\right) C_0^{(I)} \left(\sqrt{s} - M^{(I)}\right) \\ &+ \frac{1}{4f^2} \left(g_1^{(S)} + \sqrt{s} g_1^{(V)}\right) \left(\sqrt{s} - M^{(I)}\right) C_1^{(I)} \left(\sqrt{s} - M^{(I)}\right) \\ &+ \frac{1}{4f^2} \left(g_D^{(S)} + \sqrt{s} g_D^{(V)}\right) \left(\sqrt{s} - M^{(I)}\right) C_D^{(I)} \left(\sqrt{s} - M^{(I)}\right) \\ &+ \frac{1}{4f^2} \left(g_F^{(S)} + \sqrt{s} g_F^{(V)}\right) \left(\sqrt{s} - M^{(I)}\right) C_F^{(I)} \left(\sqrt{s} - M^{(I)}\right) \\ &+ \mathcal{O}\left(Q^3\right), \\ V_{[8][8]}^{(I,-)}(\sqrt{s}; 0) &= -\frac{1}{3f^2} M^{(I)} \left(g_0^{(S)} C_0^{(I)} + g_1^{(S)} C_1^{(I)}\right) M^{(I)}\end{aligned}$$

$$\begin{aligned}
& - \frac{1}{3f^2} M^{(I)} \left(g_D^{(S)} C_D^{(I)} + g_F^{(S)} C_F^{(I)} \right) M^{(I)} \\
& + \frac{1}{4f^2} \left(\sqrt{s} + M^{(I)} \right) \left(g_1^{(T)} \bar{C}_1^{(I)} + g_D^{(T)} \bar{C}_D^{(I)} \right) \left(\sqrt{s} + M^{(I)} \right) \\
& + \frac{1}{4f^2} \left(\sqrt{s} + M^{(I)} \right) g_F^{(T)} \bar{C}_F^{(I)} \left(\sqrt{s} + M^{(I)} \right) \\
& - \frac{1}{3f^2} M^{(I)} \left(g_1^{(T)} \bar{C}_1^{(I)} + g_D^{(T)} \bar{C}_D^{(I)} + g_F^{(T)} \bar{C}_F^{(I)} \right) M^{(I)} + \mathcal{O}(Q) , \\
V_{[8][8]}^{(I,+)}(\sqrt{s}; 1) & = - \frac{1}{12f^2} \left(g_0^{(S)} C_0^{(I)} + g_1^{(S)} C_1^{(I)} + g_D^{(S)} C_D^{(I)} + g_F^{(S)} C_F^{(I)} \right) \\
& - \frac{1}{12f^2} \left(g_1^{(T)} \bar{C}_1^{(I)} + g_D^{(T)} \bar{C}_D^{(I)} + g_T^{(T)} \bar{C}_F^{(I)} \right) + \mathcal{O}(Q) . \\
V_\chi^{(I,+)}(\sqrt{s}, 0) & = \frac{b_0}{f^2} \left(m_\pi^2 C_{\pi,0}^{(I)} + m_K^2 C_{K,0}^{(I)} \right) + \frac{b_D}{f^2} \left(m_\pi^2 C_{\pi,D}^{(I)} + m_K^2 C_{K,D}^{(I)} \right) \\
& + \frac{b_F}{f^2} \left(m_\pi^2 C_{\pi,F}^{(I)} + m_K^2 C_{K,F}^{(I)} \right) + \mathcal{O}(Q^3) , \tag{4.41}
\end{aligned}$$

where the diagonal baryon mass matrix $M_{ab}^{(I)} = \delta_{ab} m_{B(I,a)}$ was introduced. The notation in (4.41) implies a matrix multiplication of the mass matrix $M^{(I)}$ by the coefficient matrices $C^{(I)}$ in the 'ab' channel-space. Recall that the d-wave interaction kernel $V_{[8][8]}^{(I,-)}(\sqrt{s}, 1)$ does not receive any contribution from quasi-local counter terms to chiral order Q^3 . Similarly the chiral symmetry-breaking interaction kernel V_χ can only contribute to s-wave scattering to this order. It is pointed out that the result (4.41) is uniquely determined by expanding the meson energy according to (4.38). In particular we keep in $V_{\Phi_B}^{(I,+)}(\sqrt{s}, 0)$ the \sqrt{s} factor in front of $g^{(V)}$. Any further expansion in $\sqrt{s} - \Lambda$ with some scale $\Lambda \simeq m_N$ is refrained from. The relativistic chiral Lagrangian supplied with (4.38) leads to well-defined kinematical factors included in (4.41). These kinematical factors, which are natural ingredients of the relativistic chiral Lagrangian, can be generated also in the heavy-baryon formalism by a proper regrouping of interaction terms. The Q^3 -terms induced by the interaction kernel (4.37) are shown in [97] as part of a complete collection of relevant Q^3 -terms.

Next consider the Weinberg-Tomozawa term and the baryon octet and decuplet s-channel pole contributions

$$\begin{aligned}
V_{WT}^{(I,\pm)}(\sqrt{s}; 0) & = \frac{1}{2f^2} \left(\sqrt{s} C_{WT}^{(I)} \mp \frac{1}{2} [M^{(I)}, C_{WT}^{(I)}]_+ \right) , \\
V_{s-[8]}^{(I,\pm)}(\sqrt{s}; 0) & = - \sum_{c=1}^3 \left(\sqrt{s} \mp M_5^{(I,c)} \right) \frac{C_{[8]}^{(I,c)}}{4f^2 (\sqrt{s} \pm m_{[8]}^{(c)})} \left(\sqrt{s} \mp M_5^{(I,c)} \right) , \\
V_{s-[10]}^{(I,+)}(\sqrt{s}; 0) & = - \frac{2}{3} \sum_{c=1}^2 \frac{\sqrt{s} + m_{[10]}^{(c)}}{(m_{[10]}^{(c)})^2} \left(\sqrt{s} - M^{(I)} \right) \frac{C_{[10]}^{(I,c)}}{4f^2} \left(\sqrt{s} - M^{(I)} \right) \\
& + \sum_{c=1}^2 Z_{[10]} \frac{2\sqrt{s} - m_{[10]}^{(c)}}{3(m_{[10]}^{(c)})^2} \left(\sqrt{s} - M^{(I)} \right) \frac{C_{[10]}^{(I,c)}}{4f^2} \left(\sqrt{s} - M^{(I)} \right) \\
& + \sum_{c=1}^2 Z_{[10]}^2 \frac{2m_{[10]}^{(c)} - \sqrt{s}}{6(m_{[10]}^{(c)})^2} \left(\sqrt{s} - M^{(I)} \right) \frac{C_{[10]}^{(I,c)}}{4f^2} \left(\sqrt{s} - M^{(I)} \right)
\end{aligned}$$

$$\begin{aligned}
& + \mathcal{O}(Q^3) , \\
V_{s-[10]}^{(I,-)}(\sqrt{s}; 0) &= \sum_{c=1}^2 \frac{Z_{[10]}}{3 m_{[10]}^{(c)}} (\sqrt{s} + M^{(I)}) \frac{C_{[10]}^{(I,c)}}{4 f^2} (\sqrt{s} + M^{(I)}) \\
& - \sum_{c=1}^2 Z_{[10]}^2 \frac{\sqrt{s} + 2 m_{[10]}^{(c)}}{6 (m_{[10]}^{(c)})^2} (\sqrt{s} + M^{(I)}) \frac{C_{[10]}^{(I,c)}}{4 f^2} (\sqrt{s} + M^{(I)}) \\
& + \mathcal{O}(Q) , \\
V_{s-[10]}^{(I,+)}(\sqrt{s}; +1) &= -\frac{1}{3} \sum_{c=1}^2 \frac{C_{[10]}^{(I,c)}}{4 f^2 (\sqrt{s} - m_{[10]}^{(c)})} + \mathcal{O}(Q) , \\
V_{s-[9]}^{(I,-)}(\sqrt{s}; -1) &= -\frac{1}{3} \sum_{c=1}^2 \frac{C_{[9]}^{(I,c)}}{4 f^2 (\sqrt{s} - m_{[9]}^{(c)})} + \mathcal{O}(Q^0) \tag{4.42}
\end{aligned}$$

where terms of order Q^3 are suppressed. Furthermore observe the short hand notation

$$\left[M_5^{(I,c)} \right]_{ab} = \delta_{ab} \left(m_{B(I,a)} + R_{L,aa}^{(I,c)} \right) , \tag{4.43}$$

used in the s-channel exchange contribution. The Weinberg-Tomozawa interaction term V_{WT} contributes to the s-wave and p-wave interaction kernels with $J = \frac{1}{2}$ to chiral order Q and Q^2 respectively but not in the $J = \frac{3}{2}$ channels. Similarly the baryon octet s-channel exchange $V_{s-[8]}$ contributes only in the $J = \frac{1}{2}$ channels and the baryon decuplet s-channel exchange $V_{s-[10]}$ to all considered channels but the d-wave channel. The Q^3 -terms not shown in (4.42) are given in [97]. In (4.42) the baryon-nonet resonance contribution is expanded applying in particular the questionable formal rule $\sqrt{s} - m_{[9]} \sim Q$. To order Q^3 one then finds that only the d-wave interaction kernels are affected. In fact, the vanishing of all contributions except the one in the d-wave channel does not depend on the assumption $\sqrt{s} - m_{[9]} \sim Q$. It merely reflects the phase space properties of the resonance field. This strategy preserves the correct pole contribution in $V_{s-[9]}^{(I,-)}(\sqrt{s}; -1)$ but discards smooth background terms in all partial-wave interaction kernels. This is consistent with the discussion of chapter 4.1 which implies that those background terms are not controlled in any case. It is emphasized that the physical mass matrix $M^{(I)}$ is used in the interaction kernel rather than its chiral $SU(3)$ limit. Since the mass matrix follows from the on-shell reduction of the interaction kernel it necessarily involves the physical mass matrix $M^{(I)}$. Similarly $M_5^{(I)}$ is kept unexpanded since only this leads to the proper meson-baryon coupling strengths. This procedure is analogous to keeping the physical masses in the unitarity loop functions $J_{MB}(w)$ in (3.51).

Proceed with the baryon octet and baryon decuplet u-channel contributions. After performing their proper angular average as implied by the partial-wave projection in (4.12) their contributions to the scattering kernels are written in terms of the matrix valued functions $h_{n\pm}^{(I)}(\sqrt{s}, m)$, $q_{n\pm}^{(I)}(\sqrt{s}, m)$ and $p_{n\pm}^{(I)}(\sqrt{s}, m)$ as

$$\begin{aligned}
\left[V_{u-[8]}^{(I,\pm)}(\sqrt{s}; n) \right]_{ab} &= \sum_{c=1}^4 \frac{1}{4 f^2} \left[\tilde{C}_{[8]}^{(I,c)} \right]_{ab} \left[h_{n\pm}^{(I)}(\sqrt{s}, m_{[8]}^{(c)}) \right]_{ab} , \\
\left[V_{u-[10]}^{(I,\pm)}(\sqrt{s}; n) \right]_{ab} &= \sum_{c=1}^3 \frac{1}{4 f^2} \left[\tilde{C}_{[10]}^{(I,c)} \right]_{ab} \left[p_{n\pm}^{(I)}(\sqrt{s}, m_{[10]}^{(c)}) \right]_{ab} ,
\end{aligned}$$

$$\left[V_{u-9}^{(I,\pm)}(\sqrt{s}; n) \right]_{ab} = \sum_{c=1}^4 \frac{1}{4f^2} \left[\tilde{C}_{[9]}^{(I,c)} \right]_{ab} \left[q_{n\pm}^{(I)}(\sqrt{s}, m_{[9]}^{(c)}) \right]_{ab}. \quad (4.44)$$

The functions $h_{n\pm}^{(I)}(\sqrt{s}, m)$, $q_{n\pm}^{(I)}(\sqrt{s}, m)$ and $p_{n\pm}^{(I)}(\sqrt{s}, m)$ can be expanded in chiral powers once a formal powers to the typical building blocks

$$\mu_{\pm,ab}^{(I)}(s, m) = m_{B(I,a)} + m_{B(I,b)} - \sqrt{s} \pm m, \quad (4.45)$$

is assigned. It is counted $\mu_- \sim Q$ and $\mu_+ \sim Q^0$ but it is refrained from any further expansion. Then the baryon octet functions $h_{n\pm}^{(I)}(\sqrt{s}, m)$ to order Q^3 read

$$\begin{aligned} \left[h_{0+}^{(I)}(\sqrt{s}, m) \right]_{ab} &= \sqrt{s} + m + \tilde{R}_{L,ab}^{(I,c)} + \tilde{R}_{R,ab}^{(I,c)} - \frac{m + M_{ab}^{(L)}}{\mu_{+,ab}^{(I)}(s, m)} \left(\sqrt{s} + \right. \\ &\quad \left. + \frac{\phi_a^{(I)}(s)(\sqrt{s} - m_{B(I,b)})}{\mu_{+,ab}^{(I)}(s, m)\mu_{-,ab}^{(I)}(s, m)} + \frac{(\sqrt{s} - m_{B(I,a)})\phi_b^{(I)}(s)}{\mu_{+,ab}^{(I)}(s, m)\mu_{-,ab}^{(I)}(s, m)} \right. \\ &\quad \left. + \frac{1}{3} \frac{\phi_a^{(I)}(s)(4\sqrt{s} - \mu_{+,ab}^{(I)}(s, m))\phi_b^{(I)}(s)}{(\mu_{+,ab}^{(I)}(s, m))^2(\mu_{-,ab}^{(I)}(s, m))^2} \right) \frac{m + M_{ab}^{(R)}}{\sqrt{s}} + \mathcal{O}(Q^3), \\ \left[h_{0-}^{(I)}(\sqrt{s}, m) \right]_{ab} &= \frac{m + M_{ab}^{(L)}}{\mu_{-,ab}^{(I)}(s, m)} \left(2\sqrt{s} + \mu_{-,ab}^{(I)}(s, m) \right. \\ &\quad \left. - \frac{8}{3} \frac{m_{B(I,a)}m_{B(I,b)}}{\mu_{+,ab}^{(I)}(s, m)} \right) \frac{m + M_{ab}^{(R)}}{\mu_{+,ab}^{(I)}(s, m)} + \mathcal{O}(Q), \\ \left[h_{1+}^{(I)}(\sqrt{s}, m) \right]_{ab} &= -\frac{2}{3} \frac{(m + M_{ab}^{(L)})(m + M_{ab}^{(R)})}{\mu_{-,ab}^{(I)}(s, m)(\mu_{+,ab}^{(I)}(s, m))^2} + \mathcal{O}(Q) \\ \left[h_{1-}^{(I)}(\sqrt{s}, m) \right]_{ab} &= -\frac{32}{15} \frac{(m + M_{ab}^{(L)})m_{B(I,a)}m_{B(I,b)}(m + M_{ab}^{(R)})}{(\mu_{-,ab}^{(I)}(s, m))^2(\mu_{+,ab}^{(I)}(s, m))^3} \\ &\quad + \frac{4}{3} \frac{(m + M_{ab}^{(L)})\sqrt{s}(m + M_{ab}^{(R)})}{(\mu_{-,ab}^{(I)}(s, m))^2(\mu_{+,ab}^{(I)}(s, m))^2} + \mathcal{O}(Q^{-1}), \end{aligned} \quad (4.46)$$

where $M_{ab}^{(L)} = m_{B(I,a)} + \tilde{R}_{L,ab}^{(I,c)}$ and $M_{ab}^{(R)} = m_{B(I,b)} + \tilde{R}_{R,ab}^{(I,c)}$ were introduced. The terms of order Q^3 can be found in [97] where also the analogous expressions for the decuplet and baryon-octet resonance exchanges are presented. Two important points related to the expansion in (4.46) should be emphasized. First, it leads to a separable interaction kernel. Thus, the induced Bethe-Salpeter equation is solved conveniently by the covariant projector method of chapter 3.4. Secondly such an expansion is only meaningful in conjunction with the renormalization procedure outlined in chapter 3.2. The expansion leads necessarily to further divergences which require careful attention.

This section is closed with a more detailed discussion of the u-channel exchange. Its non-local nature necessarily leads to singularities in the partial-wave scattering amplitudes at subthreshold energies. For instance, the expressions (4.46) as they stand turn useless at energies $\sqrt{s} \simeq m_{B(I,a)} + m_{B(I,b)} - m$ due to unphysical multiple poles at $\mu_- = 0$. One needs to address

this problem, because the subthreshold amplitudes are an important input for the many-body treatment of the nuclear meson dynamics. It is stressed that a singular behavior in the vicinity of $\mu_- \sim 0$ is a rather general property of any u-channel exchange contribution. It is not an artifact induced by the chiral expansion. The partial-wave decomposition of a u-channel exchange contribution represents the pole term only for sufficiently large or small \sqrt{s} . To be explicit consider the u-channel nucleon pole term contribution of elastic πN scattering

$$\sum_{n=0}^{\infty} \int_{-1}^1 \frac{dx}{2} \frac{P_n(x)}{\mu_{\pi N}^{(+)} \mu_{\pi N}^{(-)} - 2\phi_{\pi N} x + \mathcal{O}(Q^3)}, \quad (4.47)$$

where $\mu_{\pi N}^{(\pm)} = 2m_N - \sqrt{s} \pm m_N$. Upon inspecting the branch points induced by the angular average one concludes that the partial wave decomposition (4.47) is valid only if $\sqrt{s} > \Lambda_+$ or $\sqrt{s} < \Lambda_-$ with $\Lambda_{\pm} = m_N \pm m_{\pi}^2/m_N + \mathcal{O}(Q^3)$. For any value in between, $\Lambda_- < \sqrt{s} < \Lambda_+$, the partial-wave decomposition is not converging. Therefore the following prescription for the u-channel contributions is adopted. The unphysical pole terms in (4.46) are systematically replaced by

$$\begin{aligned} m \Lambda_{ab}^{(\pm)}(m) &= m (m_{B(I,a)} + m_{B(I,b)}) - m^2 \\ &\pm \left(\left((m - m_{B(I,b)})^2 - m_{\Phi(I,a)}^2 \right) \left((m - m_{B(I,a)})^2 - m_{\Phi(I,b)}^2 \right) \right)^{1/2}, \\ \left(\mu_{-,ab}^{-1}(\sqrt{s}, m) \right)^n &\rightarrow \left(\mu_{-,ab}^{-1}(\Lambda_{ab}^{(-)}, m) \right)^n \frac{\sqrt{s} - \Lambda_{ab}^{(+)}}{\Lambda_{ab}^{(-)} - \Lambda_{ab}^{(+)}} \\ &+ \left(\mu_{-,ab}^{-1}(\Lambda_{ab}^{(+)}, m) \right)^n \frac{\sqrt{s} - \Lambda_{ab}^{(-)}}{\Lambda_{ab}^{(+)} - \Lambda_{ab}^{(-)}}, \end{aligned} \quad (4.48)$$

for $\Lambda_{ab}^{(-)} < \sqrt{s} < \Lambda_{ab}^{(+)}$ but kept unchanged for $\sqrt{s} > \Lambda_{ab}^{(+)}$ or $\sqrt{s} < \Lambda_{ab}^{(-)}$ in a given channel (a,b). The prescription (4.48) properly generalizes the $SU(2)$ sector result $\Lambda_{\pm} \simeq m_N \pm m_{\pi}^2/m_N$ to the $SU(3)$ sector. We underline that (4.48) leads to regular expressions for $h_{\pm n}(\sqrt{s}, m)$ but leaves the u-channel pole contributions unchanged above threshold. The reader may ask why such a prescription is imposed at all. Outside the convergence radius of the partial-wave expansion the amplitudes do not make much sense in any case. The prescription is nevertheless required due to a coupled-channel effect. Consider for example elastic kaon-nucleon scattering in the strangeness -1 channel. Since there are no u-channel exchange contributions in this channel the physical partial-wave amplitudes do not show any induced singularity structures. In the $\pi\Sigma \rightarrow \pi\Sigma$ channel, on the other hand, the u-channel hyperon exchange does contribute and therefore leads through the coupling of the $\bar{K}N$ and $\pi\Sigma$ channels to a singularity also in the $\bar{K}N$ amplitude. Such induced singularities are an immediate consequence of the approximate treatment of the u-channel exchange contribution and must be absent in an exact treatment. As a measure for the quality of the prescription the accuracy to which the resulting subthreshold forward kaon-nucleon scattering amplitudes satisfy a dispersion integral representation is proposed. This issue will be taken up in the result chapter.

4.3 Crossing symmetry and the $S = 1$ channels

This section addresses an issue of central importance for coupled channel analyses. To what extent do the coupled channel scattering amplitudes as constructed in the previous sections comply with the crossing symmetry constraint of quantum field theory. The discussion necessarily involves the K^+ -nucleon scattering process which is related to the K^- -nucleon scattering process by crossing symmetry.

The scattering amplitudes $T_{KN \rightarrow KN}^{(I)}$ follow from the antikaon-nucleon scattering amplitudes $T_{\bar{K}N \rightarrow \bar{K}N}^{(I)}$ via the transformation

$$\begin{aligned} T_{KN \rightarrow KN}^{(0)}(\bar{q}, q; w) &= -\frac{1}{2} T_{\bar{K}N \rightarrow \bar{K}N}^{(0)}(-q, -\bar{q}; w - \bar{q} - q) \\ &\quad + \frac{3}{2} T_{\bar{K}N \rightarrow \bar{K}N}^{(1)}(-q, -\bar{q}; w - \bar{q} - q), \\ T_{KN \rightarrow KN}^{(1)}(\bar{q}, q; w) &= +\frac{1}{2} T_{\bar{K}N \rightarrow \bar{K}N}^{(0)}(-q, -\bar{q}; w - \bar{q} - q) \\ &\quad + \frac{1}{2} T_{\bar{K}N \rightarrow \bar{K}N}^{(1)}(-q, -\bar{q}; w - \bar{q} - q). \end{aligned} \quad (4.49)$$

Consider the two important remarks. First, if the solution of the coupled channel Bethe-Salpeter equation of the antikaon-nucleon system of the previous chapters is used to construct the kaon-nucleon scattering amplitudes via (4.49) one finds real partial-wave amplitudes in conflict with unitarity. Second, in any case the antikaon-nucleon scattering amplitudes must not be applied far below the antikaon-nucleon threshold. The first point is obvious because in the kaon-nucleon channel only two-particle irreducible diagrams are summed. The reducible diagrams in the KN sector correspond to irreducible contributions in the $\bar{K}N$ sector and vice versa. Since the interaction kernel of the $\bar{K}N$ sector is evaluated perturbatively it is clear that the scattering amplitude does not include that infinite sum of reducible diagrams required for unitarity in the crossed channel. The second point follows, because the chiral $SU(3)$ Lagrangian is an effective field theory where the heavy-meson exchange contributions are integrated out. It is important to identify the applicability domain correctly. Inspecting the singularity structure induced by the light t-channel vector meson exchange contributions one observes that they, besides restricting the applicability domain with

$$\sqrt{s} < \sqrt{m_N^2 + m_\rho^2/4} + \sqrt{m_K^2 + m_\rho^2/4} \simeq 1640 \text{ MeV}, \quad (4.50)$$

from above, induce cut-structures in between the kaon- and antikaon-nucleon thresholds. This will be discussed in more detail below. Though close to the kaon and antikaon-nucleon thresholds the tree-level contributions of the vector meson exchange are successfully represented by quasi-local interaction vertices, basically the Weinberg-Tomozawa interaction term, it is not justified to extrapolate a loop evaluated with the effective antikaon-nucleon vertex down to the kaon-nucleon threshold. Thus, one should not identify the antikaon-nucleon scattering amplitudes as obtained in this work with the Bethe-Salpeter kernel of the kaon-nucleon system. This would lead to a manifestly crossing symmetric approach, a so-called 'parquet' approximation, if set up in a self consistent manner.

The fatal drawback of a parquet type of approach within the present chiral framework is reiterated: the antikaon-nucleon amplitudes would be probed far below the $\bar{K}N$ threshold at $\sqrt{s} \simeq m_N - m_K$ outside their validity domain. A clear signal for the unreliability of the antikaon-nucleon scattering amplitudes at $\sqrt{s} \simeq m_N - m_K$ is the presence of unphysical pole structures

	$C_{WT}^{(I)}$	$C_{N_{[8]}}^{(I)}$	$C_{\Lambda_{[8]}}^{(I)}$	$C_{\Sigma_{[8]}}^{(I)}$	$C_{\Delta_{[10]}}^{(I)}$	$C_{\Sigma_{[10]}}^{(I)}$	$\tilde{C}_{N_{[8]}}^{(I)}$	$\tilde{C}_{\Lambda_{[8]}}^{(I)}$	$\tilde{C}_{\Sigma_{[8]}}^{(I)}$	$\tilde{C}_{\Xi_{[8]}}^{(I)}$	$\tilde{C}_{\Delta_{[10]}}^{(I)}$	$\tilde{C}_{\Sigma_{[10]}}^{(I)}$	$\tilde{C}_{\Xi_{[10]}}^{(I)}$
$I = 0$	0	0	0	0	0	0	0	$-\frac{1}{2}$	$\frac{3}{2}$	0	0	$\frac{3}{2}$	0
$I = 1$	-2	0	0	0	0	0	0	$\frac{1}{2}$	$\frac{1}{2}$	0	0	$\frac{1}{2}$	0

Table 4.3: Weinberg-Tomozawa interaction strengths and baryon exchange coefficients in the strangeness plus one channels as defined in (4.31).

which typically arise at $\sqrt{s} < 700$ MeV. For example, the Fig. 3.1 of chapter 3.3 would show unphysical poles if extended for $\sqrt{s} < 1$ GeV.

For the above reasons the antikaon-nucleon interaction kernel is evaluated in chiral perturbation theory. Equivalently the interaction kernels, V_{KN} , could be derived from the antikaon-nucleon interaction kernels $V_{\bar{K}N}$ by applying the crossing identities (4.49). The interaction kernels $V_{KN}(\sqrt{s}; n)$ in the K^+ -nucleon channel are given by (4.41,4.42,4.44) with the required coefficients listed in Tab. 4.3 and Tab. 4.4. By analogy with the treatment of the antikaon-nucleon scattering process the kaon-nucleon interaction evaluated to chiral order Q^3 is taken as input in the Bethe-Salpeter equation. Again only those Q^3 -correction terms are considered which are leading in the $1/N_c$ expansion. The partial-wave scattering amplitudes $M_{KN}^{(I,\pm)}(\sqrt{s}; n)$ then follow

$$M_{KN}^{(I,\pm)}(\sqrt{s}; n) = \frac{V_{KN}^{(I,\pm)}(\sqrt{s}; n)}{1 - V_{KN}^{(I,\pm)}(\sqrt{s}; n) J_{KN}^{(\pm)}(\sqrt{s}; n)} \quad (4.51)$$

where the loop functions $J_{KN}^{(\pm)}(\sqrt{s}; n)$ are given in (4.11) with $m_{B(I,a)} = m_N$ and $m_{\Phi(I,a)} = m_K$. The subtraction point $\mu^{(I)}$ is identified with the averaged hyperon mass $\mu^{(I)} = (m_\Lambda + m_\Sigma)/2$.

It is pointed out that in the scheme developed here one arrives at a crossing symmetric amplitude by matching the amplitudes $M_{KN}^{(I,\pm)}(\sqrt{s}, n)$ and $M_{\bar{K}N}^{(I,\pm)}(\sqrt{s}, n)$ at subthreshold energies. The matching interval must be chosen so that both the kaon and antikaon amplitudes are still within their validity domains. A complication arises due to the light vector meson exchange contributions in the t-channel, which was already identified above to restrict the validity domain of the present chiral approach. To be explicit consider the t-channel ω -exchange. It leads to a branch point at $\sqrt{s} = \Lambda_\omega$ with

$$\Lambda_\omega = (m_N^2 - m_\omega^2/4)^{1/2} + (m_K^2 - m_\omega^2/4)^{1/2} \simeq 1138 \text{ MeV} . \quad (4.52)$$

Consequently, one expects the partial-wave kaon and antikaon amplitudes to be reliable for $\sqrt{s} > \Lambda_\omega$ only. That implies, however, that in the crossed channel the amplitude is needed for

$$\sqrt{s} > (2m_N^2 - \Lambda_\omega^2 + 2m_K^2)^{1/2} \simeq 978 \text{ MeV} < \Lambda_\omega . \quad (4.53)$$

One may naively conclude that crossing symmetry appears outside the scope of the present approach because the matching window is closed. The minimal critical point Λ_{opt} needed to open the matching window is

$$\Lambda_{\text{opt.}} \simeq \sqrt{m_N^2 + m_K^2} \simeq 1061 \text{ MeV} . \quad (4.54)$$

	$C_{\pi,0}^{(I)}$	$C_{\pi,D}^{(I)}$	$C_{\pi,F}^{(I)}$	$C_{K,0}^{(I)}$	$C_{K,D}^{(I)}$	$C_{K,F}^{(I)}$	$C_0^{(I)}$	$C_1^{(I)}$	$C_D^{(I)}$	$C_F^{(I)}$	$\bar{C}_1^{(I)}$	$\bar{C}_D^{(I)}$	$\bar{C}_F^{(I)}$
$I = 0$	0	0	0	-4	0	4	2	-1	0	-2	1	2	0
$I = 1$	0	0	0	-4	-4	0	2	1	2	0	-1	0	-2

Table 4.4: Coefficients of quasi-local interaction terms in the strangeness plus one channels as defined in (4.37).

It is determined by the condition $s = u$ at $\cos\theta = 1$. One concludes that matching the kaon and antikaon amplitudes requires that both amplitudes are within their applicability domain at $\sqrt{s} = \Lambda_{\text{opt.}}$. The point $\sqrt{s} = \Lambda_{\text{opt.}}$ is optimal, because it identifies the minimal reliability domain required for the matching of the subthreshold amplitudes. The complication implied by the t-channel vector meson exchanges could be circumvented by reconstructing that troublesome branch point explicitly; after all it is determined by a tree-level diagram. On the other hand, it is clear that one may avoid this complication altogether if one considers the forward scattering amplitudes only. For the latter amplitudes the branch cut at $\sqrt{s} = \Lambda_\omega$ cancels identically and consequently the forward scattering amplitudes should be reliable for energies smaller than Λ_ω also. For that reason, the matching will be demonstrated for the forward scattering amplitudes only. The approximate forward scattering amplitudes $T_{KN}^{(I)}(s)$ are reconstructed in terms the partial-wave amplitudes considered in this work

$$\begin{aligned}
T_{KN}^{(I)}(s) &= \frac{1}{2\sqrt{s}} \left(\frac{s + m_N^2 - m_K^2}{2m_N} + \sqrt{s} \right) M_{KN}^{(I,+)}(\sqrt{s}; 0) \\
&+ \frac{1}{2\sqrt{s}} \left(\frac{s + m_N^2 - m_K^2}{2m_N} - \sqrt{s} \right) M_{KN}^{(I,-)}(\sqrt{s}; 0) \\
&+ \frac{1}{\sqrt{s}} \left(\frac{s + m_N^2 - m_K^2}{2m_N} + \sqrt{s} \right) p_{KN}^2 M_{KN}^{(I,+)}(\sqrt{s}; 1) \\
&+ \frac{1}{\sqrt{s}} \left(\frac{s + m_N^2 - m_K^2}{2m_N} - \sqrt{s} \right) p_{KN}^2 M_{KN}^{(I,-)}(\sqrt{s}; 1) + \dots, \quad (4.55)
\end{aligned}$$

where $\sqrt{s} = \sqrt{m_N^2 + p_{KN}^2} + \sqrt{m_K^2 + p_{KN}^2}$. The analogous expression holds for $T_{\bar{K}N}^{(I)}(s)$. The crossing identities for the forward scattering amplitudes

$$\begin{aligned}
T_{KN}^{(0)}(s) &= -\frac{1}{2} T_{\bar{K}N}^{(0)}(2m_N^2 + 2m_K^2 - s) + \frac{3}{2} T_{\bar{K}N}^{(1)}(2m_N^2 + 2m_K^2 - s), \\
T_{KN}^{(1)}(s) &= +\frac{1}{2} T_{\bar{K}N}^{(0)}(2m_N^2 + 2m_K^2 - s) + \frac{1}{2} T_{\bar{K}N}^{(1)}(2m_N^2 + 2m_K^2 - s) \quad (4.56)
\end{aligned}$$

are expected to hold approximatively within some matching window centered around $\sqrt{s} \simeq \Lambda_{\text{opt.}}$. A further complication arises due to the approximate treatment of the u-channel exchange contribution in the KN -channel. Since the optimal matching point $\Lambda_{\text{opt.}}$ is not too far away from the hyperon poles with $\Lambda_{\text{opt.}} \sim m_\Lambda, m_\Sigma$ it is advantageous to investigate approximate crossing symmetry for the hyperon-pole term subtracted scattering amplitudes.

It should be stressed that the expected approximate crossing symmetry is closely linked to the renormalization condition (3.37). Since all loop functions $J^{(\pm)}(\sqrt{s}, n)$ vanish close to $\sqrt{s} =$

$(m_\Lambda + m_\Sigma)/2$ by construction, the kaon and antikaon amplitudes turn perturbative sufficiently close to the optimal matching point $\Lambda_{\text{opt.}}$. Therefore the approximate crossing symmetry of the scheme developed here follows directly from the crossing symmetry of the interaction kernel. In the result chapter the final $K^\pm N$ amplitudes are confronted with the expected approximate crossing symmetry.

Finally, for pion-nucleon scattering the situation is rather different. Given the rather small pion mass, the t-channel vector meson exchange contributions do not induce singularities in between the π^+ and π^- -nucleon thresholds but restrict the applicability domain of the chiral Lagrangian to

$$\sqrt{s} < \sqrt{m_N^2 + m_\rho^2/4} + \sqrt{m_\pi^2 + m_\rho^2/4} \simeq 1420 \text{ MeV} . \quad (4.57)$$

The approximate crossing symmetry follows directly from the perturbative character of the pion-nucleon sector.

Chapter 5

Goldstone bosons in cold nuclear matter

In this chapter a novel and covariant many-body framework to evaluate the Goldstone boson propagation in cold nuclear matter is introduced. While the formalism is quite general and applicable for pions and etas as well, the focus here is on the properties of antikaons in nuclear matter. The self consistent approach is based on the chiral SU(3) dynamics derived in the previous chapters. Besides deriving a realistic antikaon spectral function quantitative results on the in-medium structure of the s-wave $\Lambda(1405)$, p-wave $\Sigma(1385)$ and the d-wave $\Lambda(1520)$ resonances are obtained.

The starting point of any microscopic evaluation of meson propagation in nuclear matter should be a well established theory of the meson's scattering process off nucleons, the constituents of nuclear matter. According to the low-density theorem (1.3) the meson-nucleon scattering amplitudes determine the self energy of a meson at small density [74, 33]. Once the appropriate scattering amplitudes are available a difficult task remains, namely to explore what small density really means in (1.3). For the case of antikaons it was demonstrated in [41] that the density expansion stops converging at roughly $\rho \simeq 0.02 \text{ fm}^{-3}$, about one tens of the nuclear saturation density $\rho_0 \simeq 0.17 \text{ fm}^{-3}$. In contrast to that the density expansion is expected to predict solid results for the kaon self energy [41] up to about $2\rho_0$ provided that sufficiently many terms in the expansion are kept [41]. This is nicely illustrated upon studying the leading and subleading terms in the density expansion of the mass change Δm_K^2 of a kaon at rest. All what is required are the isospin zero and isospin one s-wave kaon-nucleon scattering lengths:

$$\begin{aligned} \Delta m_K^2 &= -\pi \left(1 + \frac{m_K}{m_N}\right) \left(a_{KN}^{(I=0)} + 3a_{KN}^{(I=1)}\right) \rho \\ &+ \alpha \left(\left(a_{KN}^{(I=0)}\right)^2 + 3 \left(a_{KN}^{(I=1)}\right)^2 \right) k_F^4 + \mathcal{O}(k_F^5), \end{aligned} \quad (5.1)$$

where

$$\alpha = \frac{1 - x^2 + x^2 \log(x^2)}{\pi^2 (1 - x)^2} \simeq 0.166, \quad x = \frac{m_K}{m_N}, \quad \rho = \frac{2k_F^3}{3\pi^2}. \quad (5.2)$$

Using typical values for the kaon-nucleon scattering lengths, the correction term of order k_F^4 is indeed small. At nuclear saturation density with $k_F \simeq 265 \text{ MeV}$ it increases the repulsive mass shift of the kaon from 28 MeV to 35 MeV by about 20%. Thus, the density expansion is useful in

this case. Any microscopic model consistent with the low-energy kaon-nucleon scattering data is bound to give similar results for the K^+ and K^0 propagation in nuclear matter at densities $\rho \simeq \rho_0$ sufficiently small to maintain the density expansion rapidly convergent. Applying the low density expansion (5.2) for the antikaon a leading repulsive mass shift of 23 MeV with a width of about 147 MeV arises at saturation density. The correction term results in a total repulsive mass shift of 55 MeV and a width of about 195 MeV. At nuclear saturation the density expansion for the antikaon-mode is poorly convergent if at all. Furthermore, the leading terms appear to contradict kaonic atom data [176] which suggest sizable attraction at small density.

The physical reason for the breakdown of the density expansion for antikaons is the presence of the $\Lambda(1405)$ resonance just below the antikaon-nucleon threshold. In order to obtain reliable results for the antikaon spectral function at saturation density ρ_0 or above an infinite resummation scheme is asked for. Since the breakdown of the density expansion is closely linked to a rapid in-medium change of the hyperon resonance properties it is sufficient to evaluate the antikaon and hyperon resonance spectral functions in a self consistent manner. That leads to the required infinite resummation scheme of the density expansion. Schematically this effect can be illustrated in terms of an elementary $\Lambda(1405)$ field dressed by an antikaon-nucleon loop. The repulsive $\Lambda(1405)$ mass shift due to the Pauli blocking of the nucleon is then given by:

$$\Delta m_\Lambda = \frac{g_{\Lambda NK}^2}{\pi^2} \frac{m_N}{m_\Lambda} \left(1 - \frac{\mu_\Lambda}{k_F} \arctan \left(\frac{k_F}{\mu_\Lambda} \right) \right) k_F \quad (5.3)$$

with the 'small' scale

$$\mu_\Lambda^2 = \frac{m_N}{m_\Lambda} \left(m_K^2 - (m_\Lambda - m_N)^2 \right) \simeq (144 \text{ MeV})^2 \quad (5.4)$$

and the $\Lambda(1405)$ kaon nucleon coupling constant $g_{\Lambda NK}$. The result (5.3) clearly demonstrates that a density expansion of the resonance properties must break down at $k_F \simeq \mu_\Lambda$ where one hits the convergence radius of the arctan. Since the scale μ_Λ is rather small and also sensitively dependent on a mass shift of the antikaon a self consistent scheme is indispensable to study the physics at nuclear saturation density quantitatively. The relevant Fermi momentum $k_F \simeq 270$ MeV is much larger than the small scale $\mu_\Lambda \simeq 140$ MeV and therefore a low-density expansion is inappropriate. It is evident that analogous arguments hold for the p-wave $\Sigma(1385)$ resonance which therefore should be part of a self consistent computation.

Self consistent evaluations of the antikaon spectral function in nuclear matter are so far typically based on s-wave dynamics only [41, 42, 43]. Although these calculations agree qualitatively they are based on different realizations of the coupled channel s-wave interactions and lead to significant differences in the antikaon self energy important when describing kaonic atom data [45, 43]. Moreover, since a strong momentum dependence of the antikaon spectral function is predicted, it is important to generalize these calculations and include higher partial waves [67]. The first work that considers higher partial waves in this context but relying on a quasi-particle approximation for the antikaon spectral function was by Tolos et al. [44]. A meson-exchange model of the Jülich group was applied [76]. Unfortunately, the latter model has so far been confronted with total cross section data only and therefore it remains unclear whether it describes the dynamics of higher partial waves correctly. More seriously, as was already emphasized in [76] that model leads to unrealistic scattering amplitudes at subthreshold energies, an energy domain of utmost importance for the nuclear antikaon dynamics.

5.1 Self consistent and covariant nuclear dynamics

Here a covariant framework in which self consistency is implemented in terms of the vacuum meson-nucleon scattering amplitudes is constructed. The scheme is capable to treat consistently the spectral distribution of the meson and also the in-medium mixing of partial wave amplitudes. In order to make this chapter self contained all requisites needed for the formulation are briefly recalled.

Of central importance is the free-space on-shell antikaon-nucleon scattering amplitude:

$$\begin{aligned} \langle \bar{K}^j(\bar{q}) N(\bar{p}) | T | \bar{K}^i(q) N(p) \rangle &= (2\pi)^4 \delta^4(p + q - \bar{q} - \bar{p}) \\ &\times \bar{u}(\bar{p}) T_{\bar{K}N \rightarrow \bar{K}N}^{ij}(\bar{q}, \bar{p}; q, p) u(p), \end{aligned} \quad (5.5)$$

where $u(p)$ is the nucleon isospin-doublet spinor. The isospin doublet notation is used also for the antikaons with $\bar{K} = (K^-, \bar{K}^0)$. The vacuum scattering amplitude is decomposed into its isospin zero and isospin one channels with:

$$\begin{aligned} T_{\bar{K}N \rightarrow \bar{K}N}^{ij}(\bar{q}, \bar{p}; q, p) &= T_{\bar{K}N \rightarrow \bar{K}N}^{(0)}(\bar{k}, k; w) P_{(I=0)}^{ij} + T_{\bar{K}N \rightarrow \bar{K}N}^{(1)}(\bar{k}, k; w) P_{(I=1)}^{ij}, \\ P_{(I=0)}^{ij} &= \frac{1}{4} \left(\delta^{ij} 1 + (\vec{\tau})^{ij} \vec{\tau} \right), \quad P_{(I=1)}^{ij} = \frac{1}{4} \left(3 \delta^{ij} 1 - (\vec{\tau})^{ij} \vec{\tau} \right), \end{aligned} \quad (5.6)$$

where

$$w = p + q = \bar{p} + \bar{q}, \quad k = \frac{1}{2}(p - q), \quad \bar{k} = \frac{1}{2}(\bar{p} - \bar{q}). \quad (5.7)$$

In quantum field theory the scattering amplitudes $T_{\bar{K}N}^{(I)}$ arise in terms of the Bethe-Salpeter matrix equation,

$$\begin{aligned} T(\bar{k}, k; w) &= K(\bar{k}, k; w) + \int \frac{d^4 l}{(2\pi)^4} K(\bar{k}, l; w) G(l; w) T(l, k; w), \\ G(l; w) &= -i S_N(\frac{1}{2}w + l) D_{\bar{K}}(\frac{1}{2}w - l), \end{aligned} \quad (5.8)$$

specified by the Bethe-Salpeter scattering kernel $K(\bar{k}, k; w)$, the free-space nucleon propagator $S_N(p) = 1/(p - m_N + i\epsilon)$ and kaon propagator $D_K(q) = 1/(q^2 - m_K^2 + i\epsilon)$. Following previous considerations self energy corrections in the nucleon and kaon propagators that arise in free-space are neglected. In a chiral scheme such effects are of subleading order. The Bethe-Salpeter equation (5.8) implements properly Lorentz invariance and unitarity for the two-body scattering process. The generalization of (5.8) to a coupled channel system is straightforward (see (4.3)).

The antikaon-nucleon scattering process is readily generalized from the vacuum to the nuclear matter case. It is convenient to introduce the compact notation:

$$\mathcal{T} = \mathcal{K} + \mathcal{K} \cdot \mathcal{G} \cdot \mathcal{T}, \quad \mathcal{T} = \mathcal{T}(\bar{k}, k; w, u), \quad \mathcal{G} = \mathcal{G}(l; w, u), \quad (5.9)$$

where the in-medium scattering amplitude $\mathcal{T}(\bar{k}, k; w, u)$ and the two-particle propagator $\mathcal{G}(l; w, u)$ depend now on the 4-velocity u_μ characterizing the nuclear matter frame. For nuclear matter moving with a velocity \vec{v} we write:

$$u_\mu = \left(\frac{1}{\sqrt{1 - \vec{v}^2/c^2}}, \frac{\vec{v}/c}{\sqrt{1 - \vec{v}^2/c^2}} \right), \quad u^2 = 1. \quad (5.10)$$

It is important to realize that (5.9) is well defined from a Feynman diagrammatic point of view even in the case where the in-medium scattering process is not well defined anymore due to a broad antikaon spectral function. In this work the medium modifications of the interaction kernel is not considered, i.e. the approximation $\mathcal{K} = K$ is applied. It is studied exclusively the effect of a modified two-particle propagator \mathcal{G} with

$$\begin{aligned}\Delta S_N(p, u) &= 2\pi i \Theta(p \cdot u) \delta(p^2 - m_N^2) (\not{p} + m_N) \Theta(k_F^2 + m_N^2 - (u \cdot p)^2), \\ S_N(p, u) &= S_N(p) + \Delta S_N(p, u), \quad \mathcal{D}_{\bar{K}}(q, u) = \frac{1}{q^2 - m_K^2 - \Pi_{\bar{K}}(q, u)}, \\ \mathcal{G}(l; w, u) &= -i S_N(\tfrac{1}{2}w + l, u) \mathcal{D}_{\bar{K}}(\tfrac{1}{2}w - l, u).\end{aligned}\tag{5.11}$$

For isospin symmetric nuclear matter the nucleon density ρ follows with

$$\rho = -2 \text{tr} \gamma_0 \int \frac{d^4 p}{(2\pi)^4} i \Delta S_N(p, u) = \frac{2 k_F^3}{3 \pi^2 \sqrt{1 - \vec{v}^2/c^2}},\tag{5.12}$$

where $\rho = \rho_n + \rho_p$ and $k_F = k_{F,n} = k_{F,p}$. In the rest frame of the bulk with $u_\mu = (1, \vec{0})$ one recovers with (5.12) the standard result $\rho = 2 k_F^3 / (3 \pi^2)$. In this work nucleonic correlation effects are not considered. Such effects have been estimated to be small at moderate densities [40] but should nevertheless be subject of a more complete consideration. The antikaon self energy $\Pi_{\bar{K}}(q, u)$ is evaluated self consistently in terms of the in-medium scattering amplitudes $\mathcal{T}_{\bar{K}N}^{(I)}(\bar{k}, k; w, u)$:

$$\begin{aligned}\Pi_{\bar{K}}(q, u) &= -2 \text{tr} \int \frac{d^4 p}{(2\pi)^4} i \Delta S_N(p, u) \bar{\mathcal{T}}_{\bar{K}N \rightarrow \bar{K}N}(\tfrac{1}{2}(p - q), \tfrac{1}{2}(p - q); p + q, u), \\ \bar{\mathcal{T}}_{\bar{K}N \rightarrow \bar{K}N} &= \frac{1}{4} \mathcal{T}_{\bar{K}N \rightarrow \bar{K}N}^{(I=0)} + \frac{3}{4} \mathcal{T}_{\bar{K}N \rightarrow \bar{K}N}^{(I=1)}.\end{aligned}\tag{5.13}$$

The generalization of (5.13) to asymmetric nuclear matter with $\rho_p \neq \rho_n$ is straightforward. In this case, the two isospin channels couple. Hence it is more convenient to apply the particle basis rather than the isospin basis. The relevant Clebsch Gordan coefficients are:

$$\begin{aligned}T_{K^- p \rightarrow K^- p} &= \frac{1}{2} \left(T_{\bar{K}N \rightarrow \bar{K}N}^{(0)} + T_{\bar{K}N \rightarrow \bar{K}N}^{(1)} \right), \quad T_{K^- n \rightarrow K^- n} = T_{\bar{K}N \rightarrow \bar{K}N}^{(1)} = T_{\bar{K}^0 p \rightarrow \bar{K}^0 p}, \\ T_{\bar{K}^0 n \rightarrow \bar{K}^0 n} &= \frac{1}{2} \left(T_{\bar{K}N \rightarrow \bar{K}N}^{(0)} + T_{\bar{K}N \rightarrow \bar{K}N}^{(1)} \right), \quad T_{\bar{K}^0 n \rightarrow \bar{K}^- p} = \frac{1}{2} \left(T_{\bar{K}N \rightarrow \bar{K}N}^{(0)} - T_{\bar{K}N \rightarrow \bar{K}N}^{(1)} \right)\end{aligned}\tag{5.14}$$

In order to solve the self consistent set of equations (5.9,5.11,5.13) it is convenient to rewrite the scattering amplitude in the following way

$$\mathcal{T} = K + K \cdot \mathcal{G} \cdot \mathcal{T} = T + T \cdot \Delta \mathcal{G} \cdot \mathcal{T}, \quad \Delta \mathcal{G} = \mathcal{G} - G,\tag{5.15}$$

where $T = K + K \cdot G \cdot T$ is the vacuum scattering amplitude. The idea is to start with a set of tabulated coupled channel scattering amplitudes T in terms of which self consistency is implemented. Thus, the vacuum interaction kernel K need not to be specified.

Coupled channel effects, which are known to be important for $\bar{K}N$ scattering, are included by assigning \mathcal{T} , \mathcal{G} and K the appropriate matrix structures. Here we use the convention introduced

in (4.2). For example the isospin zero loop matrix $\Delta\mathcal{G}^{(I=0)}$ reads:

$$\Delta\mathcal{G}^{(I=0)} = \begin{pmatrix} \Delta\mathcal{G}_{\bar{K}N} & 0 & 0 & 0 \\ 0 & \Delta\mathcal{G}_{\pi\Sigma} & 0 & 0 \\ 0 & 0 & \Delta\mathcal{G}_{\pi\Lambda} & 0 \\ 0 & 0 & 0 & \Delta\mathcal{G}_{K\Xi} \end{pmatrix}. \quad (5.16)$$

This work focuses on the in-medium modification of the $\bar{K}N$ channel. Ultimately it would be desirable to include also the effects of the in-medium modified $\pi\Sigma$, $\pi\Lambda$ and $K\Xi$ channels. Since this requires a realistic in-medium pion propagator to be determined ultimately also by a self consistent scheme [177] such effects will be considered in a separate work. Here approximation $\Delta\mathcal{G}_{\pi\Sigma} = 0$ and $\Delta\mathcal{G}_{\pi\Lambda} = 0$ is applied. Since the K^+ spectral density is affected only moderately by a nuclear environment it is assumed $\Delta\mathcal{G}_{K\Xi} = 0$ also. With these assumptions the coupled channel problem reduces to a single channel problem if rewritten in terms of the vacuum $\bar{K}N$ amplitude $T_{\bar{K}N \rightarrow \bar{K}N}$:

$$\begin{aligned} \mathcal{T}_{\bar{K}N \rightarrow \bar{K}N}^{(I)} &= T_{\bar{K}N \rightarrow \bar{K}N}^{(I)} + T_{\bar{K}N \rightarrow \bar{K}N}^{(I)} \cdot \Delta\mathcal{G}_{\bar{K}N} \cdot \mathcal{T}_{\bar{K}N \rightarrow \bar{K}N}^{(I)}, \\ \Delta\mathcal{G}_{\bar{K}N} &= \mathcal{G}_{\bar{K}N} - G_{\bar{K}N}. \end{aligned} \quad (5.17)$$

It should be pointed out that the self consistent set of equations (5.11,5.13,5.17) are now completely determined by the vacuum amplitudes $T_{\bar{K}N \rightarrow \bar{K}N}^{(I)}$. Even though the antikaon spectral function is a functional of the elastic $\bar{K}N \rightarrow \bar{K}N$ scattering process only, the inelastic channels $\bar{K}N \rightarrow X$ are nevertheless affected by $\Delta\mathcal{G}_{\bar{K}N}$. Simple algebra leads to:

$$\begin{aligned} \mathcal{T}_{\bar{K}N \rightarrow X}^{(I)} &= T_{\bar{K}N \rightarrow X}^{(I)} + \mathcal{T}_{\bar{K}N \rightarrow \bar{K}N}^{(I)} \cdot \Delta\mathcal{G}_{\bar{K}N} \cdot T_{\bar{K}N \rightarrow X}^{(I)}, \\ \mathcal{T}_{Y \rightarrow X}^{(I)} &= T_{Y \rightarrow X}^{(I)} + T_{Y \rightarrow \bar{K}N}^{(I)} \cdot \Delta\mathcal{G}_{\bar{K}N} \cdot \mathcal{T}_{\bar{K}N \rightarrow X}^{(I)}, \end{aligned} \quad (5.18)$$

where $X, Y \neq \bar{K}N$. In (5.18) the effect of $\Delta\mathcal{G}_{\bar{K}N} \neq 0$ on the reaction $X \rightarrow Y$ with $X, Y \neq \bar{K}N$ is demonstrated.

In the following section it is outlined how to solve the self consistent set of equations (5.11,5.13,5.17) by introducing an appropriate projector algebra. The scheme takes into account the spectral distribution of the meson as well as the medium induced mixing of partial waves usually neglected in conventional G-matrix calculations (see e.g. [44]).

5.2 Covariant projector algebra method in nuclear matter

It is useful to briefly recall the coupled channel theory of chapter 4. The scattering amplitudes were obtained in a relativistic chiral $SU(3)$ approach by decomposing the amplitudes systematically into covariant projectors $Y_n^{(\pm)}$ with good angular momentum $J = n + \frac{1}{2}$

$$\begin{aligned} T^{(I)}(\bar{k}, k; w) &= \sum_{n=0}^{\infty} Y_n^{(+)}(\bar{q}, q; w) M^{(I,+)}(\sqrt{s}, n) \\ &+ \sum_{n=0}^{\infty} Y_n^{(-)}(\bar{q}, q; w) M^{(I,-)}(\sqrt{s}, n), \end{aligned} \quad (5.19)$$

where $w^2 = s$ and $k = \frac{1}{2}(p - q)$ and $\bar{k} = \frac{1}{2}(\bar{p} - \bar{q})$. The representation (5.19) implies a particular off-shell behavior of the scattering amplitude, which was optimized as to simplify the task of solving the covariant Bethe-Salpeter equation. This is legitimate because the off-shell structure of the scattering amplitude is not determined by the two-body scattering processes in any case and moreover reflects the choice of meson and baryon interpolation fields only [172, 156]. The leading projectors relevant for the $J = \frac{1}{2}$ and $J = \frac{3}{2}$ channels are $Y_0^{(+)}$ (s-wave), $Y_0^{(-)}$ (p-wave) and $Y_1^{(+)}$ (p-wave), $Y_1^{(-)}$ (d-wave) where

$$\begin{aligned} Y_0^{(\pm)}(\bar{q}, q; w) &= \frac{1}{2} \left(\frac{\psi}{\sqrt{w^2}} \pm 1 \right), \\ Y_1^{(\pm)}(\bar{q}, q; w) &= \frac{3}{2} \left(\frac{\psi}{\sqrt{w^2}} \pm 1 \right) \left(\frac{(\bar{q} \cdot w)(w \cdot q)}{w^2} - (\bar{q} \cdot q) \right) \\ &\quad - \frac{1}{2} \left(\not{q} - \frac{w \cdot \bar{q}}{w^2} \psi \right) \left(\frac{\psi}{\sqrt{w^2}} \mp 1 \right) \left(\not{q} - \frac{w \cdot q}{w^2} \psi \right). \end{aligned} \quad (5.20)$$

For instance the projector $Y_1^{(-)}$ probes the d-wave $\Lambda(1520)$ resonance and $Y_1^{(+)}$ the p-wave $\Sigma(1385)$ resonance. For more details on the construction and the properties of these projectors see [97].

In the following the self consistent set of equations (5.17, 5.11, 5.13) is solved for $n = 0, 1$ in (5.19). The solution of the Bethe-Salpeter equation in nuclear matter is considerably complicated by the fact that the partial waves, which nicely decouple in the vacuum, start to mix in the medium. This manifests itself in the presence of further tensor structures in the scattering amplitude not required in the vacuum. For example if one starts to iterate the Bethe-Salpeter equation (5.17) in terms of the vacuum amplitudes $M^{(I, \pm)}(\sqrt{s}, n)$ incorporating $\Delta\mathcal{G}_{\bar{K}N}$ as determined by (5.13) with $\mathcal{T}_{\bar{K}N} = T_{\bar{K}N}$, one finds that $\mathcal{T}_{\bar{K}N}$ can no longer be decomposed into the projectors $Y_n^{(\pm)}(\bar{q}, q; w)$. The in-medium solution of the Bethe-Salpeter equation requires a more general ansatz for the scattering amplitude.

Some tedious algebra shows that the following ansatz solves the self consistent set of equations:

$$\begin{aligned} \mathcal{T}(\bar{k}, k; w, u) &= \mathcal{T}(w, u) + \mathcal{T}^\nu(w, u) q_\nu + \bar{q}_\mu \bar{\mathcal{T}}^\mu(w, u) + \bar{q}_\mu \mathcal{T}^{\mu\nu}(w, u) q_\nu, \\ \bar{\mathcal{T}}^\mu &= \sum_{j=3}^8 \left(\mathcal{M}_{[1j]}^{(p)} \bar{P}_{[1j]}^\mu + \mathcal{M}_{[2j]}^{(p)} \bar{P}_{[2j]}^\mu \right), \quad \mathcal{T}^\mu = \sum_{j=3}^8 \left(\mathcal{M}_{[j1]}^{(p)} P_{[j1]}^\mu + \mathcal{M}_{[j2]}^{(p)} P_{[j2]}^\mu \right), \\ \mathcal{T} &= \sum_{i,j=1}^2 \mathcal{M}_{[ij]}^{(p)} P_{[ij]}, \quad \mathcal{T}^{\mu\nu} = \sum_{i,j=3}^8 \mathcal{M}_{[ij]}^{(p)} P_{[ij]}^{\mu\nu} + \sum_{i,j=1}^2 \mathcal{M}_{[ij]}^{(q)} Q_{[ij]}^{\mu\nu}, \end{aligned} \quad (5.21)$$

where appropriate projectors $P_{[ij]}(w, u)$ which generalize the vacuum projectors $Y_n^{(\pm)}(\bar{q}, q; w)$ are introduced [98]. The matrix valued functions $\mathcal{M}_{[ij]}^{(p,q)}(w, u)$ are scalar and therefore depend only on $s = w^2$ and $w \cdot u$. The set of projectors is constructed to satisfy the convenient algebra

$$\begin{aligned} P_{[ik]} \cdot P_{[lj]} &= \delta_{kl} P_{[ij]}, \quad P_{[ik]}^\mu \bar{P}_{[lj]}^\nu = \delta_{kl} P_{[ij]}^{\mu\nu}, \quad \bar{P}_{[ik]}^\mu g_{\mu\nu} P_{[lj]}^\nu = \delta_{kl} P_{[ij]}, \\ Q_{[ik]}^{\mu\alpha} g_{\alpha\beta} P_{[lj]}^{\beta\nu} &= 0 = P_{[ik]}^{\mu\alpha} g_{\alpha\beta} Q_{[lj]}^{\beta\nu}, \quad Q_{[ik]}^{\mu\alpha} g_{\alpha\beta} P_{[lj]}^\beta = 0 = \bar{P}_{[ik]}^\alpha g_{\alpha\beta} Q_{[lj]}^{\beta\nu}, \\ Q_{[ik]}^{\mu\alpha} g_{\alpha\beta} Q_{[lj]}^{\beta\nu} &= \delta_{kl} Q_{[ij]}^{\mu\nu}, \quad P_{[ik]}^{\mu\alpha} g_{\alpha\beta} P_{[lj]}^{\beta\nu} = \delta_{kl} P_{[ij]}^{\mu\nu}. \end{aligned} \quad (5.22)$$

The projector algebra (5.22) properly implements the coupling of the partial waves in the medium. Consider for example the projectors $P_{[ij]}(w, u)$ for $i, j = 1, 2$

$$\begin{aligned} P_{[11]} &= +Y_0^{(+)} , & P_{[12]} &= -Y_0^{(+)} \frac{\gamma \cdot u}{\sqrt{1 - (w \cdot u)^2/w^2}} Y_0^{(-)} , \\ P_{[22]} &= -Y_0^{(-)} , & P_{[21]} &= -Y_0^{(-)} \frac{\gamma \cdot u}{\sqrt{1 - (w \cdot u)^2/w^2}} Y_0^{(+)} , \end{aligned} \quad (5.23)$$

which demonstrate that the vacuum projectors start to mix in the medium due to the presence of the matter 4-velocity u_μ . If we neglected the $J = \frac{3}{2}$ amplitudes $M^{(\pm)}(\sqrt{s}, 1)$ the Bethe-Salpeter equation is solved with the restricted set of projectors $P_{[ij]}$ given in (5.23). Explicit results for the remaining projectors are presented in [98]. In particular it is found

$$Y_1^{(+)} = -3\bar{q}_\mu \left(Q_{[11]}^{\mu\nu} + P_{[77]}^{\mu\nu} \right) q_\nu , \quad Y_1^{(-)} = +3\bar{q}_\mu \left(Q_{[22]}^{\mu\nu} + P_{[88]}^{\mu\nu} \right) q_\nu . \quad (5.24)$$

From the form of the algebra in (5.22) it follows that P- and Q-space projectors decouple. Whereas the $P_{[ij]}$ -projectors couple to all considered partial waves the $Q_{[ij]}$ -projectors require only the two $J = \frac{3}{2}$ partial wave amplitudes. This reflects the fact that the four polarizations of a spin $\frac{3}{2}$ fermion are no longer degenerate in a nuclear environment. By analogy with a spin 1 boson with one longitudinal and two degenerate transverse modes one expects two independent modes for a spin $\frac{3}{2}$ fermion in nuclear matter also. Such modes have been discussed for the case of the $\Delta(1232)$ isobar properties in nuclear matter (see e.g. [178]). They reflect two independent terms in its self energy, a scalar and a tensor, characterizing a non-relativistic spin 3/2 state in nuclear matter. Like for a vector meson at rest where longitudinal and transverse modes are degenerate in nuclear matter the analogous property holds for the spin 3/2 states.

With the ansatz (5.21) the antikaon-nucleon propagator $\Delta\mathcal{G}_{\bar{K}N}$ translates into the set of loop functions

$$\begin{aligned} \int \frac{d^4l}{(2\pi)^4} \Delta\mathcal{G}(l - \tfrac{1}{2}w; w, u) &= \sum_{i,j=1}^2 \Delta J_{[ij]}^{(p)}(w, u) P_{[ij]}(w, u) , \\ \int \frac{d^4l}{(2\pi)^4} l^\mu \Delta\mathcal{G}(l - \tfrac{1}{2}w; w, u) &= \sum_{j=3}^8 \left(\Delta J_{[j1]}^{(p)}(w, u) P_{[j1]}^\mu(w, u) + \Delta J_{[j2]}^{(p)}(w, u) P_{[j2]}^\mu(w, u) \right) \\ &= \sum_{j=3}^8 \left(\Delta J_{[1j]}^{(p)}(w, u) \bar{P}_{[1j]}^\mu(w, u) + \Delta J_{[2j]}^{(p)}(w, u) \bar{P}_{[2j]}^\mu(w, u) \right) , \\ \int \frac{d^4l}{(2\pi)^4} l^\mu l^\nu \Delta\mathcal{G}(l - \tfrac{1}{2}w; w, u) &= \sum_{i,j=3}^8 \Delta J_{[ij]}^{(p)}(w, u) P_{[ij]}^{\mu\nu}(w, u) + \sum_{i,j=1}^2 \Delta J_{[ij]}^{(q)}(w, u) Q_{[ij]}^{\mu\nu}(w, u) , \\ \Delta\mathcal{G}(l - \tfrac{1}{2}w; w, u) &= -i \left(\mathcal{S}_N(l, u) \mathcal{D}_K(w - l, u) - S_N(l) D_K(w - l) \right) , \end{aligned} \quad (5.25)$$

which can be decomposed in terms of the projectors $P_{[ij]}$ and $Q_{[ij]}$. The reduced loop functions $\Delta J_{[ij]}(w, u)$ acquire the generic form

$$\Delta J_{[ij]}(w, u) = \int \frac{d^4l}{(2\pi)^4} g(l; w, u) \Delta J_{[ij]}(l; w, u) ,$$

$$\begin{aligned}
g(l; w, u) = & -2\pi \Theta(l \cdot u) \delta(l^2 - m_N^2) \frac{\Theta(k_F^2 + m_N^2 - (u \cdot l)^2)}{(w-l)^2 - m_K^2 - \Pi_{\bar{K}}(w-l, u)} \\
& - \frac{i}{l^2 - m_N^2 + i\epsilon} \frac{1}{(w-l)^2 - m_K^2 - \Pi_{\bar{K}}(w-l, u)} \\
& + \frac{i}{l^2 - m_N^2 + i\epsilon} \frac{1}{(w-l)^2 - m_K^2 + i\epsilon}, \tag{5.26}
\end{aligned}$$

where the scalar polynomials $\Delta J_{[ij]}(l; w, u)$ involve typically some power of $l^2, l \cdot w$ or $l \cdot u$. They are listed in [98]. Note that the reduced loop functions $\Delta J_{[ij]}(w, u)$ are scalar and therefore depend only on w^2 and $w \cdot u$. Hence the loop functions can be evaluated in any convenient frame without loss of information. In practice the loop integration is performed in the rest frame of nuclear matter with $u_\mu = (1, \vec{0})$.

Choosing the center of mass frame of the antikaon-nucleon system with $w_\mu = (\sqrt{s}, \vec{0})$ instead does not necessarily lead to any further simplification as suggested in [66] since in this frame a nonzero bulk velocity $\vec{v} \neq 0$ is required. After performing the energy and azimuthal angle integration in (5.26) one is left with a two dimensional integration which must be evaluated numerically. Note that the scalar self energy $\Pi_{\bar{K}}(l-w, u)$ depends on the two invariants $(l-w)^2$ and $(l-w) \cdot u$ only. Consequently in the nuclear matter rest frame the first entry involves the angle $\vec{l} \cdot \vec{w}$ as compared to the frame with $w_\mu = (\sqrt{s}, \vec{0})$ which leads the angle $\vec{l} \cdot \vec{v}$ in second entry. This confirms the expected conservation of complexity. A strong 'vector' potential in the antikaon self energy, as suggested by phenomenology, actually means a strong dependence on $(l-w) \cdot u$ in (5.26). Therefore it appears unjustified to neglect that dependence as was done in [42, 28].

With (5.21, 5.22, 5.25) the in-medium Bethe-Salpeter equation (5.9) reduces to a simple matrix equation

$$\begin{aligned}
\mathcal{M}_{[ij]}^{(p)}(w, u) &= M_{[ij]}^{(p)}(\sqrt{s}) + \sum_{l,k=1}^8 M_{[ik]}^{(p)}(\sqrt{s}) \Delta J_{[kl]}^{(p)}(w, u) \mathcal{M}_{[lj]}^{(p)}(w, u), \\
\mathcal{M}_{[ij]}^{(q)}(w, u) &= M_{[ij]}^{(q)}(\sqrt{s}) + \sum_{l,k=1}^2 M_{[ik]}^{(q)}(\sqrt{s}) \Delta J_{[kl]}^{(q)}(w, u) \mathcal{M}_{[lj]}^{(q)}(w, u). \tag{5.27}
\end{aligned}$$

The isospin index I is suppressed and it is implied $s = w_0^2 - \vec{w}^2$. All nonzero vacuum matrix elements are identified with

$$\begin{aligned}
M_{[11]}^{(q)}(\sqrt{s}) &= -3 M^{(+)}(\sqrt{s}, 1), & M_{[22]}^{(q)}(\sqrt{s}) &= 3 M^{(-)}(\sqrt{s}, 1), \\
M_{[11]}^{(p)}(\sqrt{s}) &= M^{(+)}(\sqrt{s}, 0), & M_{[22]}^{(p)}(\sqrt{s}) &= -M^{(-)}(\sqrt{s}, 0), \\
M_{[77]}^{(p)}(\sqrt{s}) &= -3 M^{(+)}(\sqrt{s}, 1), & M_{[88]}^{(p)}(\sqrt{s}) &= 3 M^{(-)}(\sqrt{s}, 1). \tag{5.28}
\end{aligned}$$

Note that in fact all amplitudes $\mathcal{M}_{[ij]}^{(p)}(w, u)$ with either $i \in \{3, 4, 5, 6\}$ or $j \in \{3, 4, 5, 6\}$ are zero. That is a direct consequence of the analogous property for the amplitudes $M_{[ij]}$ in free space. In principle the vacuum scattering amplitudes could have contributions proportional to P_{33}, P_{44}, P_{55} or P_{66} also. The reason why such terms are not considered here is that they are not determined by the on-shell antikaon-nucleon scattering process. The size of such terms merely

reflects the choice of the interpolating fields [172, 156]. They acquire physical significance only, once the vacuum 3-body scattering processes are addressed systematically. It should be stressed that a detailed analysis of the loop matrices $\Delta J(w, u)$ reveals that for $u_\mu = (1, 0)$ and $\vec{w} = 0$ all off diagonal elements vanish identically [98]. This property guarantees that all partial wave amplitudes decouple in this limit.

It is left to derive expressions for the antikaon self energy more explicit than (5.13). The required formulae can be found in [98]. The antikaon self energy follows

$$\begin{aligned} \Pi_{\bar{K}}(q, u) &= - \sum_{i,j=1}^8 \int_0^{k_F} \frac{d^3 p}{(2\pi)^3} \frac{2}{E_p} c_{[ij]}^{(p)}(q; w, u) \bar{\mathcal{M}}_{[ij]}^{(p)}(w, u) \\ &\quad - \sum_{i,j=1}^2 \int_0^{k_F} \frac{d^3 p}{(2\pi)^3} \frac{2}{E_p} c_{[ij]}^{(q)}(q; w, u) \bar{\mathcal{M}}_{[ij]}^{(q)}(w, u), \end{aligned} \quad (5.29)$$

where $u_\mu = (1, \vec{0})$, $q_\mu = (\omega, \vec{q})$ and $w_\mu = (\omega + E_p, \vec{q} + \vec{p})$ with $E_p = (m_N^2 + \vec{p}^2)^{1/2}$. The scalar coefficient functions $c_{[ij]}^{(p,q)}(q; w, u)$ are listed in [98]. In (5.29) we introduced the isospin averaged amplitudes

$$\bar{\mathcal{M}}_{[ij]}(w, u) = \frac{1}{4} \mathcal{M}_{[ij]}^{(I=0)}(w, u) + \frac{3}{4} \mathcal{M}_{[ij]}^{(I=1)}(w, u), \quad (5.30)$$

appropriate for symmetric nuclear matter. The generalization to the asymmetric case is straight forward. With (5.29), (5.27) and (5.26) the final self consistent set of equations are derived. They are solved numerically by iteration. First one determines the leading antikaon self energy $\Pi_{\bar{K}}(\omega, \vec{q})$ by (5.29) with $\mathcal{M}_{[ij]} = M_{[ij]}$. That leads via the loop functions (5.26) and the in-medium Bethe-Salpeter equation (5.27) to medium modified scattering amplitudes $\mathcal{M}_{[ij]}(w_0, \vec{w})$. The latter are used to determine the antikaon self energy of the next iteration. This procedure typically converges after 3 to 4 iterations. Note that the manifest covariant form of the self energy and scattering amplitudes are recovered with $\Pi_{\bar{K}}(q^2, \omega) = \Pi_{\bar{K}}(q^2, q \cdot u)$ and $\mathcal{M}_{[ij]}(w^2, w_0) = \mathcal{M}_{[ij]}(w^2, w \cdot u)$ in a straight forward manner if considered as functions of q^2, ω and w^2, w_0 respectively .

Chapter 6

Results

In this final chapter results for the chiral $SU(3)$ analysis of the low-energy meson-baryon scattering data and for the in-medium meson-baryon scattering processes are presented. The acronym ' χ -BS(3)' is used for chiral Bethe-Salpeter dynamics of the flavor $SU(3)$ symmetry as developed in the previous chapters. The chapter falls into two different parts. First the microscopic scattering processes are discussed where the strangeness sectors are emphasized, i.e. the kaon and antikaon nucleon scattering processes. In the second part results for the self consistent solution of the antikaon and hyperon resonance propagation properties in cold nuclear matter are discussed.

The main assumptions and crucial arguments the χ -BS(3) approach is based on are briefly summarized. The number of colors (N_c) in QCD is considered as a large parameter. A systematic expansion of the scattering kernel in powers of $1/N_c$ is performed. The coupled-channel Bethe-Salpeter kernel is evaluated in a combined chiral and $1/N_c$ expansion including terms of chiral order Q^3 . Contributions of s- and u-channel baryon octet and decuplet states are included explicitly but only the s-channel contributions of the d-wave $J^P = \frac{3}{2}^-$ baryon nonet resonance states. Therewith the s-channel baryon nonet contributions to the interaction kernel are considered as a reminiscence of further inelastic channels not included in the present scheme like for example the $K \Delta_\mu$ or $K_\mu N$ channel. All baryon resonances, with the important exception of those resonances which belong to the large- N_c baryon ground states, are expected to be generated by coupled-channel dynamics. This conjecture is based on the observation that unitary (reducible) loop diagrams are typically enhanced by a factor of 2π close to threshold relatively to irreducible diagrams. That factor invalidates the perturbative evaluation of the scattering amplitudes and leads necessarily to a non-perturbative scheme with reducible diagrams summed to all orders. Indeed the χ -BS(3) approach demonstrates precursor effects of the N(1440), the $\Lambda(1600)$, $\Lambda(1890)$, $\Sigma(1750)$ and the $\Sigma(1660)$ baryon resonances once agreement with the low-energy data set is achieved [97].

The scattering amplitudes for the meson-baryon scattering processes are obtained from the solution of the coupled-channel Bethe-Salpeter scattering equation where a systematic on-shell reduction guarantees that the scattering amplitudes do not depend on the particular choice of the chiral Lagrangian. The method leads to results that are similar to those of the N/D method introduced by Chew and Mandelstam [107]. However, there are important differences linked to the fact that we constructed covariant projection operators that permit the solution of the Bethe-Salpeter equation in dimensional regularization. That novel technique constrains the many unknown subtraction constants required in the N/D method. A remaining ambiguity in the

renormalization condition of the Bethe-Salpeter equation is fixed basically by the requirement that the final scattering amplitudes are crossing symmetric approximatively. First a complete collection of the parameters as they are adjusted to the data set is presented. Particular emphasis is put on the SU(3) symmetry breaking effects in the meson-baryon and axial vector coupling constants of the baryon octet states. In the subsequent sections we report on details of the fit strategy and confront our results with the empirical data in the strangeness sectors. Details on the results in the strangeness zero sector can be found in [97], where a reasonable description of the elastic s- and p-wave pion-nucleon scattering phase shifts is documented. It follows a detailed analysis of the obtained scattering amplitudes, demonstrating their good analyticity properties as well as their approximate compliance with crossing symmetry. The result chapter will be closed with a presentation and discussion of the in-medium properties of antikaons and hyperons [98]. It will be argued that the $\Sigma(1385)$ resonance should play an important role in the microscopic understanding of the subthreshold production of antikaons in heavy-ion reactions at SIS energies.

6.1 Parameters

It should be emphasized that any fit to a data set, based on a model calculation that is less accurate in some channels than experimental errors, involving many different reactions with different statistical and systematical errors is subject to some bias. In order to obtain a uniform fit a weighting procedure of the various channels must be devised that cannot be unique. Ultimately one should judge the quality of the fit by direct comparison with the data set rather than a total chisquare. In this analysis a data point is included typically if $p_{\text{lab}} < 350$ MeV. At higher energies one would expect that further partial wave amplitudes and inelastic channels not considered in this work become important. There exist low-energy elastic and inelastic K^-p cross section data including in part angular distributions and polarizations. Also the low-energy differential $K^+p \rightarrow K^+p$ cross sections are included in the global fit. The empirical constraints set by the K^+ -deuteron scattering data above $p_{\text{lab}} > 350$ MeV are considered by requiring a reasonable matching to the single energy S_{01} and P_{03} phase shifts of [179]. This resolves an ambiguity in the parameter set. Finally, the single-energy pion-nucleon phase shifts of [180] are fitted. A uniform quality of the data description is aimed at. Therefore the χ^2 per data point is formed in each sector. The latter are added up to the total χ^2 which is minimized by the search algorithms of Minuit [181]. In cases where the empirical error bars are much smaller than the accuracy to which we expect the χ -BS(3) to work to the given order, we artificially increase those error bars in our global fit. In Tab. 6.1-6.4 the parameter set of the best fit to the data are presented. Note that part of the parameters are predetermined to a large extent and therefore fine tuned in a small interval only. It is found that the set of parameters is well determined by the available scattering data and weak decay widths of the baryon octet states.

A qualitative understanding of the typical strength in the various channels can be obtained already at leading chiral order Q . In particular the $\Lambda(1405)$ resonance is formed as a result of the coupled-channel dynamics defined by the Weinberg-Tomozawa interaction vertices (see Fig. 3.1). There are four parameters relevant to that order f , C_R , F_R and D_R . Their respective values as given in Tab. 6.1 are the result of our global fit to the data set including all parameters of the χ -BS(3) approach. At leading chiral order the parameter f determines the weak pion- and

f [MeV]	C_R	F_R	D_R
90.04	1.734	0.418	0.748

Table 6.1: Leading chiral parameters which contribute to meson-baryon scattering to order Q .

$g_F^{(V)}$ [GeV $^{-2}$]	0.293	$g_F^{(S)}$ [GeV $^{-1}$]	-0.198	$g_F^{(T)}$ [GeV $^{-1}$]	1.106	$Z_{[10]}$	0.719
$g_D^{(V)}$ [GeV $^{-2}$]	1.240	$g_D^{(S)}$ [GeV $^{-1}$]	-0.853	$g_D^{(T)}$ [GeV $^{-1}$]	1.607	-	-

Table 6.2: Chiral Q^2 -parameters resulting from a fit to low-energy meson-baryon scattering data. Further parameters to this order are determined by the large- N_c sum rules.

kaon-decay processes and at the same time the strength of the Weinberg-Tomozawa interaction vertices. At subleading order Q^2 the Weinberg-Tomozawa terms and the weak-decay constants of the pseudo-scalar meson octet receive independent correction terms. The result $f \simeq 90$ MeV is sufficiently close to the empirical decay parameters $f_\pi \simeq 92.4$ MeV and $f_K \simeq 113.0$ MeV to expect that the Q^2 correction terms lead indeed to values rather close to the empirical decay constants. The value for f is consistent with the estimate of [61] which leads to $f_\pi/f = 1.07 \pm 0.12$. The baryon octet and decuplet s- and u-channel exchange contributions to the interaction kernels are determined by the F_R, D_R and C_R parameters at leading order. Note that F_R and D_R predict the baryon octet weak-decay processes and C_R the strong decay widths of the baryon decuplet states to this order also.

A quantitative description of the data set requires the inclusion of higher order terms. Initially it was tried to establish a consistent picture of the existing low-energy meson-baryon scattering data based on a truncation of the interaction kernels to chiral order Q^2 . This attempt failed due to the insufficient quality of the kaon-nucleon scattering data at low energies. In particular some of the inelastic K^- -proton differential cross sections are strongly influenced by the d-wave $\Lambda(1520)$ resonance at energies where the data points start to show smaller error bars. Hence, on the one hand, one must include an effective baryon-nonet resonance field and, on the other hand, perform minimally a chiral Q^3 analysis to extend the applicability domain to somewhat higher energies. Since the effect of the d-wave resonances is only necessary in the strangeness minus one sector, they are only considered in that channel. The resonance parameters will be presented when discussing the strangeness minus one sector.

At subleading order Q^2 the chiral $SU(3)$ Lagrangian predicts the relevance of 12 basically unknown parameters, $g^{(S)}, g^{(V)}, g^{(T)}$ and $Z_{[10]}$, which all need to be adjusted to the empirical scattering data. It is important to realize that chiral symmetry is largely predictive in the $SU(3)$ sector in the sense that it reduces the number of parameters beyond the static $SU(3)$ symmetry. For example one should compare the six tensors which result from decomposing $8 \otimes 8 = 1 \oplus 8_S \oplus 8_A \oplus 10 \oplus \overline{10} \oplus 27$ into its irreducible components with the subset of $SU(3)$ structures selected by chiral symmetry in a given partial wave. Thus, static $SU(3)$ symmetry alone would predict 18 independent terms for the s-wave and two p-wave channels rather than the 11 chiral Q^2 background parameters, $g^{(S)}, g^{(V)}$ and $g^{(T)}$. In this work the number of parameters

was further reduced significantly by insisting on the large- N_c sum rules

$$g_1^{(S)} = 2g_0^{(S)} = 4g_D^{(S)}/3, \quad g_1^{(V)} = 2g_0^{(V)} = 4g_D^{(V)}/3, \quad g_1^{(T)} = 0,$$

for the symmetry conserving quasi-local two body interaction terms (see (2.25)). In Tab. 6.2 we collect the values of all free parameters as they result from our best global fit. All parameters are found to have natural size. This is an important result, because only then is the application of the chiral power counting rule (2.5) justified. We point out that the large- N_c sum rules derived in chapter 2 implicitly assume that other inelastic channels like $K \Delta_\mu$ or $K_\mu N$ are not too important. The effect of such channels can be absorbed to some extent into the quasi-local counter terms, however possibly at the prize that their large- N_c sum rules are violated. It is therefore a highly non-trivial result that we obtain a successful fit imposing (6.1). Note that the only previous analysis [65], which truncated the interaction kernel at chiral order Q^2 but did not include p-waves, found values for the s-wave range parameters largely inconsistent with the large- N_c sum rules. This may be due in part to the use of channel dependent cutoff parameters and the fact that that analysis missed octet and decuplet exchange contributions, which are important for the s-wave interaction kernel already to chiral order Q^2 .

The parameters b_0 , b_D and b_F to this order characterize the explicit chiral symmetry-breaking effects of QCD via the finite current quark masses. The parameters b_D and b_F are well estimated from the baryon octet mass splitting (see (2.32)) whereas b_0 must be extracted directly from the meson-baryon scattering data. It drives the size of the pion-nucleon sigma term for which conflicting values are still being discussed in the literature [159]. The values

$$b_0 = -0.346 \text{ GeV}^{-1}, \quad b_D = 0.061 \text{ GeV}^{-1}, \quad b_F = -0.195 \text{ GeV}^{-1}, \quad (6.1)$$

are rather close to values expected from the baryon octet mass splitting (2.32). The pion-nucleon sigma term $\sigma_{\pi N}$ if evaluated to chiral order Q^2 (see (2.35)) would be $\sigma_{\pi N} \simeq 32 \text{ MeV}$. That value should not be compared directly with $\sigma_{\pi N}$ as extracted usually from pion-nucleon scattering data at the Cheng-Dashen point. The required subthreshold extrapolation involves further poorly convergent expansions [159]. Here we do not attempt to add anything new to this ongoing debate. Consider the analogous symmetry-breaking parameters d_0 and d_D for the baryon decuplet states. Like for the baryon octet states the isospin averaged empirical values for the baryon masses are used in any u-channel exchange contribution. That implies $m_{[10]}^{(\Delta)} = 1232.0 \text{ MeV}$, $m_{[10]}^{(\Sigma)} = 1384.5 \text{ MeV}$ and $m_{10}^{(\Xi)} = 1533.5 \text{ MeV}$ in the decuplet exchange expressions. In the s-channel decuplet expressions the slightly different values $m_{10}^{(\Delta)} = 1223.2 \text{ MeV}$ and $m_{10}^{(\Sigma)} = 1374.4 \text{ MeV}$ are used in order to compensate for a small mass renormalization induced by the unitarization. Those values are rather consistent with $d_D \simeq -0.49 \text{ GeV}^{-1}$ (see (2.32)). All values used are quite compatible with the large- N_c sum rule

$$b_D + b_F = d_D/3.$$

The parameter d_0 is not determined by the present analysis. Its determination required the study of the meson baryon-decuplet scattering processes.

To chiral order Q^3 the number of parameters increases significantly unless further constraints from QCD are imposed. Recall for example that [182] presents a large collection of already 102 chiral Q^3 interaction terms. A systematic expansion of the interaction kernel in powers of $1/N_c$ leads to a much reduced parameter set. For example the $1/N_c$ expansion leads to only four

$h_F^{(1)}[\text{GeV}^{-3}]$	-0.129	$h_D^{(1)}[\text{GeV}^{-3}]$	-0.548	$h_F^{(2)}[\text{GeV}^{-2}]$	0.174	$h_F^{(3)}[\text{GeV}^{-2}]$	-0.221
------------------------------	--------	------------------------------	--------	------------------------------	-------	------------------------------	--------

Table 6.3: Chiral Q^3 -parameters resulting from a fit to low-energy meson-baryon scattering data. Further parameters to this order are determined by the large- N_c sum rules.

c_1	-0.0707	c_2	-0.0443	c_3	0.0624	c_4	0.0119	c_5	-0.0434
\bar{c}_1	0.0754	\bar{c}_2	0.1533	δc_1	0.0328	δc_2	-0.0043	a	-0.2099

Table 6.4: Chiral Q^3 -parameters, which break the $SU(3)$ symmetry explicitly, resulting from a fit to low-energy meson-baryon scattering data.

further parameters $h_F^{(1)}$, $h_D^{(1)}$, $h_F^{(2)}$ and $h_F^{(3)}$ describing the refined symmetry-conserving two-body interaction vertices. This is to be compared with the ten parameters established in [97], which were found to be relevant to order Q^3 if large- N_c sum rules are not imposed. In the global fit it is insisted on the large- N_c sum rules

$$h_1^{(1)} = 2h_0^{(1)} = 4h_D^{(1)}/3, \quad h_1^{(2)} = h_D^{(2)} = 0, \quad h_1^{(3)} = h_D^{(3)} = 0.$$

Note that to order Q^3 there are no symmetry-breaking 2-body interaction vertices. To that order the only symmetry-breaking effects result from the refined 3-point vertices. Here a particularly rich picture emerges. To order Q^3 we established 23 parameters describing symmetry-breaking effects in the 3-point meson-baryon vertices. For instance, to that order the baryon-octet states may couple to the pseudo-scalar mesons also via pseudo-scalar vertices rather than only via the leading axial-vector vertices. Out of those 23 parameters 16 contribute at the same time to matrix elements of the axial-vector current. Thus, in order to control the symmetry breaking effects, it is mandatory to include constraints from the weak decay widths of the baryon octet states also. A detailed analysis of the 3-point vertices in the $1/N_c$ expansion of QCD reveals that in fact only ten parameters $c_{1,2,3,4,5}$, $\delta c_{1,2}$ and $\bar{c}_{1,2}$ and a , rather than the 23 parameters, are needed to leading order in that expansion. Since the leading parameters F_R, D_R together with the symmetry-breaking parameters c_i describe at the same time the weak decay widths of the baryon octet and decuplet ground states (see Tab. 2.1,6.5), the number of free parameters does not increase significantly at the Q^3 level if the large- N_c limit is applied.

The parameter reduction achieved in this work by insisting on chiral and large- N_c sum rules is significant. In this respect it is instructive to recall that for instance the analysis by Kim [71], rather close in spirit to modern effective field theories, required already 44 parameters in the strangeness minus one sector only. As was pointed out in [183] that analysis, even though troubled with severe shortcomings [184], was the only one so far which included s- and p-waves and still reproduced the most relevant features of the subthreshold $\bar{K}N$ amplitudes. Thus, a combined chiral and large- N_c analysis leads to a scheme with a reasonably small number of parameters at the Q^3 level.

	g_A (Exp.)	χ -BS(3)	SU(3)
$n \rightarrow p e^- \bar{\nu}_e$	1.267 ± 0.004	1.26	1.26
$\Sigma^- \rightarrow \Lambda e^- \bar{\nu}_e$	0.601 ± 0.015	0.58	0.65
$\Lambda \rightarrow p e^- \bar{\nu}_e$	-0.889 ± 0.015	-0.92	-0.90
$\Sigma^- \rightarrow n e^- \bar{\nu}_e$	0.342 ± 0.015	0.33	0.32
$\Xi^- \rightarrow \Lambda e^- \bar{\nu}_e$	0.306 ± 0.061	0.19	0.25
$\Xi^- \rightarrow \Sigma^0 e^- \bar{\nu}_e$	0.929 ± 0.112	0.79	0.89

Table 6.5: Axial-vector coupling constants for the weak decay processes of the baryon octet states. The empirical values for g_A are taken from [163]. Here we do not consider small $SU(3)$ symmetry-breaking effects of the vector current. The column labelled by SU(3) shows the axial-vector coupling constants as they follow from $F_R = 0.47$ and $D_R = 0.79$ and $c_i = 0$.

6.2 Axial-vector and meson-baryon coupling constants

The result of the global fit for the axial-vector coupling constants of the baryon octet states are presented in Tab. 6.5. The six data points, which strongly constrain the parameters F_R, D_R and $c_{1,2,3,4}$, are well reproduced. The recent measurement of the decay process $\Xi^0 \rightarrow \Sigma^+ e^- \bar{\nu}_e$ by the KTeV experiment does not provide a further stringent constraint so far [185, 186]. The axial-vector coupling constant of that decay $g_A(\Xi^0 \rightarrow \Sigma^+ e^- \bar{\nu}_e) = \sqrt{2} g_A(\Xi^- \rightarrow \Sigma^0 e^- \bar{\nu}_e)$ is related to the decay process $\Xi^- \rightarrow \Sigma^0 e^- \bar{\nu}_e$ included in Tab. 6.5 by isospin symmetry. The value given in [186] is $g_A(\Xi^0 \rightarrow \Sigma^+ e^- \bar{\nu}_e) = 1.23 \pm 0.44$. As emphasized in [186] it would be important to reduce the uncertainties by more data taking. The result of [163] which favors values for $g_A(\Xi^- \rightarrow \Sigma^0 e^- \bar{\nu}_e)$ and $g_A(\Xi^- \rightarrow \Lambda e^- \bar{\nu}_e)$ which are somewhat smaller than the central values given in Tab. 6.5 is confirmed. This is a non-trivial result because in the present approach the parameters $c_{1,2,3,4}$ are constrained not only by the weak decay processes of the baryon octet states but also by the meson-baryon scattering data.

$SU(3)$ symmetry-breaking effects can be studied also in terms of the meson-baryon coupling constants. To subleading order the Goldstone bosons couple to the baryon octet states via axial-vector but also via suppressed pseudo-scalar vertices (see (2.38)). In Tab. 6.6 results are collected for all the axial-vector meson-baryon coupling constants, $A_{\Phi B}^{(B)}$, and their respective pseudo-scalar parts $P_{\Phi B}^{(B)}$. The $SU(3)$ symmetric part of the axial-vector vertices is characterized by parameters F_A and D_A

$$\begin{aligned}
 F_A &= F_R - \frac{\beta}{\sqrt{3}} \left(\frac{2}{3} \delta c_1 + \delta c_2 - a \right) = 0.270, \\
 D_A &= D_R - \frac{\beta}{\sqrt{3}} \delta c_1 = 0.726,
 \end{aligned}
 \tag{6.2}$$

where $\beta \simeq 1.12$. To subleading order the parameters F_A and D_A differ from the corresponding parameters $F_R = 0.418$ and $D_R = 0.748$ relevant for matrix elements of the axial-vector current (see Tab. 2.1) by a sizeable amount. The $SU(3)$ symmetry-breaking effects in the axial-vector coupling constants A are determined by the parameters c_i , which are already tightly constrained

	$A_{\pi N}^{(N)}$	$A_{\eta N}^{(N)}$	$A_{\bar{K}N}^{(\Lambda)}$	$A_{\pi\Sigma}^{(\Lambda)}$	$A_{\eta\Lambda}^{(\Lambda)}$	$A_{\bar{K}\Xi}^{(\Lambda)}$	$A_{\bar{K}N}^{(\Sigma)}$	$A_{\pi\Sigma}^{(\Sigma)}$	$A_{\eta\Sigma}^{(\Sigma)}$	$A_{\bar{K}\Xi}^{(\Sigma)}$	$A_{\pi\Xi}^{(\Xi)}$	$A_{\eta\Xi}^{(\Xi)}$
χ -BS(3)	2.15	0.20	-1.29	1.41	-0.64	0.12	0.73	-1.02	1.09	1.24	-0.59	-0.32
SU(3)	1.73	0.05	-1.25	1.45	-0.84	-0.07	0.65	-0.76	0.84	1.41	-0.79	-0.89
	$P_{\pi N}^{(N)}$	$P_{\eta N}^{(N)}$	$P_{\bar{K}N}^{(\Lambda)}$	$P_{\pi\Sigma}^{(\Lambda)}$	$P_{\eta\Lambda}^{(\Lambda)}$	$P_{\bar{K}\Xi}^{(\Lambda)}$	$P_{\bar{K}N}^{(\Sigma)}$	$P_{\pi\Sigma}^{(\Sigma)}$	$P_{\eta\Sigma}^{(\Sigma)}$	$P_{\bar{K}\Xi}^{(\Sigma)}$	$P_{\pi\Xi}^{(\Xi)}$	$P_{\eta\Xi}^{(\Xi)}$
χ -BS(3)	-0.01	0.16	0.04	-0.01	0.20	-0.07	-0.11	-0.00	-0.02	-0.09	0.01	0.13

Table 6.6: Axial-vector (A) and pseudo-scalar (P) meson-baryon coupling constants for the baryon octet states. The row labelled by SU(3) gives results excluding SU(3) symmetry-breaking effects with $F_A = 0.270$ and $D_A = 0.726$. The total strength of the on-shell meson-baryon vertex is determined by $G = A + P$.

by the weak decay widths of the baryon octet states, and $\delta c_{1,2}$ and a . Similarly the four parameters $\bar{c}_{1,2}$ and a characterize the pseudo-scalar meson-baryon 3-point vertices. Their symmetric contributions are determined by F_P and D_P

$$F_P = -\frac{\beta}{\sqrt{3}} \left(\frac{2}{3} \bar{c}_1 + \bar{c}_2 + a \right) = 0.004, \quad D_P = -\frac{\beta}{\sqrt{3}} \bar{c}_1 = -0.049. \quad (6.3)$$

Note that in the on-shell coupling constants $G = A + P$ the parameter a drops out. In that sense that parameter should be viewed as representing an effective quasi-local 2-body interaction term, which breaks the $SU(3)$ symmetry explicitly.

The meson-baryon coupling constants are strongly constrained by the axial-vector coupling constants. In particular a sum rule derived first by Dashen and Weinstein is reproduced [187]

$$\begin{aligned} G_{\pi N}^{(N)} - \sqrt{3} g_A(n \rightarrow p e^- \bar{\nu}_e) &= -\frac{m_\pi^2}{\sqrt{6} m_K^2} \left(G_{\bar{K}N}^{(\Sigma)} - g_A(\Sigma^- \rightarrow n e^- \bar{\nu}_e) \right) \\ &- \frac{m_\pi^2}{\sqrt{2} m_K^2} \left(G_{\bar{K}N}^{(\Lambda)} - 2 g_A(\Lambda \rightarrow p e^- \bar{\nu}_e) \right). \end{aligned} \quad (6.4)$$

We observe that, given the expected range of values for $g_{\pi NN}$, $g_{\bar{K}N\Lambda}$ and $g_{\bar{K}N\Sigma}$ together with the empirical axial-vector coupling constants, the Dashen-Weinstein relation strongly favors a small f parameter value close to f_π .

In Tab. 6.7 we confront our results with a representative selection of published meson-baryon coupling constants. For the clarity of this comparison we recall here the connection with our convention

$$\begin{aligned} g_{\pi NN} &= \frac{m_N}{\sqrt{3} f} G_{\pi N}^{(N)}, \quad g_{\bar{K}N\Lambda} = \frac{m_N + m_\Lambda}{\sqrt{8} f} G_{\bar{K}N}^{(\Lambda)}, \quad g_{\pi\Lambda\Sigma} = \frac{m_\Lambda + m_\Sigma}{\sqrt{12} f} G_{\pi\Sigma}^{(\Lambda)}, \\ g_{\bar{K}N\Sigma} &= \frac{m_N + m_\Sigma}{\sqrt{8} f} G_{\bar{K}N}^{(\Sigma)}, \quad g_{\pi\Sigma\Sigma} = \frac{m_\Sigma}{\sqrt{2} f} G_{\pi\Sigma}^{(\Sigma)}. \end{aligned} \quad (6.5)$$

Further values from previous analyses can be found in [80]. Note also the interesting recent results within the QCD sum rule approach [192, 193] and also [194]. We do not confront our values with those of [192, 193] and [194] because the $SU(3)$ symmetry-breaking effects are not yet

	χ -BS(3)	[188]	[76, 189, 190]	[78]	[69]	[191]
$ g_{\pi NN} $	12.9	13.0	13.5	13.1	-	-
$ g_{\bar{K}N\Lambda} $	10.1	13.5	14.0	10.1	13.2	16.1
$ g_{\pi\Sigma\Lambda} $	10.4	11.9	9.3	6.4	-	-
$ g_{\bar{K}N\Sigma} $	5.2	4.1	2.7	2.4	6.4	3.5
$ g_{\pi\Sigma\Sigma} $	9.6	11.8	10.8	0.7	-	-

Table 6.7: On-shell meson-baryon coupling constants for the baryon octet states (see (6.5)). We give the central values only because reliable error analyses are not available in most cases.

fully under control in these works. The analysis [188] is based on nucleon-nucleon and hyperon-nucleon scattering data where $SU(3)$ symmetry breaking effects in the meson-baryon coupling constants are parameterized according to the model of [195]. The values given in [76, 189, 190] do not allow for $SU(3)$ symmetry-breaking effects and moreover rely on $SU(6)$ quark-model relations. Particularly striking are the extreme $SU(3)$ symmetry-breaking effects claimed in [78]. The parameters result from a K-matrix fit to the phase shifts of K^-N scattering as given in [73]. We do not confirm these results. Note also the recent analysis [196] which deduces the value $g_{\pi\Lambda\Sigma} = 12.9 \pm 1.2$ from hyperonic atom data, a value somewhat larger than our result of 10.4. For the most recent and accurate pion-nucleon coupling constant $g_{\pi NN} = 13.34 \pm 0.09$ we refer to [197]. We do not compete with the high precision and elaborate analyses of this work.

In Tab. 6.8 results for the meson-baryon coupling constants of the decuplet states are collected. Again only moderate $SU(3)$ symmetry-breaking effects are found in the coupling constants. This is demonstrated by comparing the two rows of Tab. 6.8. The $SU(3)$ symmetric part is determined by the parameter C_A

$$C_A = C_R - 2 \frac{\beta}{\sqrt{3}} (\bar{c}_1 + \delta c_1) = 1.593. \quad (6.6)$$

Note that the coupling constants as given in (6.8) should not be used in the simple expressions (2.45) for the decuplet widths. For example with $A_{\pi N}^{(\Delta)} \simeq 2.62$ one would estimate $\Gamma_\Delta \simeq 102$ MeV not too close to the empirical value of $\Gamma_\Delta \simeq 120$ MeV [147]. As demonstrated in [97] nevertheless the P_{33} phase shift of the pion-nucleon scattering process, which probes the Δ resonance width, is reproduced accurately. This reflects an important energy dependence in the decuplet self energy.

	$A_{\pi N}^{(\Delta)}$	$A_{K\Sigma}^{(\Delta)}$	$A_{\bar{K}N}^{(\Sigma)}$	$A_{\pi\Sigma}^{(\Sigma)}$	$A_{\pi\Lambda}^{(\Sigma)}$	$A_{\eta\Sigma}^{(\Sigma)}$	$A_{K\Xi}^{(\Sigma)}$	$A_{\bar{K}\Lambda}^{(\Xi)}$	$A_{\bar{K}\Sigma}^{(\Xi)}$	$A_{\eta\Xi}^{(\Xi)}$	$A_{\pi\Xi}^{(\Xi)}$
χ -BS(3)	2.62	-2.03	1.54	-1.40	-1.64	1.55	-0.96	1.67	1.75	-1.29	-1.46
SU(3)	2.25	-2.25	1.30	-1.30	-1.59	1.59	-1.30	1.59	1.59	-1.59	-1.59

Table 6.8: Meson-baryon coupling constants for the baryon decuplet states. The row labelled by SU(3) gives results obtained with $C_A = 1.593$ excluding all symmetry-breaking effects.

To summarize the main findings of this section. All established parameters prove the $SU(3)$ flavor symmetry to be an extremely useful and accurate tool. Explicit symmetry breaking effects are quantitatively important but sufficiently small to permit an evaluation within the χ -BS(3) approach. This confirms a beautiful analysis by Hamilton and Oades [198] who strongly supported the $SU(3)$ flavor symmetry by a discrepancy analysis of antikaon-nucleon scattering data.

6.3 Kaon- and antikaon-nucleon scattering

Since it is impossible to give here a comprehensive discussion of the many works dealing with kaon-nucleon scattering we refer to the review article by Dover and Walker [9] which is still up-to-date in many respects. The data situation can be summarized as follows: there exist precise low-energy differential cross sections for K^+p scattering but no scattering data for the K^+ -deuteron scattering process at low energies. Thus, all low-energy results in the isospin zero channel necessarily follow from model-dependent extrapolations. The available differential cross section are included in the global fit. They are nicely reproduced as shown in [97].

It is instructive to consider the threshold amplitudes in detail. In the χ -BS(3) approach the threshold parameters are determined by the threshold values of the effective interaction kernel $V_{KN}^{(\pm)}(m_N+m_K; n)$ and the partial-wave loop function $J_{KN}^{(\pm)}(m_N+m_K; n)$ (see (4.11,4.51)). Since all loop functions vanish at threshold but the one for the s-wave channel, all p-wave scattering volumes remain unchanged by the unitarization and are directly given by the threshold values of the appropriate effective interaction kernel V_{KN} . Explicit expressions for the scattering volumes to leading order can be found in [97]. In contrast the s-wave scattering lengths are renormalized strongly by the loop function $J_{KN}^{(+)}(m_N+m_K; 0) \neq 0$. At leading order the s-wave scattering lengths are

$$\begin{aligned} 4\pi \left(1 + \frac{m_K}{m_N}\right) a_{S_{21}}^{(KN)} &= -m_K \left(f^2 + \frac{m_K^2}{8\pi} \left(1 - \frac{1}{\pi} \ln \frac{m_K^2}{m_N^2}\right) \right)^{-1}, \\ 4\pi \left(1 + \frac{m_K}{m_N}\right) a_{S_{01}}^{(KN)} &= 0, \end{aligned} \quad (6.7)$$

and lead to $a_{S_{21}}^{(KN)} \simeq -0.22$ fm and $a_{S_{01}}^{(KN)} = 0$ fm close to our final values to subleading orders as given in Tab. 6.9. In that table we collected typical results for the p-wave scattering volumes

	$a_{S_{01}}^{(KN)}$ [fm]	$a_{S_{21}}^{(KN)}$ [fm]	$a_{P_{01}}^{(KN)}$ [m_π^{-3}]	$a_{P_{21}}^{(KN)}$ [m_π^{-3}]	$a_{P_{03}}^{(KN)}$ [m_π^{-3}]	$a_{P_{23}}^{(KN)}$ [m_π^{-3}]
χ -BS(3)	0.06	-0.30	0.033	-0.017	-0.003	0.012
[199]	0.0	-0.33	0.028	-0.056	-0.046	0.025
[200]	-0.04	-0.32	0.030	-0.011	-0.007	0.007

Table 6.9: K^+ -nucleon threshold parameters. The values of the χ -BS(3) analysis are given in the first row. The last two rows recall the threshold parameters as given in [199] and [200].

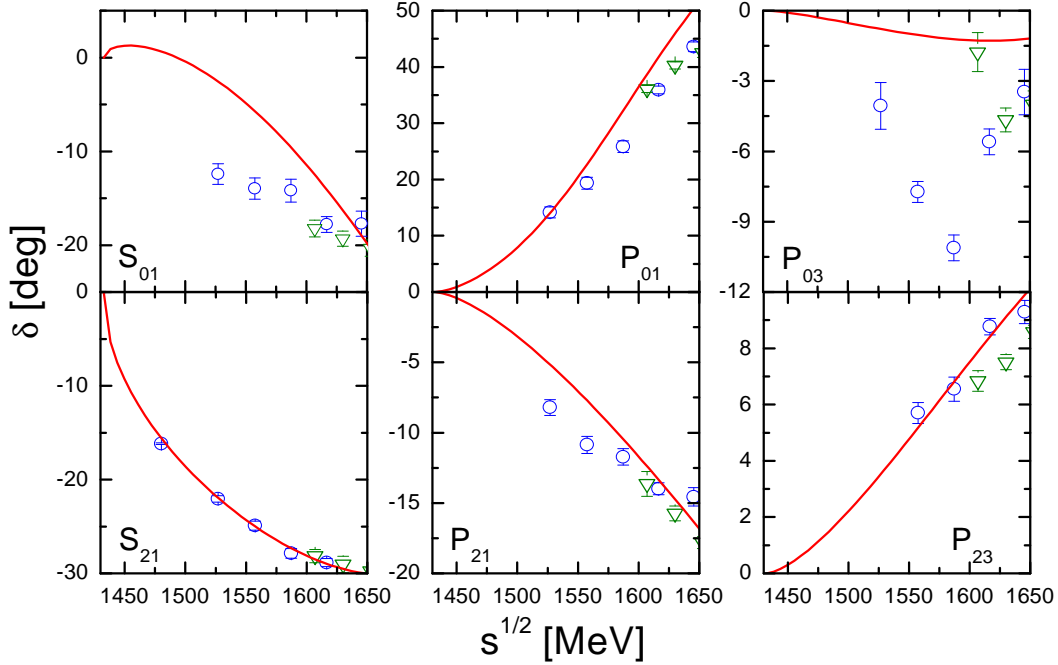


Figure 6.1: S- and p-wave K^+ -nucleon phase shifts. The solid lines represent the results of the χ -BS(3) approach. The open circles are from the Hyslop analysis [199] and the open triangles from the Hashimoto analysis [179].

also. The large differences in the isospin zero channel reflect the fact that this channel is not constrained by scattering data directly [9]. We find that some of our p-wave scattering volumes, also shown in Tab. 6.9, differ significantly from the values obtained by previous analyses. Such discrepancies may be explained in part by important cancellation mechanisms among the u-channel baryon octet and decuplet contributions (see [97]). An accurate description of the scattering volumes requires a precise input for the meson-baryon 3-point vertices. Since the χ -BS(3) approach describes the 3-point vertices in accordance with all chiral constraints and large- N_c sum rule of QCD the values for the scattering volumes presented here should be rather reliable.

In Fig. 6.1 results for the s- and p-wave K^+ -nucleon phase shifts are confronted with the most recent analyses by Hyslop et al. [199] and Hashimoto [179]. We find that our partial-wave phase shifts are reasonably close to the single energy phase shifts of [199] and [179] except the P_{03} phase for which we obtain much smaller strength. Note however, that at higher energies we smoothly reach the single energy phase shifts of Hashimoto [179]. A possible ambiguity in that phase shift is already suggested by the conflicting scattering volumes found in that channel by earlier works (see Tab. 6.9). The isospin one channel, on the other hand, seems well-established even though the data set does not include polarization measurements close to threshold, which are needed to unambiguously determine the p-wave scattering volumes.

In contrast to the kaon-nucleon scattering process the antikaon-nucleon scattering process shows a large variety of interesting phenomena. Inelastic channels are already open at threshold leading to a rich coupled channel dynamics. Also the $\bar{K}N$ state couples to many of the observed hyperon resonances for which competing dynamical scenarios are conceivable. In this work

the available data set is fitted directly rather than any partial wave analysis. Comparing for instance the energy-dependent analyses [73] and [201] one finds large uncertainties in the s- and p-waves in particular at low energies. This reflects on the one hand a model dependence of the analysis and on the other hand an insufficient data set. A partial wave analysis of elastic and inelastic antikaon-nucleon scattering data without further constraints from theory is inconclusive at present [9, 202]. For a detailed overview of former theoretical analyses, we refer to the review article by Dover and Walker [9].

As motivated above the d-wave baryon resonance nonet field is considered here. An update of the analysis [146] leads to the estimates $F_{[9]} \simeq 1.8$, $D_{[9]} \simeq 0.84$ and $C_{[9]} \simeq 2.5$ for the resonance parameters. The singlet-octet mixing angle $\vartheta \simeq 28^\circ$ confirms the finding of [145] that the $\Lambda(1520)$ resonance is predominantly a flavor singlet state. The values for $F_{[9]}$ and $D_{[9]}$ describe the decay widths and branching ratios of the $\Sigma(1670)$ and $\Xi(1820)$ reasonably well within their large empirical uncertainties. Less emphasis is put on the properties of the $N(1520)$ resonance since that resonance is strongly influenced by the $\pi\Delta_\mu$ channel not considered here. In the global fit $F_{[9]}$ and $D_{[9]}$ were fixed as given above but the mixing angle $\vartheta = 27.74^\circ$ and $C_{[9]} = 2.509$ were fine-tuned. To account for further small inelastic three-body channels the 'bare' $\Lambda(1520)$ resonance was given an energy independent decay width of $\Gamma_{\Lambda(1520)}^{(3\text{-body})} \simeq 1.4$ MeV. The total cross sections are included in the fit for $p_{\text{lab.}} < 500$ MeV. For the bare masses of the d-wave resonances the values $m_{\Lambda(1520)} \simeq 1528.2$ MeV, $m_{\Lambda(1690)} \simeq 1705.3$ MeV and $m_{\Sigma(1680)} \simeq 1690.7$ MeV were used.

In Fig. 6.2 the result of the fit for the elastic and inelastic K^-p cross sections are shown. The data set is nicely reproduced including the rather precise data points for laboratory momenta $250 \text{ MeV} < p_{\text{lab.}} < 500$ MeV. In Fig. 6.2 the s-wave contribution to the total cross section is shown with a dashed line. Important p-wave contributions are found at low energies only in the $\Lambda\pi^0$ production cross section. Note that the $\Lambda\pi^0$ channel carries isospin one and therefore provides valuable constraint on the poorly known K^- -neutron interaction. The deviation of the results from the empirical cross sections above $p_{\text{lab.}} \simeq 500$ MeV in some channels may be due in part to the fact that we do not consider the p-wave $\Lambda(1600)$ and $\Sigma(1660)$ resonances quantitatively in this work. As will be demonstrated below when presenting the partial-wave amplitudes, there is, however, a strong tendency that those resonances are generated in the χ -BS(3) scheme. Giving up some of the large- N_c sum rules and thereby increasing the number of free parameters one can easily obtain a fit of much improved quality beyond $p_{\text{lab.}} = 500$ MeV. We refrained from presenting those results because it is not clear that this procedure leads to the correct partial wave interpretation of the total cross sections. The inelastic channel $K^-p \rightarrow \Lambda\pi\pi$, not included in this work, is no longer negligible at a quantitative level for $p_{\text{lab.}} > 300$ MeV [203].

Further important information on the p-wave dynamics is provided by angular distributions for the K^-p reactions. The available data are represented in terms of coefficients A_n and B_n characterizing the differential cross section $d\sigma(\cos\theta, \sqrt{s})$ and the polarization $P(\cos\theta, \sqrt{s})$ as functions of the center of mass scattering angle θ and the total energy \sqrt{s} :

$$\begin{aligned} \frac{d\sigma(\sqrt{s}, \cos\theta)}{d\cos\theta} &= \sum_{n=0}^{\infty} A_n(\sqrt{s}) P_n(\cos\theta), \\ \frac{d\sigma(\sqrt{s}, \cos\theta)}{d\cos\theta} P(\sqrt{s}, \cos\theta) &= \sum_{n=1}^{\infty} B_n(\sqrt{s}) P_n^1(\cos\theta). \end{aligned} \quad (6.8)$$

In Fig. 6.3 the empirical ratios A_1/A_0 and A_2/A_0 are compared with the results of the χ -BS(3) approach. Note that for $p_{\text{lab.}} < 300$ MeV the empirical ratios with $n \geq 3$ are compatible

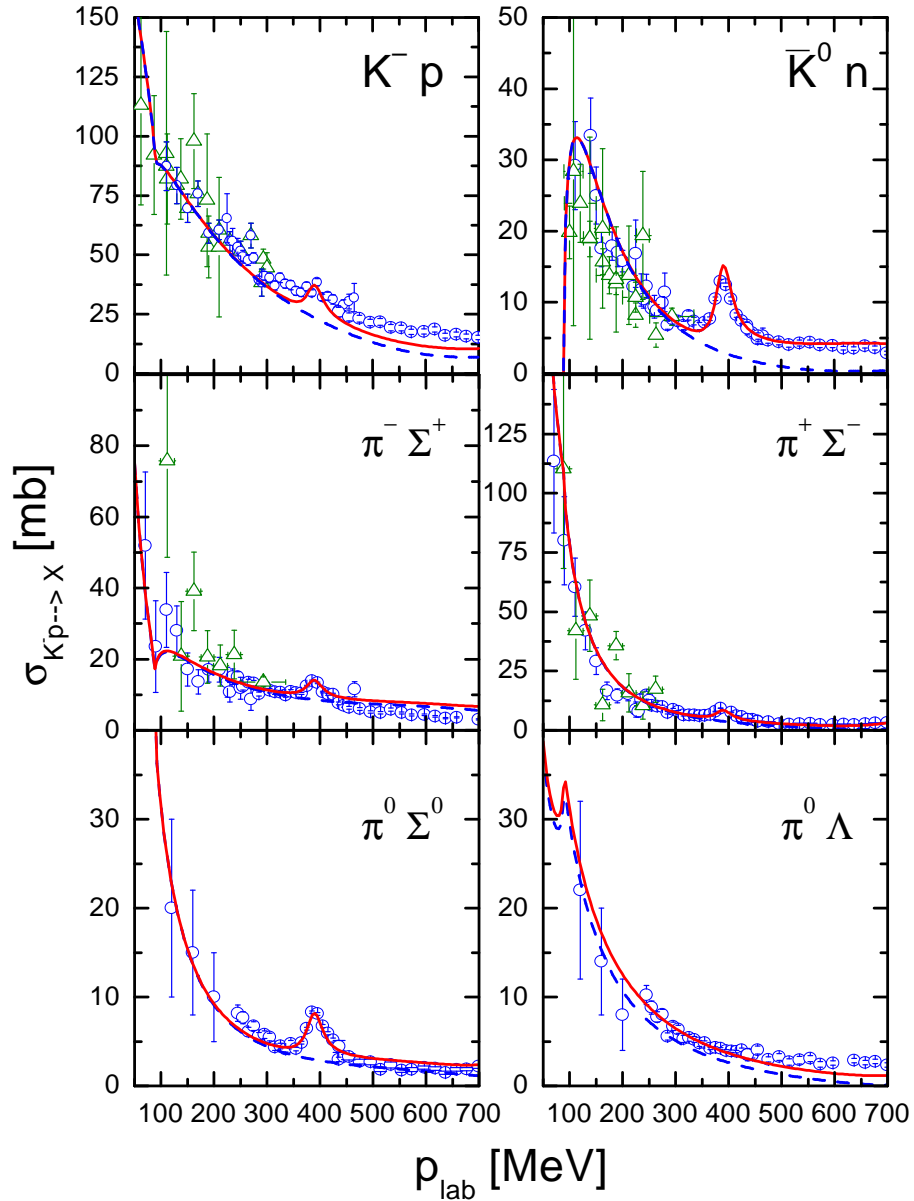


Figure 6.2: K^- -proton elastic and inelastic cross sections. The data are taken from [86, 72, 204, 205, 206, 207, 208, 209]. The solid lines show the results of the χ -BS(3) theory including all effects of s-, p- and d-waves. The dashed lines represent the s-wave contributions only. We fitted the data points given by open circles [86, 72, 204, 205, 206, 207, 208]. Further data points represented by open triangles [209] were not considered in the global fit.

with zero within their given errors. A large A_1/A_0 ratio is found only in the $K^-p \rightarrow \pi^0\Lambda$ channel demonstrating again the importance of p-wave effects in the isospin one channel. The dashed lines of Fig. 6.3, which are obtained when switching off d-wave contributions, confirm the importance of this resonance for the angular distributions in the isospin zero channel. The fact that the $\Lambda(1520)$ resonance appears more important in the differential cross sections than

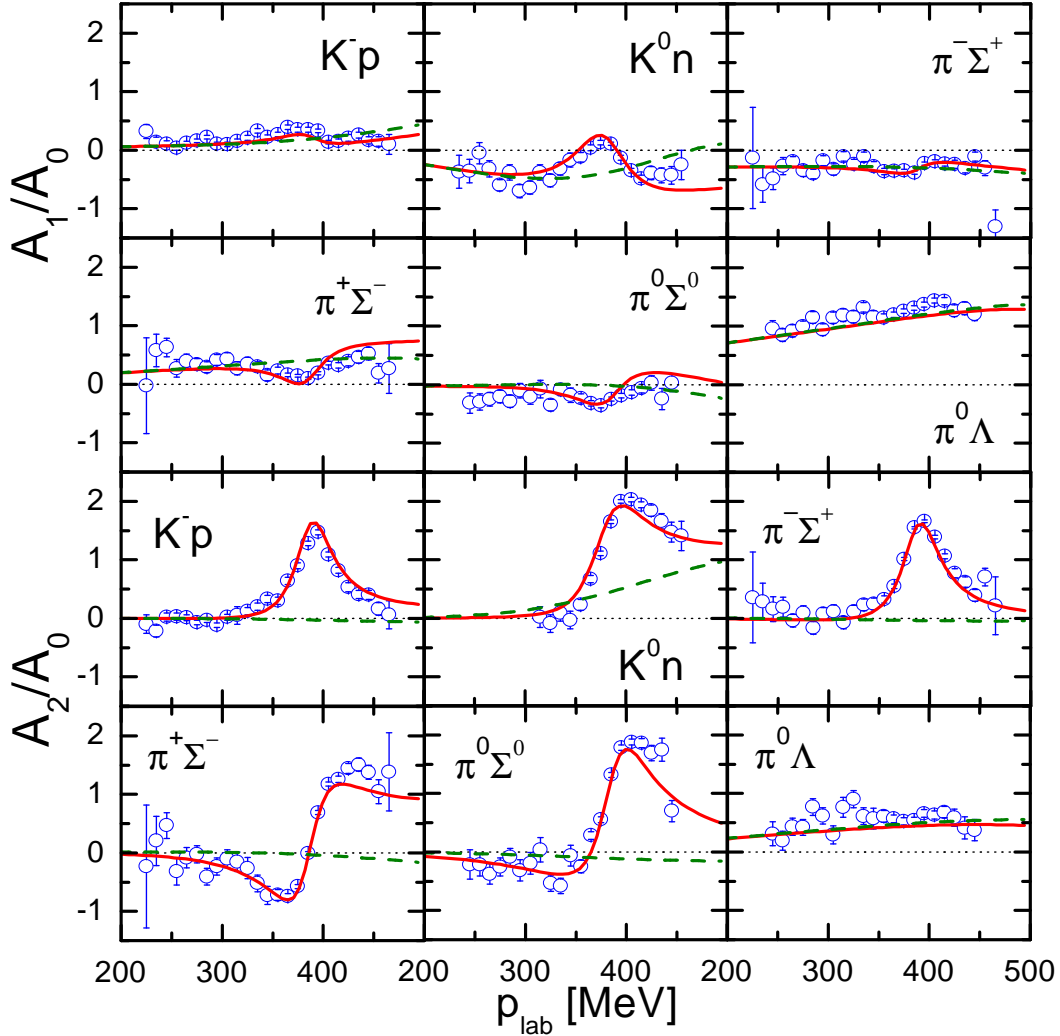


Figure 6.3: Coefficients A_1 and A_2 for the $K^-p \rightarrow \pi^0\Lambda$, $K^-p \rightarrow \pi^\mp\Sigma^\pm$ and $K^-p \rightarrow \pi^0\Sigma$ differential cross sections. The data are taken from [86, 207]. The solid lines are the result of the χ -BS(3) approach with inclusion of the d-wave resonances. The dashed lines show the effect of switching off d-wave contributions.

in the total cross sections follows simply because the tail of the resonance is enhanced if probed via an interference term. In the differential cross section the $\Lambda(1520)$ propagator enters linearly whereas the total cross section probes the squared propagator only. Note also the sizeable p-wave contributions at somewhat larger momenta seen in the charge-exchange reaction of Fig. 6.3 and also in Fig. 6.2. The constraint from the ratios B_1/A_0 and B_2/A_0 , presented in Fig. 6.4, is weak due to rather large empirical errors. New polarization data possibly with polarized hydrogen targets, would be highly desirable.

The threshold characteristics of the K^-p reaction is constrained by experimental data for

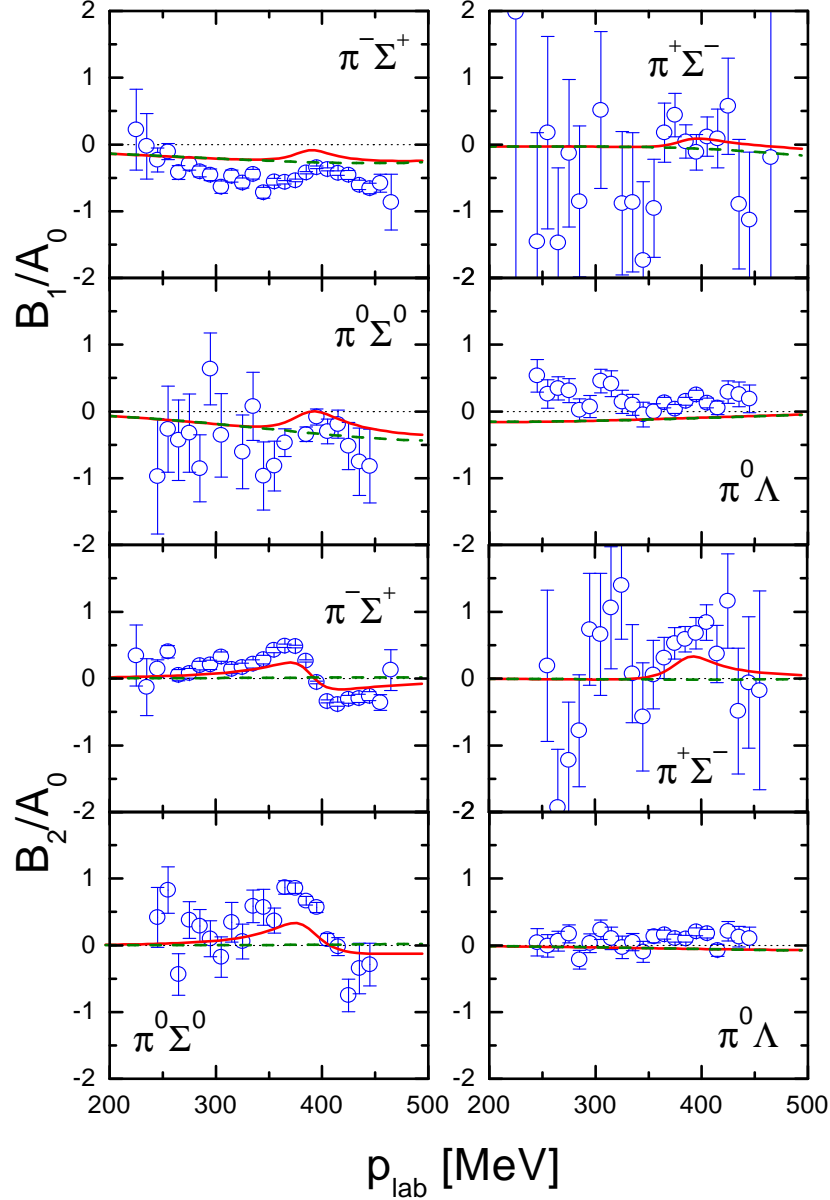


Figure 6.4: Coefficients B_1 and B_2 for the $K^-p \rightarrow \pi^\mp \Sigma^\pm$, $K^-p \rightarrow \pi^0 \Sigma$ and $K^-p \rightarrow \pi^0 \Lambda$ differential cross sections. The data are taken from [86, 207]. The solid lines are the result of the χ -BS(3) approach with inclusion of the d-wave resonances. The dashed lines show the effect of switching off d-wave contributions.

the threshold branching ratios γ , R_c and R_n where

$$\begin{aligned} \gamma &= \frac{\sigma(K^- p \rightarrow \pi^+ \Sigma^-)}{\sigma(K^- p \rightarrow \pi^- \Sigma^+)}, & R_c &= \frac{\sigma(K^- p \rightarrow \text{charged particles})}{\sigma(K^- p \rightarrow \text{all})}, \\ R_n &= \frac{\sigma(K^- p \rightarrow \pi^0 \Lambda)}{\sigma(K^- p \rightarrow \text{all neutral channels})}. \end{aligned} \quad (6.9)$$

	a_{K^-p} [fm]	a_{K^-n} [fm]	γ	R_c	R_n
Exp.	-0.78 ± 0.18 $+i(0.49 \pm 0.37)$	-	2.36 ± 0.04	0.664 ± 0.011	0.189 ± 0.015
χ -BS(3)	$-1.09 + i 0.82$	$0.29 + i 0.54$	2.42	0.65	0.19
SU(2)	$-0.79 + i 0.95$	$0.30 + i 0.49$	4.58	0.63	0.32
	$a_{P_{01}}^{(\bar{K}N)}$ [m_π^{-3}]	$a_{P_{03}}^{(\bar{K}N)}$ [m_π^{-3}]		$a_{P_{21}}^{(\bar{K}N)}$ [m_π^{-3}]	$a_{P_{23}}^{(\bar{K}N)}$ [m_π^{-3}]
χ -BS(3)	$0.025 + i 0.001$	$0.002 + i 0.001$		$-0.004 + i 0.001$	$-0.055 + i 0.021$

Table 6.10: K^- -nucleon threshold parameters. The row labelled with $SU(2)$ gives the results in the isospin limit with $m_{K^-} = m_{\bar{K}^0} = 493.7$ MeV and $m_p = m_n = 938.9$ MeV.

A further important piece of information is provided by the recent measurement of the K^- hydrogen atom state which leads to a value for the K^-p scattering length [82]. In Tab. 6.10 the empirical numbers are confronted with the present analysis. All threshold parameters are well described within the χ -BS(3) approach. The result of [65,66] that the branching ratios are rather sensitive to isospin breaking effects is confirmed. However, note that it is sufficient to include isospin breaking effects only in the $\bar{K}N$ channel to good accuracy. The empirical branching ratios are taken from [85]. The real part of our K^-n scattering length with $\Re a_{K^-n \rightarrow K^-n} \simeq 0.29$ fm turns out considerably smaller than the value of 0.53 fm found in the recent analysis [66]. In the Tab. 6.10 results for the p-wave scattering volumes are presented also. Here isospin breaking effects are negligible. All scattering volumes but the one in the P_{23} channel are found to be small. The not too small and repulsive scattering volume $a_{P_{23}} \simeq (-0.16 + i0.06)$ fm³ reflects the presence of the $\Sigma(1385)$ resonance just below the $\bar{K}N$ threshold. The precise values of the threshold parameters are of crucial importance when describing K^- -atom data which constitute a rather sensitive test of the in-medium dynamics of antikaons. In particular one expects a strong sensitivity of the level shifts on the s-wave scattering lengths.

In Fig. 6.5 the $\Lambda(1405)$ and $\Sigma(1385)$ spectral functions are shown as measured in the reactions $K^-p \rightarrow \Sigma^+\pi^-\pi^+\pi^-$ [210] and $K^-p \rightarrow \Lambda\pi^+\pi^-$ [211] respectively. The $\Lambda(1405)$ spectrum of [210] was not included in the global fit. Since the $\Lambda(1405)$ -spectrum shows a strong energy dependence, incompatible with a Breit-Wigner resonance shape, the spectral form depends rather strongly on the initial and final states through which it is measured. The empirical spectrum of [210] describes the reaction $\Sigma^+(1600)\pi^- \rightarrow \Lambda(1405) \rightarrow \Sigma^+\pi^-$ rather than the reactions $\Sigma^\pm\pi^\mp \rightarrow \Lambda(1405) \rightarrow \Sigma^+\pi^-$ accessible in our present scheme. In Fig. 6 the spectral form of the $\Lambda(1405)$ resulting from two different initial states $\Sigma^\pm\pi^\mp$ are confronted with the empirical spectrum of [210]. While the spectrum defined with respect to the initial state $\Sigma^+\pi^-$ represents the empirical spectrum reasonably well the other choice of initial state $\Sigma^+\pi^-$ leads to a significantly altered spectral form. Hence, in a scheme that does not include the $\Sigma(1600)\pi$ state explicitly it is not justified to use the $\Lambda(1405)$ spectrum of [210] as a quantitative constraint for the antikaon-nucleon dynamics.

Consider the mass spectrum of the decuplet $\Sigma(1385)$ state in Fig. 6.5. The spectral form, to good accuracy of Breit-Wigner form, is reproduced reasonably well. The result for the ratio of

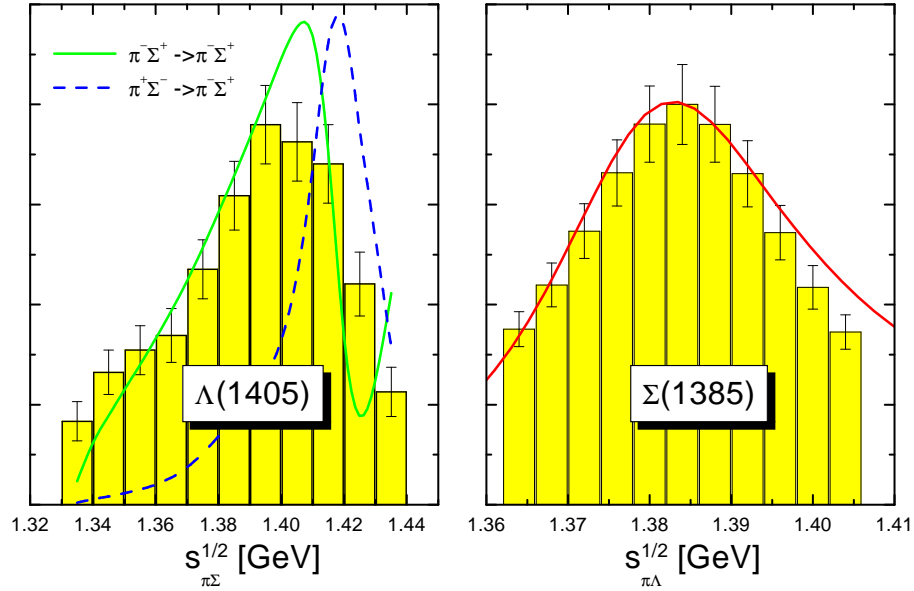


Figure 6.5: $\Lambda(1405)$ and $\Sigma(1385)$ resonance mass distributions in arbitrary units.

$\Sigma(1385) \rightarrow \pi\Lambda$ over $\Sigma(1385) \rightarrow \pi\Sigma$ of about 17% compares well with the most recent empirical determination. In [212] that branching ratio was extracted from the $K^-p \rightarrow \Sigma(1385)K\bar{K}$ reaction and found to be $20 \pm 6\%$. Note that the ratio given above was obtained from the two reaction amplitudes $\pi\Lambda \rightarrow \pi\Lambda$ and $\pi\Lambda \rightarrow \pi\Sigma$ evaluated at the $\Sigma(1385)$ pole. The schematic expression (2.45) would give a smaller value of about 15%. The value for the $\Xi(1530)$ total width of 10.8 MeV comfortably meets the empirical value of $9.9_{-1.9}^{+1.7}$ MeV given in [147].

6.4 Analyticity and crossing symmetry

It is important to investigate to what extent the multi-channel scattering amplitudes are consistent with the expectations from analyticity and crossing symmetry. As discussed in detail in chapter 4.3 the crossing symmetry constraints should not be considered in terms of partial-wave amplitudes, but rather in terms of the forward scattering amplitudes only. In the strangeness sector crossing symmetry is particularly important because that sector has a large subthreshold region not directly accessible and constrained by data. In the following the forward $\bar{K}N$ and KN scattering amplitudes are reconstructed in terms of their imaginary parts by means of dispersion integrals. The reconstructed scattering amplitudes are then confronted with the original ones. It is non-trivial that those amplitudes match even though the loop functions and effective interaction kernels are analytic functions. One can not exclude that the coupled channel dynamics generates unphysical singularities off the real axis which would then spoil the representation of the scattering amplitudes in terms of dispersion integrals. Within effective field theory unphysical singularities are acceptable, however, only far outside the applicability domain of the approach.

The analysis performed here is analogous to that of Martin [69]. However, here the dispersion-integral representation is considered as a consistency check of the theory rather than as a predictive tool to derive the low-energy kaon-nucleon scattering amplitudes in terms of the more accurate scattering data at $E_{\text{lab}} > 300$ MeV [213]. This way any subtle assumption on the number of required subtractions in the dispersion integral is avoided. Obviously the dispersion integral, if evaluated for small energies, must be dominated by the low-energy total cross sections which are not known empirically too well. A subtracted dispersion integral is written

$$\begin{aligned} T_{\bar{K}N}^{(0)}(s) &= \frac{f_{\bar{K}N\Lambda}^2}{s - m_\Lambda^2} + \sum_{k=1}^n c_{\bar{K}N}^{(0,k)} (s - s_0)^k + \int_{(m_\Sigma + m_\pi)^2}^\infty \frac{ds'}{(s' - s_0)^n} \frac{(s - s_0)^n}{s' - s - i\epsilon} \Im T_{\bar{K}N}^{(0)}(s'), \\ T_{\bar{K}N}^{(1)}(s) &= \frac{f_{\bar{K}N\Sigma}^2}{s - m_\Sigma^2} + \sum_{k=1}^n c_{\bar{K}N}^{(1,k)} (s - s_0)^k + \int_{(m_\Lambda + m_\pi)^2}^\infty \frac{ds'}{(s' - s_0)^n} \frac{(s - s_0)^n}{s' - s - i\epsilon} \Im T_{\bar{K}N}^{(1)}(s'), \end{aligned} \quad (6.10)$$

where $s_0 = \Lambda_{\text{opt.}}^2 = m_N^2 + m_K^2$ is identified with the optimal matching point of (4.54). Recall that the kaon-hyperon coupling constants,

$$f_{KNY} = \sqrt{\frac{m_K^2 - (m_Y - m_N)^2}{2m_N}} \frac{m_N + m_Y}{2f} \left(A_{\bar{K}N}^{(Y)} + P_{\bar{K}N}^{(Y)} \right), \quad (6.11)$$

with $Y = \Lambda, \Sigma$ receive contributions from pseudo-vector and pseudo-scalar vertices as specified in Tab. 6.6. The values $f_{KN\Lambda} \simeq -12.8 m_{\pi^+}^{1/2}$ and $f_{KN\Sigma} \simeq 6.1 m_{\pi^+}^{1/2}$ follow.

The forward scattering amplitude $T_{\bar{K}N}(s)$ reconstructed in terms of the partial-wave amplitudes $f_{\bar{K}N,j}^{(L)}(\sqrt{s})$ of (3.61) reads

$$T_{\bar{K}N}(s) = 4\pi \frac{\sqrt{s}}{m_N} \sum_{n=0}^{\infty} (n+1) \left(f_{\bar{K}N,n+\frac{1}{2}}^{(n)}(\sqrt{s}) + f_{\bar{K}N,n+\frac{1}{2}}^{(n+1)}(\sqrt{s}) \right). \quad (6.12)$$

The subtraction coefficients $c_{\bar{K}N}^{(I,k)}$ are adjusted to reproduce the scattering amplitudes close to the kaon-nucleon threshold. One must perform a sufficient number of subtractions so that the dispersion integral in (6.10) is dominated by energies still within the applicability range of our theory. With $n = 4$ in (6.10) we indeed find that we are insensitive to the scattering amplitudes for $\sqrt{s} > 1600$ MeV to good accuracy. Similarly, subtracted dispersion integrals for the amplitudes $T_{\bar{K}N}^{(I)}(s)$ of the strangeness +1 sector are written

$$\begin{aligned} T_{\bar{K}N}^{(0)}(s) &= -\frac{1}{2} \frac{f_{\bar{K}N\Lambda}^2}{2s_0 - s - m_\Lambda^2} + \frac{3}{2} \frac{f_{\bar{K}N\Sigma}^2}{2s_0 - s - m_\Sigma^2} \\ &+ \sum_{k=1}^n c_{\bar{K}N}^{(0,k)} (s - s_0)^k + \int_{(m_N + m_K)^2}^\infty \frac{ds'}{\pi} \frac{(s - s_0)^n}{(s' - s_0)^n} \frac{\Im T_{\bar{K}N}^{(0)}(s')}{s' - s - i\epsilon}, \\ T_{\bar{K}N}^{(1)}(s) &= \frac{1}{2} \frac{f_{\bar{K}N\Lambda}^2}{2s_0 - s - m_\Lambda^2} + \frac{1}{2} \frac{f_{\bar{K}N\Sigma}^2}{2s_0 - s - m_\Sigma^2} \\ &+ \sum_{k=1}^n c_{\bar{K}N}^{(1,k)} (s - s_0)^k + \int_{(m_N + m_K)^2}^\infty \frac{ds'}{\pi} \frac{(s - s_0)^n}{(s' - s_0)^n} \frac{\Im T_{\bar{K}N}^{(1)}(s')}{s' - s - i\epsilon}. \end{aligned} \quad (6.13)$$

The subtraction coefficients $c_{\bar{K}N}^{(I,k)}$ are adjusted to reproduce the scattering amplitudes close to the kaon-nucleon threshold. The choice $n = 4$ leads to a sufficient emphasis of the low-energy KN -amplitudes.

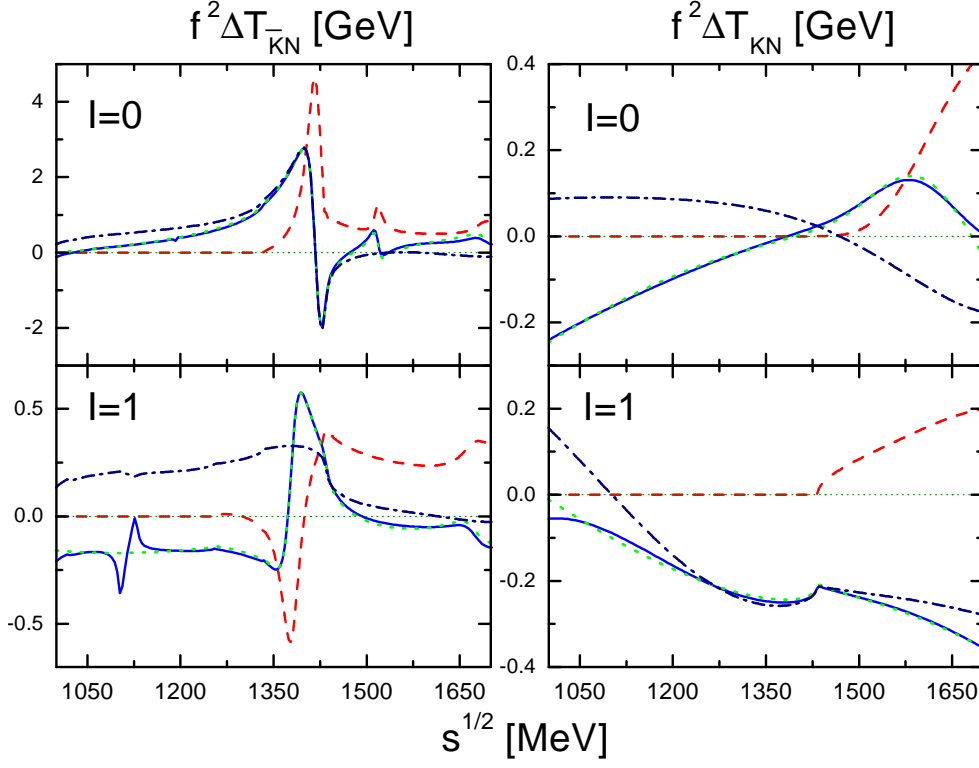


Figure 6.6: Causality check of the pole-subtracted kaon-nucleon scattering amplitudes $f^2 \Delta T_{\bar{K}N}^{(I)}$ and $f^2 \Delta T_{KN}^{(I)}$. The full lines represent the real part of the forward scattering amplitudes. The dotted lines give the amplitudes as obtained from their imaginary parts (dashed lines) in terms of the dispersion integrals (6.10) and (6.13). The dashed-dotted lines give the s-wave contribution to the real part of the forward scattering amplitudes only.

In Fig. 6.6 we compare the real part of the pole-subtracted amplitudes $\Delta T_{\bar{K}N}^{(I)}(s)$ and $\Delta T_{KN}^{(I)}(s)$ with the corresponding amplitudes reconstructed via the dispersion integral (6.10)

$$\begin{aligned} \Delta T_{\bar{K}N}^{(I)}(s) &= T_{\bar{K}N}^{(I)}(s) - \frac{f_{\bar{K}NY}^2}{s - m_H^2} - \left(A_{\bar{K}N}^{(Y)}\right)^2 \frac{2m_N^2 + m_K^2 - s - m_H^2}{8f^2 m_N} \\ &+ \left(P_{\bar{K}N}^{(Y)}\right)^2 \frac{(m_N + m_H)^2}{8f^2 m_N} + P_{\bar{K}N}^{(Y)} A_{\bar{K}N}^{(Y)} \frac{m_H^2 - m_N^2}{4f^2 m_N}, \end{aligned} \quad (6.14)$$

with $Y = \Lambda$ for $I = 0$ and $Y = \Sigma$ for $I = 1$. Whereas it is straightforward to subtract the complete hyperon pole contribution in the $\bar{K}N$ amplitudes (see (6.14)), it is less immediate how to do so for the KN amplitudes. Since not all partial wave contributions are considered in the latter amplitudes the u-channel pole must be subtracted in its approximated form as given in (4.46). The reconstructed amplitudes agree rather well with the original amplitudes. For $\sqrt{s} > 1200$ MeV the solid and dotted lines in Fig. 6.6 can hardly be discriminated. This demonstrates that the amplitudes are causal to good accuracy. Note that the discrepancy for $\sqrt{s} < 1200$ MeV is a consequence of the approximate treatment of the non-local u-channel exchanges which violates analyticity at subthreshold energies to some extent (see (4.48)). With

Fig. 6.6 it is demonstrated that such effects are well controlled for $\sqrt{s} > 1200$ MeV. In any case, close to $\sqrt{s} \simeq 1200$ MeV the complete forward scattering amplitudes are largely dominated by the s- and u-channel hyperon pole contributions absent in $\Delta T_{\bar{K}N}^{(I)}(s)$.

As can be seen from Fig. 6.6 also, there are sizeable p-wave contributions in the pole-subtracted amplitudes at subthreshold energies. This follows by comparing the dashed-dotted lines, which give the s-wave contributions only, with the solid lines which represent the complete real part of the pole-subtracted forward scattering amplitudes. The p-wave contributions are typically much larger below threshold than above threshold. The fact that this is not the case in the isospin zero KN amplitude reflects a subtle cancellation mechanism of hyperon exchange contributions and quasi-local two-body interaction terms. In the $\bar{K}N$ amplitudes the subthreshold effects of p-waves are most dramatic in the isospin one channel. Here the amplitude is dominated by the $\Sigma(1385)$ resonance. Note that p-wave channels contribute with a positive imaginary part for energies larger than the kaon-nucleon threshold but with a negative imaginary part for subthreshold energies. A negative imaginary part of a subthreshold amplitude is consistent with the optical theorem which relates the imaginary part of the forward scattering amplitudes to the total cross section for energies above threshold only. The results presented here shed some doubts on the analysis of Martin, which attempted to constrain the forward scattering amplitude via a dispersion analysis [69]. An implicit assumption of his analysis was, that the contribution to the dispersion integral from the subthreshold region, which is not directly determined by the data set, is dominated by s-wave dynamics. As was pointed out in [67] strong p-wave contributions at subthreshold energies should have an important effect on the propagation properties of antikaons in dense nuclear matter. This expectation will be confirmed in the next section.

Crossing symmetry relates the subthreshold $\bar{K}N$ and KN scattering amplitudes. As a consequence the exact amplitude $T_{\bar{K}N}^{(0)}(s)$ shows unitarity cuts not only for $\sqrt{s} > m_\Sigma + m_\pi$ but also for $\sqrt{s} < m_N - m_K$ representing the elastic KN scattering process. For the isospin zero amplitude one expects the following representation:

$$\begin{aligned} T_{\bar{K}N}^{(0)}(s) - T_{\bar{K}N}^{(0)}(s_0) &= \frac{f_{\bar{K}N\Lambda}^2}{s - m_\Lambda^2} - \frac{f_{\bar{K}N\Lambda}^2}{s_0 - m_\Lambda^2} + \int_{-\infty}^{(m_N - m_K)^2} \frac{ds'}{\pi} \frac{s - s_0}{s' - s_0} \Im T_{\bar{K}N}^{(0)}(s') \\ &+ \int_{(m_\Sigma + m_\pi)^2}^{+\infty} \frac{ds'}{\pi} \frac{s - s_0}{s' - s_0} \Im T_{\bar{K}N}^{(0)}(s'), \end{aligned} \quad (6.15)$$

where one subtraction was performed to help the convergence of the dispersion integral. An analogous representation holds for the isospin one amplitude. Comparing the expressions for $T_{\bar{K}N}^{(0)}(s)$ in (6.10) and $T_{\bar{K}N}^{(0)}(s)$ in (6.15) demonstrates that the contribution of the unitarity cut at $\sqrt{s} < m_N - m_K$ in (6.15) is effectively absorbed in the subtraction coefficients $c_{\bar{K}N}^{(I,k)}$ of (6.10). Similarly the subtraction coefficients $c_{\bar{K}N}^{(I,k)}$ in (6.13) represent the contribution to $T_{\bar{K}N}^{(I)}(s)$ from the inelastic $\bar{K}N$ scattering process. Thus, both model amplitudes $T_{\bar{K}N}^{(I)}(s)$ and $T_{\bar{K}N}^{(I)}(s)$ represent the exact amplitude $T_{\bar{K}N}^{(I)}(s)$ within their validity domains and therefore approximate crossing symmetry

$$\begin{aligned} \Delta T_{\bar{K}N}^{(0)}(s) &\simeq -\frac{1}{2} \Delta T_{\bar{K}N}^{(0)}(2s_0 - s) + \frac{3}{2} \Delta T_{\bar{K}N}^{(1)}(2s_0 - s), \\ \Delta T_{\bar{K}N}^{(1)}(s) &\simeq +\frac{1}{2} \Delta T_{\bar{K}N}^{(0)}(2s_0 - s) + \frac{1}{2} \Delta T_{\bar{K}N}^{(1)}(2s_0 - s), \end{aligned} \quad (6.16)$$

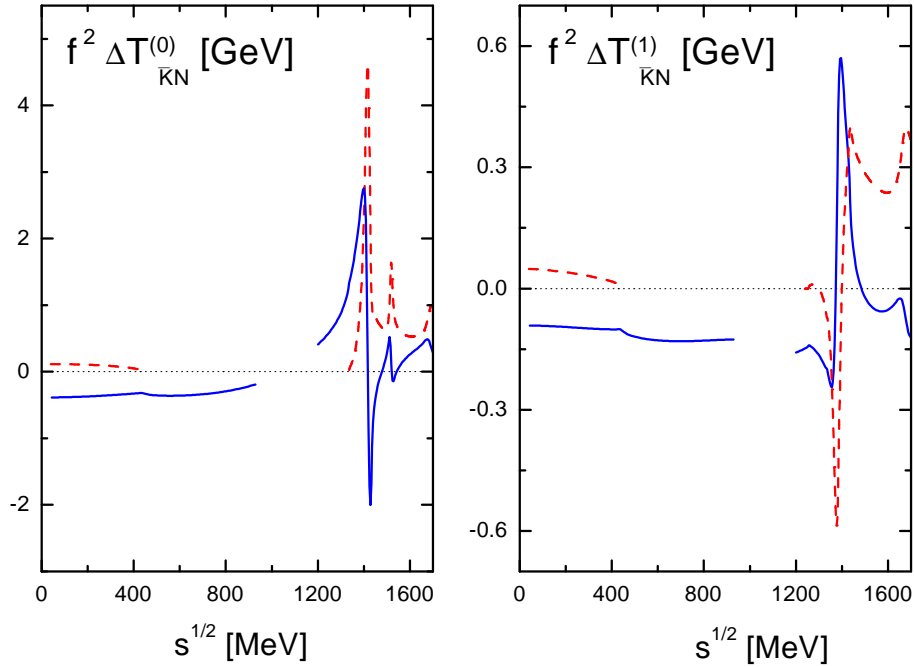


Figure 6.7: Approximate crossing symmetry of the pole subtracted kaon-nucleon forward scattering amplitudes. The lines in the left hand parts of the figures result from the KN amplitudes. The lines in the right hand side of the figures give the $\bar{K}N$ amplitudes.

is expected close to the optimal matching point $s_0 = m_N^2 + m_K^2$ only. In Fig. 6.7 we confront the pole-subtracted $\Delta T_{KN}^{(I)}$ and $\Delta T_{\bar{K}N}^{(I)}$ amplitudes with the expected approximate crossing identities (6.16). Since the optimal matching point $s_0 = m_N^2 + m_K^2 \simeq (1068)^2 \text{ MeV}^2$ is slightly below the respective validity range of the original amplitudes, one may use the reconstructed amplitudes of (6.10) and (6.13) shown in Fig. 6.6. This is justified, because the reconstructed amplitudes are based on the imaginary parts of the amplitude which have support within the validity domain of our theory only. Fig. 6.7 indeed confirms that the kaon-nucleon scattering amplitudes are approximately crossing symmetric. Close to the the point $s \simeq m_N^2 + m_K^2$ the KN and $\bar{K}N$ amplitudes match. Hence, the subthreshold antikaon-nucleon scattering amplitudes are determined rather reliably and well suited for an application to the nuclear antikaon dynamics.

6.5 Antikaons and hyperon resonances in nuclear matter

The result section is closed with a presentation of antikaon and hyperon resonance properties as they arise in the self consistent many-body approach developed in chapter 5. A resonance propagator may be identified with the appropriate antikaon-nucleon scattering amplitude of a given partial wave. In a self consistent scheme the in-medium scattering process is intimately related to the antikaon spectral function. According to (5.29) once the self consistent in-medium scattering process is established the antikaon self energy follows upon a proper Fermi averaging

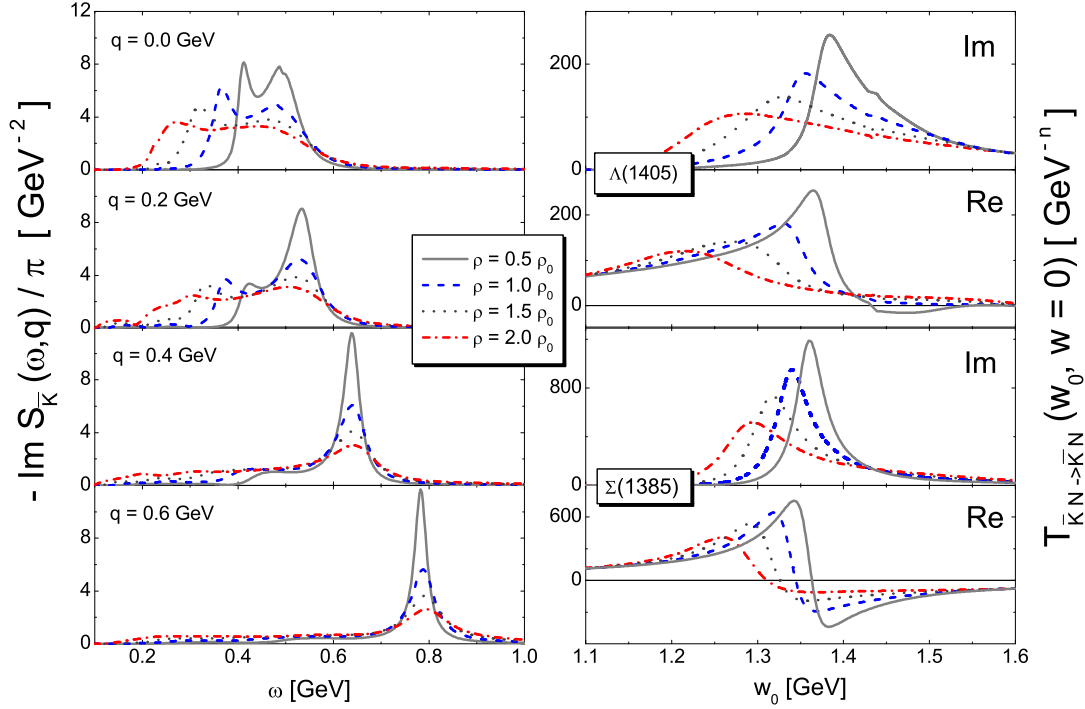


Figure 6.8: The antikaon spectral function is shown in the left hand panel as a function of the antikaon energy ω , the momentum \vec{q} and the nuclear density with $\rho_0 = 0.17 \text{ fm}^{-3}$. The right hand panel illustrates the in-medium modification of the $\Lambda(1405)$ and $\Sigma(1385)$ hyperon resonances. It is plotted the real and imaginary parts of the antikaon-nucleon scattering amplitudes in the appropriate channels. The hyperon energy and momentum are w_0 and $\vec{w} = 0$ respectively.

of the in-medium scattering amplitudes (5.29). Therefore the pertinent structures in the in-medium amplitudes already tell the characteristic features expected in the antikaon spectral function. Most important are the s-wave $\Lambda(1405)$ and the p-wave $\Sigma(1385)$ resonances. Of central importance for the derivation of a realistic antikaon spectral function are the subthreshold $\bar{K}N$ scattering amplitudes derived in the previous sections. Since the antikaon spectral function tests the $\bar{K}N$ amplitudes at subthreshold energies where they are not directly determined by empirical data it is crucial to take $\bar{K}N$ amplitudes as input for the many-body calculation which are consistent with constraints set by causality, chiral symmetry and crossing symmetry. In this work the effect of nuclear binding and short range correlation is not yet studied. The impact of the latter effects on the antikaon propagation properties are generally found to be of moderate importance at nuclear saturation density [40, 44, 43].

In Fig. 6.8 results for the spectral functions are shown at various isospin symmetric nuclear matter densities. They are based on the scattering amplitudes obtained in the previous sections. The antikaon spectral function exhibits a rich structure with a pronounced dependence on the antikaon three-momentum. That reflects the presence of hyperon resonance states in the $\bar{K}N$

amplitudes. Typically the peaks seen are quite broad and not always of quasi-particle type. For the hyperon resonances we predict attractive mass shifts and a considerable broadening with increasing density. At nuclear saturation density the attractive mass shifts for the $\Lambda(1405)$ and $\Sigma(1385)$ are about 60 MeV for both states. The resonance widths increase to about 120 MeV and 70 MeV respectively. Further results for the hyperon ground states and the $\Lambda(1520)$ resonance are reported in [98]. It is assured that the sum rule

$$-\int \frac{d\omega}{\pi} \omega \Im S_{\bar{K}}(\omega, \vec{q}) = 1, \quad (6.17)$$

is satisfied to good accuracy. Any violation of that sum rule (6.17) would indicate that the microscopic theory is in conflict with constraints set by causality. The strong in-medium modifications found for the hyperon resonance states have a simple physical interpretation. The latter is determined by the hyperon-resonance nucleon interaction. The self consistent approach includes in particular the t-channel antikaon exchange contribution, which is expected to dominate that interaction in particular when the effective antikaon mass is lowered by the nuclear environment. A dramatic in-medium modification of the antikaon spectral function, then necessarily leads to strong effects also for the hyperon states.

It is emphasized that here the in-medium effects for the $\Lambda(1405)$ are reported to be significantly stronger as compared to previous works [41, 42, 43]. In the original work [41] it was found that a self consistent evaluation, based on s-wave interactions only, that were adjusted to reproduce the amplitudes of [65], lead to almost zero mass shift of the $\Lambda(1405)$ at nuclear saturation density. The large repulsive mass shift [39, 40] predicted by the Pauli blocking effect (see (5.3)) was compensated by the attractive mass shift implied by a decreased effective antikaon mass. It is reassuring that our present scheme confirms that finding. At nuclear saturation density the in-medium change of the antikaon-nucleon loop function is largely dominated by the last two terms in (5.26). If higher partial wave contributions are switched off the $\Lambda(1405)$ resonance does not experience any significant mass shift at nuclear saturation density, merely the width increases somewhat as was observed also in [41, 42, 43].

In [42] this result is confirmed qualitatively by a calculation applying the amplitudes of [66]. The quantitative comparison of our original calculation [41] and also [98], important for the description of kaonic atoms [45, 43], is hampered by the facts that first the subthreshold amplitudes of [65, 97] and [66] differ significantly and second the computation in [42] relies on an approximation that amounts to neglecting the strong momentum dependence of the antikaon self energy (see discussion in chapter 5.2). We refrain here from a detailed comparison with the results of Tolos et al. [44]. Their many-body computation includes higher partial wave contributions. However, the applied meson exchange model [76] was confronted so far with total cross sections data only. Thus, it remains unclear whether it describes the dynamics of higher partial waves correctly.

The non-trivial dynamics implied by the presence of the hyperon resonances reflects itself in a complicated behavior of the antikaon self energy, $\Pi_{\bar{K}}(\omega, \vec{q}; \rho)$. This is illustrated by the antikaon nuclear optical potential $V_{\text{opt.}}(\vec{q}; \rho)$, defined by

$$2E_K(\vec{q})V_{\text{opt.}}(\vec{q}; \rho) = \Pi_{\bar{K}}(\omega = E_K(\vec{q}), \vec{q}; \rho), \quad E_K(\vec{q}) = \sqrt{m_K^2 + \vec{q}^2}. \quad (6.18)$$

In Fig. 6.9 the result for the optical potential is presented as a function of the antikaon momentum \vec{q} and the nuclear matter density. It is pointed out that the real part of the optical potential exhibits rather moderate attraction of about 20 MeV at nuclear saturation density and

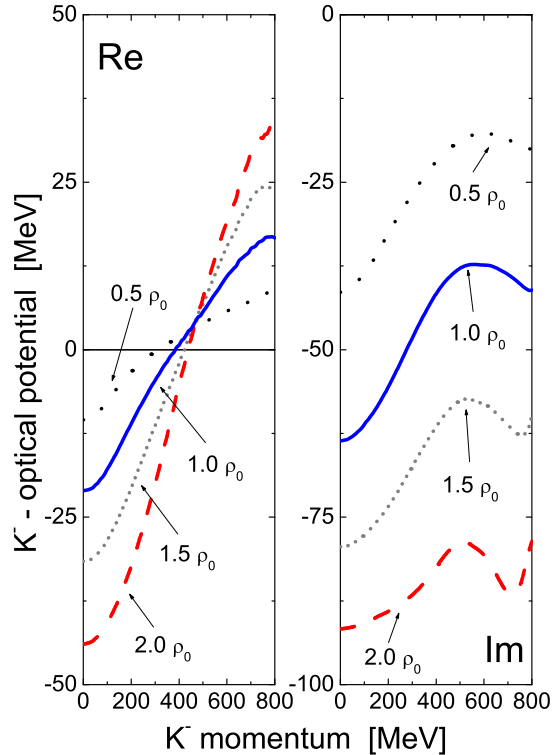


Figure 6.9: Antikaon optical potential $V_{\text{opt.}}(\vec{q}; \rho)$ for isospin symmetric nuclear matter densities. Results are shown for $0.5 \rho_0$, $1.0 \rho_0$, $1.5 \rho_0$ and $2.0 \rho_0$ where $\rho_0 = 0.17 \text{ fm}^{-3}$.

$\vec{q} = 0 \text{ MeV}$. The attraction is further diminished and even turns into repulsion as the antikaon momentum increases. On the other hand we find a rather strong absorptive part of the optical potential. This agrees qualitatively with our previous work that was based on self consistent s-wave dynamics [45] but is in striking disagreement with mean field calculations [214] that predict considerable more attraction in the antikaon optical potential. The large attraction in the antikaon spectral function of Fig. 6.8 is consistent with the moderate attraction in the optical potential of Fig. 6.9. It merely reflects the strong energy dependence of the kaon self energy induced by the $\Lambda(1405)$ and $\Sigma(1385)$ resonances. Such important energy variations are missed in a mean field approach. Hence, a proper treatment of the pertinent many-body effects is required.

Before analyzing the results in more detail it is useful to comment on the claim that the in-medium modification of the $\pi\Lambda$ and $\pi\Sigma$ channels, not considered in this work, have an important effect on the antikaon spectral function [66]. Clearly such effects probe the reaction amplitudes $\bar{K}N \rightarrow \pi\Lambda, \pi\Sigma$ at subthreshold energies. This was illustrated explicitly in chapter 5.2. Since subthreshold amplitudes are constrained by the data set only rather indirectly via crossing symmetry and analyticity it is not surprising that the more recent work by Cieply et al. [43] does not confirm that claim. The conflicting results reflect the different amplitudes those computation are based on. On naive grounds we would favor the results of Cieply et al., since we argued consistently throughout this work that subthreshold amplitudes should match

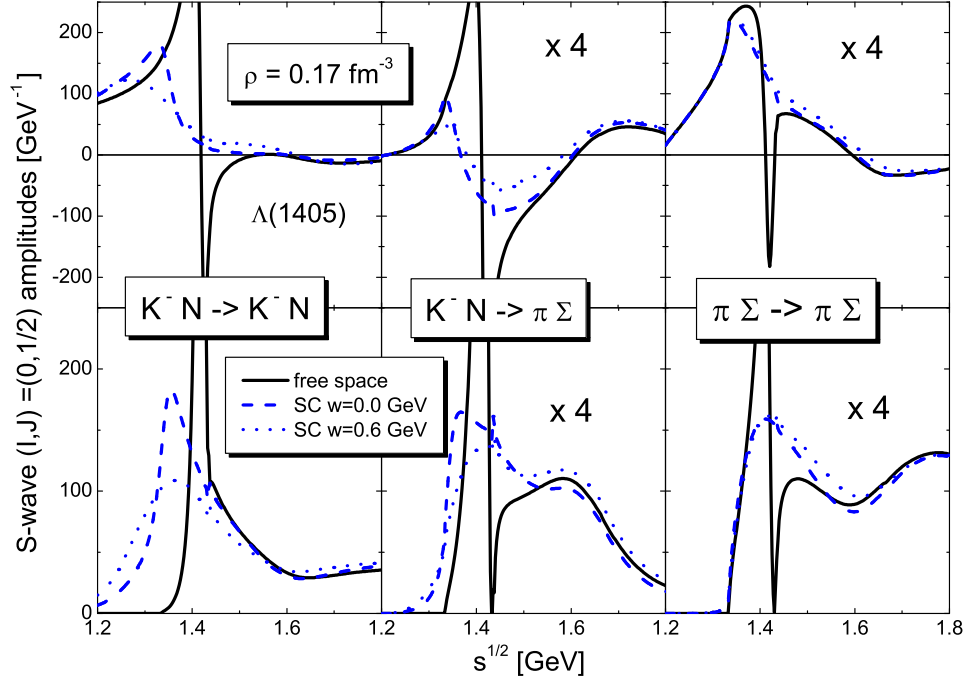


Figure 6.10: S-wave reaction amplitudes in the isospin zero channel for isospin symmetric nuclear matter $\rho = 0.17 \text{ fm}^{-3}$. The $J = 1/2$ amplitudes are the result of a self consistent calculation. The three momentum \vec{w} denotes the sum of initial three momenta defined in the rest frame of nuclear matter.

the perturbative amplitudes as they arise in χ PT, and therefore we do not see much room for significant effects implied by the pion dressing. An indication that this is indeed the case follows from the form of the in-medium reaction amplitudes $\bar{K}N \rightarrow \pi\Sigma$ as shown in Fig. 6.10 and Fig. 6.11. The dominant s-wave $I = 0$ amplitudes are plotted in Fig. 6.10 at isospin symmetric nuclear saturation density. The reaction amplitude $\bar{K}N \rightarrow \pi\Sigma$ is suppressed by a factor of 4 as compared to the diagonal amplitude $\bar{K}N \rightarrow \bar{K}N$. Therefore any additional in-medium change of the $\pi\Sigma \rightarrow \pi\Sigma$ amplitude that is induced by an in-medium pion spectral function, manifests itself only weakly in the diagonal amplitude $\bar{K}N \rightarrow \bar{K}N$. A larger ratio of $\bar{K}N \rightarrow \pi\Sigma$ to $\bar{K}N \rightarrow \bar{K}N$ amplitudes is found for the isospin one p-wave amplitudes that probe the $\Sigma(1385)$ resonance. This is illustrated in Fig. 6.11 where the various amplitudes are shown at isospin symmetric nuclear matter. Notwithstanding a detailed investigating of the effect of the pion dressing is eventually desirable also in the present scheme.

In Fig. 6.12 the antikaon spectral function evaluated at symmetric nuclear densities ρ_0 and $2\rho_0$ according to various approximation strategies is shown. In the first and third row the antikaon self energy is computed in terms of the free-space scattering amplitudes only. Here the first row gives the result with only s-wave contributions and the third row includes all s-, p- and d-wave contributions established in this work. The second and fourth row give results obtained in the self consistent approach developed in chapter 5 where the full result of the last

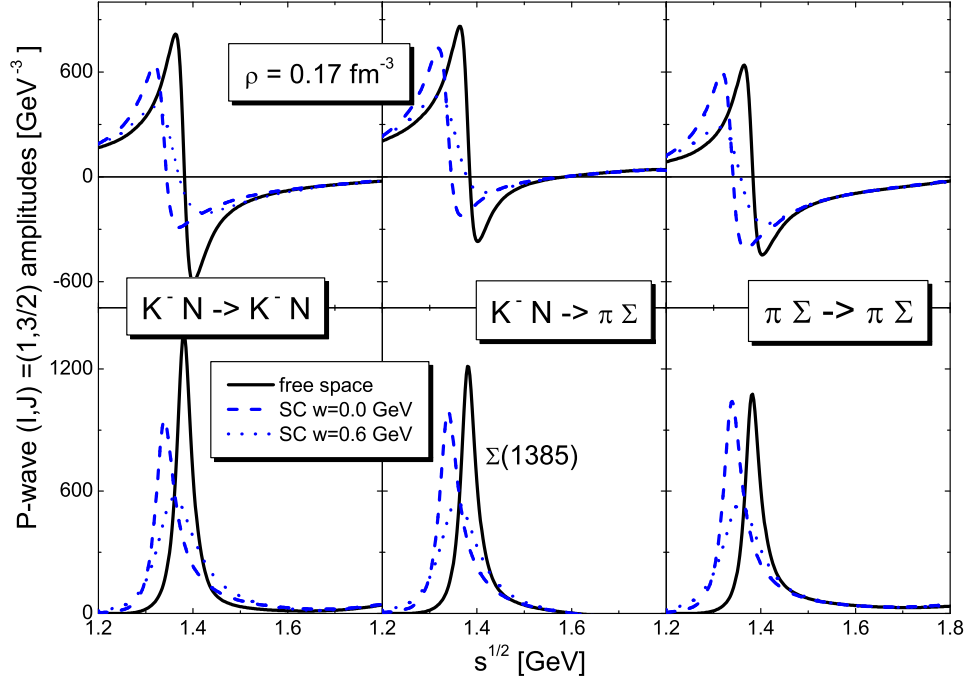


Figure 6.11: P-wave reaction amplitudes in the isospin one channel for isospin symmetric nuclear matter $\rho = 0.17 \text{ fm}^{-3}$. The $J = 3/2$ amplitudes are the result of a self consistent calculation. The three momentum \vec{w} denotes the sum of initial three momenta defined in the rest frame of nuclear matter.

row includes all partial waves and the results in the second row follow with s-wave contributions only. In all cases a self consistent evaluation of the spectral function leads to dramatic changes in the spectral function as compared to a calculation which is based on the free-space scattering amplitudes only. Moreover, as emphasized in the discussion of the $\Lambda(1405)$ resonance properties, the effects of higher partial waves are not negligible. This was anticipated in [67,45]. As is evident upon comparing the first and third rows of Fig. 6.12 the p- and d-wave contributions add quite significant attraction for small energies and large momenta. At twice nuclear saturation density we find most striking the considerable support of the spectral function at small energies. That reflects in part the coupling of the antikaon to the $\Lambda(1115)$ and $\Sigma(1185)$ nucleon-hole states. The latter explains the peak structure of the antikaon spectral functions at $\omega \simeq 250 \text{ MeV}$ seen in the ' $T\rho$ ' approximation. Upon inspecting the Lindhard function of these contributions for free-space $\Lambda(1115)$ and $\Sigma(1185)$ states [35] one finds that the antikaon spectral function should be non-zero for

$$\omega > \sqrt{m_Y^2 + (|\vec{q}| - k_F)^2} - \sqrt{m_N^2 + k_F^2}. \quad (6.19)$$

The strength of the spectral function is largest at $|\vec{q}| \sim k_F$ because of the kinematical consideration (6.19). Self consistency smears out that structure because the contribution from the dominant $\Sigma(1185)$ state receives a finite decay width [98].

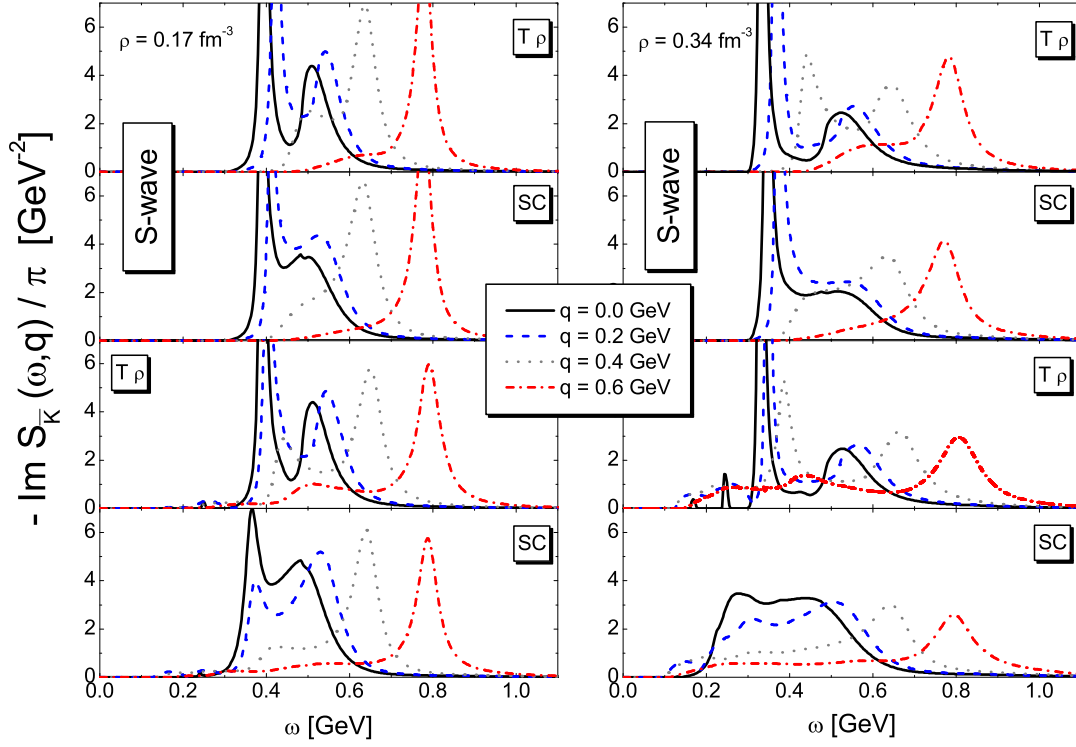


Figure 6.12: Antikaon spectral function as a function of antikaon energy ω and momentum \vec{q} . The labels 'T ρ ' and 'SC' refer to calculations obtained in terms of free-space and in-medium $\bar{K}N$ amplitudes respectively (see (5.13)). The first two rows give the results with only s-wave interactions and the last two rows with all s-, p- and d-wave contributions.

In Fig. 6.13 we present the results for the propagation properties of the $\Lambda(1405)$ and $\Sigma(1385)$ resonances as they move with finite three momentum \vec{w} in isospin symmetric nuclear matter. The peak positions in the imaginary parts of the amplitudes follow in general the naive expectation $\sqrt{(m_Y^*)^2 + \vec{w}^2}$ with the hyperon effective mass m_Y^* defined at $\vec{w} = 0$. However, we observe a systematic increase of the decay widths as \vec{w} increases. This is easily understood since the effective in-medium $Y^*N \rightarrow Y^*N$ amplitude which is responsible for the broadening allows for additional inelasticity as the hyperon momentum \vec{w} increases. An interesting phenomenon illustrated in Fig. 6.13 is the in-medium induced mixing of partial wave amplitudes with different quantum numbers J^P . At vanishing three momentum of the meson-baryon state $\vec{w} = 0$, all partial wave amplitudes decouple. In this case the system enjoys a three-dimensional rotational symmetry since there is no three-vector available to select a particular direction. However, once the meson-baryon pair is moving relative to the nuclear matter bulk with $\vec{w} \neq 0$ we find two separate channels for a given isospin only. The system is invariant under a subgroup of rotations only, namely those for which the rotational vector is aligned with the hyperon momentum \vec{w} . The three-dimensional rotational symmetry is reduced and therefore the total angular momentum J

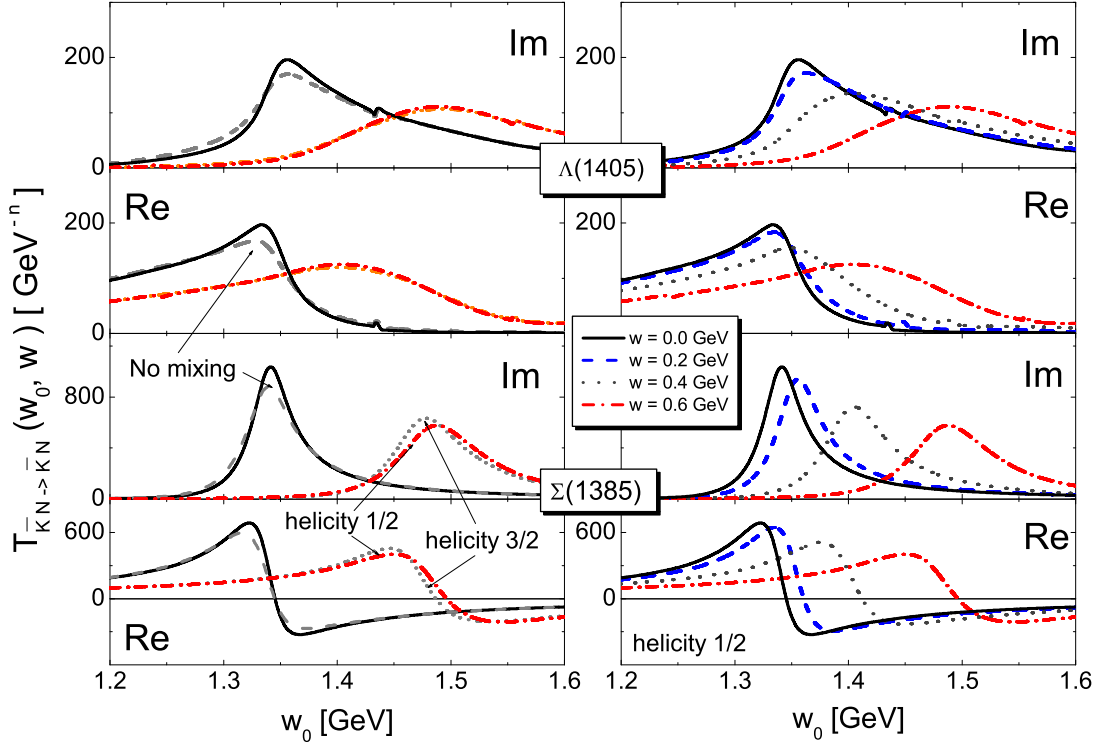


Figure 6.13: Hyperon resonance spectral functions for the $\Lambda(1405)$ and $\Sigma(1385)$ as a function of the hyperon energy w_0 and momentum \vec{w} for isospin symmetric nuclear matter. It is shown the s-wave $I=0$ and p-wave $I=1$ partial wave amplitudes at $\rho_n + \rho_p = 0.17 \text{ fm}^{-3}$. The left hand panels demonstrate the small effect of switching off the mixing of the partial wave amplitudes (dashed versus full lines) and the splitting of the 4 spin $3/2$ states into helicity one half and three half modes (dotted versus dashed-dotted lines).

is no longer a conserved quantum number. However, the total angular momentum projection onto the \vec{w} direction remains a conserved quantum number. The latter defines the helicity of a hypothetical s-channel particle exchange and therefore the in-medium scattering amplitudes decouple into an infinite tower of helicity amplitudes. Each helicity amplitude probes a well defined infinite set of partial wave amplitudes. For instance, in the P-space, all considered partial wave amplitudes S_{I1} , P_{I1} , P_{I3} and D_{I3} couple for given isospin channel I . Since the angular momentum projection of the S_{I1} channel onto \vec{w} is necessarily one half, the P-space corresponds to the first term with helicity one half. Note that reflection symmetry implies that only the absolute value of the helicity matters here. It is evident that all partial wave amplitudes contribute to this channel simply because any state with a given angular momentum L has a component where $\vec{L} \cdot \vec{w}$ vanishes and therefore the helicity is carried by the nucleon spin. In the second channel, our Q-space, only the partial wave amplitudes P_{03} and D_{03} couple. This channel corresponds to the helicity three half term. In a computation that considered all partial

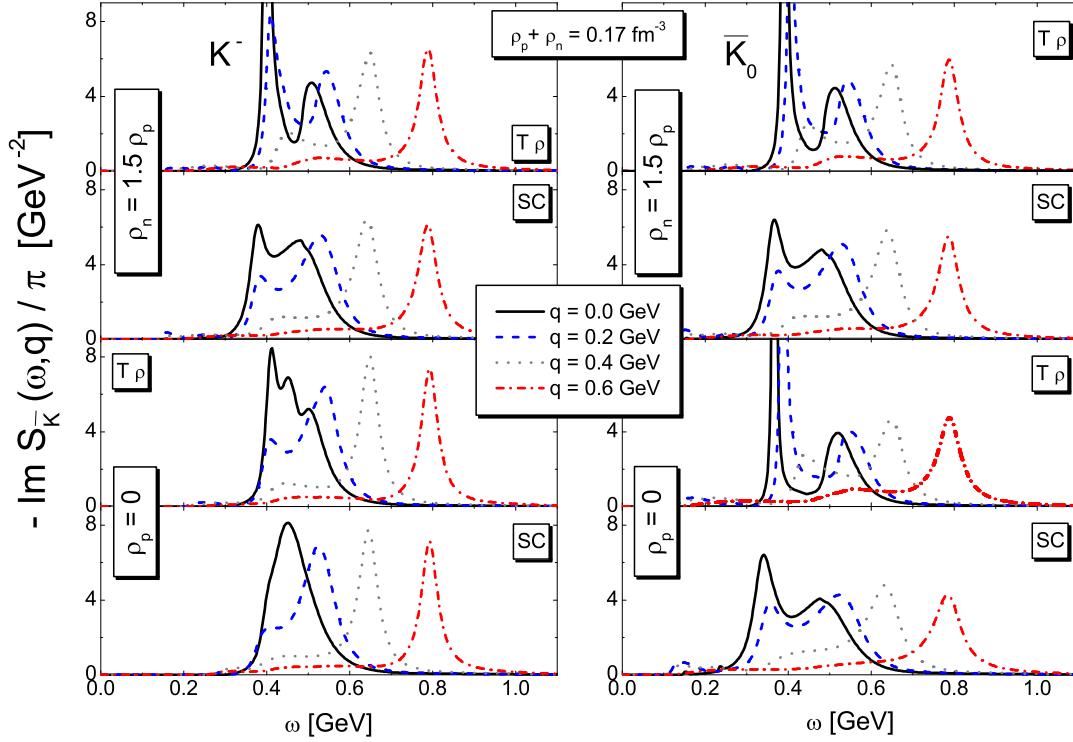


Figure 6.14: Antikaon spectral functions as a function of antikaon energy ω and momentum q in asymmetric nuclear matter with $\rho_p + \rho_n = 0.17 \text{ fm}^{-3}$. The labels 'T ρ ' and 'SC' refer to calculations obtained in terms of free-space and self consistent in-medium $\bar{K}N$ amplitudes respectively (see (5.13)). The first column gives the result for K^- , the second for the \bar{K}_0 at $\rho_n = 1.5 \rho_p$ and $\rho_p = 0$.

waves the helicity three half term would require all partial wave amplitudes except the S_{11} and P_{11} waves with $J = 1/2$. The fact that the $J = 3/2$ amplitudes P_{13} and D_{13} affect both the P- and Q-space, or the helicity one half and helicity three half terms, is not surprising, because for those states one would expect the nuclear medium to lift the degeneracy of the four spin modes. This is completely analogous to the longitudinal and transverse modes of vector mesons, which bifurcate in nuclear matter.

The splitting of the four $\Sigma(1385)$ modes is demonstrated in the left hand panel of Fig. 6.13. The helicity one and three half modes are shifted by about 5 MeV for $\vec{w} = 600$ MeV. This is a small effect and therefore it is justified to neglect the coupling of the partial waves for that density to good accuracy. Indeed a run where all off diagonal loop functions that couple waves of different angular momentum or parity are set to zero gives results that are almost indistinguishable to those obtained in the full scheme. This is demonstrated by the dashed lines in the left hand panel of Fig. 6.13. At $\vec{w} = 0$ the results of the two computations, dashed and solid lines are quite close. This finding has a simple interpretation. One expects

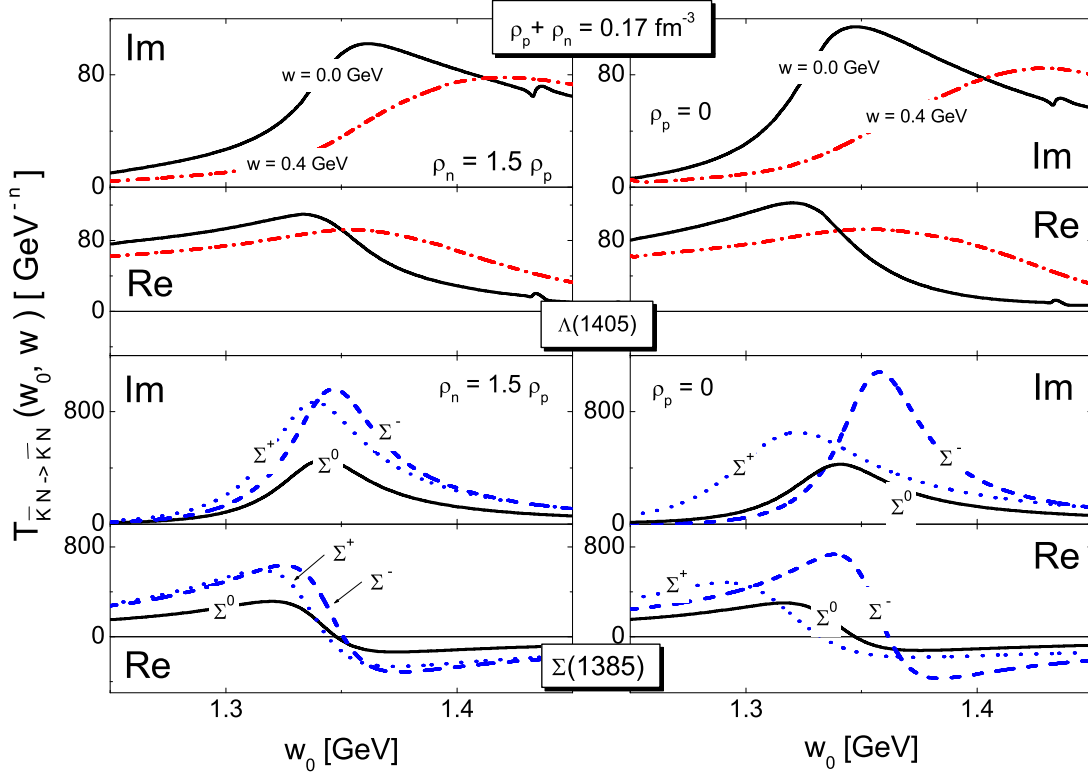


Figure 6.15: $\Lambda(1405)$ and $\Sigma(1385)$ hyperon resonance propagators as a function of hyperon energy w_0 and momentum \vec{w} for asymmetric nuclear matter. It is shown the s-wave $K^-p \rightarrow K^-p$ (for $\vec{w} = 0$ MeV and $\vec{w} = 400$ MeV) and p-wave $\bar{K}^0n \rightarrow \bar{K}^0n$, $\bar{K}^0p \rightarrow \bar{K}^0p$ and $K^-n \rightarrow K^-n$ reaction amplitudes (for $\vec{w} = 0$ MeV) at $\rho_n + \rho_p = 0.17 \text{ fm}^{-3}$.

sizeable effects from the in-medium mixing of the partial-wave amplitudes only if two partial wave amplitudes that mix show both significant strength at a given energy w_0 . This is not the case here. The dominant partial waves S_{01} and P_{13} decouple because they carry different total isospin. Therefore it is natural to obtain small mixing effects. This may, however, change once isospin asymmetric matter where the two isospin channels couple is considered.

A presentation of results obtained for asymmetric nuclear matter follows. Two cases are considered here both with $\rho_n + \rho_p = 0.17 \text{ fm}^{-3}$. In Fig. 6.14 results for $\rho_n = 1.5 \rho_p$, which corresponds to the condition met in the interior of lead, and for $\rho_p = 0$, which describes neutron matter, are shown. The asymmetry breaks up the isospin doublet (K^-, \bar{K}_0) leading to distinct spectral functions for the charged and neutral antikaons. In all cases considered a significant effect from the self consistency is found at small antikaon momenta. This is illustrated by comparing the entries of Fig. 6.14 labelled with 'T ρ ' and 'SC'. Whereas the effect of the asymmetry is surprisingly small for the lead scenario, the spectral functions of the charged and neutral antikaons differ strongly in neutron matter with $\rho_p = 0$. In Fig. 6.15 the corresponding

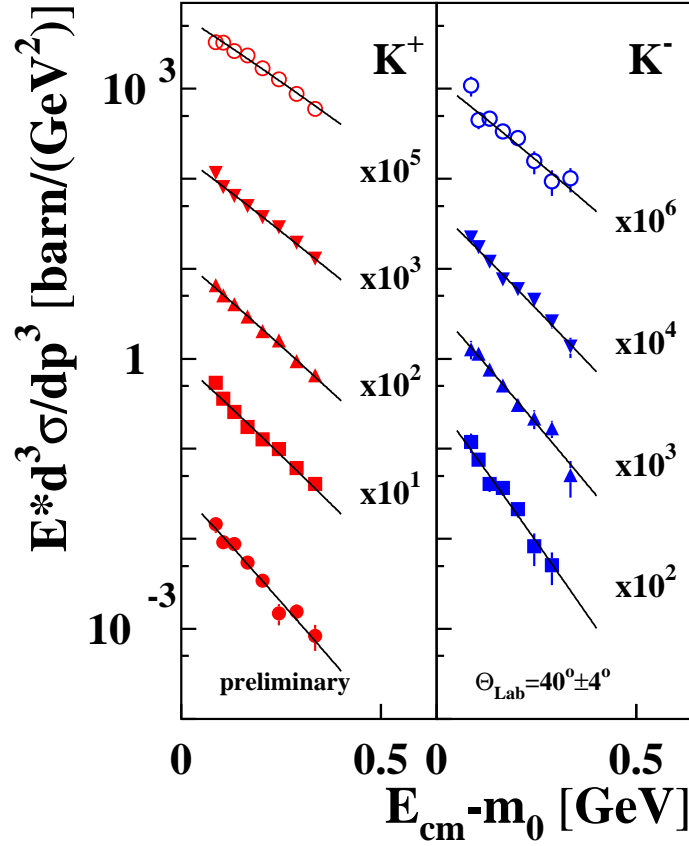


Figure 6.16: Invariant cross sections for K^+ and K^- in Au + Au collisions at $E_{\text{beam}} = 1.5$ AGeV for five centrality classes [215]. The open circles depict the most central data with decreasing centrality from the top to the bottom of the figure. The solid lines are the result of a fit with a Boltzmann distribution.

properties of the hyperon resonances are shown. Again, like one observed for the isospin doublet (K^- , \bar{K}^0) the isospin asymmetry of the matter breaks up the isospin triplet state $\Sigma(1385)$ introducing a medium-induced splitting pattern. The $\Lambda(1405)$ resonance is presented in terms of the in-medium $K^-p \rightarrow K^-p$ s-wave amplitude, the neutral and charged $\Sigma(1385)$ states by p-wave amplitudes $\bar{K}^0n \rightarrow \bar{K}^0n$, $\bar{K}^0p \rightarrow \bar{K}^0p$ and $K^-n \rightarrow K^-n$. In free space the latter amplitudes are determined by the isospin one amplitude in case of the charged hyperon states but by the mean of the two isospin amplitudes in case of the neutral hyperon state. Thus, the isospin one component, the $\Sigma(1385)$ couples to in free space, is smaller by a factor of two for the neutral amplitude $\bar{K}^0n \rightarrow \bar{K}^0n$ as compared to the amplitudes describing the charged hyperon states. This reflects itself in amplitudes for the $\Sigma^0(1385)$ in Fig. 6.15 that are typically smaller by a factor two as compared to the amplitudes of the $\Sigma^\pm(1385)$. Whereas the $\Lambda(1405)$ resonance is not affected much by the asymmetry, the splitting of the three $\Sigma(1385)$ states shows a strong dependence on the asymmetry. For neutron matter with $\rho_n = 0.17 \text{ fm}^{-3}$ we find a mass difference of about 30 MeV for the charged states.

The result chapter is closed with a brief discussion of the results presented here as they may

be relevant for antikaon production in heavy ion reactions at subthreshold energies. Strictly speaking the results do not apply for the conditions present inside a fireball created after the collision of two heavy nuclei. The quantitative description of such a process requires a transport theoretical description capable to model physics of finite systems off equilibrium. The latter requires as input hadronic cross sections, or more precisely hadronic transition rates, that are taken from experiment or theory. Calculations performed in the idealized world of infinite but hot and dense nuclear matter are nevertheless a useful tool to discuss and understand effects on a qualitative level. In certain channels transition rates that are typically derived from free-space cross sections may be significantly changed in a hot and dense nuclear environment. Of course one may object to the application of our calculations to the heavy ion scenario because they are performed at zero temperature. However, since the dominant effect found in this work is quite insensitive to the Pauli blocking effect, it is natural to anticipate that the inclusion of small temperatures of up to $T \simeq 80$ MeV typical for SIS energies at GSI, does not affect the results significantly. This argument relies on the naive picture that temperature effects may be interpreted as an effective reduction of the Pauli blocking effect.

One may argue that if the antikaon spectral function evaluated for infinite hot nuclear matter shows considerable strength at energies smaller than the free kaon mass, it is energetically easier to produce antikaons in a fireball than if the effective antikaon mass distribution was not reduced. In this case one may expect to see some type of enhancement of antikaon production rates. It is a challenge to verify the above simple but physical interpretation of the observed kaon and antikaon yields in terms of transport model simulations. In Fig. 6.16 preliminary results of the KaoS collaboration [215] for the kaon and antikaon transverse spectra for Au+Au at $E_{\text{beam}}=1.5$ AGeV are shown. The spectra shown are typical for most observed particle multiplicities. They are fitted well by a simple Boltzmann distribution

$$\sim \exp(- (E_{cm} - m_K)/T), \quad (6.20)$$

in terms of an effective temperature parameter T . The effective temperatures in Fig. 6.16 of the K^+ are about 20 MeV larger than the ones for the K^- . It is important to realize that the Boltzmann type behavior of the spectra does not imply that the kaons and antikaons are necessarily equilibrated. Estimates for the kaon mean free path, which are based on the empirical kaon-nucleon cross section, suggest that the kaons do not have a chance to reach equilibrium conditions in a typical heavy ion collision at SIS energies. That may be different for antikaons as will be discussed in some detail below.

Since at subthreshold energies the mean energy available by one nucleon is not sufficient to produce an antikaon in an elementary nucleon-nucleon collision by definition, one visualizes the production process to occur in a series of successive reactions [216, 217, 218, 219],

$$N N \rightarrow N \Delta \rightarrow N N \pi, \quad N N \rightarrow N Y K, \quad \pi Y \rightarrow \bar{K} N, \quad (6.21)$$

where $Y = \Lambda(1115), \Sigma(1185)$. Here we do not intend to provide a complete listing of reactions included in transport model simulations rather we would like to discuss the main effects qualitatively. A heavy ion reaction produces, besides photons and leptons, dominantly pions, the lightest hadronic degrees of freedom available. For SIS energies at GSI this production is thought to be driven by the isobar production process $N N \rightarrow N \Delta \rightarrow N N \pi$. The kaon production is determined by the primary $N N \rightarrow N Y K$ reaction far above threshold but by the secondary reaction $\pi N \rightarrow K Y$ at subthreshold energies. Because of strangeness conservation the antikaon

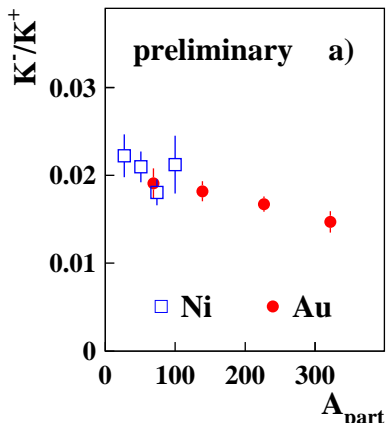


Figure 6.17: It is shown the ratio of the K^-/K^+ yields in the Ni + Ni and Au + Au collisions at $E_{\text{beam}} = 1.5$ AGeV as a function of the number of nucleons A_{part} , that participate in the reaction [215]. The data are taken at $\theta_{\text{lab}} = 40^\circ$.

production threshold in nucleon-nucleon collisions is much larger than the threshold of kaon production. The former is determined by the $NN \rightarrow NNK\bar{K}$ reaction leading to

$$\sqrt{s_{\text{thres}}^{(\bar{K})}} - \sqrt{s_{\text{thres}}^{(K)}} = m_K + m_N - m_\Lambda \simeq 320\text{MeV}. \quad (6.22)$$

It is therefore plausible that antikaons are dominantly produced in the secondary $\pi Y \rightarrow \bar{K}N$ reaction in particular at subthreshold energies. Consequently these reactions received considerable attention in the study of subthreshold antikaon production [216, 217, 28]. A clear hint that the antikaon production in nucleus-nucleus collisions is indeed driven by the secondary $\pi Y \rightarrow \bar{K}N$ reaction follows from the centrality dependence of the measured ratio K^-/K^+ [215] as shown in Fig. 6.17. The number of nucleons, A_{part} that participate in a Ni on Ni or Au on Au collision is a measure for the inverse size of the impact parameter. Since both, the kaon and antikaon yields depend strongly on the impact parameter [220] the empirical observation that the ratio of the yields is almost insensitive to it signals that the production mechanisms of the kaons and antikaons must be strongly related.

The importance of the $\pi Y \rightarrow \bar{K}N$ reactions suggests that it may be useful to investigate the latter within the χ -BS(3) scheme. In Fig. 6.18 the isospin averaged cross sections of the channels $\bar{K}N$, $\pi\Sigma$ and $\pi\Lambda$ as obtained in the chiral coupled channel analysis [97] are shown. The results in the first row repeat in part the content of Fig. 6.2 only that here the cross sections are confronted with typical parameterizations used in transport model calculations. The cross sections in the first column are determined by detailed balance from those of the first row. Uncertainties are present nevertheless, reflecting the large empirical uncertainties of the antikaon-nucleon cross sections close to threshold. The remaining four cross sections in Fig. 6.18 are true predictions of the χ -BS(3) approach. It should be emphasized that the results are quantitatively reliable only for $\sqrt{s} < 1600$ MeV. It is remarkable that nevertheless the cross sections agree with the parameterizations in [223] qualitatively up to much higher energies except in the $\bar{K}N \leftrightarrow \pi\Sigma$ reactions where they overshoot those parameterizations somewhat. Besides some significant deviations of our results from [222, 223] at $\sqrt{s} - \sqrt{s_{\text{th}}} < 200$ MeV, an energy range where the results are quantitatively reliable, we find interesting the sizeable cross section of about

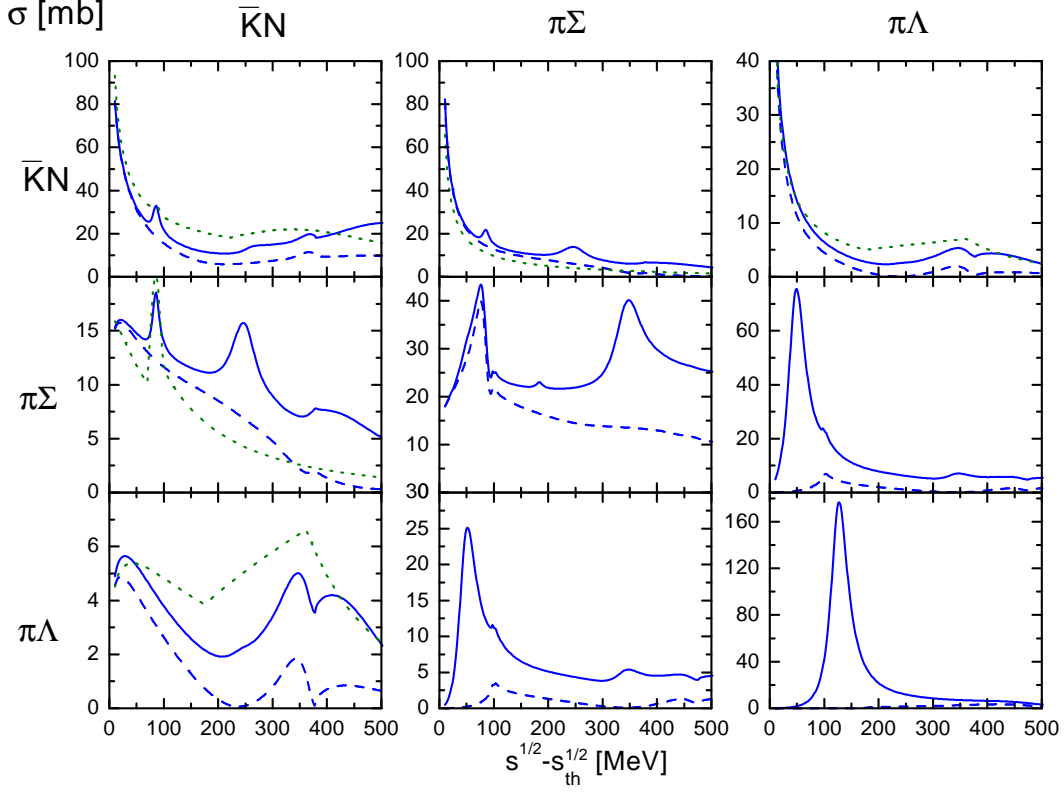


Figure 6.18: Total cross sections $\bar{K}N \rightarrow \bar{K}N$, $\bar{K}N \rightarrow \pi\Sigma$, $\bar{K}N \rightarrow \pi\Lambda$ etc relevant for subthreshold production of kaons in heavy-ion reactions. The solid and dashed lines give the results of the χ -SB(3) approach with and without p- and d-wave contributions respectively. The dotted lines correspond to the parameterizations given in [223].

30 mb for the elastic $\pi\Sigma$ scattering. As demonstrated by the dotted line in Fig. 6.18, which represent the χ -BS(3) approach with s-wave contributions only, the p- and d-wave amplitudes are of considerable importance for elastic $\pi\Sigma$ scattering. A further striking effect is seen in the elastic $\pi\Lambda$ cross section that has a maximum of about 160 mb at $\sqrt{s} \simeq 1385$ MeV. That reflects a strong coupling of the $\pi\Lambda$ state to the p-wave $\Sigma(1385)$ resonance. This resonance cannot be seen in the $\bar{K}N$ reactions because it is below the antikaon nucleon threshold. It is evident that the large cross sections found for the $\pi Y \rightarrow \pi Y$ reactions will help significantly to drive hyperons produced in nucleus-nucleus collisions towards a statistical phase space distribution. As it will be argued in detail below the presence of the $\Sigma(1385)$ resonance will play a crucial role for antikaon production in nucleus-nucleus collisions at subthreshold energies.

So far most transport model simulations of antikaon production rely on rough approximations. For instance the complicated antikaon spectral function is substituted by a quasi-particle ansatz parameterized in terms of an effective antikaon mass that drops basically linearly with the nuclear density [216,217]. Technically this is implemented by incorporating an appropriate mean field modifying the trajectories of the antikaon between collisions in the fireball. The width of the quasi particle is then modelled by including the inelastic cross sections like $\bar{K}N \rightarrow \pi Y$. For cross sections involving antikaons in initial or final states simple substitution rules like e.g.

$\sqrt{s} \rightarrow \sqrt{s} - \Delta m_{\bar{K}}$ are applied. Such computations confirm the expectation that the antikaon yield is quite sensitive to an attractive mean field of the antikaon [216, 217]. Runs where an attractive mean field and the absorption cross sections are both switched off or on are reported to be fairly close to the measured multiplicities [216, 217]. Neglecting, however the attractive mean field but including the antikaon absorption cross sections underestimates the antikaon yield up to a factor 5 [216, 217].

A more sophisticated simulation was performed by Schaffner, Effenberger and Koch [28] in which the consequences of two effects were studied. First, the effect of in-medium modifications of the $\pi Y \rightarrow \bar{K}N$ reactions was studied. And second, a momentum dependence of the antikaon potential was considered. The momentum dependence was chosen such that at moderate antikaon momenta of about 300-400 MeV the attractive mean field was basically switched off. This was motivated by microscopic many-body evaluations of the antikaon self energy which predicted that type of behavior [41]. The in-medium modification of the production cross sections $\pi Y \rightarrow \bar{K}N$ were assumed to be dominated by the Pauli blocking effect [34] that shifts the $\Lambda(1405)$ resonance from $\sqrt{s} = 1405$ MeV to larger energies, about $\sqrt{s} \simeq 1490$ MeV at nuclear saturation density. As a consequence the authors report an enhancement factor for the $\pi\Sigma \rightarrow \bar{K}N$ reaction of about 20 close to $\sqrt{s} = 1490$ MeV. Both effects, the attractive mean field and the increased $\pi Y \rightarrow \bar{K}N$ cross section gave rise to a similar effects in the antikaon yield. Together the two mechanism predict an enhancement factor of about 4 as compared to a computation that applies the empirical cross sections and discards any mean field effects. However, as was pointed out by Schaffner, Effenberger and Koch [28], once the momentum dependence of the attractive mean field was incorporated together with the fact that in their model the enhancement of the cross section disappears already at moderate temperatures $T \simeq 80$ MeV, the results are quite close to the reference calculation with no medium effects. All together the empirical antikaon yields are not described, they are underestimated by about a factor 3-4.

In a more recent work by Aichelin, Hartnack and Oeschler [218, 219] a further interesting aspect was emphasized. Since the antikaon production is driven by the $\pi Y \rightarrow \bar{K}N$ reaction the total antikaon yield should be sensitive to the kaon production mechanism. A repulsive mass shift for the kaon can therefore compensate for the effect implied by an attractive mean field for the antikaon. It is argued, however, that the computation by Aichelin and Hartnack [218] most likely overemphasizes this effect due to a too large mass shift for the kaon (about 70 MeV at $2\rho_0$ [214]). This objection is based on a recent calculation based on the kaon-nucleon s- and p-wave phase shifts [221] that demonstrates that a kaon produced with momenta of about 400 MeV at $2\rho_0$ the repulsive mass shift is only about 45 MeV, smaller than the value of 70 MeV used in [218]. The conclusions of Aichelin, Hartnack and Oeschler [218, 219] depend also sensitively on the magnitude of the attractive mean fields for the nucleons and hyperons as well as on the poorly known $N\Delta \rightarrow NYK$ reaction rates. In order to reduce such uncertainties it would be useful to describe not only total yields of kaons, antikaons and hyperons but at the same time achieve quantitative agreement with the azimuthal emission pattern [225, 226, 19]. The mean fields used in [218, 219] for the hyperons show a strong non-linear behavior in the nuclear density [214]. In particular at twice saturation density the hyperons' mean fields are zero approximatively. We would conclude from the self consistent antikaon dynamics [98], that the $\Lambda(1115)$ should experience an attractive mass shift of about 20-40 MeV at twice saturation density instead [98]. We do not find any sign of a strong non-linear behavior in density. Such a strong non-linear density behavior in the hyperon self energy may be questioned. It is a consequence of a mean field picture that relies on a scalar iso-scalar σ degree of freedom. If, on

the other hand, the physics of the nucleon self energy is driven by the many-body dynamics of pions instead as suggested in [227], a strong non-linear behavior for the Λ ground state is not expected. The non-linearities should be significantly reduced because the analogous (reducible) diagrams that drive the nuclear saturation mechanism in [227] do not exist in case of the Λ . Even for the Σ ground state, which permits the analogous reducible diagrams of [227], one would expect significantly smaller effects simply because only one of the two baryon lines is affected in strangeness zero nuclear matter. Thus, one may expect that the hyperon self energies are dominated by the antikaon t-channel exchange. The latter contribution was studied in [98] but no indication for a strong non-linear density dependence was found despite the non-trivial form of the antikaon spectral function in nuclear matter. Of course it is impossible at this stage to make rigorous estimates of the hyperon self energy at twice nuclear saturation density simply because the hyperon-nucleon interaction is at present not too well constrained by the data set [230,231]. It is interesting to observe, however, that a Brueckner-Hartree-Fock evaluation [229] based on the Nijmegen soft-core hyperon-nucleon interaction [230] suggests about 30 MeV attraction for the $\Lambda(1115)$ mean field at twice nuclear saturation density. As a consequence in nucleus-nucleus collisions the net effect of increased kaon mass and decreased hyperon mass would then tend to cancel in the total kaon yield. An investigation of further observable quantities like the azimuthal emission pattern at mid rapidity, which discriminate among the various effects, reveals that a small repulsive mean field for the kaon is favored by the data set [224, 225, 226, 19]. Aichelin, Hartnack and Oeschler [218,219] affirm that the K^-/K^+ ratio is insensitive to the details of the kaon production and therefore should be considered as a superior observable to test the antikaon dynamics. In their work [219] the possible importance of in-medium modified cross sections is studied. Within their scenario, which does not consider a momentum dependence of the antikaon mean field, they observe an enhancement of the K^-/K^+ ratio by a factor 2 if the $\pi Y \rightarrow \bar{K}N$ cross sections are enlarged by a factor three. However, the impact parameter dependence of that ratio is affected strongly by this ad-hoc procedure leading to a dependence that appears incompatible with the behavior shown in Fig. 6.17. It is argued that the antikaons are produced at a late stage of the collision even though the difference of absorption and production rates shows a clear maximum in the high density initial phase. Increasing the $\pi Y \rightarrow \bar{K}N$ cross sections only affects the antikaon absorption process at the late stage of the fireball expansion since the typical pions and hyperons do not have sufficient kinetic energy to produce antikaons anymore. This would lead to a drop of the K^-/K^+ ratio with increasing impact parameter. Moreover, their claim, that including an attractive mean field for the antikaon into the simulation does not affect the total antikaon yield, remains puzzling. This contradicts the typical enhancement factors 2-4 as were obtained in previous simulations [216,217,23,28].

The above discussion implies that it is important to obtain an improved understanding of the $\pi Y \rightarrow \bar{K}N$ cross sections as they may change in a nuclear environment [28]. In Fig. 6.19 the result of a computation based on the self consistent scheme introduced in this work are presented. In the upper panel we show the isospin averaged $\pi\Sigma \rightarrow \bar{K}N$ and $\pi\Lambda \rightarrow \bar{K}N$ cross sections where the in-medium scattering amplitudes (see e.g. Figs. 6.10,6.11) are used together with the antikaon spectral function defining the final-state phase space (see Fig. 6.8). Comparing the solid with the dashed and dotted lines one realizes a dramatic enhancement for the $\pi\Lambda$ reaction but a much more moderate enhancement for the $\pi\Sigma$ reaction. The dashed and dotted lines correspond to the situation where the sum of initial three-momenta is 0 MeV and 600 MeV respectively. To explain the source of this effect the figure shows in its lower panel the same cross sections evaluated in two different schematic ways. The dotted lines give the result

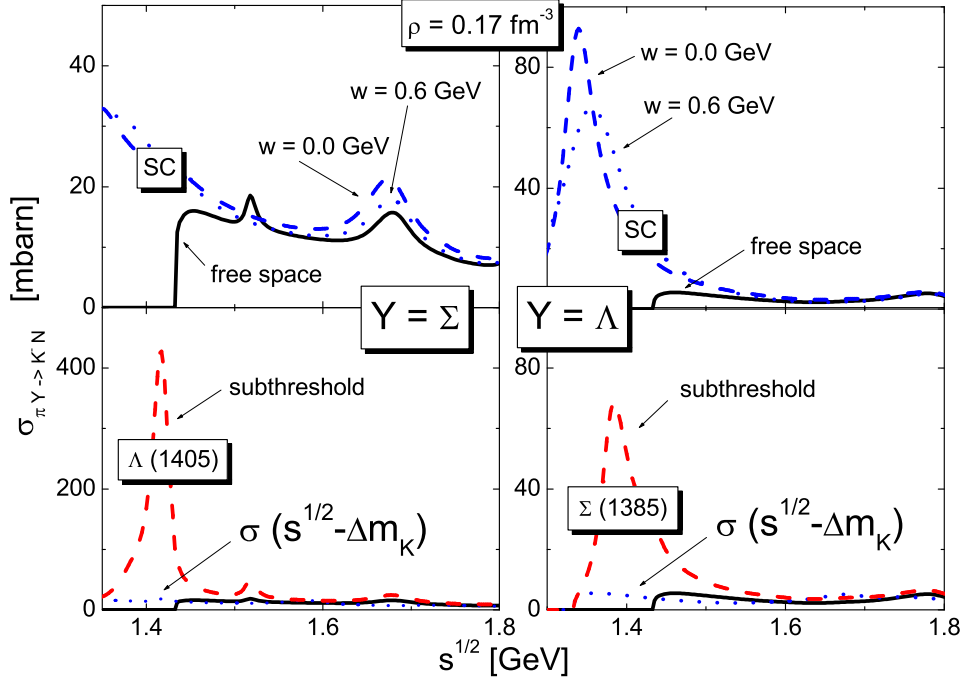


Figure 6.19: The upper panels show the pion induced cross sections of antikaons obtained in a self consistent many-body evaluation (dashed for $\vec{w} = 0$ MeV and dotted lines for $\vec{w} = 600$ MeV) at nuclear saturation density as compared to the free-space cross sections (full lines). The lower panels give the results of schematic evaluations. The dotted lines are the free-space cross section shifted in \sqrt{s} by $\Delta m_{\bar{K}} = -100$ MeV. The dashed lines follow with computations that are based on the subthreshold free-space amplitudes as predicted by the χ -BS(3) approach together with a final state phase space evaluated with a reduced kaon mass.

obtained according to the prescription $\sqrt{s} \rightarrow \sqrt{s} - \Delta m_{\bar{K}}$ as commonly applied in transport model simulations. It is used $\Delta m_{\bar{K}} = -100$ MeV typically for the amount of attraction found for the antikaon at saturation density. The cross sections remain as small as they are in free-space. A striking enhancement is shown by the dashed lines in the lower panel. Here we use the free-space scattering amplitude and evaluate the cross section with the final state phase space determined by a reduced kaon mass of 394 MeV. As a result this cross section probes the scattering amplitudes at subthreshold energies a kinematical region where they are not directly constrained by the scattering data. Since the χ -BS(3) scheme predicts considerable strength in the subthreshold amplitudes from the s-wave $\Lambda(1405)$ and p-wave $\Sigma(1385)$ resonances the former cross sections are dramatically enhanced as compared to the free-space cross sections ¹.

¹The results for the $\pi Y \rightarrow \bar{K}N$ transition rates may change somewhat once the in-medium spectral functions for the pion, nucleon and hyperons are used. One would expect that the effect of the attractive shifts in the mass distributions of the nucleons and hyperons tend to cancel in the transition rates. The inclusion of the pion spectral function will most likely broaden the $\Sigma(1385)$ resonance peak in the $\pi\Lambda \rightarrow \bar{K}N$ transition rate. This issue deserves further studies.

Comparing the lower with the upper panel demonstrates that the latter cross section, though providing a simple physical interpretation of the enhancement, do not adequately reproduce the full computation as it arises in a self consistent framework. In particular the large cross section of the $\pi\Sigma \rightarrow \bar{K}N$ reaction predicted by the free-space amplitudes is significantly reduced in the self consistent scheme. Here one should note that the s-wave and p-wave final-state phase space factors probe the antikaon spectral function in different ways. Thus, the net result is a combined effect depending on the in-medium amplitude and a projection of the antikaon spectral function that depends on the angular momentum.

The moderate enhancement for the $\pi\Sigma \rightarrow \bar{K}N$ reaction confirms the results of our previous work [41], in which it was pointed out that a self consistent antikaon dynamics does not generate the large enhancement factor predicted by a scheme that considers Pauli blocking only [34, 28]. Since an enhancement factor that is driven by the Pauli blocking effect will eventually disappear once a finite temperature is allowed for, it can not explain enlarged cross sections to be used in heavy ion reactions in any case. The striking effect induced by the $\Sigma(1385)$ resonance in the $\pi\Lambda \rightarrow \bar{K}N$ reaction is novel. It is the result of our detailed analysis of the kaon and antikaon scattering data which predicts that there is a strong coupling of the $\Sigma(1385)$ resonance to the $\pi\Lambda$ and $\bar{K}N$ channels at subthreshold energies. The self consistent many-body computation presented here suggests that this strong coupling persists in the nuclear medium giving rise to the large enhancement factor found for the in-medium $\pi\Lambda \rightarrow \bar{K}N$ reaction. This effect should have important consequences for the antikaon yield in nucleus-nucleus collisions at SIS energies.

As demonstrated in [219] the ad-hoc increase of the $\pi Y \rightarrow \bar{K}N$ cross section away from its free-space limit does increase the total antikaon yield. This demonstrates that transport model simulations of the antikaon yield that are based on free-space cross sections do not reach equilibrium conditions. Of course beyond some critical enhancement factor one would expect the yield to saturate implying that phase space is populated statistically. To put it in another way an enhancement factor 40 will not increase the yield by a factor of 40. However, we argue that a strong enhancement factor is rather welcome since that implies that the enhancement should be strong enough exceeding the critical value required for driving the antikaons towards equilibrium conditions even at smaller density or equivalently larger impact parameter. Therefore we would expect that the impact parameter dependence of the K^-/K^+ yield should be weak as seen in Fig. 6.17 and predicted by the statistical model of Cleymans, Oeschler and Redlich [228]. Here we would deviate from the line of arguments put forward by Aichelin, Hartnack and Oeschler who argued that with their ad-hoc enhancement the impact parameter dependence of the K^-/K^+ yield decreases with increasing impact parameter. Since the unscaled cross sections predict a flat behavior in their simulation, more consistent with Fig. 6.17, one may favor the free-space cross sections. This conclusion would be based, however, on a simple energy independent enhancement factor of the $\pi Y \rightarrow \bar{K}N$ transition rate. In contrast Fig. 6.19 suggests that even at a rather late stage of the fireball expansion the pions and hyperons need very little kinetic energy to produce a virtual antikaon. That should lead to a flattening of the number of antikaons with increasing reaction time contradicting the results shown by Aichelin, Hartnack and Oeschler [219].

It would be very useful to incorporate the dynamics of the $\Sigma(1385)$ into transport model simulations. If it can be confirmed that that the description of the antikaon yield requires an in-medium enhancement of the $\pi Y \rightarrow \bar{K}N$ rates we would interpret this as a clear signal for an attractive shift in the antikaon mass distribution ². Only if the in-medium $\bar{K}N$ phase

²One may argue that an attractive mean field of the nucleon gives rise to a similar enhancement. However, our results predict that this effect would be annihilated by the attractive mass shift of the $\Sigma(1385)$ resonance.

space has significant overlap with the $\Sigma(1385)$ resonance the $\pi \Lambda \rightarrow \bar{K} N$ rate can be enhanced significantly.

Chapter 7

Summary and outlook

In this work the relativistic chiral $SU(3)$ Lagrangian was applied to the meson-baryon scattering processes. Within the χ -BS(3) approach a unified description of pion-nucleon, kaon-nucleon and antikaon-nucleon scattering was established. A large amount of scattering data and also the empirical axial vector coupling constants for the baryon octet ground states are described. We derived the Bethe-Salpeter interaction kernel at chiral order Q^3 and then computed the scattering amplitudes by solving the Bethe-Salpeter equation within a systematic on-shell reduction scheme that preserves covariance, analyticity and two-body unitarity. Moreover, the number of colors (N_c) in QCD was considered as a large parameter performing a systematic $1/N_c$ expansion of the interaction kernel. This led to a significant reduction of the number of parameters. The analysis provides first reliable estimates of poorly known s- and p-wave parameters. An important result of the work is that the strength of all quasi-local 2-body interaction terms are consistent with the large- N_c sum rules of QCD. Further intriguing results were obtained for the meson-baryon coupling constants. The chiral $SU(3)$ flavor symmetry was found to be an extremely useful and accurate tool. Explicit symmetry breaking effects are quantitatively important but sufficiently small to permit an evaluation within chiral perturbation theory. Two essential ingredients for a successful application of the chiral Lagrangian to the meson-baryon dynamics were derived. First it was found that the explicit s- and u-channel decuplet contributions are indispensable for a good fit to the data set. Second, it is crucial to employ the relativistic chiral Lagrangian. It gives rise to well defined kinematical structures in the quasi-local 4-point interaction terms which imply a mixing of s-wave and p-wave parameters. Only in the heavy-baryon mass limit, not applied in this work, the parameters decouple into the s-wave and p-wave sector. A projector formalism was constructed which decouples the Bethe-Salpeter equation into covariant partial wave equations. This formalism permits the application of dimensional regularization crucial for a proper renormalization of the scattering equation. A novel minimal chiral subtraction prescription within the dimensional regularization scheme was developed that complies manifestly with the chiral counting rules. A consistency check of the forward scattering amplitudes was performed by confronting them with their dispersion-integral representations. The analysis showed that the scattering amplitudes are compatible with their expected analytic structure. Moreover it was demonstrated that the kaon-nucleon and antikaon-nucleon scattering amplitudes are approximately crossing symmetric in the sense that the KN and $\bar{K}N$ amplitudes match at subthreshold energies. An important test of the analysis could be provided by new data on kaon-nucleon scattering e.g. from the DAΦNE facility [79]. In particular further polarization data possibly obtained with a polarized hydrogen or deuteron

target would be extremely useful.

The results for the $\bar{K}N$ amplitudes have interesting consequences for antikaon propagation in dense nuclear matter as for example probed in heavy ion collisions [31]. According to the low-density theorem [74, 33] an in-medium antikaon spectral function with support at energies smaller than the free-space kaon mass, probes the antikaon-nucleon scattering amplitudes at subthreshold energies. The required amplitudes are well established in this work. In particular sizeable contributions from p-waves not considered systematically so far [35, 41, 42] were found. The microscopic χ -BS(3) dynamics was applied to antikaon and hyperon resonance propagation in cold nuclear matter in a manifestly covariant and self consistent manner. For the antikaon spectral function a pronounced dependence on the three-momentum of the antikaon is predicted. The spectral function shows typically a rather wide structure invalidating a simple quasi-particle description. For instance at $\rho = 0.17 \text{ fm}^{-3}$ the strength starts at the quite small energy, $\omega \simeq 200$ MeV. Furthermore, at nuclear saturation density attractive mass shifts for the $\Lambda(1405)$, $\Sigma(1385)$ and $\Lambda(1520)$ of about 60 MeV, 60 MeV and 100 MeV are predicted. The hyperon states are found to show at the same time an increased decay width of about 120 MeV for the s-wave $\Lambda(1405)$, 70 MeV for the p-wave $\Sigma(1385)$ and 90 MeV for the d-wave $\Lambda(1520)$ resonances. It would be interesting to explore whether it is feasible to confirm the strong in-medium modifications of hyperon resonance by suitable experiments at ELSA or MAMI.

The importance of the p-wave $\Sigma(1385)$ resonance for the antikaon production in heavy ion collisions as studied at GSI was pointed out. The presence of the latter resonance implies a substantially enhanced $\pi\Lambda \rightarrow \bar{K}N$ reaction rate in nuclear matter. Contrary to naive expectations only a small enhancement of the $\pi\Sigma \rightarrow \bar{K}N$ reaction was derived even though it couples to the s-wave $\Lambda(1405)$ resonance. It was argued that the incorporation of the $\Sigma(1385)$ resonance into transport model simulations of nucleus-nucleus collisions at SIS energies should help to obtain a quantitative and microscopic understanding of the empirical antikaon yields.

The analysis is expected to pave the way for a microscopic description of kaonic atom data. The latter are known to be a rather sensitive test of the antikaon-nucleon dynamics [176]. An extended domain of applicability for the microscopic chiral theory is foreseen once additional inelastic channels are considered systematically. Also an application of the covariant and self consistent many-body dynamics, developed in this work, to the propagation properties of pions, vector-mesons and nucleon resonances is being pursued. Here interesting in-medium effects due to mixing of the s-, p- and d-wave nucleon resonances are expected. Before a quantitative application of the results to heavy-ion reactions it is necessary to extend the approach to finite temperatures.

Bibliography

- [1] G. E. Brown and W. Weise, Phys. Rept. **22** (1975) 279.
- [2] A. B. Migdal, E. E. Saperstein, M. A. Troitsky and D. N. Voskresensky, Phys. Rept. **192** (1990) 179.
- [3] E. Oset, H. Toki and W. Weise, Phys. Rept. **83** (1982) 281.
- [4] W. Weise, *Quarks, hadrons and dense nuclear matter*, Les Houches, France, 30 July - 30 August 1996.
- [5] R. Rapp and J. Wambach, Adv. Nucl. Phys. **25** (2000) 1.
- [6] G. Chanfray, Nucl. Phys. **A 685** (2001) 328c.
- [7] U. Mosel, in Proc. of *28th Int. Workshop on Gross Properties of Nuclei and Nuclear Excitation: Hadrons in Dense Matter*, Hirschegg, Austria, 16-22 January 2000.
- [8] J. Hufner, Phys. Rept. **21** (1975) 1.
- [9] C.D. Dover and G.E. Walker, Phys. Rep. **89** (1982) 1.
- [10] C.J. Batty, E. Friedman and A. Gal, Phys. Rep. **287** (1997) 385.
- [11] V. Metag, in Proc. of *Int. Symposium on Nuclei and Nucleons*, Darmstadt, Germany, October (2000), to appear in Nucl. Phys. **A**.
- [12] V. Metag, in Proc. of *N* 2001 workshop on the physics of excited nucleons*, Mainz, Germany, 7-10 March 2001, to appear in World Scientific.
- [13] P. Braun-Munzinger and J. Stachel, Nucl. Phys. **A 606** (1996) 320.
- [14] P. Braun-Munzinger, I. Heppe and J. Stachel, Phys. Lett. **B 465** (1999) 15.
- [15] J. Cleymans, et al., Phys. Rev. **C 60** (1999) 054908; Phys. Rev. Lett. **81** (1998) 5284.
- [16] J.S. Hamieh, K. Redlich and A. Tounsi, Phys. Lett. **B 486** (2000) 61.
- [17] C. Fuchs, D.S. Kosov, A. Faessler, Z.S. Wang and T. Waindzoeh, Phys. Lett. **B 434** (1998) 245; Z.S. Wang, A. Faessler, C. Fuchs, V.S. Uma Maheswaria and T. Waindzoeh, Phys. Rev. **C 57** (1998) 3284.
- [18] T. Gaitanos, C. Fuchs and H. H. Wolter, Nucl. Phys. **A 650** (1999) 97.

- [19] E. L. Bratkovskaya, W. Cassing and U. Mosel, Nucl. Phys. **A 622** (1997) 593.
- [20] S. A. Bass et al., Prog. Part. Nucl. Phys. **41** (1998) 225.
- [21] C.M. Ko, V. Koch and G. Li, Annu. Rev. Nucl. Part. Sci. **47** (1997) 505.
- [22] C. David, C. Hartnack, J. Aichelin, Nucl. Phys. **A 650** (1999) 358.
- [23] W. Cassing and E.L. Bratkovskaya, Phys. Rep. **308** (1999) 65.
- [24] M. Effenberger and U. Mosel, Phys. Rev. **C 60** (1999) 051901.
- [25] St. Leupold, Nucl. Phys. **A 672** (2000) 475.
- [26] Yu. B. Ivanov, J. Knoll and D. N. Voskresensky, Nucl. Phys. **A 672** (2000) 313.
- [27] W. Cassing and S. Juchem, Nucl. Phys. **A 672** (2000) 417.
- [28] J. Schaffner-Bielich, V. Koch and M. Effenberger, Nucl. Phys. **A 669** (2000) 153.
- [29] J.P. Blaizot, *The physics of the quark gluon plasma*, Frontiers in nuclear physics 262, Canberra (1998).
- [30] U. Heinz and M. Jacob, nucl-th/0002042.
- [31] F. Laue, Ch. Sturm et al., Phys. Rev. Lett. **82** (1999) 1640.
- [32] G.E. Brown, K. Kubodera, M. Rho, V. Thorsson, Phys. Lett. **B 291** (1992) 355; G.E. Brown, C.H. Lee, M. Rho, V. Thorsson, Nucl. Phys. **A 567** (1994) 937; C.-H. Lee, G.E. Brown, D.-P. Min, M. Rho, Nucl. Phys. **A 385** (1995) 481.
- [33] M. Lutz, A. Steiner and W. Weise, Nucl. Phys. **A 574** (1994) 755.
- [34] V. Koch, Phys. Lett. **B 337** (1994) 7.
- [35] E.E. Kolomeitsev, D.N. Voskresensky and B. Kämpfer, Nucl. Phys. **A 588** (1995) 889.
- [36] V.R. Pandharipande, C.J. Pethick and V. Thorsson, Phys. Rev. Lett. **75** (1995) 4567.
- [37] C.-H. Lee, D.-P. Min and M. Rho, Nucl. Phys. **A 602**, 334 (1996).
- [38] G.E. Brown and M. Rho, Nucl. Phys. **A 596**, 503 (1996).
- [39] T. Waas, N. Kaiser and W. Weise, Phys. Lett. **B 365** (1996) 12, Phys. Lett. **B 379** (1996) 34.
- [40] T. Waas, M. Rho and W. Weise, Nucl. Phys. **A 617** (1997) 449.
- [41] M. Lutz, Phys. Lett. **B 426** (1998) 12; M.F.M. Lutz, in Proceedings "APCTP Workshop on Astro-Hadron Physics", Seoul, 25.- 31. Oktober 1997, nucl-th/9802033.
- [42] A. Ramos and E. Oset, Nucl. Phys. **A 671** (2000) 481.
- [43] A. Cieply, E. Friedman, A. Gal and J. Mares, Nucl. Phys. **A 696** (2001) 173.
- [44] L. Tolos, A. Ramos, A. Polls and T.S. Kuo, Nucl. Phys. **A 690** (2001) 547.

- [45] M.F.M. Lutz and W. Florkowski, *Act. Phys. Pol.* **31** (2000) 2567.
- [46] G.E. Brown and H.A. Bethe, *Astrophys. Jour.* **423** (1994) 659.
- [47] G.Q. Li, C.-H.Lee, G.E. Brown, *Phys. Rev. Lett.* **79** (1997) 5214; *Nucl. Phys. A* **625** (1997) 372.
- [48] R.S. Hyano, S. Hirenzaki and A. Gillitzer, *Eur. Phys. J. A* **6** (1999) 99.
- [49] G.A. Sokol, nucl-ex/0012010.
- [50] M.A. Nowak, M. Rho and I. Zahed, *Chiral nuclear dynamics*, World Scientific, Singapore (1996).
- [51] F. Karsch, *Nucl. Phys. B* (Proc. Suppl.) 83-84 (2000) 14.
- [52] G. Boyd, et al. *Phys. Lett. B* **349** (1995) 170.
- [53] T. Hatsuda, hep-ph/0104139.
- [54] S. Weinberg, *The quantum theory of fields*, Vol. II, University Press, Cambridge (1996).
- [55] J. Gasser, H. Leutwyler, M.P. Locher and M.E. Sainio, *Phys. Lett. B* **213** (1988) 85.
- [56] V. Bernard, N. Kaiser and U.-G. Meißner, *Nucl. Phys. A* **615** (1997) 483.
- [57] N. Fettes, U. Meissner and S. Steininger, *Nucl. Phys. A* **640** (1998) 199.
- [58] N. Fettes and U.-G. Meißner, *Nucl. Phys. A* **676** (2000) 311.
- [59] N. Fettes and U.-G. Meißner, *Nucl. Phys. A* **693** (2001) 693.
- [60] A. Krause, *Helv. Phys. Acta* **63** (1990) 3.
- [61] J. Gasser and H. Leutwyler, *Nucl. Phys. B* **250** (1985) 517.
- [62] S. Weinberg, *Phys. Rev. Lett.* **17** (1966) 616.
- [63] Y. Tomazawa, *Nuov. Cim. A* **46** (1966) 707.
- [64] S. Weinberg, *Phys. Lett. B* **251** (1990) 288.
- [65] N. Kaiser, P.B. Siegel and W. Weise, *Nucl. Phys. A* **594** (1995) 325; N. Kaiser, T. Waas and W. Weise, *Nucl. Phys. A* **612** (1997) 297.
- [66] E. Oset and A. Ramos, *Nucl. Phys. A* **635** (1998) 99.
- [67] M. Lutz and E. Kolomeitsev, in *Proc. of 28th Int. Workshop on Gross Properties of Nuclei and Nuclear Excitations: Hadrons in Dense Matter*, Hirschegg, Austria, 16-22 January 2000.
- [68] J.A. Oller and U.-G. Meißner, *Phys. Lett. B* **500** (2001) 263; U.-G. Meißner and J.A. Oller, *Phys. Rev. D* **64** (2001) 014006.
- [69] A.D. Martin, *Nucl. Phys. B* **179** (1981) 33.

- [70] B.R. Martin and M. Sakit, Phys. Rev. **183** (1969) 1345; 1352.
- [71] J.K. Kim, Phys. Rev. Lett. **14** (1965) 29.
- [72] M. Sakit et al., Phys. Rev. **139** (1965) B719.
- [73] G.P. Gopal et al. Nucl. Phys. **B 119** (1977) 362.
- [74] C.D. Dover, J. Hüfner and R.H. Lemmer, Ann. Phys. **66** (1971) 248.
- [75] G. C. Oades, in Proc. of *Int. Workshop on Low and Intermediate-Energy Kaon-Nucleon Physics*, Rome, Italy, 24-28 March 1980, (eds. E. Ferrari, G. Violini), D. Reidel Publishing, Dordrecht (1980).
- [76] A. Müller-Groeling, K. Holinde and J. Speth, Nucl. Phys. **A 513** (1990) 557.
- [77] R.H. Dalitz and A. Deloff, J. Phys. **G 17** (1991) 289.
- [78] M.Th. Keil, G. Penner and U. Mosel, Phys. Rev. **C 63** (2001) 045202.
- [79] L. Maiani, G. Pancheri and N. Pavers eds, "*The Second DAΦNE Physics Handbook*", (I.N.F.N., Frascati 1995), Vol. I and II.
- [80] O. Dumbrajs et al., Nucl. Phys. **B 216** (1983) 277.
- [81] T. Barnes and E.S. Swanson, Phys. Rev. **C 49** (1994) 1166.
- [82] M. Iwasaki et al., Phys. Rev. Lett. **78** (1997) 3067.
- [83] V.R. Veirs and R.A. Burnstein, Phys. Rev. **D 1** (1970) 1883.
- [84] G. Höhler, in Landolt-Börstein, Vol. I/9b2, (ed. H. Schopper), Springer, Berlin (1983).
- [85] D.N. Tovee et al., Nucl. Phys. **B 33** (1971) 493; R.J. Nowak et al., Nucl. Phys. **B 139** (1978) 61; W.E. Humphrey and R.R. Ross, Phys. Rev. **127** (1962) 1305.
- [86] T.S. Mast et al., Phys. Rev. **D 11** (1975) 3078.
- [87] G. 't Hooft, Nucl. Phys. **B 72** (1974) 461.
- [88] E. Witten, Nucl. Phys. **B 160** (1979) 57; G. Adkins, C. Nappi and E. Witten, Nucl. Phys. **B 228** (1983) 552.
- [89] T. Becher and H. Leutwyler, Eur. Phys. J. **C 9** (1999) 643.
- [90] M. Lutz, Nucl. Phys. **A 677** (2000) 241.
- [91] J. Gegelia, G. Japaridze and X.Q. Wang, hep-ph/9910260.
- [92] P.B. Siegel and W. Weise, Phys. Rev. **C 38** (1988) 2221.
- [93] R. Dashen, E. Jenkins and A.V. Manohar, Phys. Rev. **D 49** (1994) 4713.
- [94] Ch.D. Carone, H. Georgi and S. Osofsky, Phys. Lett. **B 322** (1994) 227.
- [95] M. Luty and J. March-Russell, Nucl. Phys. **B 426** (1994) 71.

- [96] S. Kondratyuk, A.D. Lahiff and H.W. Fearing, Phys. Lett. **B 521** (2001) 204.
- [97] M.F.M. Lutz and E.E. Kolomeitsev, Nucl. Phys. **A700** (2002) 193.
- [98] M.F.M. Lutz and C.L. Korpa, Nucl. Phys. **A700** (2002) 309.
- [99] M.F.M. Lutz, Gy. Wolf and B. Friman, Nucl. Phys. **A 661** (1999) 526c.
- [100] M.F.M. Lutz, Gy. Wolf and B. Friman, Nucl. Phys. **A**, in print.
- [101] V. Bernard, N. Kaiser, U.-G. Meißner, Int. J. Mod. Phys. **E 4** (1995) 193.
- [102] T. Ericson and W. Weise, *Pions and Nuclei*, Clarendon Press, Oxford (1988).
- [103] H.W. Wyld, Phys. Rev. **155** (1967) 1649.
- [104] R.H. Dalitz, T.C. Wong and G. Rajasekaran, Phys. Rev. **153** (1967) 1617; R.H. Dalitz, Rev. Mod. Phys. **33** (1961) 471.
- [105] J.A. Oller and E. Oset, Phys. Rev. **D 60** (1999) 074023.
- [106] U.-G. Meißner and J.A. Oller, Nucl. Phys. **A 673** (2000) 311.
- [107] G.F. Chew and S. Mandelstam, Phys. Rev. **119** (1960) 467.
- [108] J. Caro Ramon, N. Kaiser, S. Wetzel and W. Weise, Nucl. Phys. **A 672** (2000) 249.
- [109] J. Nieves and E.R. Arriola, Phys. Rev. **D 64** (2001) 11608.
- [110] D.M. Manley and E.M. Saleski, Phys. Rev. **D 45** (1992) 4002; Phys. Rev. **D 30** (1984) 904.
- [111] Ch. Sauerman, B. Friman and W. Nörenberg, Phys. Lett. **B 341** (1995) 261.
- [112] T. Feuster and U. Mosel, Phys. Rev. **C 58** (1998) 457.
- [113] T. Feuster and U. Mosel, Phys. Rev. **C 59** (1999) 460.
- [114] T.P. Vrana, S.A. Dytman and T.-S. H. Lee, Phys. Rept. **328** (2000) 181.
- [115] T.R. Hemmert, B.R. Holsteinn and J. Kambor, J. Phys. **G 24** (1998) 1831.
- [116] N. Fettes and U.G. Meißner, Nucl. Phys. **A 679** (2001) 629.
- [117] R. Dalitz and S.F. Tuan, Ann. Phys. (N.Y.) **10** (1960) 307.
- [118] N. Isgur and G. Karl, Phys. Rev. **D 18** (1978) 4187.
- [119] S. Capstick and W. Roberts, Prog. Part. Nucl. Phys. **45** (2000) 241.
- [120] L.Ya. Glozman and D.O. Riska, Phys. Rep. **268** (1996) 263.
- [121] H. Georgi, in Proc. of *3rd International Conference In Quark Confinement And Hadron Spectrum*, Newport News, Virginia, 7-12 June 1998; Singapore, World Scientific, 2000.

- [122] P. Zenczykowski, *Ann. Phys.* **169** (1986) 453; W. Blask, M.G. Huber and B. Metsch, *Z. Phys.* **A 326** (1987) 413; B. Silvetre-Brac and C. Gignoux, *Phys. Rev.* **D 43** (1991) 3699.
- [123] Ch.D. Carone, H. Georgi, L. Kaplan and David Morin, *Phys. Rev.* **D 50** (1994) 5793.
- [124] C.E. Carlson, Ch.D. Carone, J.L. Goity and R.F. Lebed, *Phys. Rev.* **D 59** (1999) 114008.
- [125] C.L. Schatt, J.L. Goity and N.N. Scoccola, *Phys. Rev. Lett.* **88** (2002) 102002.
- [126] R. Dashen and A.V. Manohar, *Phys. Lett.* **B 315** (1993) 438.
- [127] H. Georgi, talk presented to the 1994 Chiral Dynamics Workshop at MIT.
- [128] M. Kimura et al., *Phys. Rev.* **C 62** (2000) 015206.
- [129] J.S. Ball and W.R. Frazer, *Phys. Rev.* **7** (1961) 204.
- [130] R. Aaron and R.D. Amado, *Phys. Rev. Lett.* **27** (1971) 1316.
- [131] R. Aaron, in *Proc. Summer Symp. on New Directions in Hadron Spectroscopy*, Argonne National Laboratory, July 7-10, 1975, (eds. S.L. Kramer and E.L. Berger), Argonne report ANL-HEP-CP-75-58.
- [132] N. Kaiser, P.B. Siegel, W. Weise, *Phys. Lett.* **B 362** (1995) 23.
- [133] T. Inoue, E. Oset, M.J. Vicente Vacas, *Phys. Rev.* **C 65** (2002) 035204.
- [134] A. Müller Groeling, K. Holinde and J. Speth, *Nucl. Phys.* **A 513** (1990) 557; J. Speth, O. Krehl, S. Krewald and C. Hanhart, *Nucl. Phys.* **A 680** (2000) 328.
- [135] Y. Nambu, *Phys. Rev.* **D 210** (1974) 4262.
- [136] J.S. Kang and H.J. Schnitzer, *Phys. Rev.* **D 12** (1975) 841.
- [137] T.D. Cohen and L.Ya. Glozman, *Phys. Rev.* **D 65** (2002) 016006.
- [138] T.D. Cohen and L.Ya. Glozman, hep-ph/0201242.
- [139] K.G. Wilson, *Phys. Rev.* **179** (1969) 1499.
- [140] L.Ya. Glozman, *Phys. Lett.* **B 475** (2000) 329; hep-ph/0105225.
- [141] P.D.B. Collins, *An introduction to Regge Theory and High Energy Physics*, Cambridge University Press, 1977.
- [142] D.I. Diakonov and V.Yu. Petrov, unpublished preprint 1988; private communications with D.I. Diakonov.
- [143] S. Kondratyuk and O. Scholten, *Nucl. Phys.* **A 677** (2000) 396.
- [144] R.D. Tripp et al., *Nucl. Phys.* **B 3** (1967) 10.
- [145] R.D. Tripp, R.O. Bangerter, A. Barbaro-Galtieri and T.S. Mast, *Phys. Rev. Lett.* **21** (1968) 1721.

- [146] D.E. Plane et al., Nucl. Phys. **B 22** (1970) 93.
- [147] Particle Data Tables, Eur. Phys. J. **C 15** (2000) 1.
- [148] U.-G. Meißner and J.A. Oller, Nucl. Phys. **A 679** (2001) 671.
- [149] E. Jenkins and A. Manohar, Phys. Lett. **B 255** (1991) 558.
- [150] G.P. LePage, nucl-th/9706029.
- [151] L.B. Okun, *Leptons and Quarks*, Amsterdam, North-Holland (1982).
- [152] P.J. Ellis and H-B. Tang, Phys. Lett. **B 387** (1996) 9; Phys. Rev. **C 57** (1998) 3356.
- [153] E. Jenkins, Phys. Rev. **D 53** (1996) 2625.
- [154] R. F. Dashen, E. Jenkins and A. V. Manohar, Phys. Rev. **D 51** (1995) 3697.
- [155] Ch.-H. Lee, G.E. Brown, D.-P. Min and M. Rho, Nucl. Phys. **A 585** (1995) 401.
- [156] S. Scherer and H.W. Fearing, Phys. Rev. **D 52** (1995) 6445; H.W. Fearing and S. Scherer, Phys. Rev. **C 62** (2000) 034003.
- [157] G. Müller and U.-G. Meißner, Nucl. Phys. **B 492** (1997) 379.
- [158] J. Gasser, H. Leutwyler and M.E. Sainio, Phys. Lett. **B 253** (1991) 252.
- [159] P. Büttiker and U.-G. Meißner, Nucl. Phys. **A 668** (2000) 97.
- [160] J.L. Goity, R. Lewis, M. Schvellinger and L. Zhang, Phys. Lett. **B 454** (1999) 115.
- [161] C.A. Dominguez, Rivista del Nuovo Cimento **8** (1985) 1.
- [162] V. Stoks, R. Timmerman and J.J. de Swart, Phys. Rev. **C 47** (1993) 512.
- [163] J. Dai, R. Dashen, E. Jenkins and A.V. Manohar, Phys. Rev. **D 53** (1996) 273; R. Flores-Mendieta, E. Jenkins and A.V. Manohar, Phys. Rev. **D 58** (1998) 094028.
- [164] J. Bijnens, H. Sonoda and M.B. Wise, Nucl. Phys. **B261** (1985) 185.
- [165] E. Jenkins and A.V. Manohar, Phys. Lett. **B 255** (1991) 558; Phys. Lett. **B 259** (1991) 353.
- [166] E. Jenkins, Nucl. Phys. **B 375** (1992) 561.
- [167] M.A. Luty and M. White, hep-ph/9304291.
- [168] R. Blankenbecler and R. Sugar, Phys. Rev. **142** (1966) 1051.
- [169] F. Gross and Y. Surya, Phys. Rev. **C 47** (1993) 703.
- [170] V. Pascalutsa and J.A. Tjon, Phys. Rev. **C 61** (2000) 054003.
- [171] A.D. Lahiff and I.R. Afnan, Phys.Rev. **C 60** (1999) 024608.
- [172] S. Kamefuchi, L. O’Raifeartaigh and A. Salam, Nucl. Phys. **28** (1961) 529.

- [173] J. Gasser, M. E. Sainio and A. Svarč, Nucl. Phys. **B 307** (1988) 779.
- [174] V. Bernard, N. Kaiser, J. Kambor and U.-G. Meißner, Nucl. Phys. **B 388** (1992) 315.
- [175] D.B. Kaplan, M.J. Savage and M.B. Wise, Nucl. Phys. **B 534** (1998) 329.
- [176] E. Friedmann, A. Gal and C.J. Batty, Nucl. Phys. **A 579** (1994) 518.
- [177] C.L. Korpa and R. Malfiet, Phys. Rev. **C 52** (1995) 2756.
- [178] E. Oset and L.L. Salcedo, Nucl. Phys. **A 468** (1987) 631.
- [179] K. Hashimoto, Phys. Rev. **C 29** (1984) 1377.
- [180] R.A. Arndt, I.I. Strakovsky, R.L. Workman and M.M. Pavan, Phys. Rev. **C 52** (1995) 2120.
- [181] F. James, MINUIT functional minimization and error analysis, Version 94.1, CERN Program Library Long Writeup D506, CERN (1994).
- [182] G. Müller and U.-G. Meißner, Nucl. Phys. **B 492** (1997) 379.
- [183] R. Hurtado, Heavy Ion Physics **11** (2000) 383.
- [184] P.M. Gensini, R. Hurtado and G. Violini, π N Newsletter, **13** (1997) 291.
- [185] N. Solomey for the KTeV Collaboration, Nucl. Phys. **A 639** (1998) 287c.
- [186] N. Solomey, hep-ex/0011074.
- [187] R. Dashen and M. Weinstein, Phys. Rev. **188** (1969) 2330.
- [188] V.G.J. Stoks and Th.A. Rijken, Phys. Rev. **C 59** (1999) 2009.
- [189] B. Holzenkamp, K. Holinde and J. Speth, Nucl. Phys. **A 513** (1990) 557.
- [190] R. Büttgen, K. Holinde and A. Müller-Groeling, Nucl. Phys. **A 506** (1990) 586.
- [191] R.H. Dalitz, J. McGinley, C. Belyea and S. Anthony, in Proc. *Int. Conf. on hypernuclear and kaon physics*, (ed. B. Povh), Heidelberg, 20-25 June 1982.
- [192] H. Kim, T. Doi, M. Oka and S.H. Lee, Nucl. Phys. **A 678** (2000) 295.
- [193] H. Kim, T. Doi and M. Oka, Phys. Rev. **C 62** (2000) 055202.
- [194] A.J. Buchmann and E.M. Henley, Phys. Lett. **B 484** (2000) 255.
- [195] L. Mica, Nucl. Phys. **B 10** (1969) 521; R. Carlitz and M. Kisslinger, Phys. Rev. **D 2** (1970) 336.
- [196] B. Loiseau and S. Wycech, Phys. Rev. **C 3** (2001) 034003 .
- [197] T.E.O. Ericson, B. Loiseau and A.W. Thomas, hep-ph/0009312.
- [198] J. Hamilton and G.C. Oades, Phys. Rev. **D 16** (1977) 2295.

- [199] J.S. Hyslop, R.A. Arndt, L.D. Roper and R.L. Workman, Phys. Rev. **D 46** (1992) 961.
- [200] B.R. Martin, Nucl. Phys. **B 94** (1975) 413.
- [201] M. Alston-Garnjost, R.W. Kenney, D.L. Pollard, R.R. Ross and R.D. Tripp, Phys. Rev. **D 18** (1978) 182.
- [202] P.M. Gensini, R. Hurtado and G. Violini, nucl-th/9804024; nucl-th/9811010.
- [203] M.B. Watson, M. Ferro-Luzzi and R.D. Tripp, Phys. Rev. **131** (1963) 2248.
- [204] D. Evans, J.V. Major, E. Rondio et al., J. Phys. **G 9** (1983) 885.
- [205] J. Ciborowski, J. Gwizdz, D. Kielczewska et al., J. Phys. **G 8** (1982) 13.
- [206] T.S. Mast et al., Phys. Rev. **D 14** (1976) 13.
- [207] R.O. Bangerter et al., Phys. Rev. **D 23** (1981) 1484.
- [208] R. Armenteros et al., Nucl. Phys. **B 21** (1970) 13.
- [209] W. Kittel, G. Otter and I. Wacek, Phys. Lett. **21** (1966) 349; W.E. Humphrey and R.R. Ross, Phys. Rev. **127** (1962) 1305; G.S. Abrams and B. Sechi-Zorn, Phys. Rev. **139** B454.
- [210] R.J. Hemingway, Nucl. Phys. **B 253** (1985) 742.
- [211] F. Barreiro et al., Nucl. Phys. **B 126** (1977) 319.
- [212] C. Dionisi, R. Armenteros, G. Dias et al., Phys. Lett. **B 78** (1978) 154.
- [213] A.D. Martin, N.M. Queen and G. Violini, Nucl. Phys. **B 10** (1969) 481.
- [214] J. Schaffner, J. Bondorf and I.N. Mishustin, Nucl. Phys. **A 625** (1997) 325.
- [215] A. Förster for the KaoS Collaboration, nucl-ex/0202010.
- [216] W. Cassing et al., Nucl.Phys. **A 614** (1997) 415.
- [217] G.Q. Li and G.E. Brown, Phys. Rev. **C 58** (1998) 1698.
- [218] J. Aichelin and Ch. Hartnack, nucl-th/0011050.
- [219] J. Aichelin, H. Oeschler and Ch. Hartnack, nucl-th/0109016.
- [220] M. Menzel et al., Phys. Lett. **B 495** (2000) 26.
- [221] M.F.M. Lutz, E.E. Kolomeitsev and C.L. Korpa, J. Phys. G, im Druck
- [222] J. Cugnon, P. Deneye and J. Vandermeulen, Phys. Rev. **C 41** (1990) 170.
- [223] G.Q. Li, C.-H. Lee and G.E. Brown, Nucl. Phys. **A 625** (1997) 372.
- [224] Y. Shin et al., Phys. Rev. Lett. **81** (1998) 1576.
- [225] G.Q. Li, C.M. Ko and B.A. Li, Phys. Rev. Lett. **74** (1995) 235.

- [226] Z.S. Wang et al., Eur. Phys. J. **A 5** (1999) 275.
- [227] M. Lutz, Nucl. Phys. **A 642** (1998) 171c; M. Lutz, B. Friman und Ch. Appel, Phys. Lett. **B 474** (2000) 7.
- [228] J. Cleymans, H. Oeschler and K. Redlich, Phys. Lett. **B 485** (2000) 27.
- [229] H.-J. Schultze et al., Phys. Rev. **C 57** (1998) 704.
- [230] P. Maessen, Th. Rijken and J. de Swart, Phys. Rev. **C 40** (1989) 2226.
- [231] A. Reuber, K. Holinde and J. Speth, Nucl. Phys. **A 570** (1994) 543.

Acknowledgements

I would like to thank E. Kolomeitsev and C. Korpa for enjoyable and very fruitful collaboration. The writing of my habilitation thesis depended crucially on being part of a very stimulating and supportive environment present at GSI. The project profitted significantly by the constant support and encouragement of W. Nörenberg. Many thanks also to H. Feldmeier, B. Friman, H. van Hees and J. Knoll for their never ending readiness to discuss and help.

Particular encouragement I received by the many discussions with P. Senger and Ch. Sturm from the KaoS collaboration. Also I would like to express my gratitude to W. Florkowski, M. Soyeur and G. Wolf who I collaborate with on projects not part of this thesis.

Thanks also to the frequent visitors of the theory group, K. Redlich and D. Voskresensky with who I had many useful discussions.